MICROFLUIDIC ACOUSTIC SYSTEM TO GENERATE AGED YEAST

FOR CELL AGING STUDIES

A Thesis

by

KEITH EDWARD KRENEK

Submitted to the Office of Graduate and Professional Studies of
Texas A&M University
in partial fulfillment of the requirements for the degree of

MASTER OF SCIENCE

Chair of Committee,	Arum Han
Committee Members,	Jun Kameoka
	Samuel Palermo
	Michael Polymenis
Head of Department,	Miroslav Begovic

May 2015

Major Subject: Electrical Engineering

ABSTRACT

The mechanisms and causes of aging, the greatest risk factor of disease, are poorly understood. This lack of knowledge—specifically in relation to the aging of single biological cells—results from limitations in the methods traditionally used in cell aging studies, including inefficiencies of manually culturing cells and constraints in analyzing cells with sufficient spatial and temporal resolution. Microfluidic technologies solve these deficiencies that have prevented researchers from fully understanding cell aging; therefore, to improve aging studies utilizing yeast as a model organism, a high-throughput microfluidic system has been developed to generate aged yeast for subsequent biochemical analyses.

The microfluidic system starts with a mixed-size yeast population and leverages size-based differences of acoustic forces to remove smaller, younger daughter yeast and isolate a substantial quantity of larger, aged mothers. Repeated separation of yeast by size during system operation increases the yield of the aged mother population, and microfluidic agitation to break up cell clumps improves size-based separation efficiency.

With this aged yeast generator, researchers can potentially produce a large population of aged cells without the need for time-consuming, error-prone purification steps or genetic modification. Experiments employing such a system may reveal new insights into aging at the cellular and molecular levels. This improved understanding of aging can be applied when treating age-related diseases, including sarcopenia, osteoporosis, macular degeneration, neurodegeneration, and cancer.

To the people in my life, for being one of the greatest blessings I've ever known

ACKNOWLEDGEMENTS

TABLE OF CONTENTS

LIST OF FIGURES

ix

xi

xiv

xv

xvii

LIST OF TABLES

1. INTRODUCTION

In this work, we develop an unprecedented microfluidic large-scale aged yeast generator to provide researchers large quantities of old yeast suitable for subsequent biochemical analyses. Studies involving the aged yeast can supplement existing cell aging knowledge and thereby produce a more holistic understanding of aging in general and improve treatments for age-related disorders.

1.1. Molecular causes of aging are poorly understood

One reason limiting our understanding of aging, especially of the molecular causes of aging in single biological cells, results from conventional cell aging studies still relying on limited, cumbersome cell analysis techniques.[1] In other words, traditional methods of culturing and studying cells have not allowed researchers to draw collective conclusions about aging, which is currently the greatest risk factor for disease.[2]

To increase understanding of aging and thereby improve treatments for age-related diseases, researchers often study the individual biological cells whose characteristics manifest in the aging of larger organisms like humans. Of the model eukaryotic cells used in such studies, budding yeast (*Saccharomyces cerevisiae*) is chosen most often by researchers. Although yeast is a relatively simple organism, yeast aging studies have revealed significant ambiguity in the molecular causes of cell aging. Figure 1 and several examples illustrate this uncertainty. Fehrmann *et al.* discovered that (i) cells abruptly enter a post-replicative stage called senescence and (ii) the loss of mitochondrial membrane potential is independent of age.[3] Both conclusions contradict prior hypotheses that cells gradually enter senescence and the entry results from loss of mitochondrial membrane potential. In general, researchers have not been able to explain the

relationships between environmental conditions, genetics, oxidative damage,[2] apoptosis[4] and replicative life span (defined in § 1.5) of yeast cells. Similar studies have shown that chronological life span of yeast may be related to oxidative stress, dysfunction and reactive oxygen species, reduced autophagy, nuclear DNA damage, mutagenesis, replicative stress, metabolic alterations, extrinsic stress, and other factors.[2] The diversity of and lack of agreement about factors that influence yeast life span underscore the needs for more studies in this field and improved instruments to perform analyses.
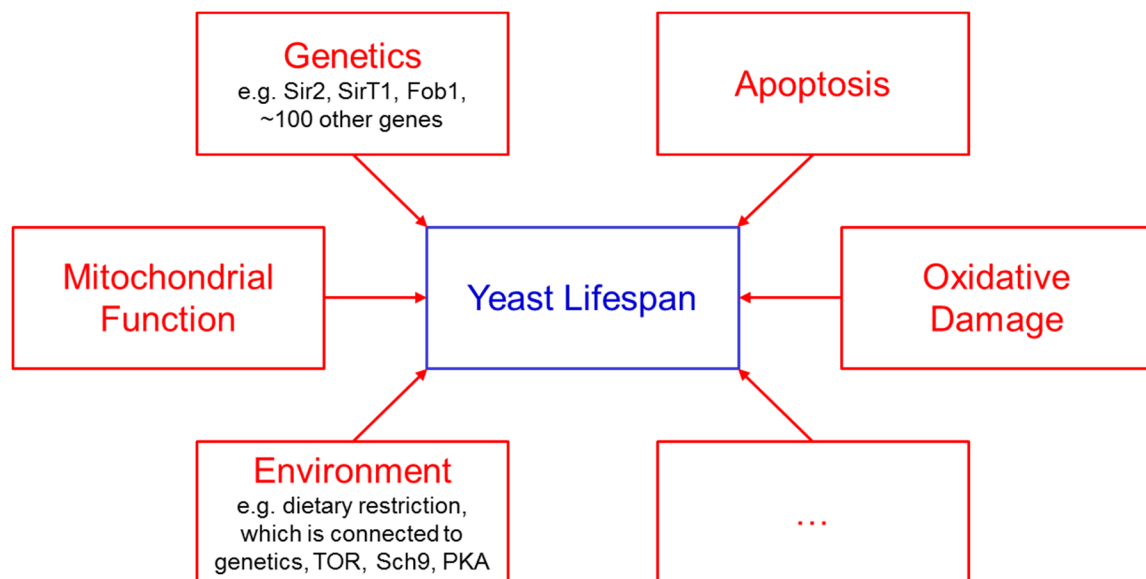
Figure 1. Researchers have found several factors that appear to influence yeast lifespan. Overall, yeast aging studies have revealed ambiguity in the molecular causes of cell aging (see refs. 2,4), and conflicting conclusions prevent a holistic understanding of aging.

1.2. Aging studies can improve how we treat age-related diseases

To harmonize the largely varied conclusions from past aging studies, in this work we develop a biomedical research tool that can generate old yeast for aging studies. Large quantities of aged yeast are needed in order to analyze molecular and biochemical factors related to cell aging.[5] We discuss below how conventional and microfluidic methods currently cannot produce a sufficient

quantity of cells. Without a high-throughput tool to generate aged yeast cells, our knowledge about the molecular causes of aging is incomplete. The new knowledge gained from studies of aged yeast cells can be used for treating age-related diseases, including sarcopenia, osteoporosis, macular degeneration, neurodegeneration, and cancer.[6]

1.3. Single-cell studies gather data unobtainable by studying higher organisms

To improve treatments of age-related diseases, research needs a deeper understanding of the microscale cells that combine to create the large-scale aging observed in whole organisms. Understanding aging at the single-cell level is important for several reasons. First, characteristics and functions of individual cells contribute to overall well-being of an organism. For example, cancerous cells in the body are observed to follow different cell-regulation processes compared to healthy cells. The cancerous cells can grow and divide even when not needed in the body, for instance, and create benign or malignant tumors. Second, studying individual cells is required to understand cell physiology of certain processes such as those that occur asynchronously or on limited timescales.[7] Signaling pathways, for example, or responses to rapid environmental stimuli cannot be studied when averaging the response across a large cell population. Third, heterogeneity among individual cells in a population is masked when biological data is averaged across the population.[8] Single-cell studies are needed to reveal these differences that can significantly impact cellular decision-making.[9] The responses of genetically identical cells to different stimuli can vary greatly. For instance, Lippuner *et al.* reported how older yeast are less sensitive (respond less) to pheromone compared to younger yeast.[10]

1.4. Yeast aging studies can reveal pathways that influence aging in humans

Single-cell studies of simple organisms, in addition to providing information that is not obtainable when studying larger organisms, can help researchers uncover knowledge about the cells of higher organisms. For instance, aging studies of unicellular eukaryotic organisms have revealed several pathways that influence aging in more complex organisms, including mammals. For this reason, simple organisms like yeast have emerged as ideal model systems for understanding aging in humans and other multicellular species.[4] Researchers have published >70,000 articles in which they used yeast as a model system. Benefits of studying yeast include short replication time (~90 min); amenability to straightforward, inexpensive, high-throughput experimental approaches; and similarities with mammalian cells.[11] Additionally, yeast has a well-characterized genome and its genetics can be manipulated relatively easily,[2] especially compared to complex rodents and humans.[12] Recently, researchers hypothesized that aging is influenced to some degree by ancestral evolutionary origins, and so researchers are actively trying to determine which characteristics of yeast aging have analogs in mammals and other multicellular eukaryotes.[2] This promise makes yeast an even more attractive tool with which to gain a better understanding of aging in more complex organisms.[4] Already, studying yeast has identified several mammalian genes and signal pathways that impact aging (e.g. the sirtuin pathway and the TOR signaling pathway).[2] Finally, because yeast has emerged as a model organism, much technology has been developed for studying it; new instruments are allowing researchers to uncover aging causes that would likely have remained hidden if not for the novel technologies.[9,13-19]

1.5. Yeast aging models

For studying yeast aging, three models are commonly used: replicative life span, chronological life span, and clonal senescence.[4,20] Replicative life span (RLS) is defined as the number of daughters produced by a mother cell before senescence. More specifically, a mother yeast divides 20-25 times (produces ~25 daughters) and then enters the post-replicative state (senescence) followed by lysis.[11] Figure 2 shows a schematic of RLS as well as a time-lapse yeast culture. Throughout their lifespans, mothers accumulate damage and bud scars, illustrated in the upper portion of Fig. 2 by circular rings that appear after each cell division. Notice the differences in mother and daughter sizes in the time-lapse culture (Fig. 2 bottom), a characteristic often exploited in yeast aging studies. The most common method of studying yeast RLS, first used in 1959,[21] involves manually separating daughter cells from mothers with a standard tetrad dissection microscope and micromanipulator. We discuss this and alternative methods of studying RLS in sections below.
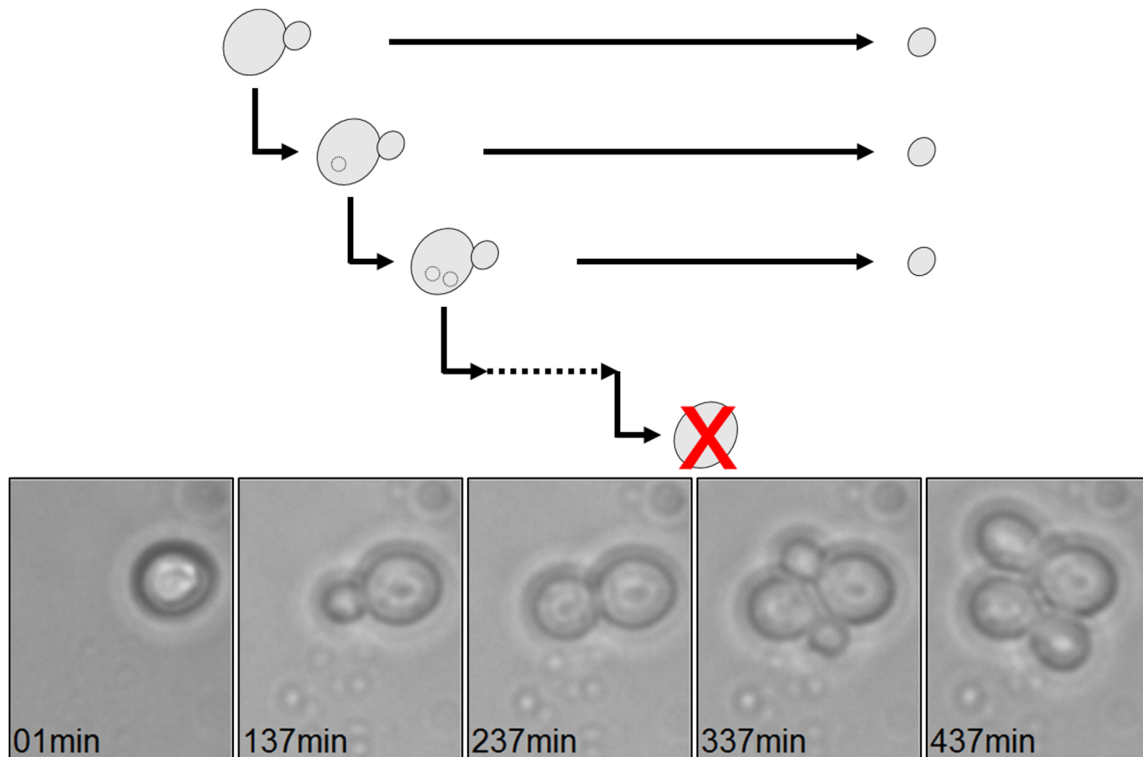
Figure 2. At top, schematic illustration of yeast replicative lifespan (RLS), defined as the number of daughter cells produced by a mother before cell death. Yeast age throughout their RLS, illustrated by the bud scars (circular rings) that appear after each division. At bottom, time-lapse of a single mother and two generations of its offspring.

Chronological lifespan (CLS) experiments examine how long a yeast cell survives after exiting the cell cycle, that is, the length of time a yeast cell survives in stationary (non-replicating) phase. Yeast exit the cell cycle and enter stationary phase after the post-diauxic state, which occurs when cells deplete extracellular glucose, decrease growth, and metabolize using mitochondrial respiration ~24 hr after a yeast culture begins.[2] Yeast cells that have stopped dividing once they deplete their environment of nutrients and enter the post-diauxic phase can survive a few days to several weeks. Environmental conditions including temperature, nutrients, pH, acetic acid concentration and genotype can affect CLS.[11] Three methods are commonly used to study yeast CLS, all of which monitor cell survival but differ in growth conditions. In one

6

method, cells are grown in 2% glucose through the post-diauxic phase and into stationary phase. The second technique is similar to the first except cells are transferred to water during the post-diauxic phase. In the third well-established method, cells are cultured on 2% glucose agar plates containing all nutrients except tryptophan.[2]

Clonal senescence of yeast cells, which is similar to the Hayflick limit observed in mammalian cell cultures, is indicated by the finite number of times a cell population can divide. Clonal senescence, also known as clonogenic survival, is quantified by colony-forming units (CFU). CFUs are calculated by scoring the ability of each yeast cell from a pre-determined number of cells to divide/reproduce and form a mini-colony on day 3 of a culture, known as the "100% survival point."[11] Other approaches to measure clonogenic survival are also used, such as the FUN-1 assay that measures metabolic activity of a population.

Researchers hypothesize that RLS studies may reveal insight into aging of mitotic/stem cells and cells with finite RLS, such as fibroblasts and lymphocytes, in multicellular eukaryotes like humans, and that CLS studies can be used to understand aging of post-mitotic tissues, non-dividing cells (e.g. neurons), and cells having long stationary phases.[11] Researchers most commonly study RLS and CLS in yeast cells, and these models complement each other.[2]

1.6. Yeast phenotypes relevant to replicative lifespan

With the microfluidic system in this work, we aim to produce a large number ($>10^5$) of aged yeast cells (>15 generations), thus the characteristics associated with replicative aging in yeast deserve discussion here. In general, yeast phenotypes change throughout their replicative lifespans. Researchers have observed bud scar accumulation, enlargement of cell size, decreasing cell cycle and fertility rates,[22] and thickening of the cell wall[12] as effects of replicative aging. Yeast undergo asymmetric budding, so older mothers are generally larger than their daughters

when they exit mitosis. To isolate large quantities of aged mothers in this work we exploit these size differences between mothers and daughters. Zhang *et al*. plotted yeast daughter size versus mother size at 10, 20, and 40 hr time points,[23] showing that at these measurement times the mother is always larger in size than the daughter.

In addition to yeast mothers generally being larger than their daughters, other cell properties distinguish mothers from daughters. For instance, a mother yeast keeps most of its cell wall throughout its lifetime, whereas the daughter cell wall is newly synthesized.[20] In other words, none of a mother's cell wall is inherited by its daughter; the daughter is grown with an entirely new cell wall. This characteristic underpins the successes of some of the methods that have been used to separate mother and daughter yeast (e.g. MACS) as discussed in § 1.8. Just as a mother's cell wall is not passed to its progeny, neither are many other manifestations of aging[10]; however, recent experiments have discovered that some age characteristics like morphology are inherited by yeast daughters.[18]

1.7. Challenges of generating a large, highly-pure population of aged yeast cells

To isolate a large number of aged yeast, the microfluidic system in this work must overcome several challenges. First, yeast grow exponentially in number. One cell divides to produce 2 cells, which divide into 4, then 8, 16, etc. Within hours, a single mother can be surrounded by millions of its progeny. If not removed, daughter cells quickly overtake the majority of nutrients and space in the environment around a mother cell. Both competition for nutrients and excreted waste from daughters can impact the aging of the mother. Second, because the number of yeast cells in a growing culture exponentially increases, a very small fraction of the total population will be very old mothers. For instance, a cell that is 15 generations old is 1 out of 2^{15} cells. Thus very old cells (>15 generations) are extremely rare in a population. Third, the difference in size

between mother and daughter yeast can be very small at the beginning and end of the yeast lifespan.[22] In other words, researchers have observed that very young and very old mother yeast produce daughters that are similar in size to the mother. This lack of difference can prove problematic when relying on size-based separation to remove daughters from mothers. Fourth, daughters remain attached to mothers close in time to when the next daughter starts budding (see § 2.2.11). Because a mother spends a majority of the time budding, somewhat rarely is the mother not attached to one of its daughters. When relying on non-optical size-based separation to differentiate between mothers and daughters, a mother still attached to its budding daughter may be seen as a single object equal to the combined mother and daughter sizes. This error may worsen the purity and resolution of many size-based separation techniques.

1.8. Micromanipulation and purification to study yeast lifespan

To study aged yeast cells, researchers typically utilize two methods: micromanipulation and purification. Micromanipulation has been used for >50 years. More recently, researchers have turned to high-throughput purification methods including selectively killing daughter cells and employing microfluidics to remove daughters from mothers; however, these alternatives have not replaced the manual dissection method as the "gold-standard life span assay"[2] for reasons discussed below.

Micromanipulation, first used in 1959,[21] is the most common method of studying yeast RLS. The technique leverages the fact that daughter yeast cells are smaller in size than their mothers.[2] Experimenters manually separate daughter cells from mothers using a standard tetrad dissection microscope with micromanipulator. Specific instructions for performing such a micromanipulation experiment are discussed elsewhere (e.g. ref. 22). In general, a researcher skilled at using a micromanipulator cultures ~40 virgin cells arrayed on an agar plate. Because of

9

significant variations among individual cells, 40 or more cells must be studied to obtain reliable

data. As each cell divides, the researcher identifies the daughter and carefully removes it with a

glass pipette tip attached to the micromanipulator. Removal of the daughter is important so that

the mother is not obstructed visually and to prevent the mother's offspring, which increase in

number exponentially, from stealing nutrients and influencing the mother's normal life span. If

each cell produces ~25 daughters, then ~1,000 cells must be removed in a single experiment,

which takes 10-14 days.[5,12] Although ~40 cells can be analyzed, larger quantities of cells

(thousands to millions) simply cannot be studied in a single aging experiment because of

limitations in manually keeping track of all mother cells.

Although micromanipulation to study RLS in yeast is most accurate especially when

precise ages in number of cell divisions are needed, this conventional method has several

disadvantages. Any contamination may ruin the RLS study, so researchers must practice extreme

caution when handling the cultures so extensively.[22] They must also work diligently not to dry-

out the cultures during removal of daughters.[12] Only a limited number of cells (~40) can be

studied and they are isolated on an agar plate, so the aged mothers cannot be used in subsequent

immunofluorescence or biochemical experiments.[22] This approach to study RLS is low-

throughput, labor intensive, and time-consuming.[5] Micromanipulation may damage cells and

invalidate experimental data. Because most of the experiments are not carried out continuously,

yeast must spend time in cold storage to prevent a surplus of daughters around each mother.[11]

Some studies claim incubation at low temperatures does not significantly impact RLS; however,

growth rate varies (e.g. mother cells bud on average once every ~2 hr at 30°C, once every 12 hr

at 10°C, and stop dividing at 4°C),[22] and growth rate may impact RLS.[2] Thus low temperatures

may indeed influence RLS. Natural variations in growth rate (those not induced by temperature

or other environmental conditions) also complicate the experiment because researchers must

then conform to the varying replication schedule of cells. For example, yeast at the very beginning of their life spans divide once every 70-90 min at 30°C, while aged mothers sometimes may not divide for several hours—an occurrence resembling replicative senescence—and then continue proliferation. This phenomenon complicates determining whether a mother has finished dividing.[22] Much experience is required for the manual micromanipulation RLS experiments, not only for operating the equipment but also recognizing subtle aspects of the yeast lifespans. For instance, differentiating between mothers and daughters is difficult during the first few cell divisions before the mother has grown very large. Finally, aged mothers are especially fragile and should not be dissected too often because over-dissection may shorten lifespan.[12]

One of the most significant disadvantages of the micromanipulation technique relative to this work is the inability to generate a large quantity ($>10^5$) of aged yeast (>15 generations) for subsequent biochemical analyses. To overcome this limitation, large-scale purification methods like centrifugal elutriation and magnetic-activated cell sorting have been developed. Studies using these high-throughput isolation techniques have revealed important factors associated with cell aging, including nucleolar fragmentation, movement of the Sir complex from telomeres to nucleolus, and accumulation of rDNA circles.[22]

Centrifugal elutriation is one high-throughput purification strategy. Similar to the micromanipulation method, centrifugal elutriation also utilizes differences in yeast mother and daughter sizes to retain larger cells and remove (elute) daughters.[24] Centrifugal elutriation successfully and efficiently produces a highly pure population of synchronized virgin yeast cells[25,26] but has experimentally shown to produce old yeast with low purity.[24] Woldringh *et al.*, after running a centrifugal elutriator for 26 hr, generated a cell population consisting of 71% cells that were 10 or more generations old, 12% that were 1-9 generations old, and 17% virgin

cells having no bud scars. In an attempt to produce 29-generation yeast, Woldringh *et al.* found that the resulting elutriated population consisted of 25% virgin cells with only 50% being 15+ generations old. In addition to requiring repeated run-times with expensive equipment to generate old yeast with relatively poor purity, centrifugal elutriation is very "elaborate", sensitive to changes in flow rate, and suffers from risk of contamination.[24] The process is also not amenable to high-throughput operation and may harm cells.[27] A similar technique, sucrose gradient centrifugation, also produces only a modestly pure population of aged yeast (~90%) after repeated purification. Rather than generating aged yeast, centrifugal elutriation and its variants are far more useful at producing a population of synchronized virgin yeast. The microfluidic system developed in this work aims to improve on the drawbacks of centrifugation, including producing low purity in the resulting old yeast population, relying on expensive equipment, and risking contamination and harm to cells.

One of the most successful methods for obtaining a large, pure population of aged yeast requires tagging the mother cell wall with a label that is not passed to daughters. The cell membranes of daughter yeast are newly synthesized, so no parts of the previously synthesized mother cell membrane are passed to any of its daughters. Using this property, researchers have successfully isolated labeled mother cells after any desired number of cell divisions. One such labeling system described by Smeal *et al.* produced a large number of aged mother cells by selectively coating mothers with biotin.[28] The biotin remained attached to the mother's cell wall even after cell division because the daughter cell wall is newly synthesized. Isolation of biotin-labeled mother yeast for subsequent analysis is accomplished using either fluorochrome-conjugated avidin and fluorescence-activated cell sorting (FACS) or streptavidin-coated paramagnetic iron beads and magnetic-activated cell sorting (MACS). The technique employing FACS can produce an aged yeast population that is >99% pure; however, expensive instruments

are needed to accomplish this isolation, and the population of aged cells is relatively small (10^4 cells). A single run of magnetic sorting method separates a much larger quantity of cells (10^8) that are 7-12 generations old. Unfortunately with these techniques, several manipulation and sample processing steps are needed, especially to obtain a very pure population and one in which cells are older than 12 generations. In addition to the repeated sorting steps, increased risks of contamination that can ruin the experiment decrease the attractiveness of these cell sorting methods.[22] Although FACS and MACS are considered high-throughput techniques, they may damage cells and are not label-free.[27]

The above-mentioned techniques, centrifugal elutriation and FACS/MACS, suffer from several disadvantages. Exponential proliferation of daughter yeast limits the replicative age of cells that can be obtained from a single purification run. Purifying a yeast culture once produces cells that are only 7-12 generations old. Repeating the purification steps can, however, produce cells older than 7-12 generations, but the additional sample processing and greater risk of adverse effects including contamination reduce the usefulness of these techniques.[20] Other drawbacks are low yield, contamination by daughter cells, and manual, time-consuming experimental steps (e.g. several sample washes).

Other large-scale purification schemes rely on genetically modifying a yeast population to aid in isolation of aged mothers. In one genetic manipulation approach that arrests proliferation of daughters, thereby helping to isolate aged mothers,[29] the RLS of mothers was significantly decreased.[20] This major drawback precludes the use of this technique for our target application.

Another large-scale purification approach termed the Mother Enrichment Program (MEP) genetically modifies daughter yeast by removing essential genes and stopping cell division.[20] Therefore, in a yeast population experiencing MEP, genetically modified daughters

do not divide, and so a mother's offspring do not limit the mother's nutrients or impact normal aging. In other words, lifespan of mothers is not changed, but replicative ability of daughters is turned off. With the MEP, researchers can reliably study genetic and environmental factors that affect RLS of old yeast. The MEP can also produce a sufficient quantity of yeast at any point in their replicative lifespans for subsequent biochemical analyses. MEP has several drawbacks, however, because it relies on genetic selection. A researcher must genetically modify a strain of interest. Mutations of modified strains and yeast that escape genetic modification both decrease the effectiveness of MEP and introduce contamination into the aged-mother population. In numbers, MEP selectively kills all but ~8% of daughters.[12] Additionally, daughters in MEP cultures can remain metabolically active in M-phase and grow for ~24 hr before lysis.[20] Metabolically active daughters can impact normal environmental and growth conditions of mothers. The negative effects of active daughters are likely emphasized when the mothers are older than ~20 generations because the replication rate of the mother slows and the mother experiences more effects of old age. These drawbacks limit the use of MEP for generating a large number of aged cells.

In summary, biochemical analyses of factors that influence yeast aging are limited by an inability to isolate large numbers ($>10^5$) of old yeast (>15 generations) using any of the current purification techniques. Micromanipulation, which requires costly equipment and skilled professionals, cannot yield a sufficient quantity of cells. The large-scale techniques developed to replace micromanipulation suffer from several drawbacks, including not being able to produce yeast older than 7-12 generations in a single run due to nutrient depletion and needing to purify a culture in several steps such that risks become significantly concerning. For instance, purifying a culture repeatedly can result in contamination and low yield/viability of aged cells.[20] Even for techniques like the Mother Enrichment Program (MEP), which overcomes drawbacks like

extensive sample processing, the resulting isolation of aged mothers is only modestly pure (~8%
of daughters are not killed by the MEP). The drawbacks associated with conventional
micromanipulation and large-scale purification techniques have sparked the developments of
further-improved systems utilizing microfluidics.
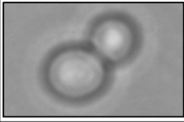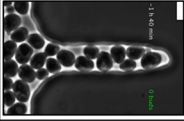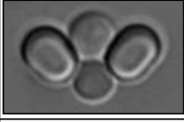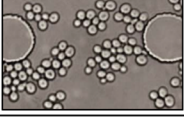
1.9. Microfluidics to study yeast aging

To overcome the limitations of micromanipulation and large-scale purification for studying yeast
aging, researchers turned to microfluidics. Before being applied to yeast aging, microfluidics
were introduced for studying single cells due to—among other reasons—two disadvantages of
traditional cell culture techniques. First, during cell culture, the exponential increase in the
number of cells quickly makes individual cell tracking challenging, if not impossible.
Researchers cannot acquire high-resolution time-lapse images throughout an experiment, and
progeny of mothers compete for nutrients and excrete waste in the mothers' environments, both
of which impact the growth and lifespans of mothers. Second, researchers cannot reliably and
efficiently study individual cell responses to different outside stimuli when the cells are in dense
cultures. Instead, researchers must average their findings over the entire cell population, which
may hide important findings and limit the variety of data that can be collected. Microfluidics
promises to solve these problems.

Microfluidics is the science and technology of manipulating small quantities of liquids
and gases using devices with small dimensions.[30] Microfluidic devices dedicated to culturing
cells[31-38] have already provided significant advantages over conventional cell culture techniques,
including increased automation, lower risks of contamination, higher-throughput, decreased use
of reagents, and greater reliability and repeatability. To leverage these advantages of

microfluidics for studying yeast aging, researchers have developed numerous microfluidic systems[3,9,13-19,23,39-51] that can be classified generally as shown in Table 1.

Table 1. Microfluidic systems applied to study yeast aging

Method to Immobilize Mother	Method to Remove Daughters	Example Image	Mean Lifespan (# divisions)	Disadvantages	References
Cultured on agar	Micromanipulation		27 (Polymenis), 31 (Fehrmann)	- Labor intensive - Cells cannot be used in subsequent tests	3, 21
Micro-chamber fills with yeast	Fluid flow removes cells near chamber entrance		25.3 (SCD/Fehrmann)	- Nutrient competition - Daughters are not removed selectively	3, 16, 17, 48, 50
Hydrodynamically trapped	Fluid flow		22.4 (XY w/ 2% glucose/Crane)	- Operational problems - Throughput depends on device geometry - Design depends on cell-type	9, 13, 42, 49
Mechanically trapped	Fluid flow		25 (SCD/Lee), 27 (YPD/Denoth, median), 23.6 (YPD/Zhang)	- Operational problems - Throughput depends on device geometry - Design depends on cell-type	23, 39, 44, 51, 53
Attached with label to channel wall	Fluid flow		18 (YPD/Xie)	- Requires a label - Yeast exhibit much shorter lifespan	19, 45
Confined to single imaging plane	None		Not measurable	- Nutrient competition - Daughters are not removed selectively	14, 15, 41, 43, 46, 47

Studies employing the novel microfluidic systems have revealed new knowledge in the field of cell aging. As examples, Lee *et al.*[18] observed age-related changes in cell phenotypes, and Xie *et al.*[19] found a molecular marker that is a "good predictor" for the lifespan of cells. With further development, these microfluidic systems may enable high-throughput studies,[5] but as of recently, the systems still have not replaced the conventional micromanipulation method or the purification methods for several reasons. For the microfluidic systems having a relatively large culture chamber (Table 1, row 3), yeast are allowed to divide to confluence which leads to

competition for nutrients among cells. These systems also cannot selectively remove daughter yeast nor isolate a large quantity of aged mothers. The same disadvantages also limit the usefulness of those systems that confine yeast to a single imaging plane but do nothing to remove cell progeny (Table 1, bottom row). The systems employing a mechanical or hydrodynamic trap (Table 1, rows 4 and 5) theoretically remove daughter cells efficiently, but this ideal mother-daughter dissection is not often observed in practice. The traps may retain >1 cell. For these systems, throughput depends solely on device geometry. In other words, the number of trapping sites determines the maximum number of cells that can be studied in a given experiment; to study 1,000 cells, >1,000 trapping sites are required because not all of the sites will successfully trap a single cell throughout its lifetime. Image acquisition of such experiments also limits the maximum number of cells that can be studied. For instance, to study 1,000 cells with 20 min time resolution may not be possible using some microscopy setups. Furthermore, the traps must be designed for specific cell types and strains, which means a single device or design is typically useful only for a particular cell. For example, wild-type yeast (75-80 fL mean volume) would require different traps compared to strains sfp1 (47 fL) and clu3 (150 fL). The fabrication techniques to produce microfluidic device features on the scale of single cells (<10 µm) are also more expensive than the conventional and more widely available processes used in the microfluidics field. The microfluidic systems that immobilize cells by attaching a labeled yeast to the channel wall (Table 1, row 6) require extra process steps and reagents, and the label may influence normal yeast aging. Finally, differences in experimental results of the microfluidic devices show they must have some bias. The fifth column of Table 1 lists mean lifespan in number of cell divisions for yeast used in the different microfluidic systems (rows 3-7) or in a standard micromanipulation experiment (row 2). In the column, lifespan is reported along with medium type and reference in parenthesis. YPD refers to yeast extract peptone dextrose medium,

17

and SCD for synthetic complete dextrose. As shown by reported mean lifespans, the microfluidic systems in general measure shorter lifespans compared to the micromanipulation technique. For example, mean replicative lifespan results obtained by Lee *et al.* (25 cell divisions), Xie *et al.* (18 cell divisions), and conventional micromanipulation (27 cell divisions) all differ.[5] The most significant disadvantage of these microfluidic systems—relative to this work—is the inability to generate large numbers of old yeast for biochemical tests. The mother-enrichment program (MEP), in which daughter cells are genetically altered so that they cannot reproduce, is a better method for these types of experiments[5]; however, even MEP suffers from drawbacks including failing to kill ~8% of daughter yeast which can impact aging of mothers.

1.10. Research needs an improved method of producing aged yeast

In summary, the conventional micromanipulation technique, although the "gold standard life span assay"[2] for >50 years, cannot generate a large number (>10^5) of aged yeast (>15 generations) and suffers from other disadvantages (see § 1.8). Purification techniques, including labeling the mothers for subsequent separation and genetically modifying daughters so that they cannot replicate, still do not provide researchers with an efficient and straightforward method of isolating a large number of aged yeast. Finally, the microfluidic systems aimed at studying yeast aging also have not solved the problem of generating a sufficient quantity of aged cells for large-scale screening analyses.

Because researchers do not have a method to produce large quantities of aged yeast for subsequent analyses,[5] high-throughput biochemical experiments of age-associated phenotypes have not yet been possible. These analyses of aged yeast are required to answer unsolved questions about cell aging. For example, the microfluidic systems have allowed—for the first time—tracking of a single yeast throughout its RLS and have found significant heterogeneity in

yeast aging especially at the end of a yeast's life.[9,10,18,19,23,41] This ambiguity at the end of a cell's lifespan and other poorly understood factors of cell aging underscore the need for a high-throughput microfluidic aged yeast generator.

1.11. High-throughput microfluidic aged yeast generator

In this work, we aim to provide researchers with a new tool for producing a highly pure population of $>10^5$ yeast that are >15 generations old. Ideally, approximately 24 hr after loading a sample yeast population into the microfluidic system, a researcher should be able to extract a large, pure population of aged yeast that can then undergo biochemical analyses. No further sample processing would be required, and the processing should be label-free. The automated system should produce aged yeast with higher purity (>90%) than the most successful purification techniques (elutriation, MACS/FACS, MEP) and should produce a quantity larger than what is possible using the current yeast aging microfluidic devices (>1000 cells) and with fewer limitations (e.g. needing to design the device geometry for a particular cell type or strain).

To accomplish these goals, our aged yeast generator consists of three subsystems: size-based separation of mother yeast from daughters, continuous or repeated separation to age the mothers, and agitation to break up cell clumps that would otherwise worsen separation purity. Figure 3 depicts these three subsystems of our aged yeast generator. Yeast enter the device at top left and flow through the separation region after which smaller daughters exit the device and mothers flow through a recirculation channel. The yeast of interest grow and bud, then pass through the agitation subsystem that breaks up cell clumps, and flow toward the separation region. This cycle repeats until a final aged yeast population suitable for subsequent analyses is produced. In § 2, we discuss the development of each subsystem.
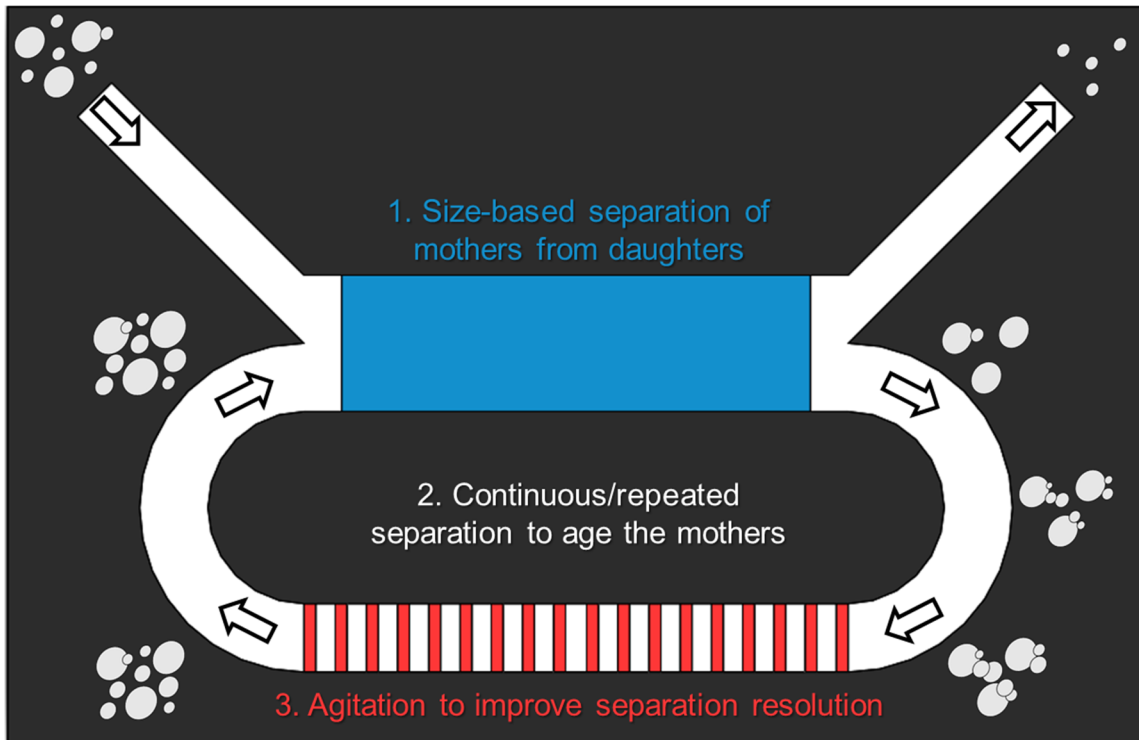
Figure 3. The aged yeast generator consists of three subsystems: size-based separation, continuous or repeated separation, and an agitation mechanism. Mother and daughter yeast enter the device at top left and are separated by size (subsystem 1). Daughters exit the device while mothers are kept to undergo repeated separation (subsystem 2). The mothers grow and bud, pass through the agitation region (subsystem 3) that breaks up cell clumps, and continue growing until they enter the separation region where the daughters are again removed and mothers remain in the device. After several hours of repeated separation, a large number of aged yeast can be generated from a mixed population of cells.

2. EXPERIMENTAL METHODS AND RESULTS

2.1. Size-based separation

2.1.1. General approach to separate yeast by size

The first subsystem of the aged yeast generator involves the size-based separation of larger mother yeast from smaller daughters. Figure 4 illustrates this separation. A heterogeneous population of mother and daughter yeast, i.e. cells of all sizes, is loaded into a microfluidic device through one inlet that combines with YPD loaded into another inlet (upper left in Fig. 4). At the intersection of the inlets, laminar flow between adjacent fluid streams focuses the yeast to the center of the microfluidic channel. This focusing helps ensure that all cells enter the separation region at approximately the same location, thereby improving size-based separation resolution. As yeast flow through the separation region, they are deflected toward the channel center by forces that vary by cell size; larger cells experience larger separation forces and thus deflect more than smaller cells. By the end of the separation region, cells should be spread out by size (inset above separation region in Fig. 4), and two outlets then finalize the separation. For our system, the smaller daughter yeast are removed from the device and the larger mothers are kept for additional separations (see § 2.2). This continuous flow-through separation is more amenable to high-throughput handling of large numbers of cells compared to traps which immobilize wanted cells while removing unwanted cells by fluid flow. In this section, we discuss our choice of using acoustic separation as the technique for removing daughter yeast from mothers.
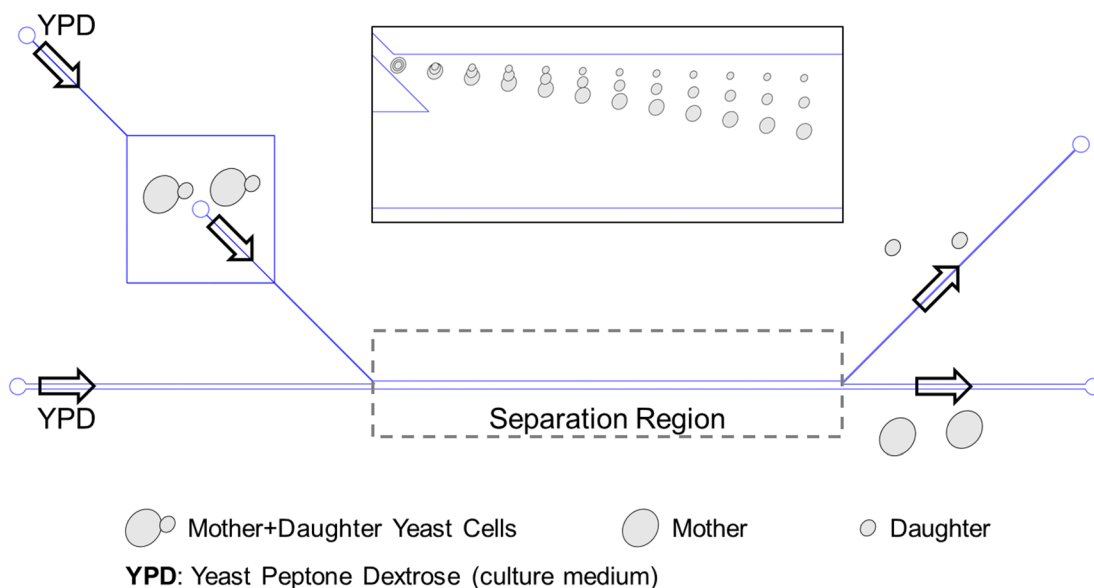
Figure 4. General approach to separate yeast by size. Mother and daughter yeast enter the device at top left and are flow-focused into the separation region by buffers on both sides. In the separation region, larger cells are deflected toward the channel center more than smaller cells (inset at top). At the outlet, smaller cells flow into the upper right outlet while larger cells flow into a separate outlet.

2.1.2. Yeast culture and device preparation for calibrating separation size cut-off

Before choosing a particular size-based separation technique, we first quantified the required separation resolution for mother and daughter yeast. Yeast cell sizes were measured for (i) our own experiments with wild-type cells and (ii) yeast images available from published sources.[9,18,19] For the in-house cultures, we fabricated Polydimethylsiloxane (PDMS) devices for holding cells/medium using a Professional Laser Series (PLS) 6.120D Laser Engraving and Cutting System (Universal Laser Systems, Inc.). A 10:1 resin to curing-agent PDMS mixture was degassed, poured into a petri dish, and cured in an 80°C oven overnight (>8 hr) to create a thin slab of PDMS (~4 mm thick). The PDMS slab was engraved using the laser micromachine so that the resulting pattern had an inlet, main chamber, and outlet. Inlet/outlet holes were punched, the PDMS was cleaned using DI water and IPA, and the slab was bonded to a glass

slide using oxygen plasma treatment (Harrick Plasma). Plastic tubing (Tygon, 0.01-inch i.d.) was manually inserted into the inlets/outlets.

Wild-type yeast (CEN.PK) were prepared by first combining Yeast Extract Peptone Dextrose medium (YPD) with a small streak of yeast colonies from a culture stock grown on an agar plate (obtained from a Texas A&M University collaborator, Dr. Michael Polymenis). The cells and media were incubated (Thermo Scientific MaxQ6000) at 30°C overnight (>12 hr) and grown to stationary phase. The overnight culture was transferred to fresh YPD and grown for ~3 hr in the incubator immediately before the experiment. This allowed cells to resume exponential growth, at which time they were placed in fresh, warmed YPD and loaded into the microfluidic device for time-lapse imaging. To introduce yeast into the device, the yeast were placed in a syringe (BD with Luer-Lok Tip) capped with a flat needle tip that was inserted into the plastic tubing of the microfluidic inlet channels. Before loading cells, the microfluidic device was primed by sterilizing it in UV light for ~15 min or by flowing ethanol, DI water, and warmed culture medium.

The microfluidic device with yeast was placed on the stage of an upright microscope (Nikon Eclipse LV100) with camera (Hamamatsu ORCA-Flash4.0 V2 C11440-22CU) and supporting software (NIS-Elements Br Microscope Imaging Software). Time-lapse images were captured every 1 min overnight (7-8 hr).

2.1.3. Yeast size distribution for time-lapse experiment

Figure 5 shows sequences of images taken at selected time points during the yeast culture. The times are measured from the beginning of the time-lapse experiment, that is, 0 min corresponds to the beginning of the time-lapse. The images show how the exponential increase in number of yeast leads to the offspring of the original cells quickly filling all spaces around the mothers.

23
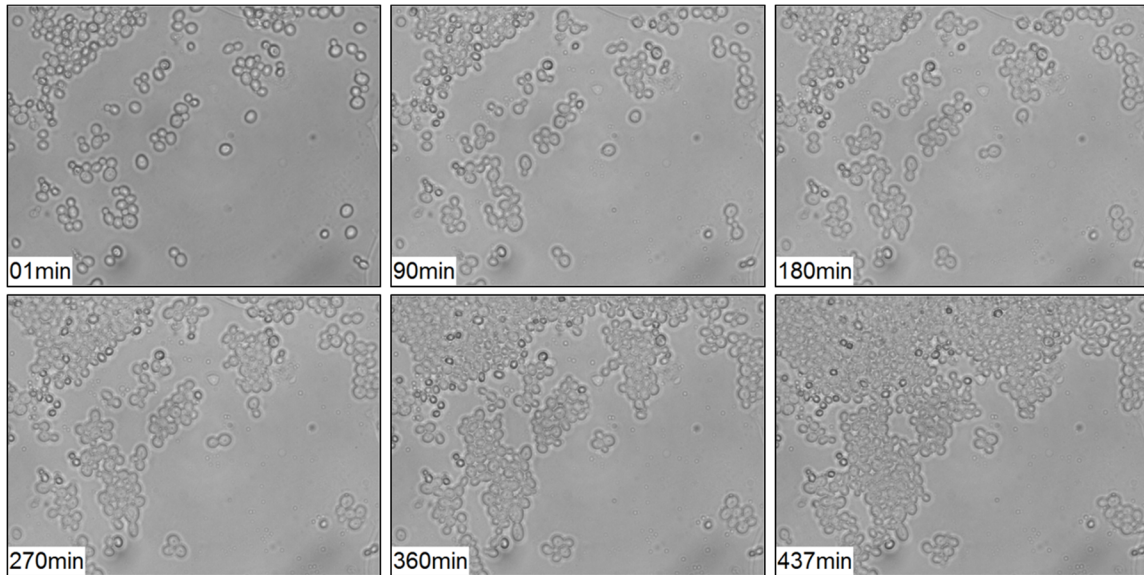
Figure 5. Time-lapse culture of wild-type yeast in yeast extract peptone dextrose (YPD) showing the exponential proliferation of yeast and daughters quickly overcrowding the mothers. The times at lower left in the images are measured from the beginning of the time-lapse experiment.

Figure 6 magnifies 2 mothers in the sequence and highlights how offspring can overcrowd the mothers, compete for nutrients, and excrete waste, all of which influence the normal aging of mothers. The temperature of the experiment was relatively low (~23°C), which explains the slow cell growth rate.
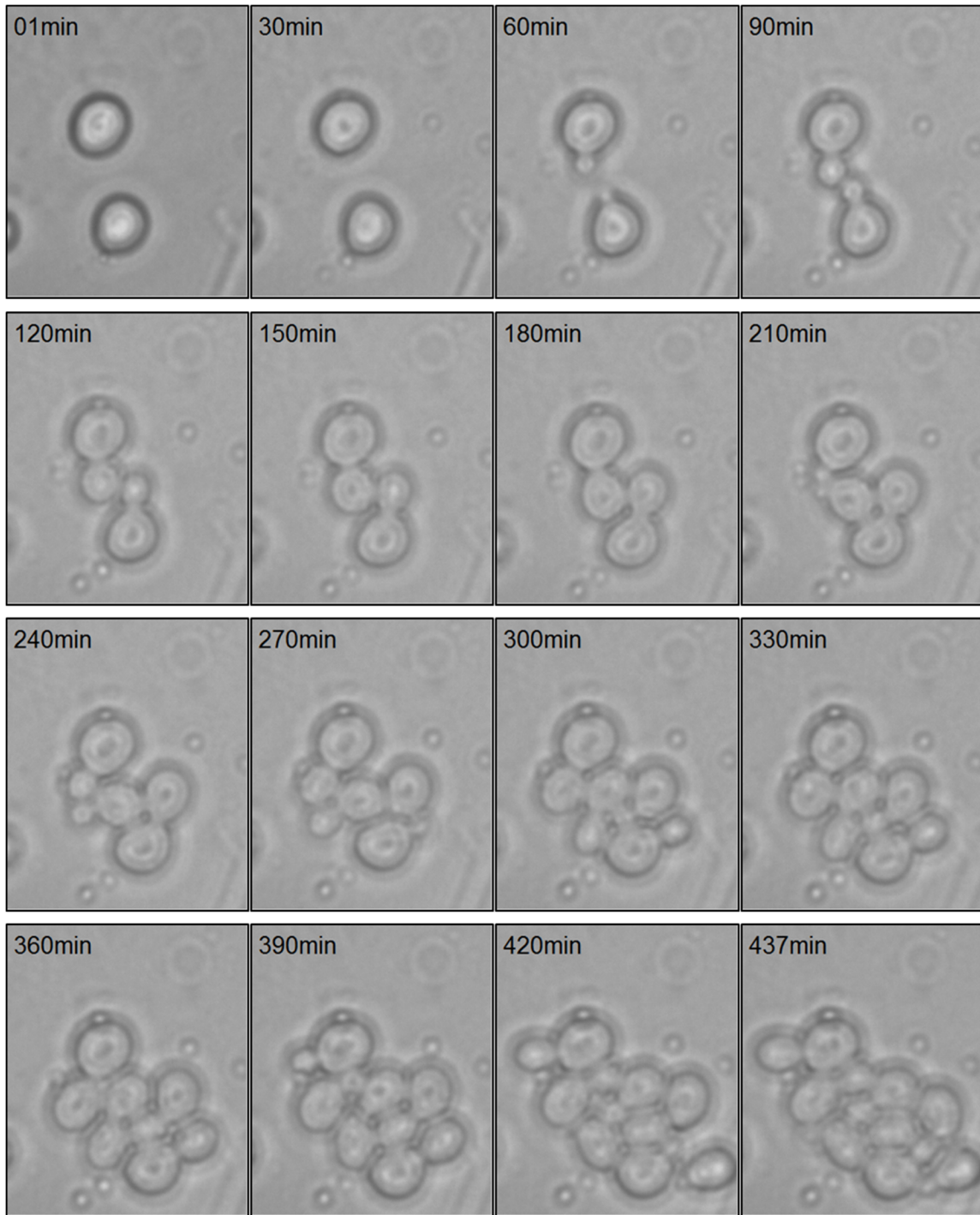
Figure 6. Magnified view of two mother yeast in the time-lapse culture. The offspring of the mothers compete for nutrients and excrete waste, both of which can influence the normal aging of the mothers.

As a first step in quantifying yeast sizes, we processed images from the time-lapse using MATLAB (MathWorks). Because individual cells were not easy differentiate using image thresholding and similar image processing techniques, we fitted circles to the yeast in images by using a built-in MATLAB function from the Image Processing Toolbox. We further discuss the circle-fit procedure for a similar yeast size measurement in § 2.1.24. Figure 7 shows how the yeast sizes trend over time. As the yeast proliferate exponentially, the number of cells with diameters in the 2-3 μm range greatly increased because more and more daughters were born.

To confirm the sizes obtained by fitting yeast to circles, we measured the size distribution of a wild-type yeast population using a Beckman Coulter Z2 Particle Count and Size Analyzer with Z2 AccuComp Software. Before a sample's size distribution was measured, the sample (~20-50 μL) was mildly sonicated to break up cell clumps and then diluted in 10 mL of buffer (Isoton II Diluent). The analyzer needs only 5,000 – 10,000 cells for a single measurement but can accommodate up to ~400,000. The software automatically generates measurements including mean birth size, and the size data for debris smaller and larger than yeast was removed before calculating these results. The yeast size data, given in volume, was converted to diameter by assuming yeast are approximately spherical.
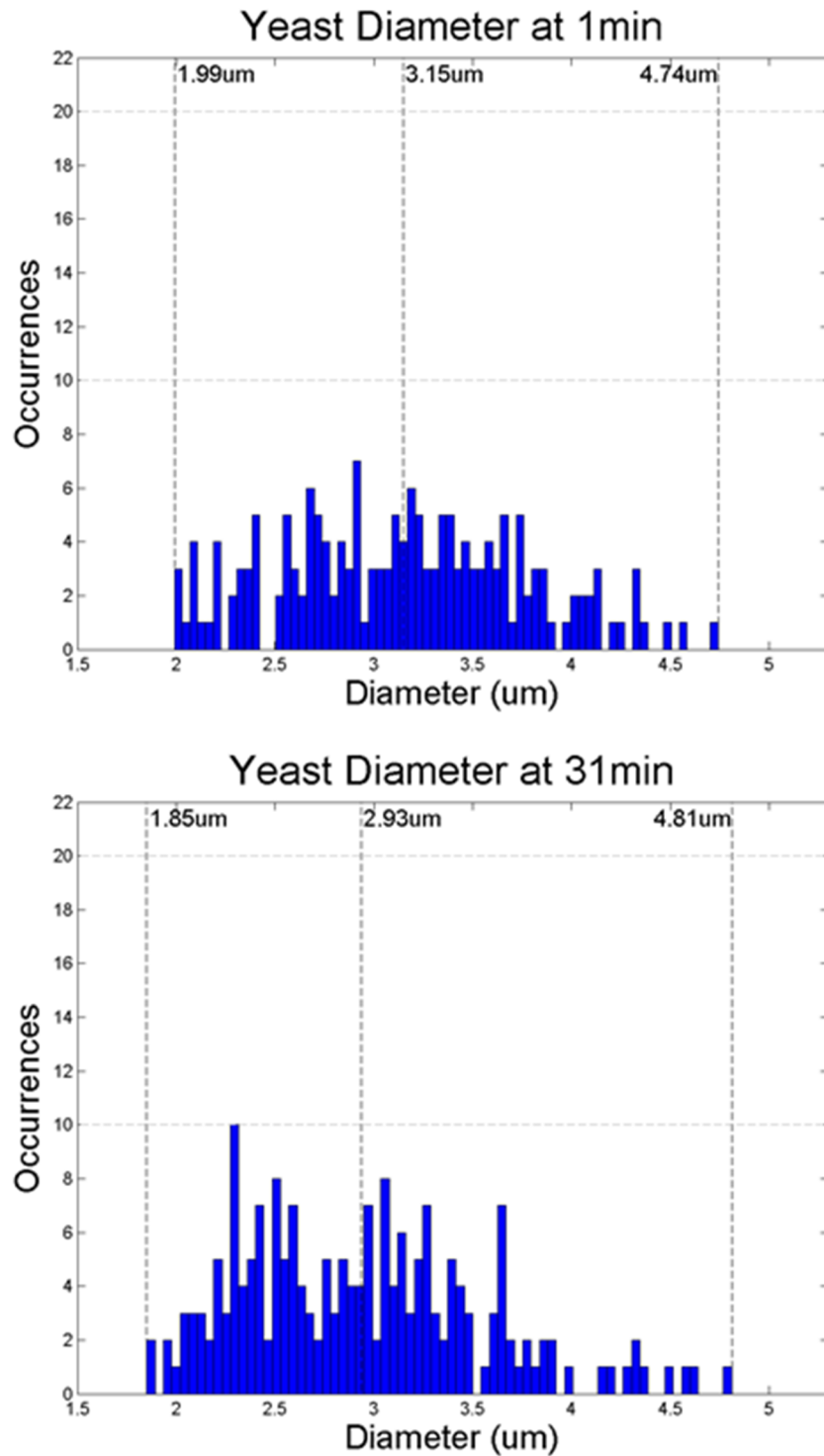
Figure 7. Size distributions of the yeast from the time-lapse experiment in Fig. 5. Yeast cells were fit to circles, and the circle diameters are plotted here. Although the size distribution evolves over time in a way that is consistent with exponential proliferation of cells, the diameters measured through image processing are smaller than the actual yeast sizes.
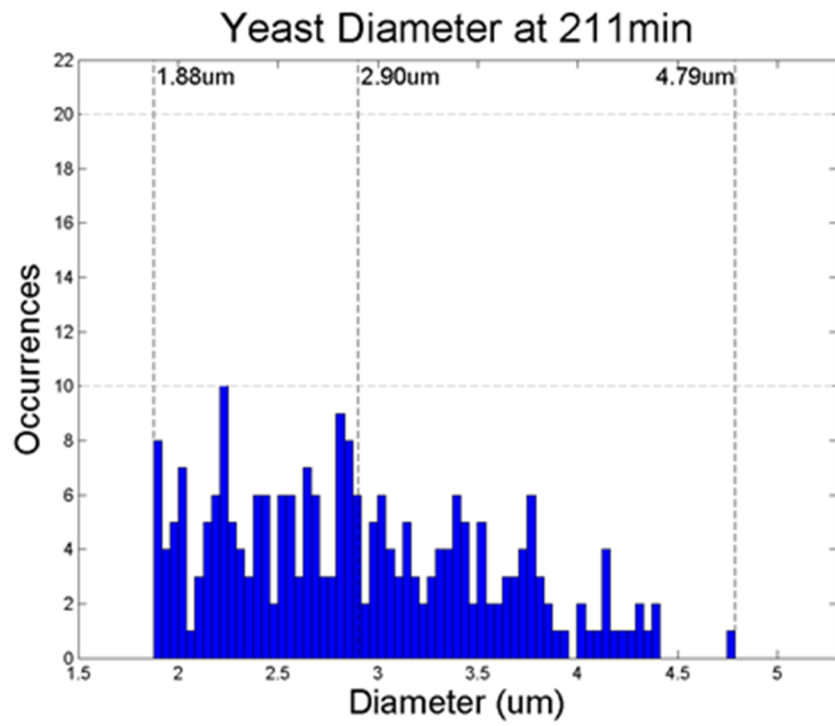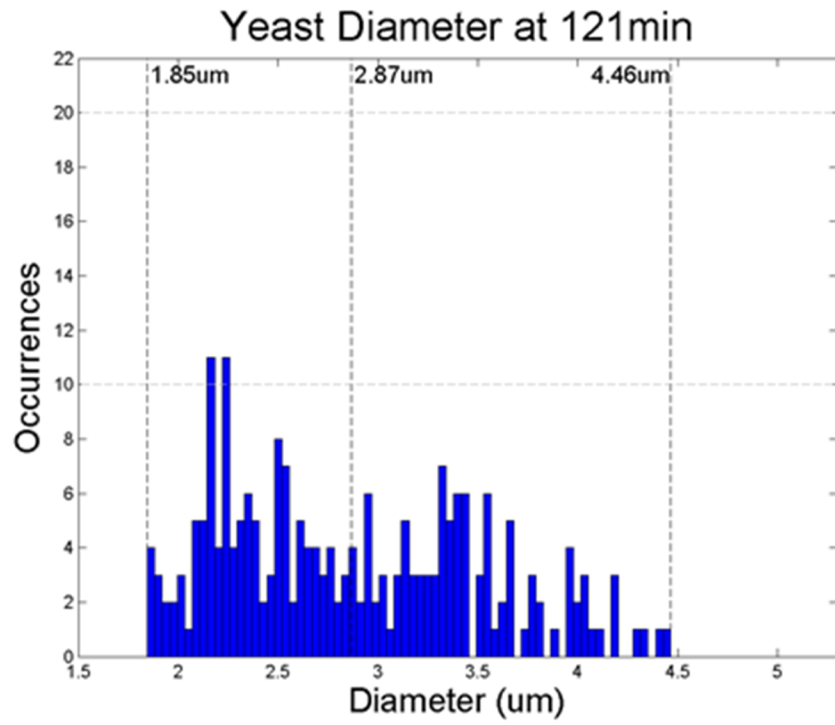
Figure 7. (continued)
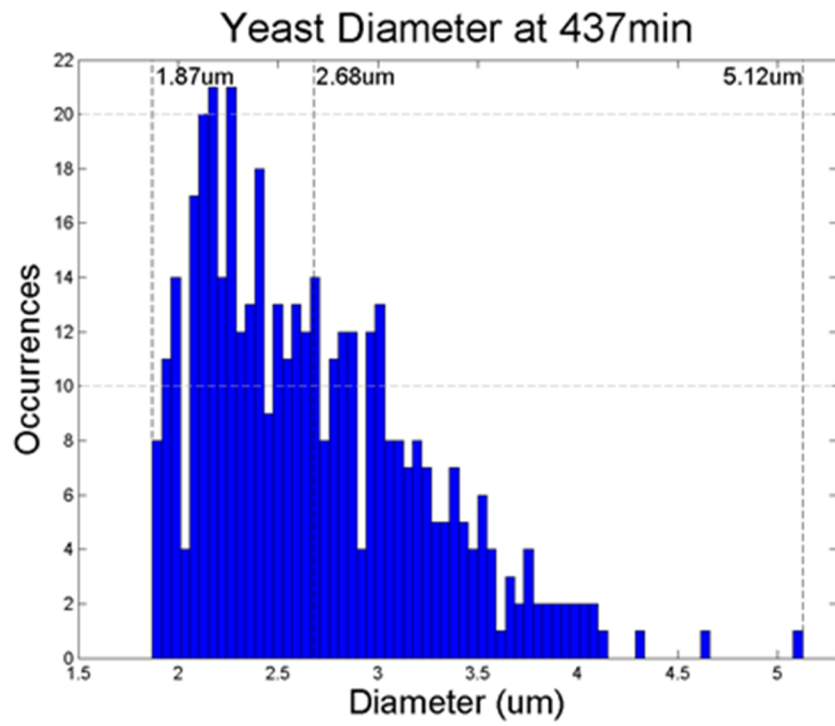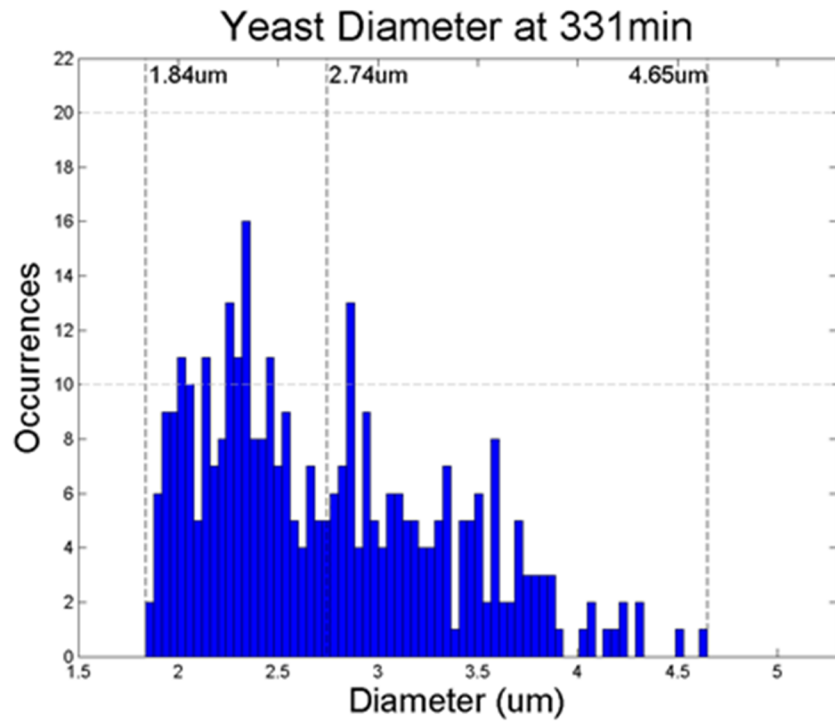
Figure 7. (continued)

Figure 8 plots the size distribution for ~400,000 wild-type yeast. The overall mean diameter was 4.61 µm, and the mean birth diameter (calculated as in ref. 52) is 3.45 µm. For reference, the upper 10% of cells sorted by size all have diameters >5.68 µm. Because the number of yeast increased exponentially as shown in the inset table at right in Fig. 8, for the population shown in the size distribution, a very small percentage of cells (0.005%) is >15 generations old.
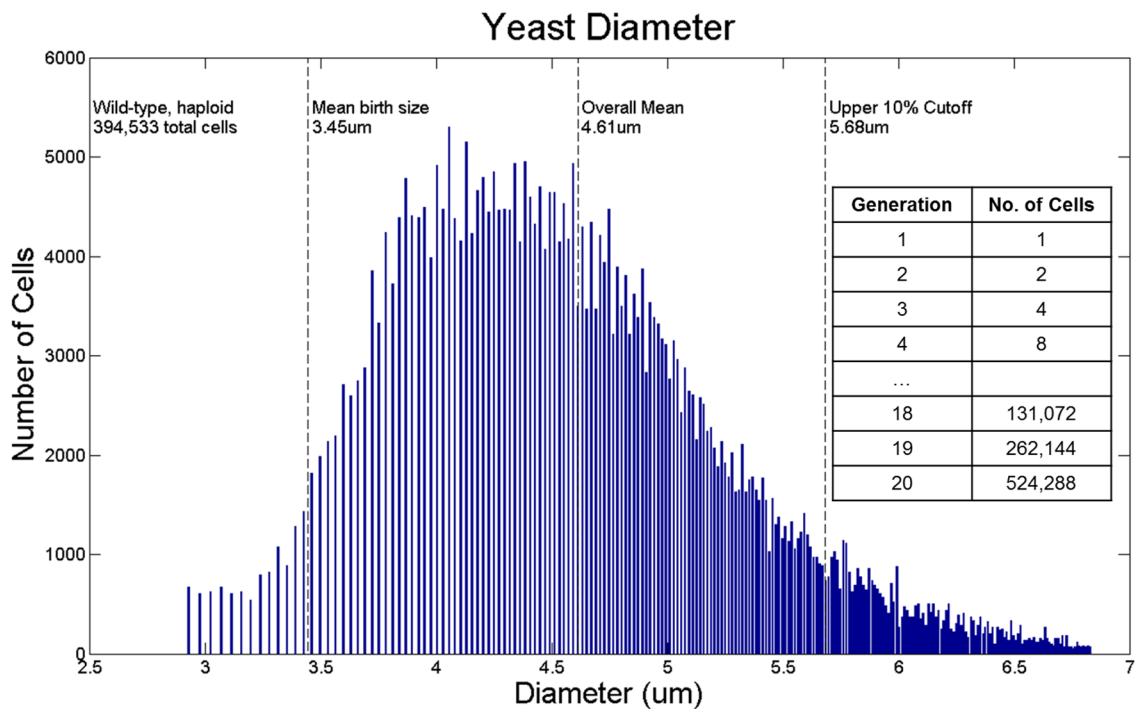
Figure 8. Cell Coulter Counter measurement of wild-type yeast diameters. The mean birth size of 3.45 µm was calculated by the Coulter Counter, and 10% of the cells had diameters >5.68 µm. The inset table at right lists the number of yeast at each generation starting with a single cell, illustrating that a very small percentage of the cells in this measurement (0.005%) is >15 generations old.

2.1.4. Image-processing and Coulter Counter produced different size measurements

The size data obtained by processing images in MATLAB (Fig. 7) is similar but varies in some ways from the histogram produced by the Beckman Coulter Counter (Fig. 8). The overall trend

in the evolution of yeast sizes throughout the time-lapse experiment agreed with expectations: as time passed, the proportion of smaller cells grew and the overall mean diameter of the population decreased. This behavior resulted from the exponential increase in cell numbers and indicates a healthy culture. The values of diameters extracted from MATLAB, however, are smaller than those obtained from the commercial particle size counter, which agree very well with expectations for a healthy wild-type, haploid yeast culture; therefore, our image processing technique must have some error. The discrepancies are likely due to (i) imaging cells out of focus and (ii) fitting circles to oval-shaped yeast. Imaging the cells out of focus blurs the cell boundaries, which must be clear and well-defined for MATLAB to detect the boundary accurately. Fitting a circle to a non-circular shape obviously produces differences between the observed and actual cell sizes. Another cause of this size data discrepancy results from how we converted yeast size data reported by the commercial counter. The Beckman Coulter Counter measured yeast cell volume, and we converted volume to diameter for our analyses by approximating the yeast cells as spheres. As shown in Figs. 5 and 6, yeast are not perfectly spherical, and this approximation may have produced differences between data obtained in MATLAB and in the cell counter. For all future analyses that involved calculating cell size in MATLAB, we relied on difference measurements rather than absolute values. For instance, we calculated percent size difference between mothers and daughters when determining the required resolution of our separation method using image-processing.

2.1.5. Yeast mothers and daughters differ in size by ~20%

To quantify the size differences between mother and daughter yeast, we used multiple MATLAB image-processing approaches on (i) in-house yeast cultures and (ii) experimental images published by other researchers. First, we developed a MATLAB tool that allows users to trace

the yeast size manually and then calculates two-dimensional percent difference using the areas of the traced regions. This software was useful for obtaining more precise size measurements that were not skewed due to poor image quality or little contrast between cells and their surrounding environments. Using images from the in-house stationary yeast culture, we measured the size differences at select time points (Fig. 9): shortly before the mother outlined in blue started to bud again after the daughter outlined in red had finished budding (left of Fig. 9), and at the end of the time-lapse experiment when cell sizes were the largest available (right of Fig. 9). This analysis showed that the mother yeast is at least 20% larger in area than the 2 generations of daughters that budded at the selected time points.
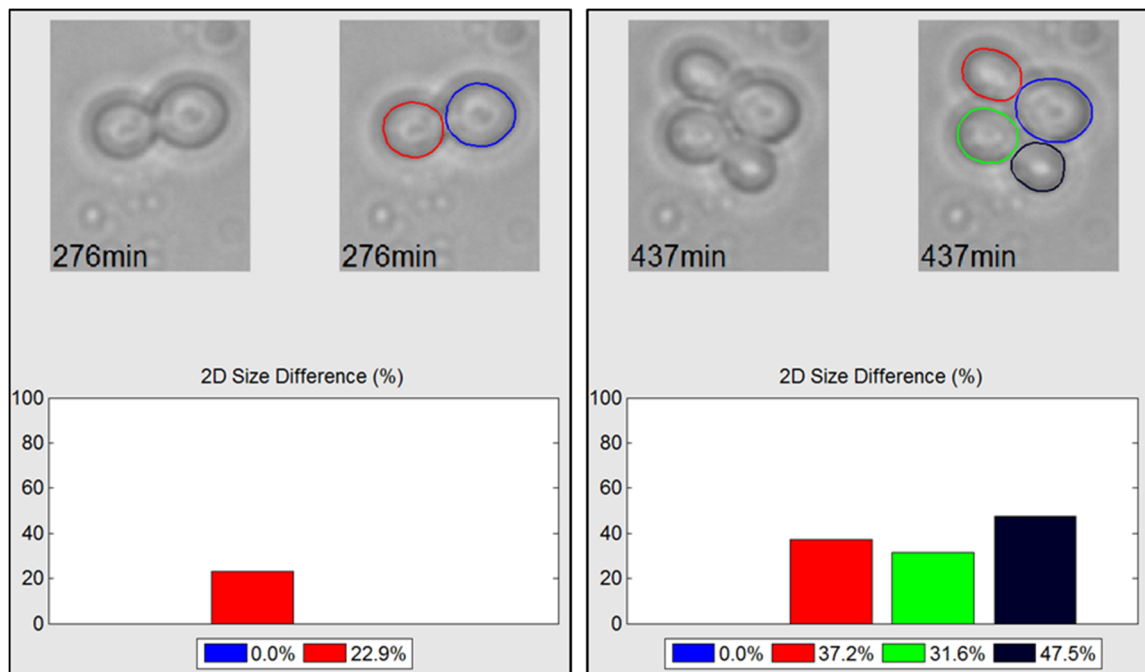
Figure 9. Mother and daughter yeast in the time-lapse experiment differ in two-dimensional size by >20% at the selected time points.
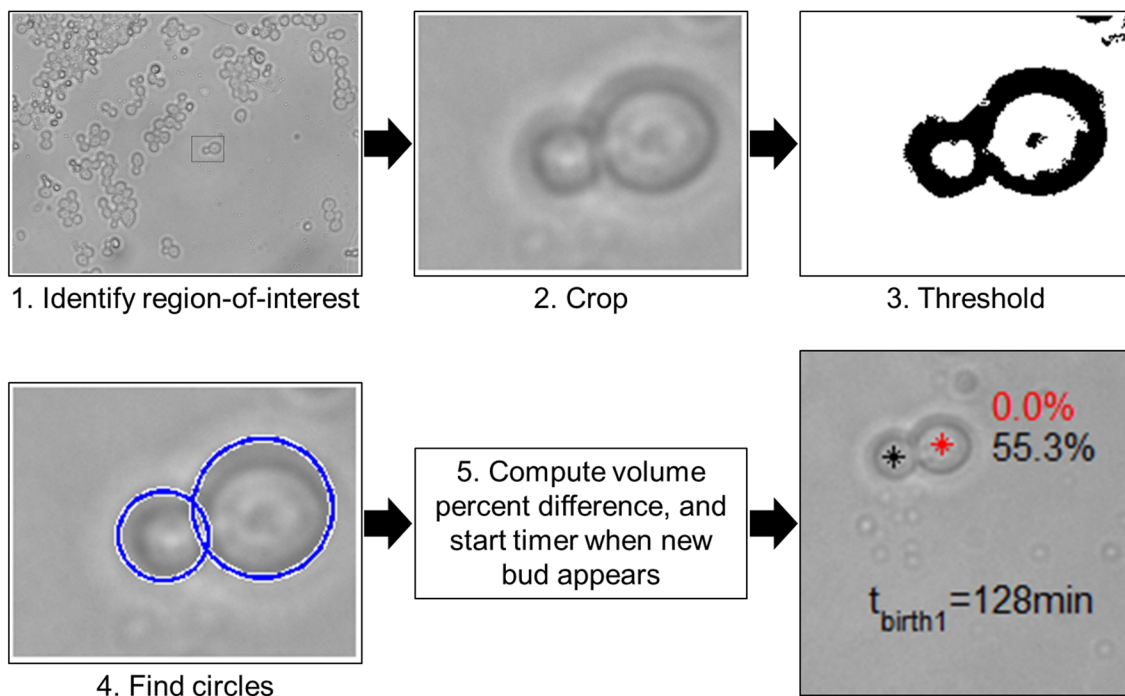
Figure 10. Procedure for calculating volume percent difference among yeast in the time-lapse experiment. A region-of-interest (step 1) was cropped (step 2) and black/white thresholded (step 3). Circles were fit to the yeast in the region-of-interest (step 4), and the volume percent different and bud time were calculated (step 5) and displayed on the original image. Size difference is color coded and measured relative to the cell with 0% difference. For example, the yeast identified with a black asterisk at bottom right has 55.3% volume difference compared to the yeast with red asterisk.

Using all time-lapse images of this particular yeast cluster, we computed the cell volume percent differences using the following procedure illustrated in Fig. 10. First, specific regions-of-interest were chosen and cropped from the overall image. The cropped image was gray-thresholded so that the cells could be fit to a circle using a built-in MATLAB function from the Image Processing Toolbox. Several input parameters of the function can be adjusted depending on the image (e.g. size of circles to fit, edge threshold, circle metric, etc.). After cells were fit to circles, we computed and displayed volume percent difference, which is measured relative to the cell showing 0% difference. Volume difference was calculated here because several of the size-

based separation strategies including acoustic and dielectrophoresis manipulate particles using forces that depend on particle volume.

Example images from this procedure are displayed in Fig. 11. The percent difference text in the images is matched to the cells by color. For example, at bottom right in Fig. 11, the cell with a black star plotted on top has ~220% volume difference compared to the cell identified by a red star. To gauge the division time, we manually searched through all time-lapse images captured in 1 min intervals to determine when the bud was first noticeable. We then programmed the bud's birth timer to start counting upward starting at that image and continuing to the end of the sequence. After processing the time-lapse series in this way, we found that volume percent differences between these mother and daughter yeast were >15%. At the time when the youngest-generation cells start budding, the oldest daughter (the first bud in the time-lapse) is 20-40% smaller in volume compared to the original mother.
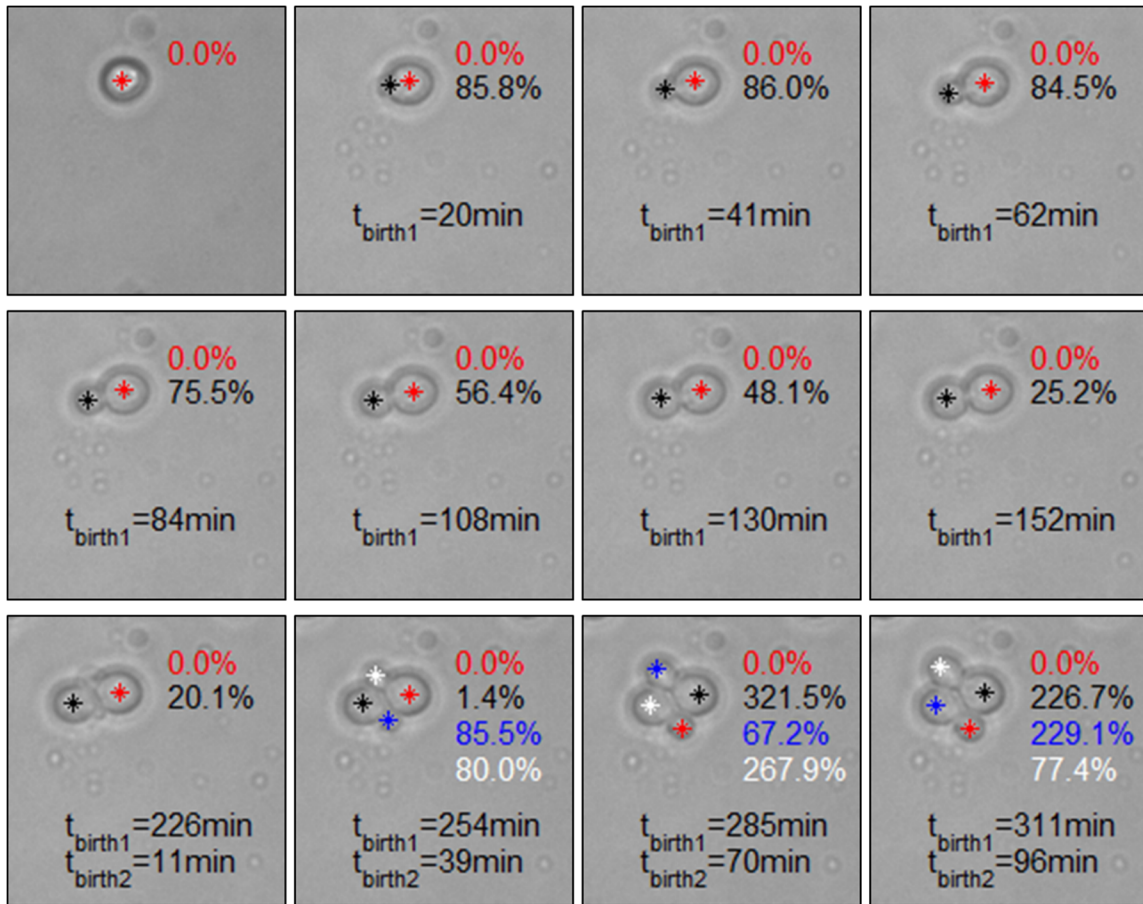
Figure 11. Volume percent difference and bud times were calculated for the yeast in each frame of the time-lapse culture following the procedure in Fig. 10. Volume percent differences are color coded and calculated relative to the cell identified with 0%. For example, at top right, the smaller cell with black asterisk has 84.5% volume difference compared to the cell with red asterisk. Up until the original mother starts budding a second time, its volume differs from its first bud by >20%.

These size analyses provide an estimate of how fine the size-based resolution must be for the separation method we select for our aged yeast generator. We found similar size differences for other mother-daughter yeast groups in this and other stationary, in-house time-lapse cultures. In general, yeast mothers are 20-40% larger in size compared to their daughters at the point in time when the daughter has finished budding. To verify this estimate, we processed yeast time-lapse images from cultures performed by other researchers who employed novel

microfluidic systems. Xie *et al.* utilized a device in which mother yeast are tagged with a label and attached to the fluidic channel bottom.[19] The device in Crane *et al.* hydrodynamically trapped mothers using two angled pillars,[9] and the system in Lee *et al.* physically trapped mothers with PDMS micropads.[53] In all 3 systems, fluid flow carried away daughters throughout the mother's lifespan, and the groups captured time-lapse images throughout the process. An important characteristic of the experimental results of these selected publications is that the daughter yeast are dissected from the mother after they have finished budding. By analyzing the images immediately before the daughter is removed from the field-of-view, we can best estimate the mother-daughter size difference that is most relevant for our system. That is, we can approximate the required resolution for our system by studying size differences at the moment in time when the daughters completely separate from their mothers. Figure 12 shows the mother-daughter size differences for wild-type yeast at 4 instances immediately prior to the daughter leaving the field-of view. The daughters in this culture were typically 45-55% smaller in area than their mothers. In similar analyses, we calculated area differences of 15-30% for the yeast with S288C genetic background in Crane *et al.* (Fig. 13). Finally, by analyzing the time-lapse of the S288C genetic background yeast in Lee *et al.*, we found daughter volume differed from mother volume by 30-50% at the beginning of the mother lifespan (during the first few cell divisions) and by 60-80% during the middle of the mother's lifespan. Daughter sizes were comparable to the mother size during the last few cell divisions before the mother died. These size differences obtained from analyzing experimental data from published journal articles are similar to our findings for the in-house stationary cultures.
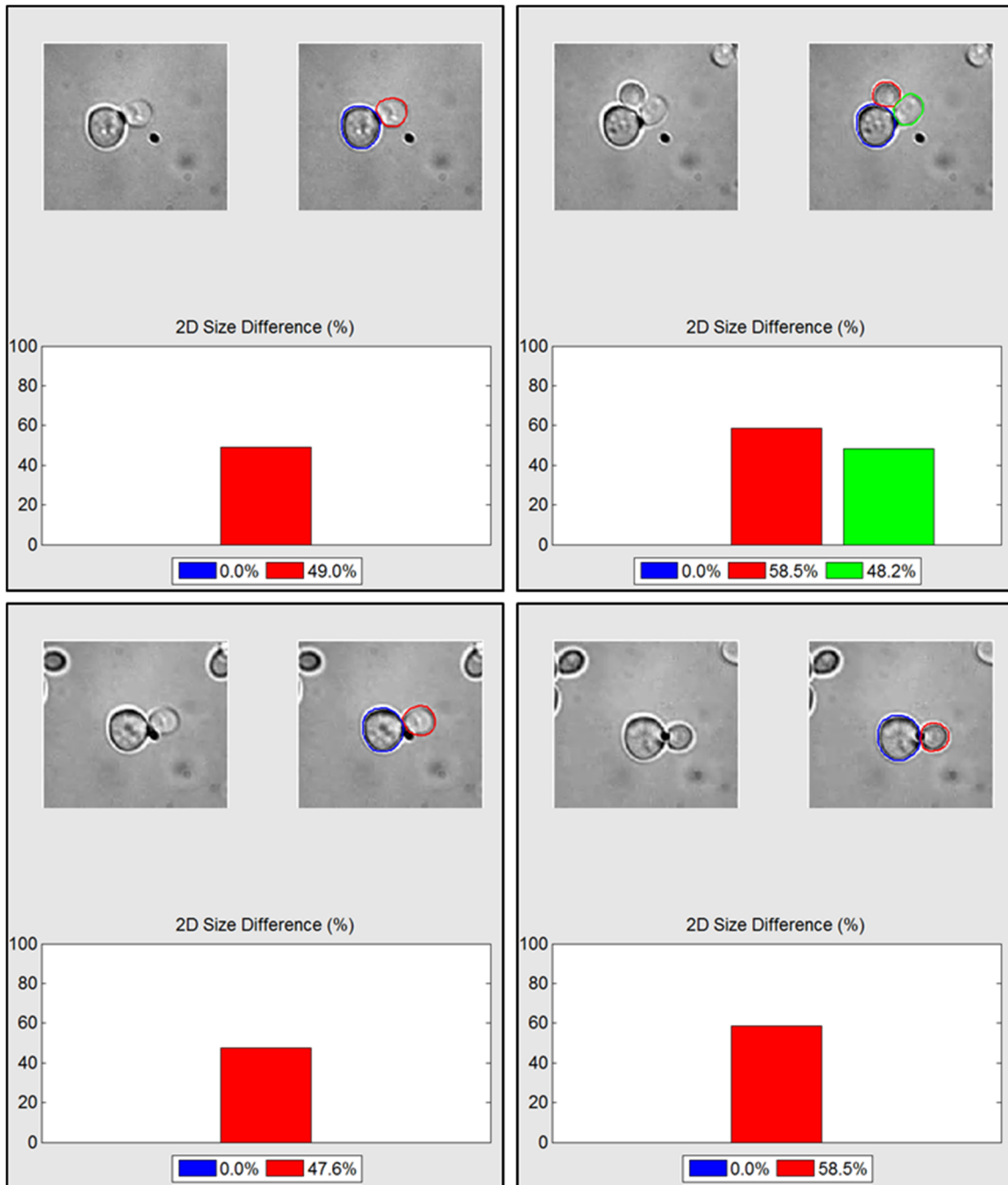
Figure 12. In an experiment from ref. 19, a mother yeast was immobilized to a microfluidic channel wall while fluid flow removed its daughters. Yeast sizes were analyzed in four frames from a time-lapse video captured during the experiment. Each frame shows the cells immediately before a daughter was removed from the field-of-view. At these instances when the mother/daughter yeast exited the cell cycle and the daughter was removed, the daughter sizes were 45-55% smaller than the mother size.
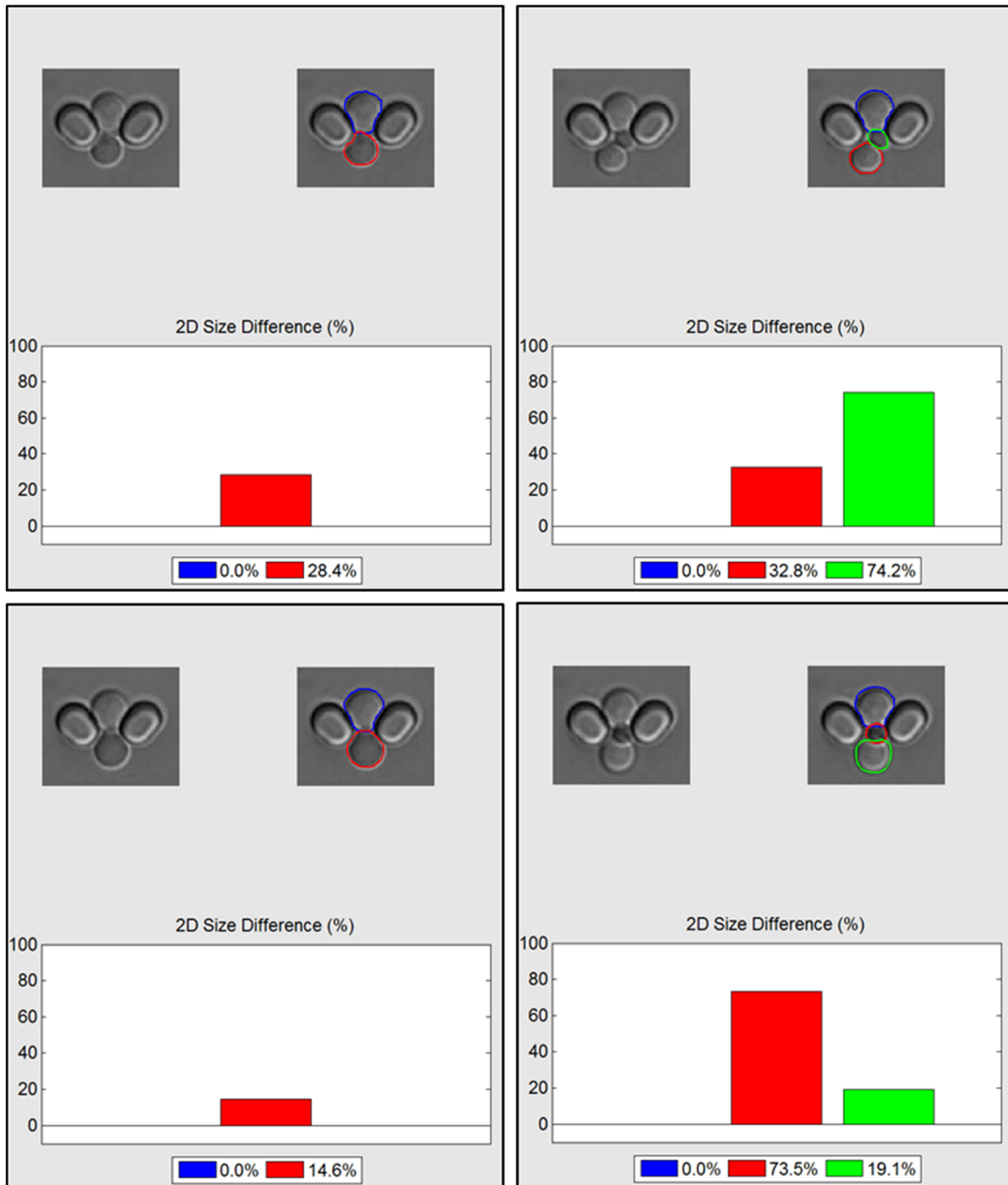
Figure 13. In an experiment from ref. 9, a mother yeast was trapped by V-shaped PDMS pillars in a microfluidic channel wall while fluid flow removed its daughters. Yeast sizes were analyzed in four frames from a time-lapse video captured during the experiment. Each frame shows the cells immediately before a daughter was removed from the field-of-view. At these instances when the mother/daughter yeast exited the cell cycle and the daughter was removed, the daughter sizes were 15-30% smaller than the mother size.

In summary, the mother-daughter yeast size differences range typically ~20% for cells cultured in-house and in experiments performed by other researchers. This size difference suggests daughters can indeed be removed from mothers by leveraging the fact that mothers are larger than daughters at most points during the mothers' lifespans. By quantifying the size difference here we also define the required resolution of the size-based separation strategy chosen for our aged yeast generator, i.e., we must select a separation method that can separate sub-10 μm particles that differ in size by ~20%. For yeast with diameters in the 2-7 μm range, this percent difference translates to 0.5-1.5 μm resolution (the separation method must be able to separate yeast with diameters that differ by 0.5-1.5 μm). In addition to quantifying the separation resolution, these analyses motivate the need to remove daughter cells with a certain repetition frequency. The aged yeast generator must periodically remove daughters with relatively high frequency so that daughters are not given enough time to grow larger than the size-threshold such that they stay with the mothers instead of being removed from the device with small cells. We further discuss the need for repeated separation in § 2.2.

2.1.6. Available size-based separation strategies

For the aged yeast generator to produce old mothers, it must remove daughters having ~20% size differences compared to mothers, which translates to 0.5-1.5 μm resolution for yeast with 2-7 μm diameters. Particle separation methods reported in the literature fall into 2 categories: active and passive. Figure 14 shows the categorization of separation strategies most commonly used in the field of micro-electro-mechanical systems (MEMS). Excellent reviews of these and other separation and sorting techniques can be found elsewhere.[54-57]

39
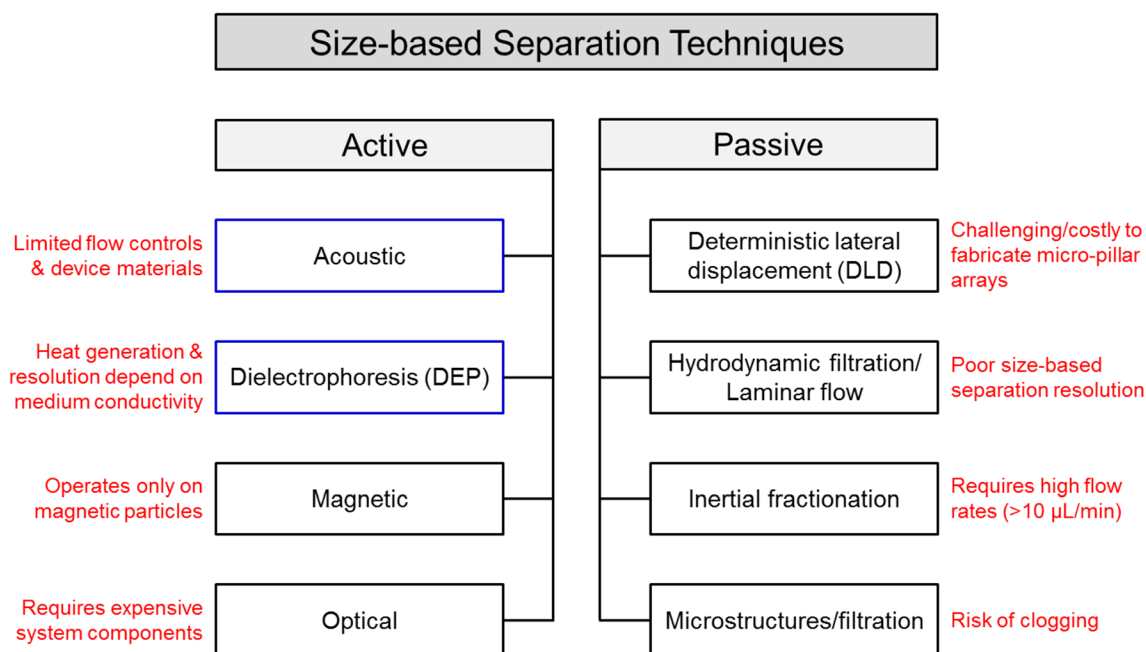
Figure 14. Common particle sorting techniques capable of separation by size. Methods fall under two broader categories: active and passive. Key disadvantages of each technique are added in red.

In the figure, key disadvantages of each technique are added in red text. We can immediately dismiss some of the strategies as candidates for the aged yeast generator in this work. Starting with the active methods, magnetic sorting can differentiate particles having magnetic properties (e.g. paramagnetic), so this technique cannot be applied to un-labeled yeast. Optical sorting can be relatively low-throughput because typical systems can process only 1 particle at a time. Optical setups can also be expensive and challenging to build especially for lasers and detectors sensing at the microscale. Acoustic and dielectrophoresis (DEP) methods are discussed in greater detail below because we decided to investigate these techniques in this work. For the passive techniques, inertial fractionation requires high flow rates (>10 µL/min) and thus needs special fabrication processes and materials to support such flow rates. Inertial microfluidics are also relatively new compared to many of the other methods, so inertial fractionation is somewhat less developed. Deterministic lateral displacement (DLD) has great

40

size-based separation resolution (sub-1 μm) but requires more expensive fabrication processes and materials to create microstructures on the same size-scale as biological cells (<10 μm). DLD also risks clogging due to cell clumps which is also a significant disadvantage for many of the filtration techniques. Finally, pinched-flow fractionation and hydrodynamic filtration do not have separation resolution suitable for separating mother-daughter yeast (e.g. see refs. 58, 59, 60, 61).

Of the available size-based separation methods in Fig. 14, dielectrophoresis (DEP) and acoustic showed great promise for separating mother-daughter yeast in our aged yeast generator. Microfluidic devices involving DEP can be fabricated in PDMS thereby leveraging the flexibility and cost-effectiveness of PDMS microfluidics. Because of this amenability to using PDMS, more flow controls including microvalves that increase functionality can be added to DEP systems. DEP is a well-developed technology with much literature to support its development. High flow rates cannot be used with DEP, however, because the DEP force can be relatively weak. Low flow rates can lead to low throughput which might hinder our ability to generate large numbers of aged yeast. Also, the choice of medium used in DEP microfluidics greatly influences how much electromagnetic heating is generated by the DEP electrodes (see § 2.1.12). Even moderate heat levels can be harmful to biological cells, so the particular medium used and/or the passivation applied over the DEP electrodes must accommodate for potential heat generation. Because the medium and electrode passivation choices influence the electric-field magnitude in a fluidic microchannel near the DEP electrodes, these choices also impact the resulting size-based separation resolution.

Acoustic separation is gentle, label-free, and efficient. As discussed in detail in § 2.1.20, acoustic forces can separate particles by size, density, and compressibility; therefore, when applied to separating mother-daughter yeast, acoustic may be the only method capable of separating mother-daughter yeast when they have similar sizes (e.g. during the last few divisions

before the mother dies) by utilizing differences in density or compressibility (e.g. mother yeast have more chitin deposits from bud scaring than do their daughters, which may create compressibility and/or density differences). Because acoustic separation devices must be fabricated out of certain materials that can accommodate acoustic waves, a limited variety of materials can be used for acoustic devices. Glass and silicon are typical acoustic device materials, and both require more complex and expensive fabrication techniques compared to polymers like PDMS. These rigid materials also limit the use of flow controls. Acoustic forces are not affected by pH, salt concentration, and other medium properties, so the separation performance of acoustic devices does not depend on medium choice. In other words, reagents and cell types (e.g. different strains of yeast) can change without drastically altering the separation performance. Also, acoustic forces acting perpendicular to the flow of biological cells impose minimal stress on the cells; therefore, acoustophoresis is useful in experiments involving delicate cells such as aged yeast.[14]

Although the disadvantages of the separation techniques guided our decision to investigate acoustophoresis and DEP for our yeast application, one of the greatest discriminators was how well the reported resolutions for the various techniques matched our goal of separating 2-7 μm diameter yeast with 0.5-1.5 μm resolution. Table 2 shows a small portion of the size-based separation publications we consulted for our decision. Each journal paper shown in the table was selected primarily because its separation was performed on a sample having size similar to that of yeast. In general, the purity/efficiency column should not be compared among the different publications because the value was often calculated in a way that is specific to the publication; not all references calculated purity/efficiency in the same way. Taken together with the sample sizes, however, the purity/efficiency indicates how successful the particular method was at separating the different-sized samples.

Table 2. Demonstrated performances of the size-based separation strategies

Method	Sample	Purity/Efficiency	Reference
Acoustic	PS beads (2, 5, 8, 10 µm), RBCs, platelets, leukocytes	62-94%	62
Acoustic	PS beads (0.71, 3.0, 3.2, 3.4, 4.2, 4.5, 5.0 µm)	Not reported	63
Acoustic	PS beads (0.5, 1.0, 2.0, 3.1, 5.0 µm), yeast (6-8 µm) from MS2 bacteriophage (30 nm)	80-90%	64
Dielectrophoresis	RBCs and platelets (5-6 µm), lymphocytes (7-8 µm), granulocytes (8-9 µm), monocytes (9-10 µm)	Not reported	65
Dielectrophoresis	PS beads (1, 5 µm), yeast cells separated from 3 µm particles	>90%	66
Dielectrophoresis	Latex spheres (1, 2 µm)	100%	67
Deterministic lateral displacement	PS beads (0.4, 0.6, 0.7, 0.8, 0.9, 1.03 µm), bacterial chromosomes	Not reported	68
Centrifugal elutriation	PS beads (1, 3, 5 µm)	Not reported	69
Gravity	PS beads (3, 5, 20 µm), <6 µm perfluorocarbon liquid droplets from droplet emulsions	99.97%	70
Inertial	PS beads (1.0, 2.1, 3.2 µm)	87-93%	71
Inertial	PS beads (1, 5 µm)	>99%	72
Laminar flow	PS beads (0.5, 0.86 µm)	100%	73
Magnetic	Super-paramagnetic (1.6 µm), non-magnetic particles (2 µm)	92%	74
Mechanical filters	Human metastatic cells in whole blood	90%	75
Optical	Silica spheres (2.3, 3.0, 5.17, 6.84 µm)	100%	76

2.1.7. Dielectrophoresis and acoustophoresis chosen as candidates for aged yeast generator

Of the separation strategies in the table, most might be capable of separating mother-daughter yeast. In particular, both acoustic and DEP have proven successful at separating particles having sizes similar to yeast. Few researchers are able to quantify the best separation resolution capable with their system because of the difficulties associated with measuring down to the smallest size difference. Although the reported systems do not provide resolution estimates against which we could compare our value of 20% size difference or 0.5-1.5 µm resolution, the successes of the reported systems considering the sample of interest indicate that DEP and acoustophoresis are

good candidates for our application. Additionally, the disadvantages associated with DEP and acoustic techniques are easier to overcome compared to other methods. For example, being confined to lower flow rates in DEP or fewer fabrication materials in acoustophoresis can be accommodated much more easily than the higher costs in optical or DLD. Finally, DEP devices are relatively easy to fabricate and test with yeast, and acoustic systems have few operational parameters (microfluidic flow rates and applied voltage driving a piezoelectric transducer) that must be defined for separating yeast. These advantages simplify the tasks of investigating DEP and acoustic separation for the aged yeast generator.

We now discuss the theory, device design, and experimental results for our experiments evaluating DEP for separating mother-daughter yeast. After showing why DEP will not work for our application, we present results with acoustic separation of yeast.

2.1.8. Theory for size-based separation in dielectrophoresis (DEP)

Particles or cells suspended in a liquid medium within a microchannel near a spatially varying electric field experience a dielectrophoretic force given by[77]

$$F_{DEP} = \frac{3}{2} V_c \varepsilon_m \, Re[f_{CM}(\omega)] \, \nabla E_{rms}^2$$

$$f_{CM}(\omega) = \frac{\varepsilon_c^* - \varepsilon_m^*}{\varepsilon_c^* + 2\varepsilon_m^*}$$

$$\varepsilon^* = \varepsilon - \frac{i\sigma}{\omega}$$

where V_c is the particle/cell volume, ε_m is relative permittivity of medium in which particle is suspended, $Re[f_{CM}(\omega)]$ is the real part of the Clausius-Mossotti (CM) factor, E_{rms} is the root-mean-square of the electric field, ε^* is the complex permittivity of the cell (ε_c^*) or medium (ε_m^*), $i = \sqrt{-1}$, σ is electric conductivity, and ω is the electric field angular frequency. The two most

important equation variables relevant to this work are $Re[f_{CM}(\omega)]$ and V_c. The real part of the CM factor determines the direction of the DEP force on the suspended cell. Figure 15A models 2 electrodes (thin rectangles at the top of the larger block) connected to a liquid medium (the larger block). The horizontal and vertical rainbow-colored cut-planes in the model represent the electric field magnitude resulting from a potential applied to one of the electrodes while the other is grounded. Red and blue colors in the planes respectively signify high and low electric-field magnitudes.

A

$$F_{DEP} = \frac{3}{2}V_c\varepsilon_m\, Re[f_{CM}(\omega)]\, \nabla E_{rms}^2$$

$$f_{CM}(\omega) = \frac{\varepsilon_c^* - \varepsilon_m^*}{\varepsilon_c^* + 2\varepsilon_m^*}$$

$$\varepsilon^* = \varepsilon - \frac{i\sigma}{\omega}$$

$f_{CM} > 0, \text{pDEP} \qquad f_{CM} < 0, nDEP$

B

C
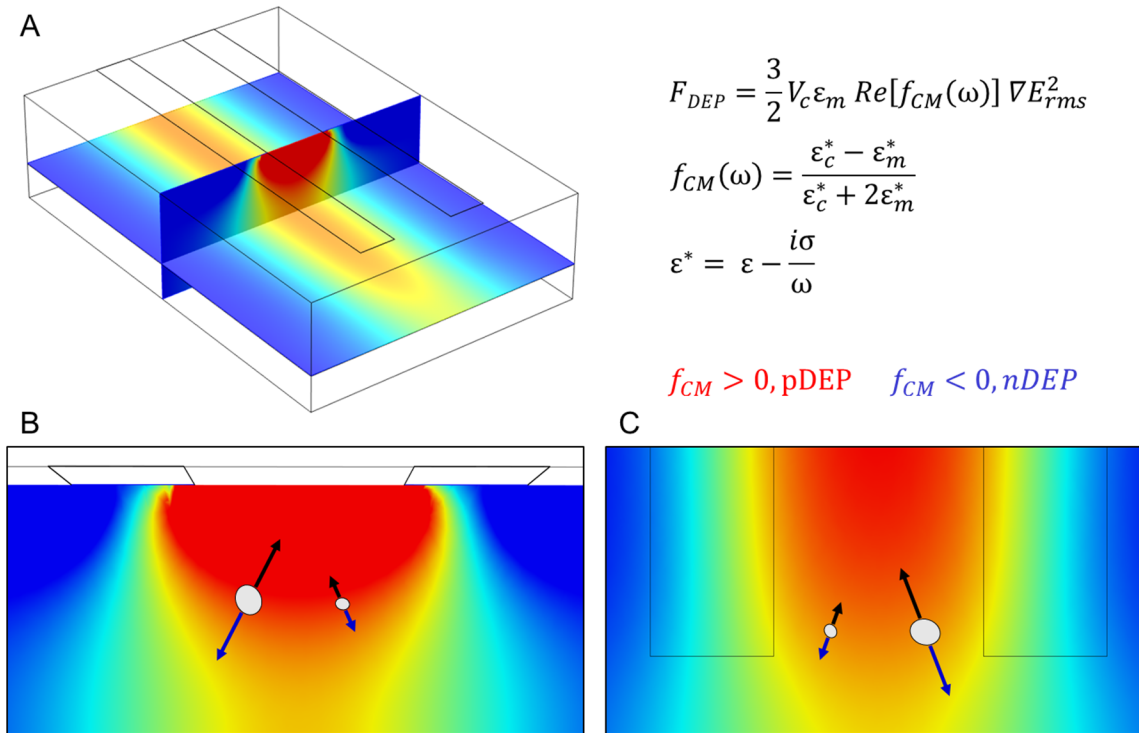
Figure 15. Dielectrophoresis (DEP) forces on a particle suspended in a fluid medium can attract (positive DEP) or repel (negative DEP) the particle depending on the sign of the Clausius-Mossotti (CM) factor (f_{CM}). A) A pair of electrodes are modeled along with the electric-field magnitude of a vertical and horizontal plane. B) The vertical cut-plane from (A) shown with particles that are attracted toward regions of higher electric-field when the CM factor is positive (black arrows) and repelled toward lower electric-field magnitudes when the CM factor is negative (blue arrows). C) The horizontal cut-plane from (A). The magnitude of the DEP force depends on particle volume; larger particles experience greater DEP forces compared to smaller particles.

Figure 15B and C show the vertical and horizontal cut-planes of the 3D model from A along with particles or cells and 2 sets of arrows per cell denoting the directions of positive and negative DEP forces. Positive DEP (pDEP) results whenever $Re[f_{CM}(\omega)]>0$, and cells are forced to regions of high electric-field as indicated by the black arrows in the figures. When $Re[f_{CM}(\omega)]<0$, cells are forced toward regions of low electric-field (negative DEP, nDEP) shown with the blue arrows. The DEP force direction relative to the electrodes is important when considering how DEP is used to separate mother-daughter yeast. Also depicted with the arrows originating from the cells in the images are the relative magnitudes of the DEP forces for each cell. Larger arrows are drawn from the larger cells because the DEP force is theoretically greater for larger cells ($F_{DEP} \propto V_c$). This dependence of F_{DEP} on V_c promises the ability to separate larger mother yeast from smaller daughters.

2.1.9. DEP is typically applied to separate live and dead yeast

Although a yeast population can theoretically be separated into different groups of varying sizes using DEP, researchers have conventionally applied DEP to separate live and dead yeast. Live and dead yeast have significantly different conductivities, and so the sign of the CM factor— which determines the direction of the DEP force—is different for live and dead cells as long as the electric-field frequency and medium conductivity are chosen appropriately. Li *et al.* plotted $Re[f_{CM}(\omega)]$ across frequency for live and dead yeast.[78] Up to ~200 kHz, both live and dead yeast have $f_{CM}<0$ in a NaCl medium with conductivity 140 μS/cm. For frequencies above 200 kHz, $f_{CM}>0$ for live yeast while $f_{CM}<0$ for dead yeast. Thus in this example if the electric-field frequency is >200 kHz and live/dead yeast are suspended in a medium with conductivity 140 μS/cm, the live yeast will be attracted toward regions of high electric-field while dead yeast are

repelled from high electric-fields. Several researchers have leveraged this difference in DEP force direction to separate live and dead yeast.[77-81]

2.1.10. Electrode design simulations motivate choosing planar over 3D electrodes

Because most published DEP work involving yeast aimed at separating cells by viability (live or dead) rather than by size, we first investigated the performances of planar and three-dimensional (3D) electrodes for generating the electric-field that manipulates yeast. We aimed to quantify the electric-field differences between planar and 3D electrodes and choose the best option for size-based separation of yeast. Figure 16 shows geometries for these options.
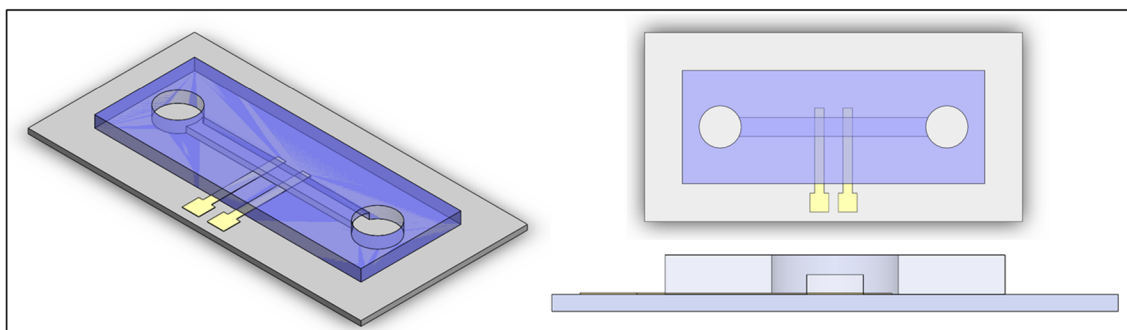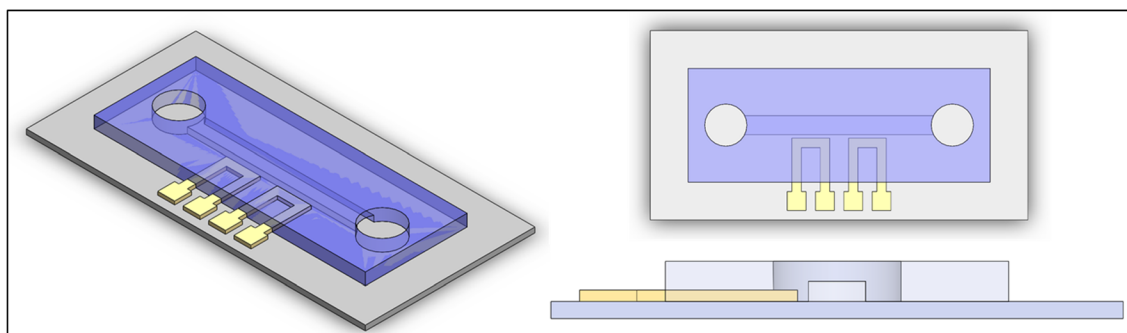
Figure 16. Models of planar and three-dimensional (3D) electrodes with integrated microfluidics. The performances of these electrode variations were simulated in COMSOL to determine the better option if dielectrophoresis (DEP) were used in the size-based separation subsystem.

The planar electrodes in the top half of Fig. 16 are fabricated as a thin film on a substrate and are then sandwiched between the substrate and a polymer containing a fluidic microchannel (running between the inlet/outlet holes in the blue-colored polymer). In the bottom half of Fig. 16, the 3D electrodes are also sandwiched between the substrate and polymer but differ from the planar electrodes in important ways. The 3D electrodes are much thicker than the planar electrodes, and the 3D electrodes do not enter the fluidic channel. These differences result from fabrication and operational differences between planar and 3D electrodes that motivated this investigation to quantify the electric-field differences between the electrode options. The planar electrodes can be fabricated on a glass substrate using conventional metal deposition and photolithography. Because of their thin height, the planar electrodes can be positioned such that they intersect with the fluidic microchannel. In this way, cells flowing through the microchannel must pass directly over the electrodes. Because the electrodes are exposed to the fluid medium within the microchannel, passivation is often added directly over the electrodes to prevent unwanted bubbles and heat that may be generated by the electrodes. Although the passivation prevents bubble and heat generation, it can complicate the integration of the electrodes with the polymer microchannel; the passivation must be chosen such that it can provide a leak-proof bond with the polymer. For example, if the polymer is PDMS, silicon dioxide (SiO_2) passivation is a better option than silicon nitride (Si_3N_4) because PDMS bonds more readily to SiO_2 than to Si_3N_4; however, the SiO_2 passivation may affect the electric-field in different ways than the Si_3N_4 would. On the other hand, the 3D electrodes can be fabricated such that they do not lie within the fluidic channel at all, thereby mitigating the need to add a separate passivation layer that increases processing costs. This ability to place electrodes outside the fluidic channel results from using thick electrodes that have a significant fringing electric-field that can pass through the fluidic channel, much higher compared to the fringing electric-field generated at the ends of

planar electrodes. Additionally, the 3D electrodes can be made out of liquid metal instead of deposited or electroplated thin-films. Using liquid metal simplifies the electrode fabrication and integration with the polymer microchannel because the liquid metal channels can be patterned in the polymer at the same time as the fluidic channels; therefore the electrode fabrication consists of only loading channels with liquid metal. For instance, the master mold for PDMS microfluidics can include the liquid metal channels along with the fluidic channels. Integrating the PDMS with a glass slide would also be straightforward, so the 3D electrodes do not have the same bonding concerns as do the passivated planar electrodes. The 3D electrodes are not without passivation, though, because a polymer layer must exist between the liquid metal and fluidic microchannel to separate the liquid metal from the fluid medium. This passivation also limits the electric-field generated by the 3D electrodes similar to the planar passivation that limits the planar electric-field. Because of the simpler and cheaper fabrication of the 3D electrodes, we considered this option for our DEP application and decided to quantify the electric-field differences between planar and 3D electrodes in order to choose which option is better for our application.

In order to choose either planar or 3D electrodes for our DEP experiments, we evaluated the options based on two criteria: (i) at an applied direct-current (DC) voltage of 10 V, which electrode variation generates the greatest electric-field magnitude, and (ii) which configuration would work best for high-throughput separation of yeast by size. For the second criterion, we considered the design and number of electrodes relative to the fluidic microchannel that carries yeast. For instance, we could design the electrodes in the same way as the models in Fig. 16, for which the yeast would experience a single electric-field peak between the electrodes. An alternative design would be an interdigitated electrode (IDE) array (see Fig. 19) that generates several electric-field peaks for manipulating cells flowing near the IDE array.

For the first criterion, we simulated planar and 3D electrodes in COMSOL Multiphysics. Figure 17 shows the models which were designed with the same material parameters and dimensions that would be used if we were actually fabricating the electrodes. Starting at the topmost z-coordinate of the planar electrode model, a pair of 200nm-thick copper (Cu) electrodes are separated by 300 µm. Each electrode is 100 µm wide, and the electrode lengths are not very relevant for the simulation. Immediately below the Cu electrodes is a 100 nm passivation layer of Si_3N_4, which is sandwiched between the electrodes and PDMS or a fluid channel modeled to simulate phosphate buffered saline (PBS). The fluid channel has 50 µm depth and runs perpendicular to the electrode length. PDMS surrounds the fluidic channel on all sides except that which interfaces with the electrode passivation.

The 3D electrode COMSOL model consists of a fluid medium containing PBS (rectangular prism at bottom of model). The fluid medium extends 250 µm from the PDMS interface that separates the liquid metal from the medium. Liquid metal fills the u-shaped channels of the model. The liquid metal channels were designed similar to the electrodes of a microfluidic device that was being used by a collaborator for an unrelated application. The shortest distance between the liquid metal and the fluid medium is 20 µm, and PDMS fills all of this space. This dimension was chosen because it abides by the approximate minimum feature size that can be patterned in PDMS using an SU-8 master mold fabricated using a film mask, which is a common process used to create PDMS microfluidics. The entire model thickness (i.e. the depth of the model into the page) is 50 µm. The material parameters of the models are provided in Tables 3 and 4. The density and heat capacity of the fluid medium depend on temperature, and their values are calculated automatically in COMSOL.
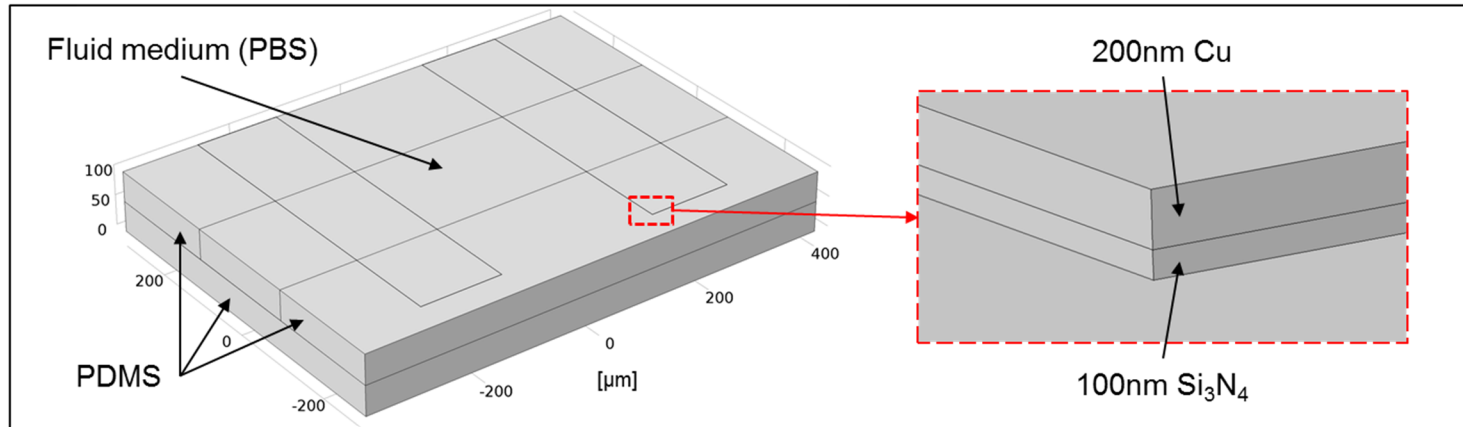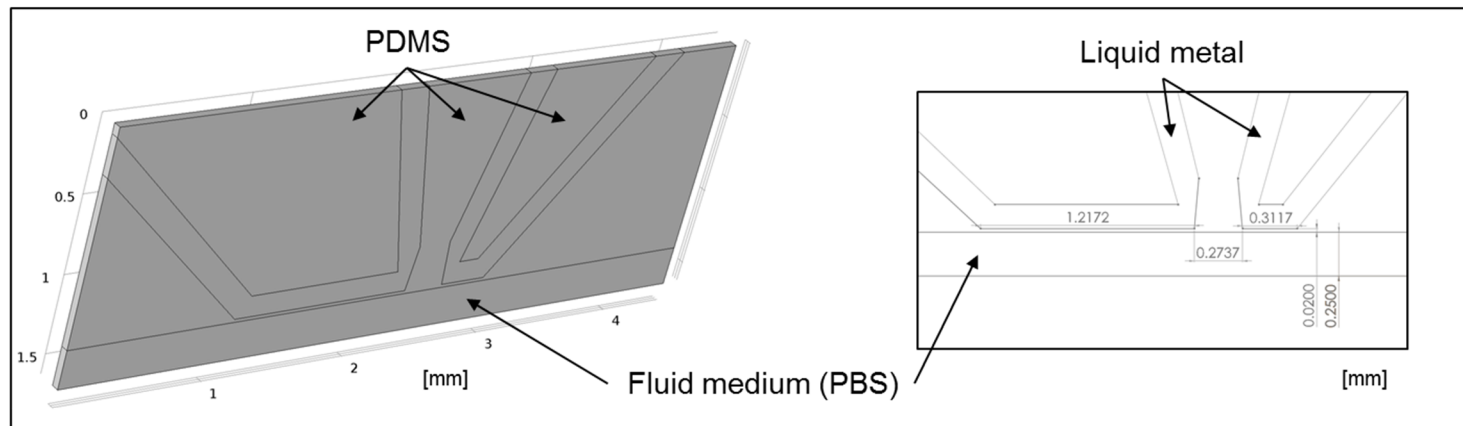
Figure 17. COMSOL models of the planar and 3D electrode variations from Fig. 16. The models were designed with the materials and dimensions that would be used if we were actually fabricating the electrodes and microfluidics.

Table 3. Material parameters of planar electrode model

Material Parameter	Electrode	Passivation	Fluid Medium	PDMS
Density [kg/m^3]	8700	3000	rho(T)	0.97
Heat Capacity [J/(kg*K)]	385	0.7	Cp(T)	1460
Relative Permittivity	1	7	80	2.3
Electrical Conductivity [S/m]	5.998e7	10e-10	0.5	2.5e-14

Table 4. Material parameters of 3D electrode model

Material Parameter	Electrode	Fluid Medium	PDMS
Density [kg/m^3]	8700	rho(T)	0.97
Heat Capacity [J/(kg*K)]	385	Cp(T)	1460
Relative Permittivity	1	80	2.3
Electrical Conductivity [S/m]	5.998e7	0.5	2.5e-14

After simulating the COMSOL models with 10 V applied to one of the electrodes while the other is grounded, we plotted the electric-field magnitude that a particle would experience while traveling through the fluid medium. Because the DEP force depends on the root-mean-square of the electric-field, the electrode option that creates a higher electric-field magnitude will manipulate cells with larger DEP force. Figure 18 shows the electric-field norms for the planar and 3D electrodes at cut-planes in the centers of the fluid medium channels (left half of Fig. 18).
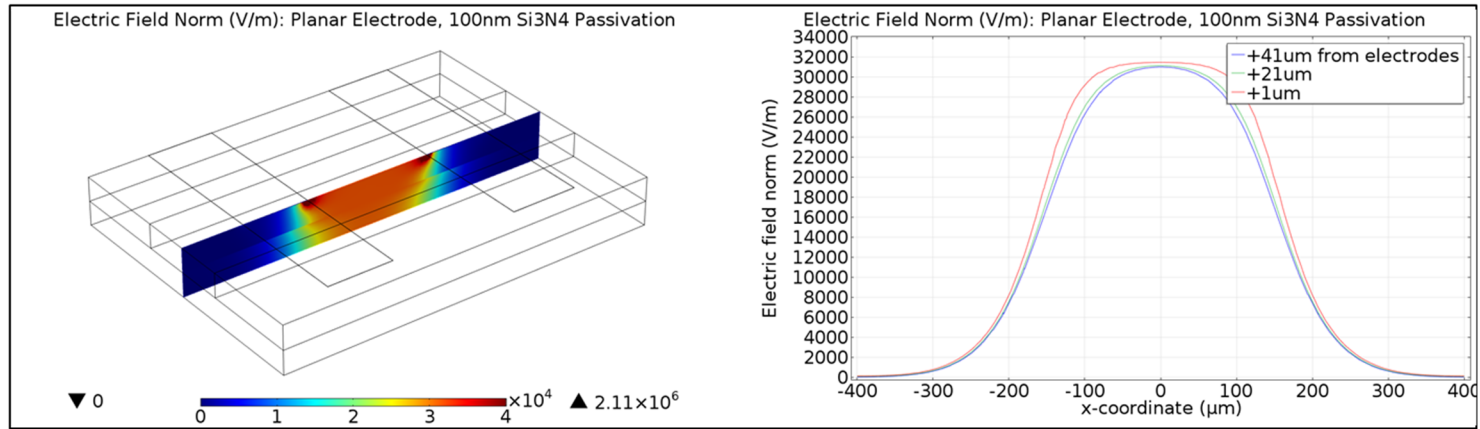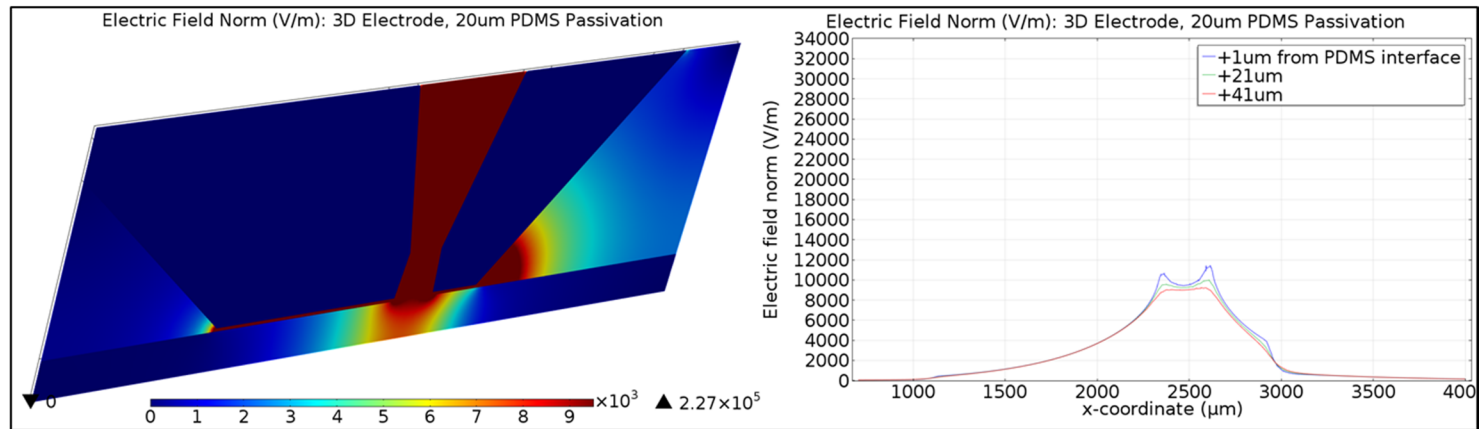
Figure 18. Simulation results for the planar and 3D electrode models. At left, a cut-plane through the models shows the electric-field magnitudes that a particle traveling through the microfluidic channel would experience as it passed near the electrodes. At right, the electric-field norms are plotted for three lines parallel to the cut-planes at left and at three distances from the passivation/fluid interface (1, 21, 41 μm). The planar electrodes produced ~3x greater electric-field magnitude compared to the 3D electrodes.

53

The plots at right of Fig. 18 show the electric-field norms for 3 lines along the lengths of the cut-planes (3 lines for each of the cut-planes). The 3 lines are at distances of 1, 21, and 41 µm from the interfaces of the fluid medium channels and passivations (Si_3N_4 for planar electrodes and PDMS for 3D electrodes). Thus the plots show the electric-field a cell would experience as it travels through a fluidic channel at 3 distances from the electrodes. The electric-field norm plots have similar y-scales, showing that planar electrodes generate ~3x higher electric-field magnitude than 3D electrodes if both are designed as if we were actually fabricating the electrode devices. Considering our first criterion above, planar electrodes would produce higher DEP forces for separating yeast by size compared to 3D electrodes. This difference in electric-field magnitudes for planar and 3D electrodes results from the passivation thickness and material that separates the electrodes from the fluid medium. The electrode material does not significantly influence the simulation because electric-field predictions in COMSOL depend on assigning potentials (e.g. 10 V and ground) to specific geometry interfaces such as the interfaces between the electrodes and passivations; the electrode material (Cu or liquid metal) does not change the electric-field as it propagates away from the electrode-passivation interface and into the fluid medium.

2.1.11. Planar, interdigitated electrode array designed for the yeast DEP device

Although using planar electrodes may require adding electrode passivation that complicates bonding the microfluidic channels to the electrode array, our criterion to select a configuration that allows high-throughput separation of yeast with suitable resolution further supported the use of planar electrodes. Han *et al.* utilized DEP from an angled interdigitated electrode (IDE) array to separate red blood cells, T cells, B cells, granulocytes, and monocytes by size.[65] These blood components (5-10 µm diameter) have sizes similar to yeast cells (2-7 µm diameter), and Han *et*

al. successes at separating blood cells by size makes their DEP design promising for our yeast application. Han *et al.* accomplished this separation by choosing the DEP frequency and medium conductivity that pushed blood cells away from the IDE array patterned on the channel bottom (negative DEP, nDEP) until the cells were confined at the channel top. Once the cells were restrained from moving any further from the electrodes, the horizontal component of the DEP force continuously nudged cells perpendicular to their flow directions. Larger cells were deflected laterally more than smaller cells because $F_{DEP} \propto V_c$. We discuss this principle of operation in § 2.1.17. The IDE array described in Han *et al.* spread completely across the microfluidic channel width and several mm down the channel length. By designing the electrodes in this way, cells flowing over the array experience DEP forces for more time compared to having only a single pair of electrodes. By increasing the DEP manipulation time, the cells are continuously nudged or deflected, which can produce finer size-based resolution using lower electric-field magnitudes.

Figure 19 shows the design for our DEP device, modeled after the design in Han *et al.*[65] The angled IDE array is deposited and patterned on a glass slide. Microfluidic channels are patterned in PDMS, which is then bonded to the electrode substrate. Microfluidic inlets and outlets are designed (i) to equalize fluidic resistances at the outlets, (ii) to allow flexibility in focusing cells toward one of the channel walls as they enter the separation region, and (iii) to provide symmetry so that cells could enter the separation region from either end of the channel which is helpful for repeating the separation by simply reversing the flow (discussed in § 2.2).
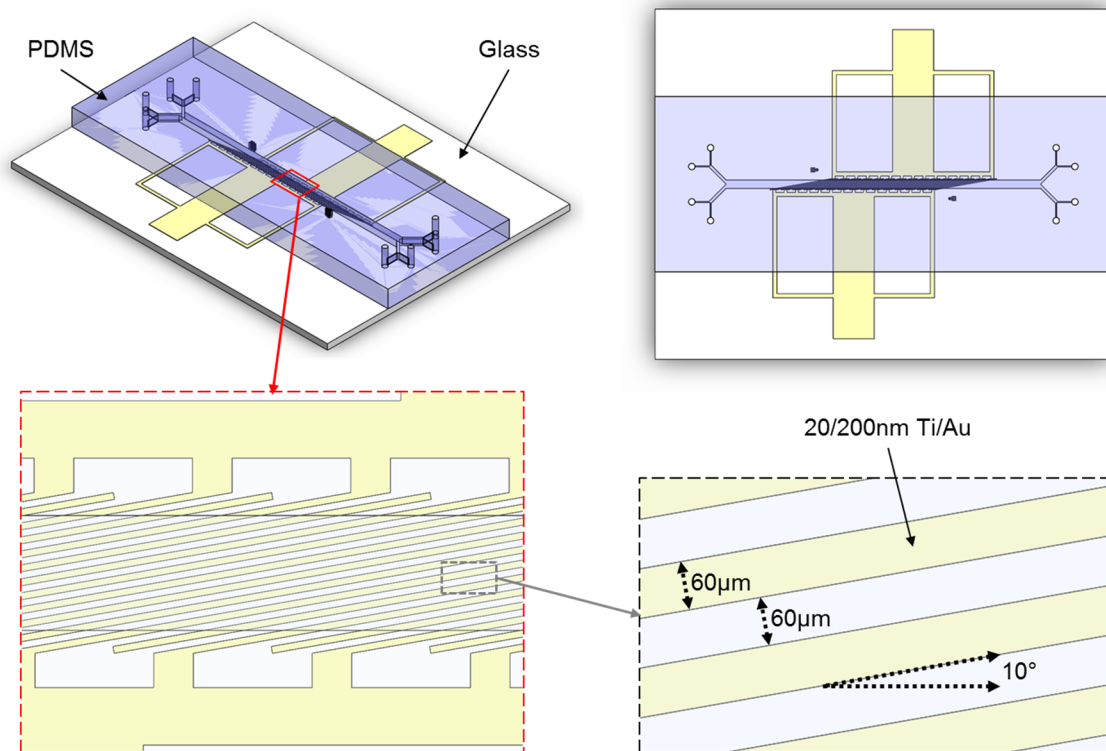
Figure 19. Dielectrophoresis (DEP) device design used in this work for investigating the separation of yeast by size. At top, an interdigitated electrode (IDE) array was patterned on a glass slide and integrated with PDMS microfluidics. The IDE array was angled relative to the flow direction in the microchannel (bottom right) to increase the perpendicular deflection of yeast as they traveled along the microchannel length.

The electrodes in the IDE array were designed similar to those used in Han *et al.* The electrode width and spacing are equal so that the electric-field pattern generated by the array also varies equally across the channel width. The electrode angle relative to the flow vector of cells traveling parallel to the channel length was chosen as small as possible because Han *et al.* found that the lateral displacement of particles is proportional to cos(θ) where θ is the angle between the flow and electrode length.[82]

2.1.12. Electric-field and Joule heating simulations for the DEP device

Before fabricating our DEP device design, we simulated the electric-field and electromagnetic Joule heating in COMSOL to verify that the DEP force and temperature within the microchannel would prove favorable for separating yeast. Figure 20 shows the geometry defined in COMSOL.
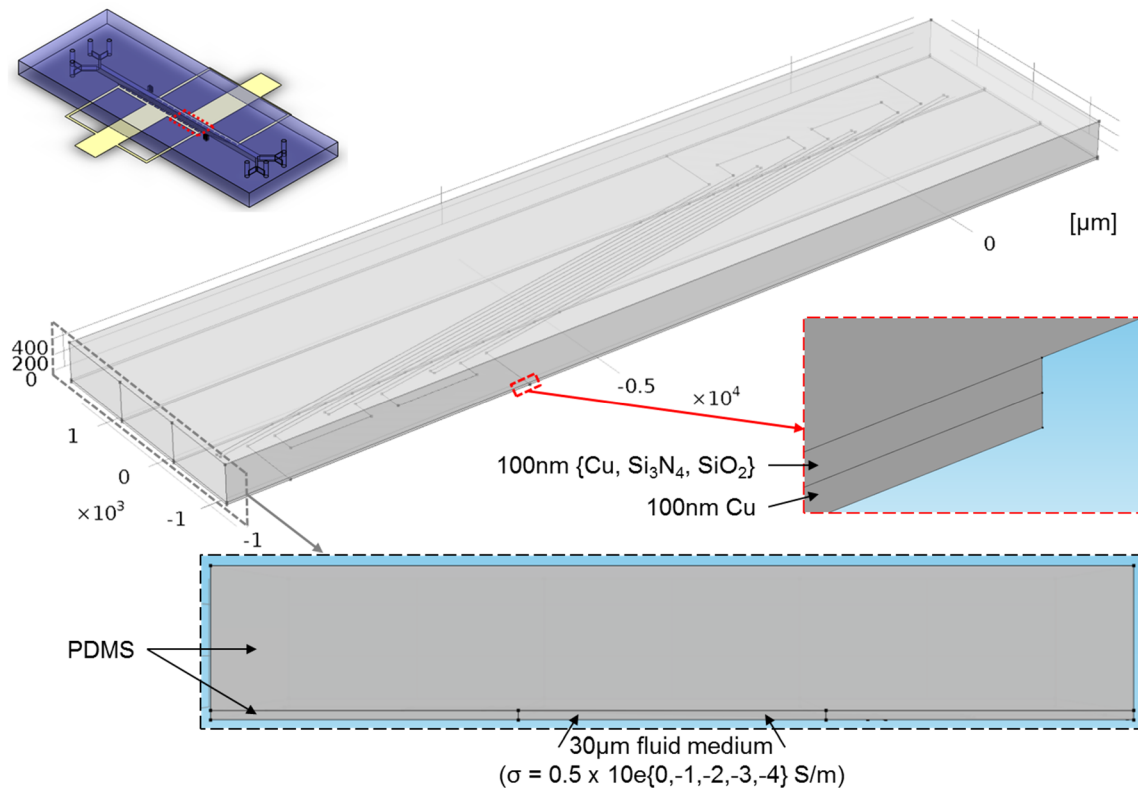
Figure 20. COMSOL model of the dielectrophoresis (DEP) device from Fig. 19. A small cross-section of the device without glass slide (top left) was simulated with three different electrode passivations (mid-right) and several fluid medium conductivities (bottom), which influenced the Joule heating from the electrodes in the fluid medium.

The model consists of the electrodes, fluidic channel, and PDMS (glass substrate is not included). Only a small segment of the overall geometry was simulated for convenience. Starting at the bottom-most z-coordinate of the model, 100 nm Cu electrodes are passivated by 100 nm of either Cu (in which case the electrodes are not passivated), Si_3N_4, or SiO_2. We discuss below

how the passivation material reduced both the electric-field magnitude and Joule heating. Similar

to the previous electrode simulations, the electrode material (whether copper, gold, etc.) is not

relevant in the simulation (see § 2.1.10). Connected to the passivation layer is either the fluid

medium or PDMS depending on the x/y-coordinates of interest. The 30 μm thick fluid medium

contacts only the center of the IDE array and runs parallel to the model length. The medium is

assigned 5 different conductivities to illustrate how lower medium conductivity limited the Joule

heating. The highest conductivity (0.5 S/m) corresponds to that of typical yeast medium (yeast

extract peptone dextrose, YPD). A relatively thick PDMS layer (~500 μm) covers all other sides

of the fluid medium. The material parameters used in the COMSOL simulations are listed in

Tables 5 and 6. A 10 V potential was applied to one of the electrodes while the other was

grounded.

Table 5. Material parameters for interdigitated electrode array models

Material Parameter	Electrode	Passivation	Fluid Medium	PDMS
Density [kg/m^3]	8700		rho(T)	0.97
Heat Capacity [J/(kg*K)]	385		Cp(T)	1460
Thermal Conductivity [W/(m*K)]	400	Table 6	k(T)	0.15
Relative Permittivity	1		80	2.3
Electrical Conductivity [S/m]	5.998e7		0.5e {0,-1,-2,-3,-4}	2.5e-14

Table 6. Passivation material parameters for interdigitated electrode array models

Material Parameter	Cu Passivation	Si$_3$N$_4$ Passivation	SiO$_2$ Passivation
Density [kg/m^3]	8700	2500	2200
Heat Capacity [J/(kg*K)]	385	500	1000
Thermal Conductivity [W/(m*K)]	400	30	1.4
Relative Permittivity	1	7	3.9
Electrical Conductivity [S/m]	5.998e7	10e-10	10e-10
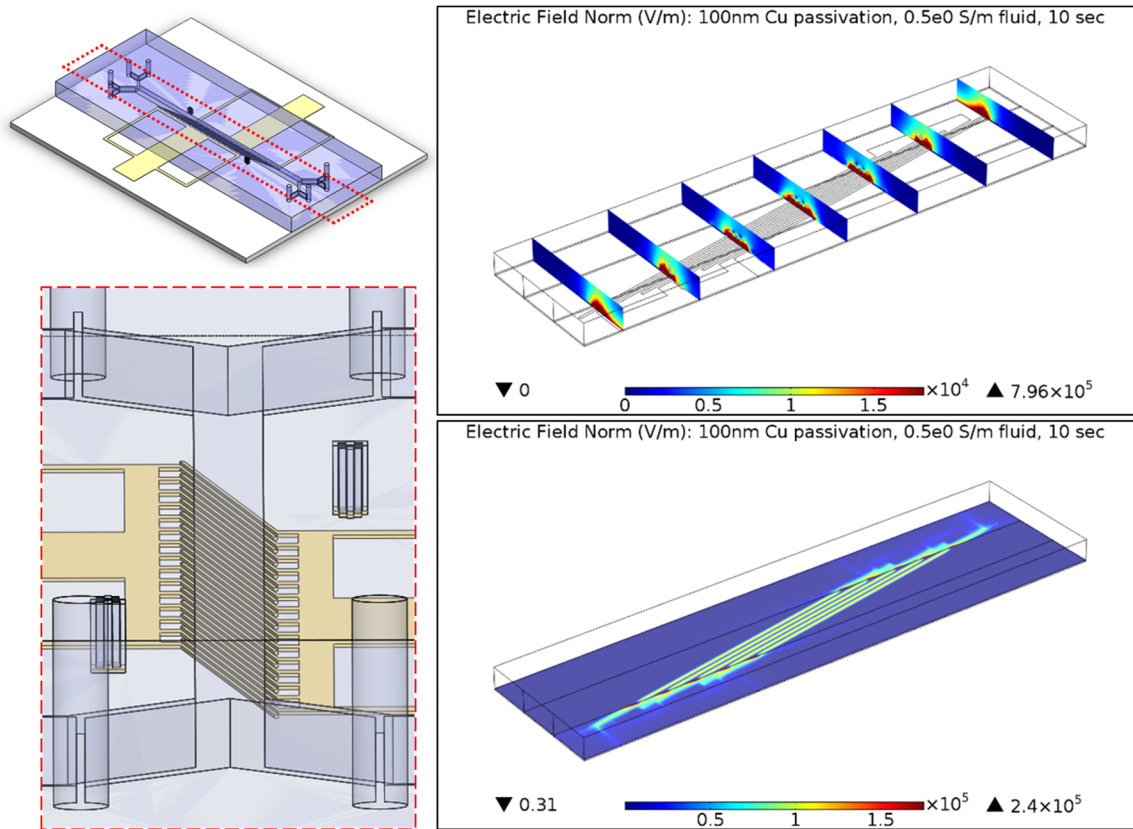
Figure 21. Electric-field simulations of the interdigitated electrode (IDE) array with no passivation and 10 V applied. A particle traveling through the microchannel at left of figure would experience the spatially-varying electric-field pattern simulated at right.

The diagrams and simulations in Fig. 21 show the electric-field magnitude a particle would experience as it travels through the microchannel over the IDE array. A particle would flow through the device from one end of the channel to the other (along the channel at left in Fig. 21), and the particle would experience the spatially varying electric-field pattern simulated at right in Fig. 21.
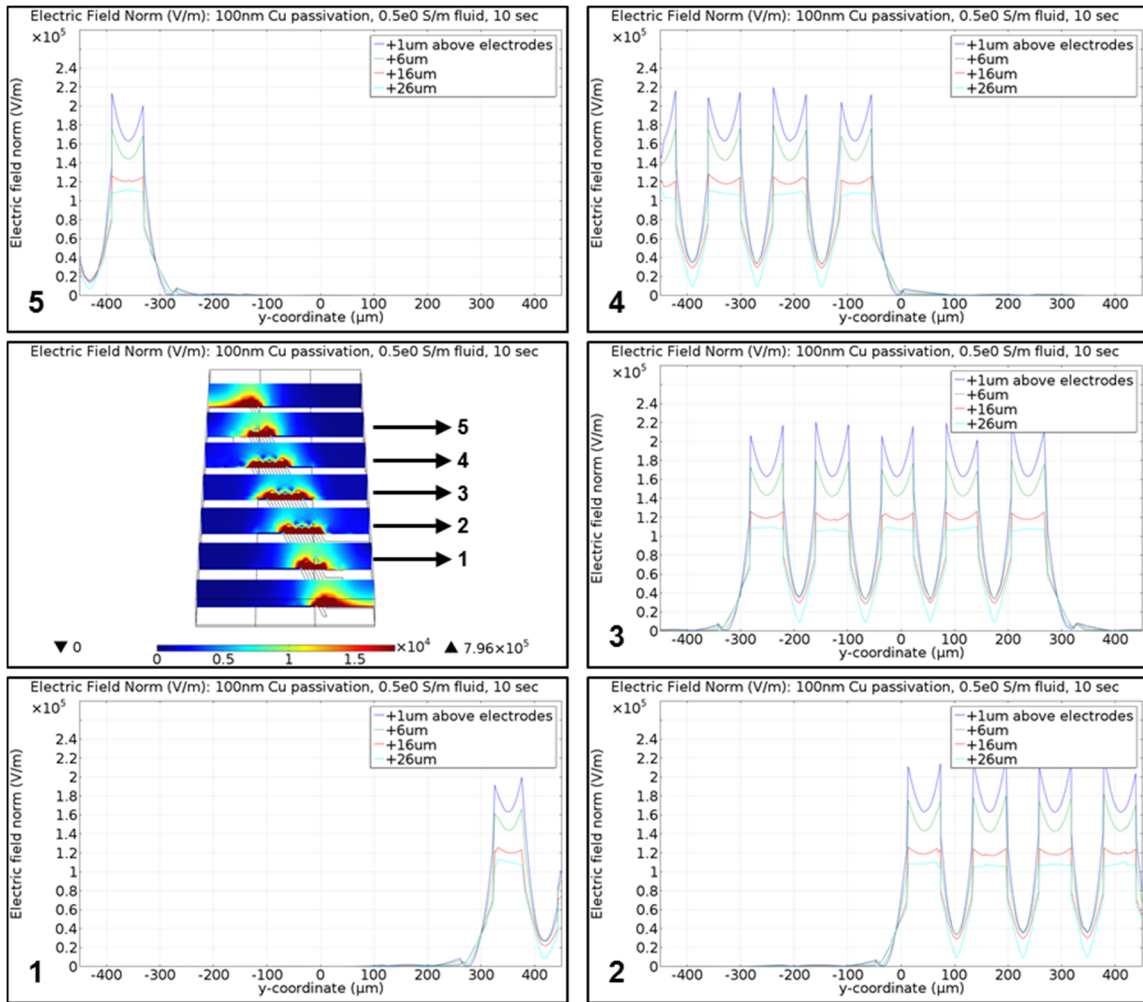
Figure 22. Electric-field magnitude plots for various cut-planes along the microchannel over the interdigitated electrode (IDE) array with no passivation and 10 V applied. The electric-field is maximum at the edges of the electrodes and minimum at the electrode centers. As a particle flows through the microchannel over the IDE array, the electric-field peaks and valleys shift laterally to follow the angled electrodes.

The electric-field norms for various cut-planes of the COMSOL model are shown in Fig. 22. As a particle enters the region above the electrodes from one end of the channel, it sees several electric-field peaks that align with the spaces between the electrode fingers. The electric-field is highest at the electrode edges and smallest at the centers of the electrode fingers. As the particle flows down the channel length, these electric-field maxima and minima shift

60

horizontally and trace the electrodes. Han *et al.* was able to deflect blood cells horizontally as they traveled through the microchannel because as the cells experienced negative DEP and were forced to the top of the microchannel at regions of low electric-field (at the minima of the electric-field plots), the angled electrodes shifted the minima horizontally and the cells followed the minima accordingly. The numerical electric-field norm plots each show four lines taken from the corresponding cut-planes at distances of 1, 6, 16, and 26 μm from the channel bottom that interfaces with the electrode passivation. Consistent with expectations, the electric-field peaks decrease by ~50% as distance from electrodes increases from 1 μm to 26 μm. The electric-field norm is symmetric about the channel center parallel to its length, which is beneficial so that cells would be deflected laterally perpendicular to the channel length in similar ways regardless from which end of the channel they enter the separation region. In the simulations of Figs. 21 and 22, the passivation was Cu, so the results present the case of effectively no passivation. The fluid medium conductivity was defined as 0.5 S/m, comparable to typical yeast medium (YPD). In summary, the simulations in Figs. 21 and 22 show that the electric-field generated by an angled IDE array varies such the particles flowing parallel to the channel length would experience perpendicular DEP forces in the same direction that the electrodes are angled.
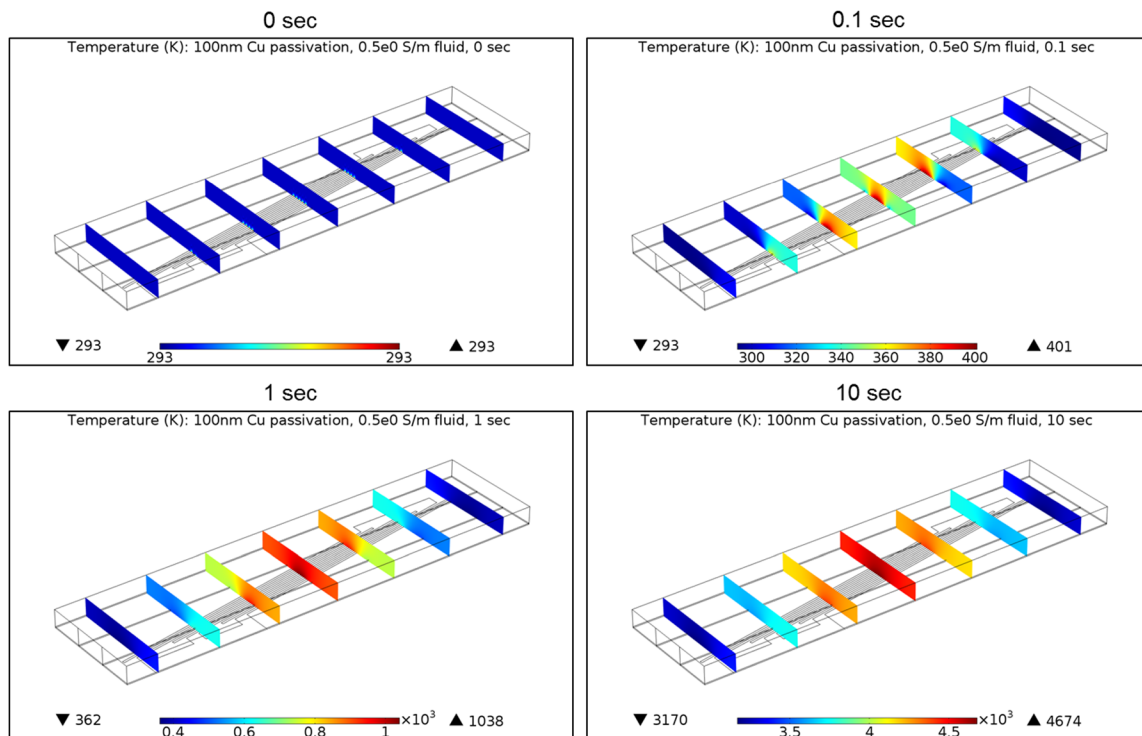
Figure 23. Joule heating simulations of the dielectrophoresis (DEP) device with no electrode passivation and high fluid medium conductivity (0.5 S/m) at 0, 0.1, 1, and 10 s after 10 V was applied. These high temperatures would be harmful to biological cells flowing in the microchannel of the device.

After simulating the electric-field magnitude of the IDE array, we investigated Joule heating in the fluid medium above the electrodes. Joule heating is the heat dissipation that results from current flowing through a conductor and is especially important to consider here so that we ensure a biocompatible environment for the yeast by limiting the heat to biologically-safe levels. Figure 23 shows temperatures for various cut-planes of the model at 0, 0.1, 1, and 10 s after applying 10 V to one electrode while the other is grounded. The model used to produce these simulation results had 100 nm Cu passivation (equivalent to no passivation) and fluid medium with 0.5 S/m conductivity. After only 0.1 s, the temperature within the microchannel increased from 293 K to 400 K which would instantly kill any yeast in the fluid medium. After 1 s of applied voltage, the temperature was over 1000 K. The 4670 K temperature after 10 s is

somewhat misleading because the applied potential was direct-current (alternating-current would be used in the actual DEP experiment) and the model does not include any way to dissipate heat. If the simulation time were run to infinity, the temperature would also increase to infinity because the model is essentially a box. The model could be increased in size to add volume in which heat can be dissipated; however, for the purposes of showing what factors influence Joule heating, we do not perform such simulations.

As discussed above, Fig. 23 shows how electrodes with no passivation generate biologically harmful heat within a fluidic channel of relatively high conductivity (0.5 S/m). Because of such heat, we must question the ability of the DEP device to maintain biocompatibility for yeast. To limit the Joule heating, we investigated adjusting two model parameters: decreasing the fluid medium conductivity and adding electrode passivation. In Fig. 24, we show the temperatures within the microchannel 1 s after 10 V is applied for fluid medium conductivities of 0.5e{-1,-2,-3,-4} S/m. The temperatures for all of the models at 0 s were 293 K. All parameters for the models are the same except for the fluid medium conductivity. The temperature in the microchannel with $\sigma = 0.5 \times 10^{-1}$ S/m increased from 293 K to >360 K after 1 s, which is still too high for yeast biocompatibility. For the microchannel with $\sigma = 0.5 \times 10^{-2}$ S/m, the temperature was ~300 K. Thus by decreasing the fluid medium conductivity by 2 orders of magnitude, we keep Joule heating within biologically-safe levels. Further decreasing the conductivity reduces the Joule heating even more. For $\sigma = 0.5 \times 10^{-3}$ S/m temperature was 294 K, and for $\sigma = 0.5 \times 10^{-4}$ S/m temperature was 293 K indicating virtually no Joule heating in the microchannel. To maintain yeast biocompatibility for our DEP device, if the electrodes are not passivated, we would need to reduce fluid medium conductivity to between 0.5×10^{-2} S/m and 0.5×10^{-3} S/m.
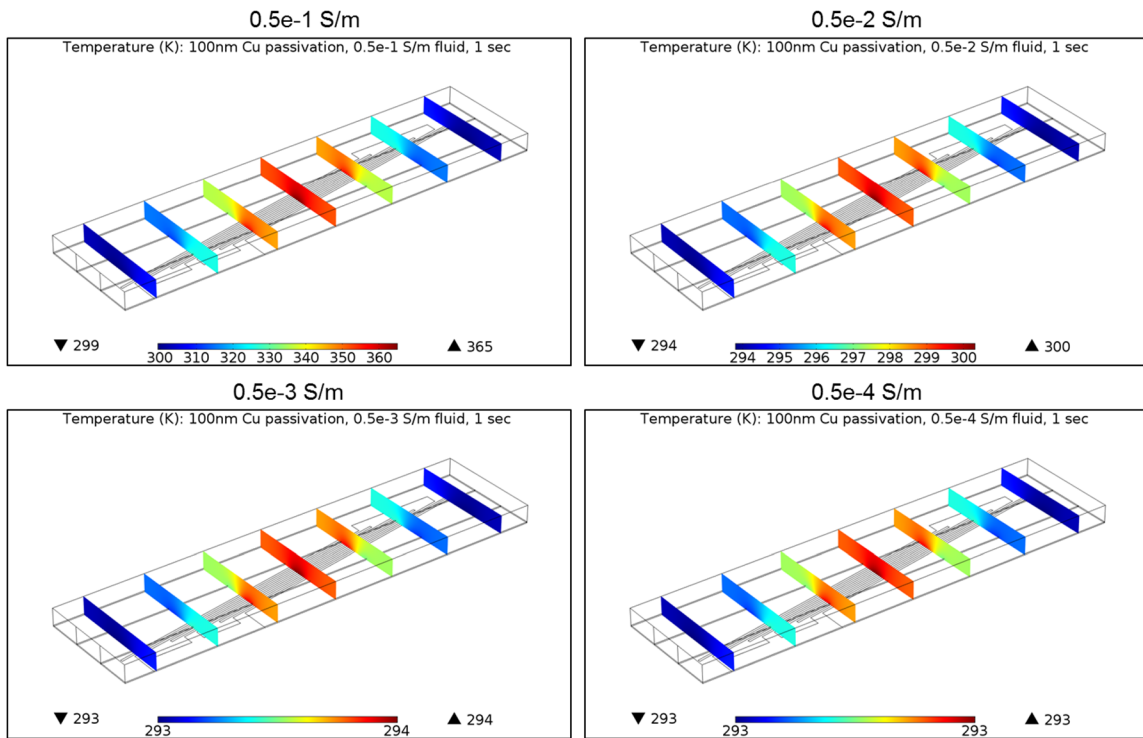
Figure 24. Joule heating simulations of the dielectrophoresis (DEP) device with no electrode passivation and fluid medium conductivities of 0.5e-1, 0.5e-2, 0.5e-3, and 0.5e-4 S/m at 1 s after 10 V was applied. Reducing the fluid medium conductivity by 2-3 orders of magnitude (compared to the model that produced the results in Fig. 23) limits the electromagnetic heating and thus improves biocompatibility for cells in the DEP device.

Adjusting medium conductivity does not impact the electric-field magnitude in the microchannel. Figure 25 shows the electric-field norms for the same models of Fig. 24; electric field did not change as the conductivity decreased. In summary, reducing the conductivity of fluid medium through a microchannel above an un-passivated IDE array reduced the Joule heating to temperatures safe for biological cells but did not affect the electric-field magnitude.
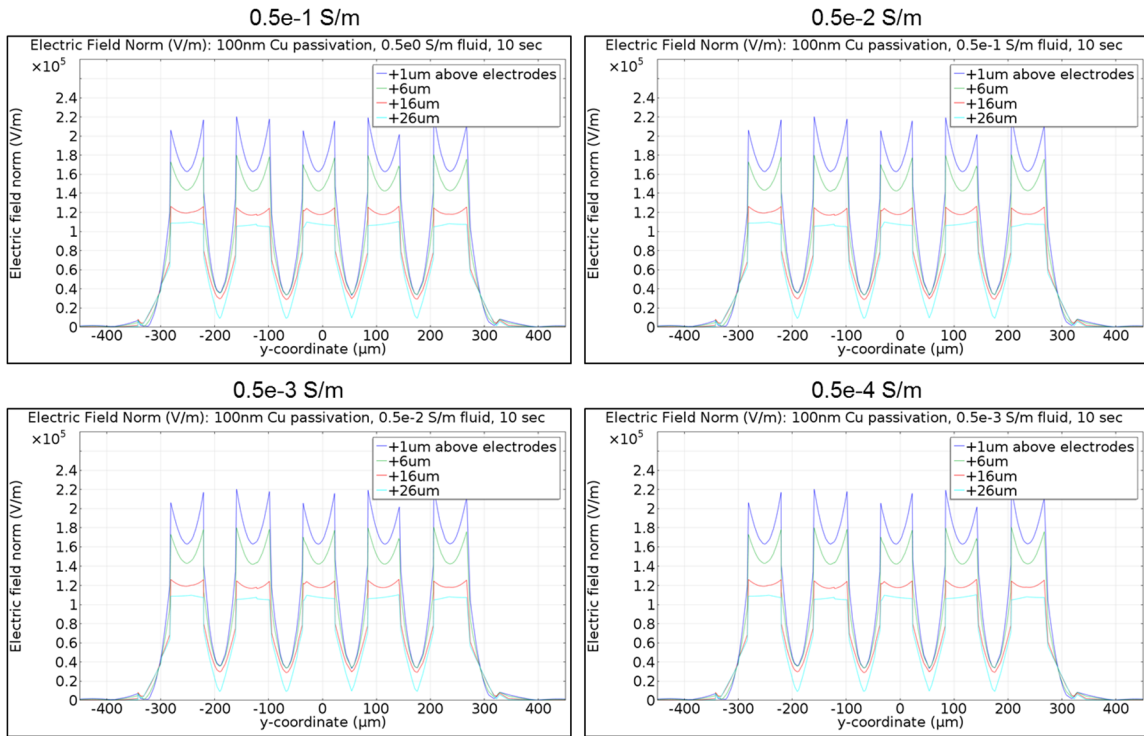
Figure 25. Electric-field magnitude plots for the same models used to produce the results in Fig. 24, showing that reducing fluid medium conductivity does not change the electric-field within the microchannel.

Another method we investigated for reducing the Joule heating was adding passivation between the electrodes and the fluid medium. Figure 26 shows the temperatures of various cut-planes of 3 models 10 s after 10 V was applied. The models were the same except for changing the material parameters (density, heat capacity, thermal conductivity, relative permittivity, electrical conductivity) for the passivation. Silicon nitride (Si_3N_4) and silicon dioxide (SiO_2) were chosen for the simulations because these materials are readily available for deposition at our process facility. Table 6 shows the passivation material parameters for each model.
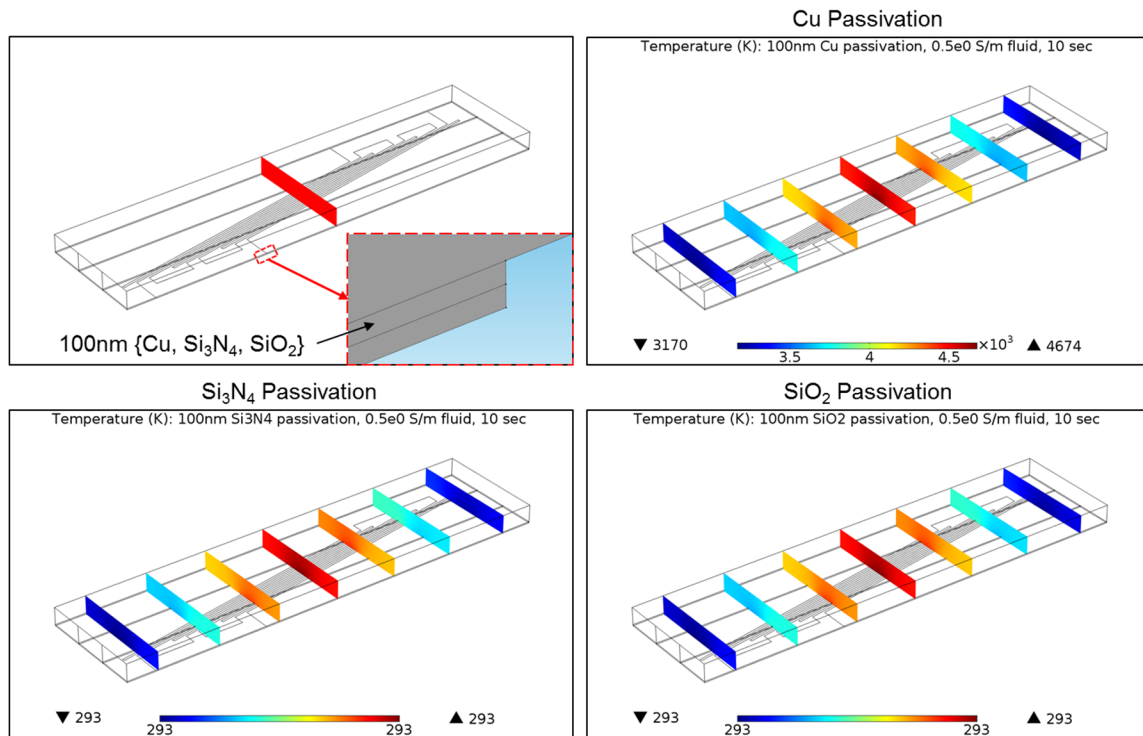
Figure 26. Joule heating simulations of the dielectrophoresis (DEP) device with three variations of electrode passivation (none, silicon nitride, and silicon dioxide) and fluid medium conductivity of 0.5 S/m at 10 s after 10 V was applied. The addition of electrode passivation appears to limit heat generation that can potentially harm biologically cells flowing in the microchannel. Additional simulations showed that passivation only decreases electric-field such that Joule heating is negligible. Increasing electric-field (e.g. by increasing applied voltage) results in Joule heating even with passivated electrodes.

The temperature of the model with Cu passivation increased from 293 K to >4600 K, while the temperatures of the models with Si_3N_4 and SiO_2 stay at 293 K. These simulations appear to show that adding electrode passivation limits the Joule heating to biologically acceptable temperatures; however, the passivation significantly reduced the electric-field magnitude generated by the IDE array in the microchannel. Figure 27 shows the electric-field norms for the models with Cu, Si_3N_4, and SiO_2 passivation. The plots show several lines parallel to the red cut-plane of the model diagram at top left. The lines are 1, 6, 16, and 26 µm away from the interface between the passivation and fluid medium. As shown in the plots, the electric-field

of passivated electrodes was reduced by ~5 orders of magnitude compared to the case with no passivation. Additionally, the passivation seemed also to reduce the number of electric-field maxima and minima across the cut-plane. The loss of maxima/minima results from an inability of the electric-field to penetrate through the passivation. The electric-field originates from certain electrodes of the IDE array (half of the fingers of the IDE array) and must pass through the passivation twice if it is to reach the grounded electrodes (the other half of the fingers) by fringing through the fluid medium. In other simulations, we found that the loss of maxima/minima is first noticed when the passivation conductivity decreased below ~10e-4 S/m. By increasing the applied voltage from 10 V to 1000 V, the overall electric-field magnitude had increased, but the loss of maxima/minima was still observed.

Although the passivation appeared to reduce Joule heating within the microchannel, it significantly decreased the electric-field. Additional simulations showed that the passivation actually did not limit Joule heating; it only reduced the electric-field such that Joule heating was negligible. In summary, passivation cannot reduce Joule heating. Because it significantly reduces electric-field magnitude, higher applied voltages must be used. Electrode passivation, therefore, is useful primarily to limit bubble generation in liquids from the electrodes. To control Joule heating, fluid medium conductivity must be reduced.
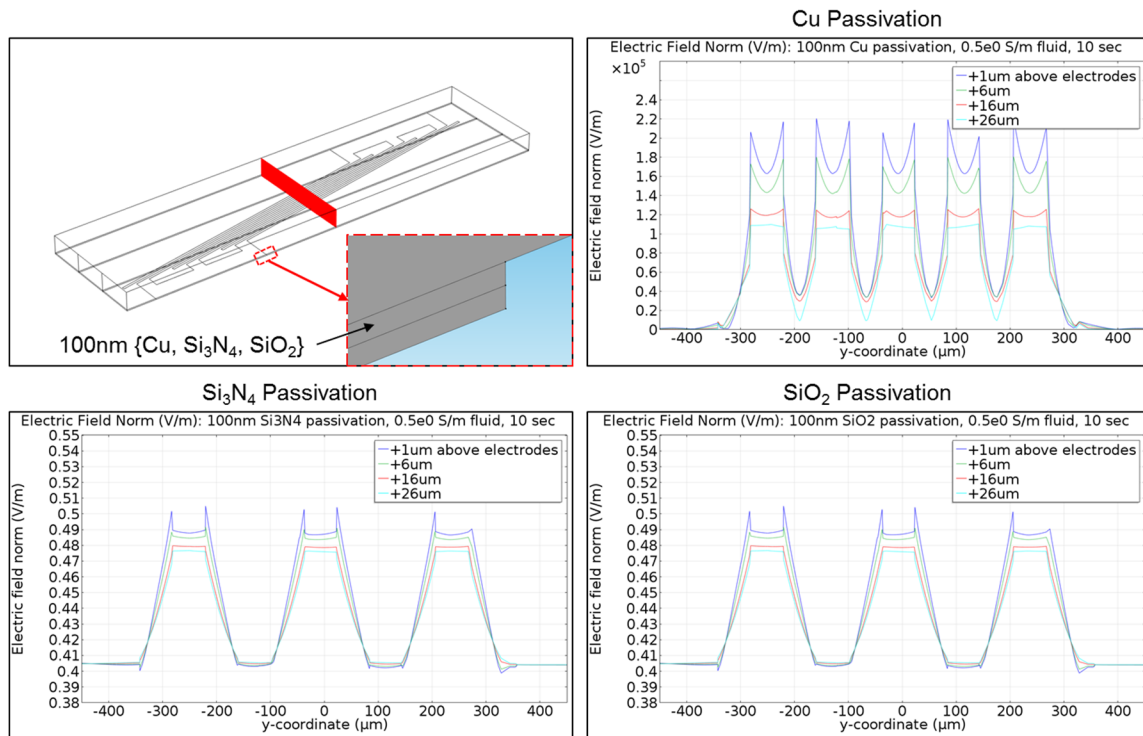
Figure 27. Electric-field magnitude plots for the same models used to produce the results in Fig. 26. The plots correspond to the red cut-plane in the model at top left. Adding electrode passivation decreases the electric-field magnitude by ~5 orders of magnitude.

From our COMSOL simulations of electric-field and Joule heating for the proposed DEP device, we found that the electric-field with no electrode passivation varies spatially such that it can deflect particles perpendicular to the channel length as the particles flow through the channel. An un-passivated electrode, however, generates heat in the microchannel that may be harmful to yeast. Additionally, an un-passivated electrode may create unwanted bubbles whenever the electric-field frequency is too low or applied voltage is too high. Reducing the fluid medium conductivity decreases Joule heating to biologically safe temperatures and does not affect the electric-field magnitude. Adding electrode passivation also controls Joule heating but significantly limits the electric-field. From these analyses, we concluded our best option would

be an IDE array with no passivation and a microchannel carrying fluid with relatively low conductivity ($1 \times 10^{-3} - 1 \times 10^{-2}$ S/m).

2.1.13. Low conductivity medium reduces Joule heating but worsens separation resolution

Although using low conductivity medium for our DEP device would reduce unwanted Joule heating that can harm yeast, low conductivity medium can also lead to positive DEP (pDEP) forces manipulating cells toward the electrodes rather than away. Han *et al.* used negative DEP (nDEP) forces to separate blood cells by size because the resolution for size-based separation is best when cells are repulsed from the electrodes, restrained by the channel top, and continuously deflected by the lateral component of the nDEP force. Consider the cross-section of our DEP device in Fig. 28.
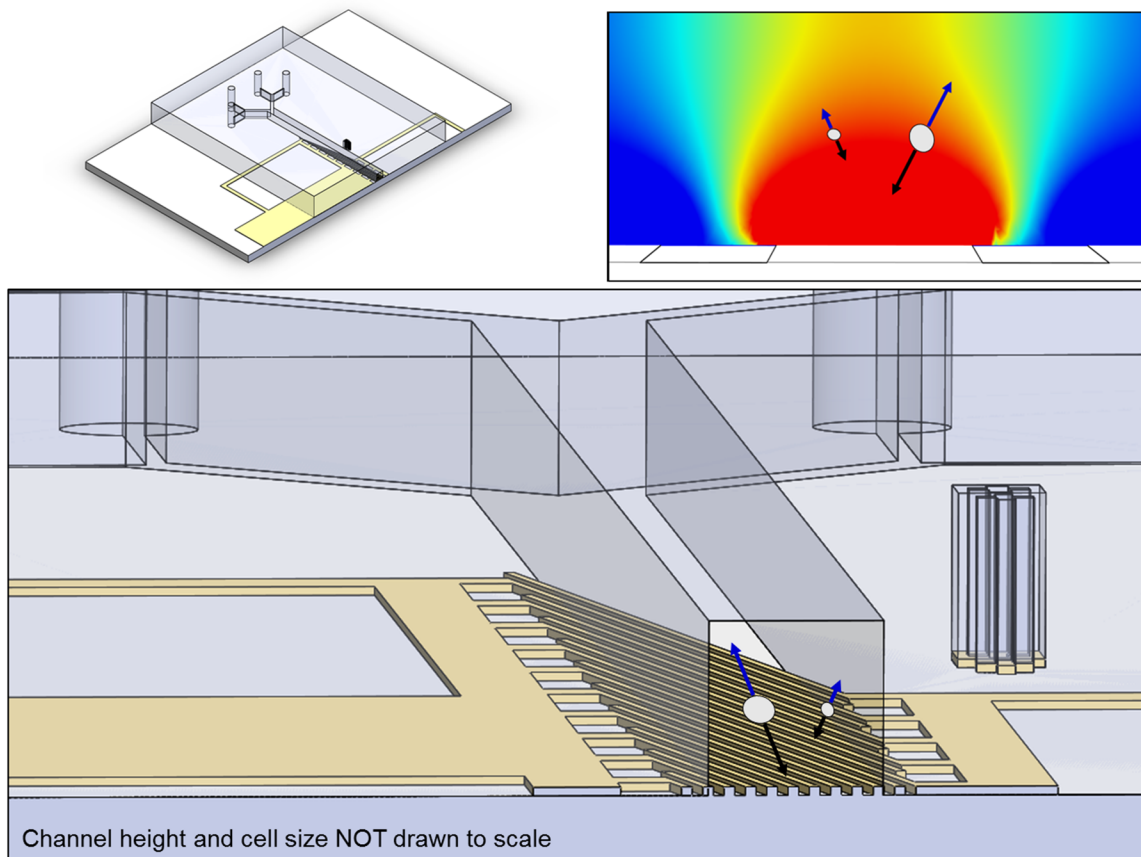
Figure 28. Dielectrophoresis (DEP) forces can attract particles to the electrodes (positive DEP, black arrows radiating from the particles) or repel them toward the channel top (negative DEP, blue arrows). The diagram at bottom is the cross-section of the DEP device at top left.

Positive DEP forces (represented by black arrows originating from the cells in the diagrams) attract cells toward the IDE array on the channel bottom while nDEP forces (blue arrows) repel cells toward the channel top. For ideal size-based separation using DEP from these angled electrodes, yeast flowing through the microchannel should be repelled away from the electrode array until they are confined by the channel top (Fig. 29).
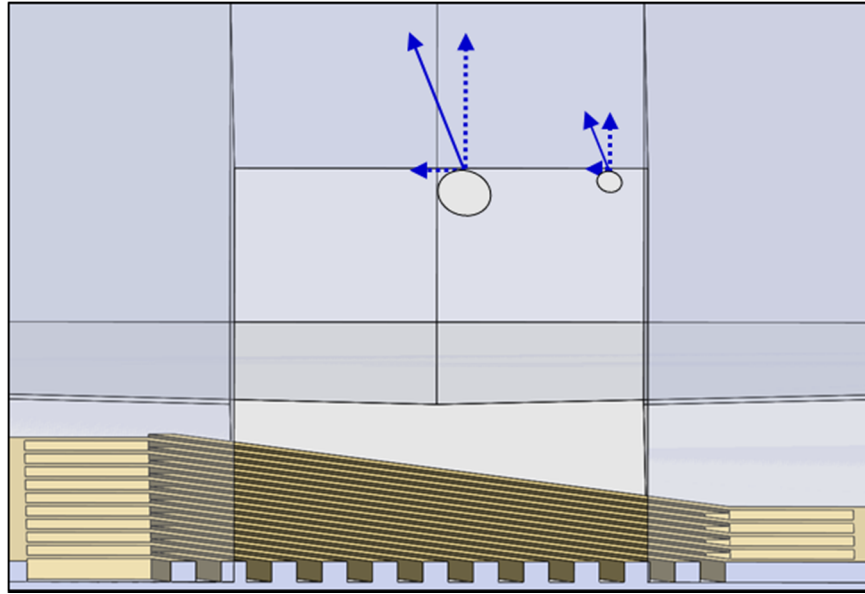
Figure 29. For the best size-based separation resolution of yeast flowing over the interdigitated (IDE) array of the dielectrophoresis (DEP) device, negative DEP (blue arrows radiating from the yeast) should force cells away from the electrodes. Once cells are confined at the channel top, the lateral component of the DEP force should deflect the yeast perpendicular to their flow directions. Larger cells should deflect laterally more than smaller cells because they experience larger DEP forces at equivalent distances away from the electrodes.

Once all cells are restrained by the channel top to stay at approximately the same distance away from the electrodes, the cells can move only laterally due to the horizontal component of the DEP force. Because $F_{DEP} \propto V_c$, larger cells experience larger DEP forces and thus are deflected perpendicular to the channel length more than smaller cells because of their larger lateral DEP force component (illustrated in Fig. 29 by the difference in lengths of the blue arrows radiating from the cells away from the electrode array). Because the IDE array electric-field varies horizontally as shown in Fig. 22, yeast cells would deflect laterally as they flow down the channel length because they are forced toward the regions of lower electric-field magnitude (i.e. the minima in the electric-field norm plots of Fig. 22). This behavior that results from nDEP has better size-based resolution compared to the results of pDEP because the former eliminates the dependence of DEP force on distance away from electrodes. If we were using

pDEP forces, cells closer to the channel bottom would experience greater forces than cells further away from the electrodes. This z-dependence only worsens the ability to separate yeast by size because the DEP device as designed does not ensure consistency in z-position among cells of different sizes. For example, a very small cell may be closer to the electrode array than a larger cell (or vice versa), and the small cell would experience a larger positive DEP force simply because it is much closer than the larger cell (and vice versa). Additionally, as discussed in § 2.1.16, in experiments with yeast cells undergoing attractive forces toward the electrodes, we observed smaller cells becoming more easily influenced by pDEP to flow such that they traced the edge of an electrode where electric-field magnitude is largest. In these experiments, larger cells were visually deflected toward the electrodes but still flowed toward the microchannel outlet instead of precisely tracing the electrode edge (see § 2.1.16).

To separate yeast by size using nDEP in our device, we can adjust the electric-field frequency or the fluid medium conductivity. From the equations describing DEP force, $F_{DEP}>0$ when $f_{CM}>0$ and pDEP results, and $F_{DEP}<0$ when $f_{CM}<0$ for nDEP. The sign of f_{CM} depends on the electrical properties of the fluid medium and the particles suspended in the medium as well as on the frequency at which the electric-field varies. We discussed in § 2.1.8 how live and dead yeast experience different DEP force directions because of their different electrical properties. For our device to separate live yeast by size, we can adjust the medium conductivity and the electric-field frequency to achieve the desired DEP force direction. Khoshmanesh *et al.* plotted Re[f_{CM}] vs frequency for live and dead yeast and for relatively high and low medium conductivities (see Fig. 4 of ref. 77). The figure shows that live yeast in low conductivity medium (0.01 mS/cm) have $f_{CM}>0$ and thus experience pDEP across all frequencies of interest. By increasing the medium conductivity to 1.4 mS/cm, live yeast have $f_{CM}<0$ and experience nDEP for frequencies up to ~1 MHz. For frequencies >1 MHz, $f_{CM}>0$ and the yeast experience

pDEP. For the best size-based separation resolution, we prefer to utilize nDEP similar to how Han *et al.* separated blood cells by size in medium with sigma = 1.7 mS/cm at 100 kHz electric-field frequency. Negative DEP cannot be achieved when yeast are in low conductivity medium regardless of the electric-field frequency, so low conductivity media will worsen the ability to separate yeast by size. Instead, we need relatively high conductivity media (sigma ~ 1 mS/cm) and low to moderate electric-field frequencies (100 Hz – 500 kHz). Unfortunately, using high conductivity medium promotes Joule heating that can harm yeast. If high conductivity medium must be used, we can add electrode passivation at the cost of reduced electric-field magnitude, but limiting the electric-field may weaken the DEP forces such that they do not affect the yeast at all.

2.1.14. High and low conductivity media selected for yeast DEP testing

Considering that we can adjust medium conductivity and electric-field frequency to produce nDEP forces to manipulate yeast in our device, we first measured the conductivities of various media to determine the corresponding electric-field frequency ranges. Using a handheld conductivity meter (Mettler Toledo, Education Series EL3), we measured the conductivities of selected media >10 times for each solution. The averages are shown in Table 7 along with conductivities for media used in selected DEP publications.[65,77,78]

Table 7. Conductivities of media considered in this and other DEP applications

Medium	Conductivity (mS/cm)
DI water + methanol +/- Trypan blue (ref. 77)	0.01, 1.4
NaCl (ref. 78)	0.14
Inositol (ref. 65)	1.7
Yeast Peptone Dextrose (YPD)	2.68 - 7.75
Synthetic Defined (SD)	9.52
Yeast Nitrogen Base (YNB)	1.685
Low Conductivity Medium	0.0645
Phosphate Buffered Saline (PBS)	16.65

We selected yeast extract peptone dextrose (YPD) because it is rich medium commonly used for culturing yeast. Yeast, however, can survive in a range of media richnesses, although their growth rate varies depending on the medium composition. In addition to YPD, yeast can be cultured in minimal or synthetic defined (SD) medium, and so we measured the conductivity of SD to determine what electric-field frequencies can be applied to achieve nDEP forces on yeast in SD. This particular medium consists of yeast nitrogen base (YNB), nitrogen typically in the form of ammonium sulfate, and carbon in the form of glucose. In order to grow and divide, yeast require at least YNB and sources of nitrogen and carbon, which can be added to YNB in varying concentrations. Thus by measuring the conductivity of YNB, we limit one end of the conductivity range that is relevant for our application. For example, starting with YNB which has $\sigma = 1.685$ mS/cm, we can add carbon and nitrogen sources to ensure yeast growth and adjust conductivity to a value closer to that of YPD ($\sigma \sim 5$ mS/cm), SD ($\sigma = 9.52$ mS/cm), or potentially higher. The low conductivity medium consists of inositol, calcium acetate, magnesium acetate, and 1-histidine prepared as described in Steenbakkers *et al.*[83] Phosphate buffered saline (PBS) at 1X concentration was included in the table because it represents an estimated maximum conductivity of ~20 mS/cm for the range of conductivities we could

potentially use in our DEP experiments. With the medium conductivities relevant to this application ranging between 1.685 mS/cm (for YNB) and 8 mS/cm (for YPD), the ideal electric-field frequency range is <1 MHz to ensure that $f_{CM}<0$ and yeast experience nDEP. Ideally, we should use frequencies <100 kHz so that the magnitude of f_{CM} (and thus F_{DEP}) is largest; however, electric-field frequency cannot be too low (not < ~100 Hz) because the risk for bubble generation is higher for un-passivated electrodes driven at low frequencies. Considering the small conductivity range between YNB (1.685 mS/cm) and YPD (8 mS/cm), we did not believe the DEP behavior on yeast in YPD would be significantly different than in minimal medium consisting of YNB and nitrogen/carbon sources. For this reason, we tested only YPD and low conductivity medium in our experiments described below.

2.1.15. DEP device fabrication and experimental protocol

After determining the ideal electric-field frequencies to use for the higher conductivity YPD and low conductivity medium, we fabricated the DEP device using standard microelectronics and microfluidics processing. As shown in Fig. 19, the device consists of 2 components: an IDE array patterned on a glass slide and a PDMS microfluidic network. The electrodes and microfluidics were designed in DWG Editor (SolidWorks), and the designs were converted into a film mask by CAD/Art Services, Inc. To fabricate the IDE array, glass slides were first cleaned with Piranha solution for ~10 min, then submerged in 95°C de-ionized (DI) water for ~3 min, and finally rinsed with room temperature DI water. Titanium and gold films were deposited onto the glass to thicknesses of 20 nm and 200 nm, respectively and in that order, using a Lesker PVD 75 Ebeam Evaporator. Next, Shipley 1818 was spin-coated onto the Ti/Au-covered glass at 500 rpm for 5 s followed by 3500 rpm for 30 s. The resist was soft-baked at 110°C for 5 min, exposed at 85.25 mJ/cm² using a Karl Suss MA6 Mask Aligner, developed in MF319 for ~40 s,

rinsed in DI water, hard-baked at 120°C for 10 min, rinsed with isopropyl alcohol (IPA), and dried with nitrogen. The Au was etched by Gold Etchant for 30-40 s, and the Ti was etched by HF acid for <10 s. The sample was immediately rinsed in DI water after each etch step was finished. We did not deposit any passivation over the electrodes. Finally, the resist was removed by rinsing with Acetone, IPA, and DI water. We thank Nebras Sobahi for assistance with electrode fabrication.

The microfluidics layer was fabricated using soft lithography. After designing the channel in DWG Editor and receiving a film mask from CAD/Art Services, Inc., the master mold was fabricated by first cleaning silicon (Si) wafers in Piranha solution for ~10 min. SU-8 2050 (Microchem) was spin-coated onto the Si wafers at 500 rpm for 10 s followed by 3000 rpm for 60 s to produce resist with 50 μm thickness. To produce 30 μm thick resist, SU-8 2025 (Microchem) was spin-coated at 500 rpm for 10 s followed by 2400 rpm for 60 s. The resist was soft-baked at 65°C for 10 min immediately followed by 95°C for 35 min. After soft-baking, the wafer was exposed at 170 mJ/cm^2 using the mask aligner and then hard-baked at 65°C for 5 min followed by 95°C for 10 min. The resist was developed in Thinner P for >2 min (until the unexposed resist was completely removed), rinsed in IPA, and dried with nitrogen. The completed SU-8 master molds were coated with tridecafluoro-1, 1, 2, 2-tetrahydrooctyl)-1-trichlorosilane (TFS) by placing the molds and TFS in a desiccator for ~10 min.

After fabricating the SU-8 master mold, PDMS (Sylgard 184, Dow Corning) was prepared by mixing pre-polymer and curing agent at a ratio of 10:1 and then degassing in a desiccator for ~10 min. The mixture was poured onto the mold and degassed for another ~20 min or until no air bubbles could be seen in the mixture. The degassed mold was cured in an 80°C oven overnight (>8 hr). After curing, the PDMS was removed from the mold, excess PDMS was cut from the structure, and inlet and outlet holes were punched using a syringe tip.

To integrate the PDMS layer and IDE array, both components were treated with oxygen plasma (Harrick Plasma) at 100 W in 100 mTorr for 1.5 min. Before placing the layers together, a small amount of methanol was applied as lubricant so that the microfluidic channel could be aligned appropriately with the IDE array. After aligning the layers and allowing some of the methanol to evaporate for ~5 min, the device was placed at 65°C for ~4 hr to allow the rest of the methanol to evaporate and the PDMS to bond irreversibly with the glass slide.

After bonding the IDE array with the PDMS microfluidics, plastic Tygon tubing was inserted into the inlets/outlets and electrical wiring was soldered to the electrode pads. Before loading cells, the microfluidic device was primed by flowing ethanol, DI water, and YPD.

Wild-type yeast were prepared as described in § 2.1.2. After the culture had resumed exponential growth by transferring cells into fresh YPD and incubating ~3 hr before the DEP experiment, the yeast were placed in either YPD or low conductivity medium and withdrawn into a syringe (BD with Luer-Lok Tip) capped with a flat needle tip. We tested yeast in YPD, which has relatively high conductivity, and in low conductivity medium because the DEP behavior was expected to vary for the different media as discussed in § 2.2.13. The syringe was then inserted into the plastic tubing of the microfluidic inlet channel. Several syringes were loaded with YPD or low conductivity media and connected to the tubing of all remaining inlets of the microfluidic device. These YPD or low conductivity medium buffers were used when the cells were in YPD or low conductivity medium, respectively. All syringes were fastened to syringe pumps (Chemyx Fusion 400 Touch Syringe Pump) which were programmed such that the cumulative flow within the main microchannel crossing the IDE array ranged from 40 µL/hr to 150 µL/hr. The flow rates used for introducing yeast into the device ranged from 5 µL/hr to 20 µL/hr, and the buffer inlets were programmed with much higher flow rates in order to focus the yeast hydrodynamically against the microfluidic channel wall.

The microfluidic device with either YPD or low conductivity media was placed on the stage of an upright microscope (Nikon Eclipse LV100) with camera (Hamamatsu ORCA-Flash4.0 V2 C11440-22CU) and supporting software (NIS-Elements Br Microscope Imaging Software). The electrical wiring that was soldered to the electrode pads was clipped to alligator connectors of a function generator (Tektronix AFG 3021B Single Channel Arbitrary/Function Generator). The function generator was programmed with frequency within 100 Hz to 100 MHz and peak-to-peak voltage V_{pp} between 1 V and 20 V. The exact combination of frequency and voltage are shown for selected experimental results in the following sections.

For continuous flow-through experiments as yeast flowed into the main channel, over the IDE array, and into the outlets, the function generator output was either ON or OFF, and videos were captured at various locations along the channel length. With the function generator ON, at each location along the channel length the yeast would have experienced DEP forces for varying amounts of time. If the function generator had just changed from ON to OFF (or vice versa), videos were not taken for >30 s to allow yeast currently over the IDE array to exit the device.

For stationary DEP experiments, all flow was stopped and the yeast were dispersed in the medium above the IDE array. Videos were captured continuously several seconds before and after the function generator was switched to ON so that the DEP manipulation could be observed in real time.

After capturing videos for flow-through and stationary DEP experiments, the videos were selectively combined and compressed using Windows Live Movie Maker (Windows 7). Text indicating the experimental conditions including applied voltage and frequency was added to the videos also using Windows Live Movie Maker.

2.1.16. Experimental pDEP agreed with theoretical expectations

We investigated how DEP manipulates yeast in low conductivity medium (σ = 0.0645 mS/cm) and YPD (σ = 5 mS/cm) over frequencies ranging from 100 Hz to 100 MHz. Depending on the combination of frequency and medium conductivity, f_{CM} was positive or negative (see § 2.1.9) and DEP attracted yeast to or repelled yeast from the IDE array. Figure 30 shows typical yeast behavior in the main channel above the IDE array when the fluid medium had low conductivity. In the images, yeast flowed from right to left and enter the field-of-view as indicated by the red arrows at the top of the main channel, which can be identified by the horizontal black lines near the tops and bottoms of the images. The left image shows yeast as they enter the first part of the IDE array, and the right shows yeast near the IDE array center. The electric-field frequency and applied voltage are provided as titles for the images.

Because f_{CM}>0 for yeast in low conductivity medium over all frequencies (see § 2.1.9), yeast experienced positive DEP (pDEP) forces that attracted them to the IDE array as they flowed through the microchannel. We observed this attraction in our device across all frequencies of interest. More specifically, pDEP attracts yeast to regions of highest electric-field magnitudes which occur at the edges of electrodes. The yeast circled in red in the images were tracking the electrode edges in the direction indicated by the dotted red arrows, that is, the yeast were exactly tracing the electrode edge even though medium was flowing from right to left.
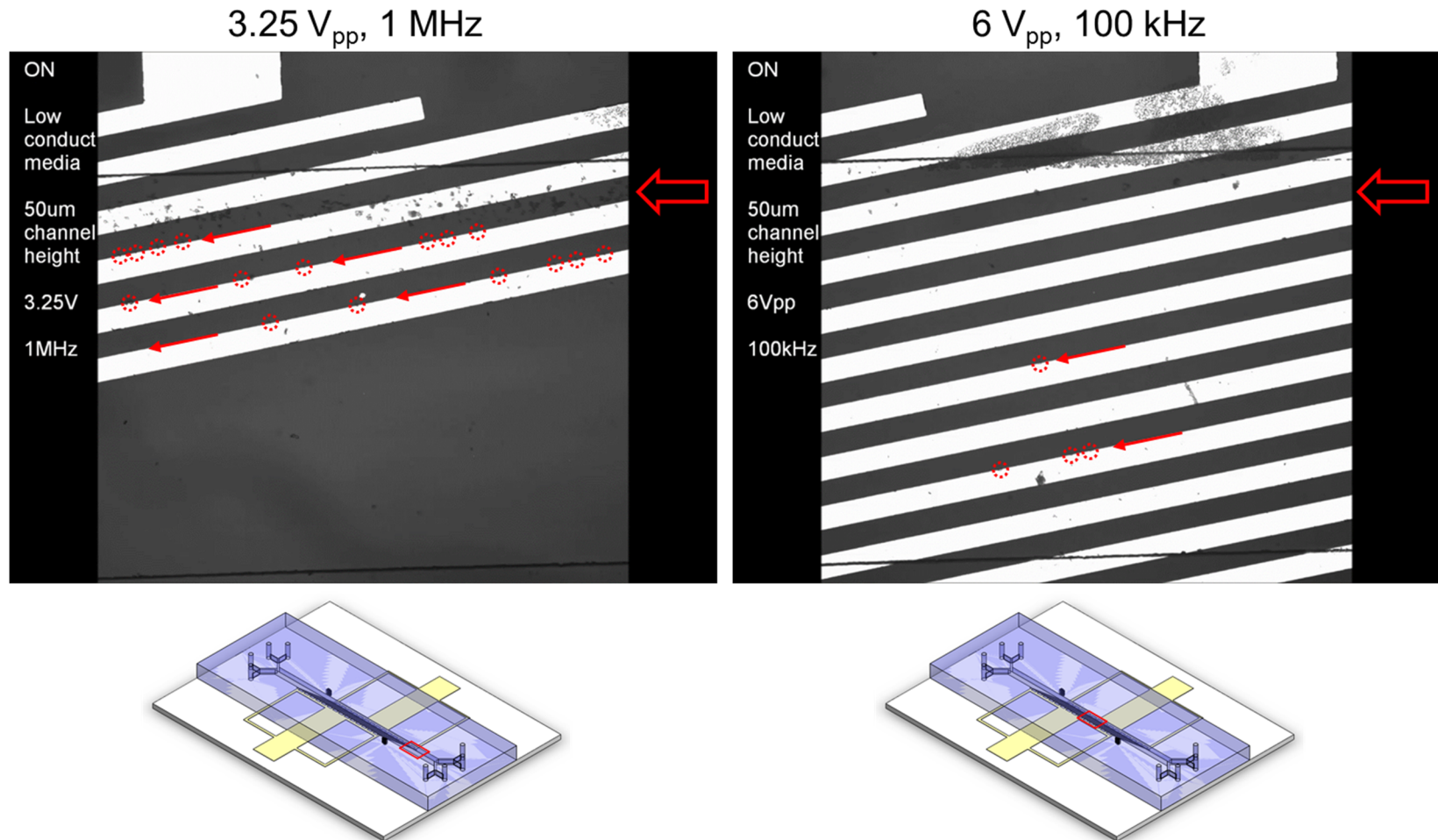
Figure 30. Yeast flowing over the interdigitated electrode (IDE) array of the dielectrophoresis (DEP) device in low conductivity medium (~0.065 mS/cm) experienced positive DEP forces that attracted them to the electrode edges where electric-field was maximum. Yeast enter the image fields-of-view from the right (large red arrows). Some cells were forced to track the electrode edge (red-dotted circles) even though fluid moved from right to left. The locations of these results in the DEP device are shown below the images.

We observed in testing that decreasing the electric-field frequency caused fewer yeast to precisely trace the electrode edges, suggesting that the DEP force decreased in magnitude as frequency was reduced. This decrease in DEP force likely resulted from a smaller f_{CM} magnitude as frequency decreased. At 3.25 V_{pp} and 1 MHz, yeast were immediately attracted all the way to the electrodes (i.e. attracted strongly enough that cells traced the electrode edge) rather than flowing toward the outlet. On the other hand, at 6 V_{pp} and 100 kHz, very few yeast were forced to trace the electrodes immediately as they entered the IDE array. As these yeast traveled further down the IDE array, the pDEP force attracted cells toward the channel bottom until some were forced to trace the electrode edge. We observed smaller yeast become more easily trapped and forced to trace the electrode edge compared to larger yeast and cell clumps. As mentioned in § 2.2.13, although low conductivity medium reduces Joule heating in the microchannel, size-based separation resolution can be improved by using negative DEP (nDEP) forces.

2.1.17. Experimental nDEP did not manipulate yeast as expected

To manipulate yeast using nDEP forces, higher conductivity medium and low to moderate electric-field frequencies should be used. In Fig. 31, we show DEP of yeast in YPD when the channel height was 50 μm. We observed that as yeast entered the separation region from one side of the channel, they were deflected by nDEP forces toward the same side from which they originated.
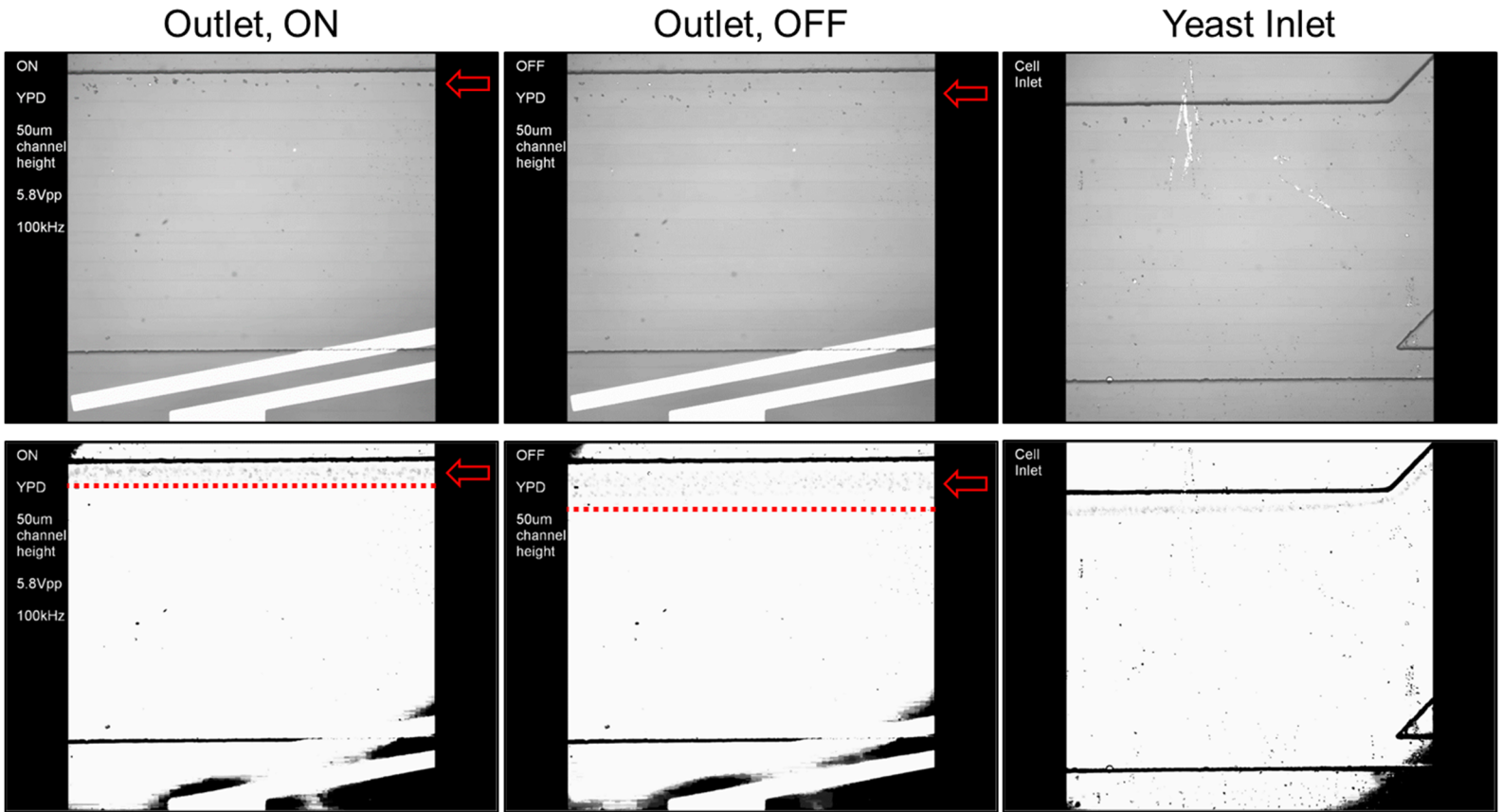
Figure 31. Yeast flowing over the interdigitated electrode (IDE) array of the dielectrophoresis (DEP) device in YPD medium (~5 mS/cm) were expected to deflect perpendicular to the flow direction toward the opposite channel wall. The three images of each row show the inlet (far right) and the outlet with DEP OFF (middle) and ON (far left). Yeast entered the image fields-of-view from the right (red arrows) and flowed into the main microchannel from the right side (top of image). The bottom row of images shows several stacked, black/white thresholded frames of a video captured under the experimental conditions shown in the black pane at left of each image. Cells were expected to deflect toward the opposite channel wall (toward bottom of image), following the electrode angle; however, upon DEP application, the cells deflected toward the right channel wall (top of image). The yeast in the black/white images at the device outlet were all confined between the red-dotted lines and the channel wall (horizontal black line).

Starting at far right of the top row in the figure, yeast entered the main channel through an inlet at the top right of the image. The yeast were flow focused toward the top of the image (toward the right in the channel from the point-of-view of the yeast flow direction) by a buffer inlet (not shown in the image). The middle image of the top row shows the end of the IDE array near the device outlet for the case when DEP was OFF. The far left image shows the outlet when DEP was ON. The red arrows indicate the locations where yeast enter the image field-of-view. Each image in the bottom row is the sum of several black/white thresholded images from videos captured under the experimental conditions of the images in the top row. For example, the black/white image below the yeast inlet is the stack of several frames of a video of yeast flowing into the main channel. By thresholding and stacking the images, the yeast are more easily noticeable (relatively high density of black dots near one side of the channel) and many more yeast can be viewed simultaneously than what can be observed in a single image. The black/white images of the outlets when DEP was OFF and ON have red-dotted horizontal lines marking the furthest that yeast are located from the channel wall at the image top (i.e. that farthest that yeast flow away from the wall from which they originated as they traveled over the IDE array). As described in § 2.1.13 and in Han *et al.*,[65] we expected DEP to deflect yeast toward the center of the microchannel, and larger cells would deflect more than smaller cells because the DEP force is greater for cells with larger volume. As shown in the black/white inlet image, however, yeast enter the separation region (i.e. the IDE array) focused closely against the channel side at top of the image or near the right side of the channel relative to the yeast flow direction. With DEP OFF, the yeast were spread out within the space between the channel wall and red-dotted line. With DEP ON, the yeast were more closely confined to the channel wall; thus cells deflected in the direction opposite to what we expected.

83

To test the deflection of yeast as they enter the IDE array from the opposite side of the main fluidic channel, we loaded yeast into the device as shown in Fig. 32. In this figure, laid out similar to Fig. 31, yeast entering the IDE array from the left channel wall (bottom of image) were deflected away from the channel center toward the channel wall from which the cells originated. All yeast were confined between the left channel walls and red-dotted lines in the images for DEP ON and OFF.

To sum up our experiments thus far, as yeast entered the IDE array from the left (or right) side of the channel, DEP deflected them away from the channel center toward the left (or right) side from which the cells originated. Decreasing frequency and/or increasing applied voltage increased how much the yeast were deflected, but no combination of frequency and voltage produced the expected behavior in which yeast deflect toward the opposite channel wall.

After observing DEP forces deflect yeast in the direction opposite to what was expected, we fabricated a device with the microfluidic channel reduced from 50 μm to 30 μm. By decreasing the channel height for the case when yeast experience nDEP and are repelled away from the IDE array and toward the top of the channel, we can constrain the cells closer to the electrodes so that they experience greater DEP forces. As shown in Figs. 18 and 22, the electric-field magnitude decreases as distance from electrodes increases; thus if we keep all cells closer to the electrodes we potentially might improve the ability to separate them by size. Figure 33 shows the results for yeast traveling in the middle of the channel length, which are similar to what was observed at the device outlet in Fig. 31: even though the channel height was reduced, yeast entering the device from the right side of the main channel (top of image) experienced nDEP forces toward the right wall from which they originated, i.e. in the direction opposite to what we expected.
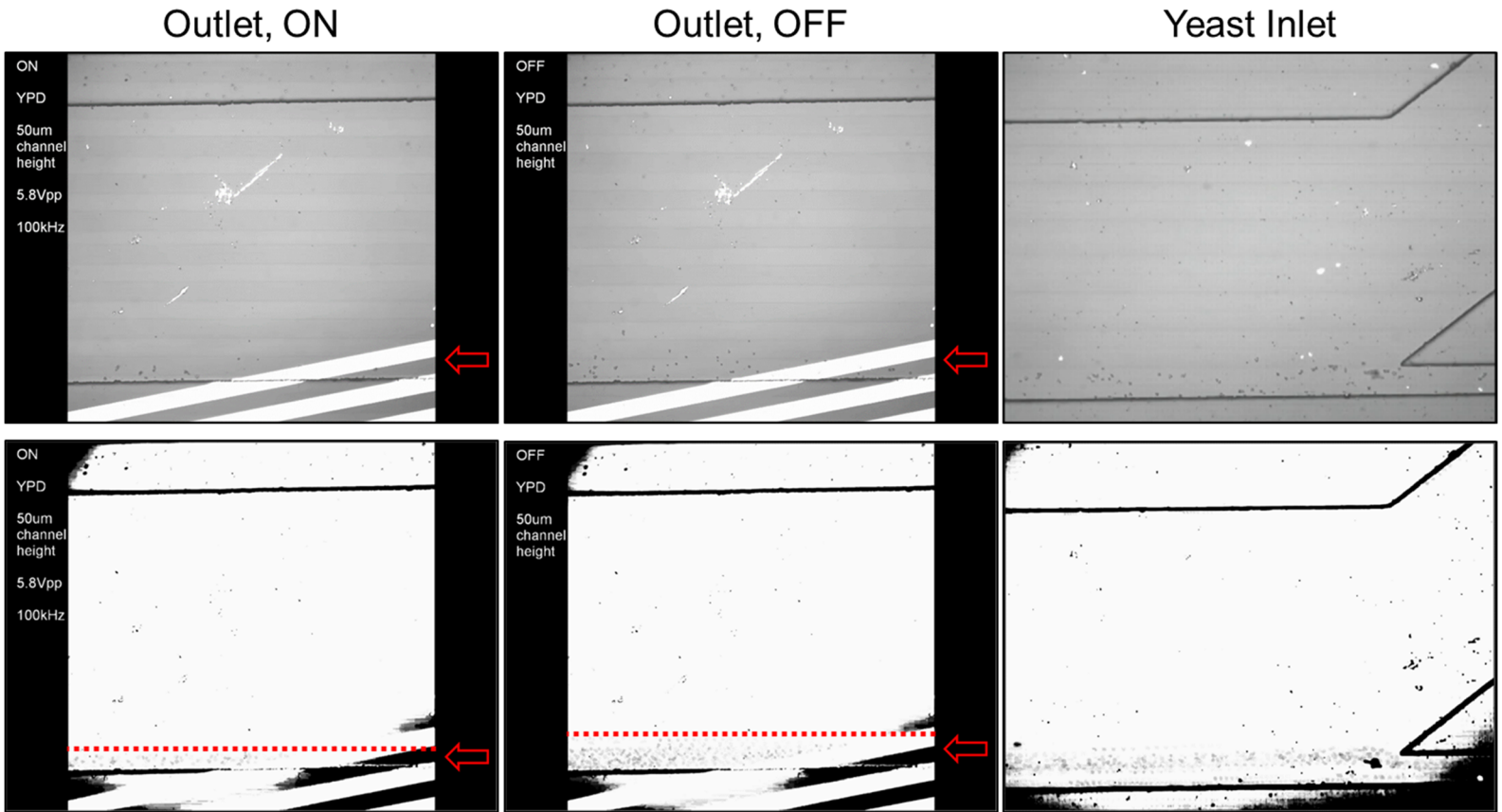
Figure 32. Yeast flowing over the interdigitated electrode (IDE) array of the dielectrophoresis (DEP) device in YPD medium (~5 mS/cm) were expected to deflect perpendicular to the flow direction toward the opposite channel wall. The three images of each row show the inlet (far right) and the outlet with DEP OFF (middle) and ON (far left). Yeast entered the image fields-of-view from the right (red arrows) and flowed into the main microchannel from the left side (bottom of image). The bottom row of images shows several stacked, black/white thresholded frames of a video captured under the experimental conditions shown in the black pane at left of each image. Cells were expected to deflect toward the opposite channel wall (toward top of image); however, upon DEP application, the cells deflected toward the left channel wall (bottom of image). The yeast in the black/white images at the device outlet were all confined between the red-dotted lines and the channel wall (horizontal black line).
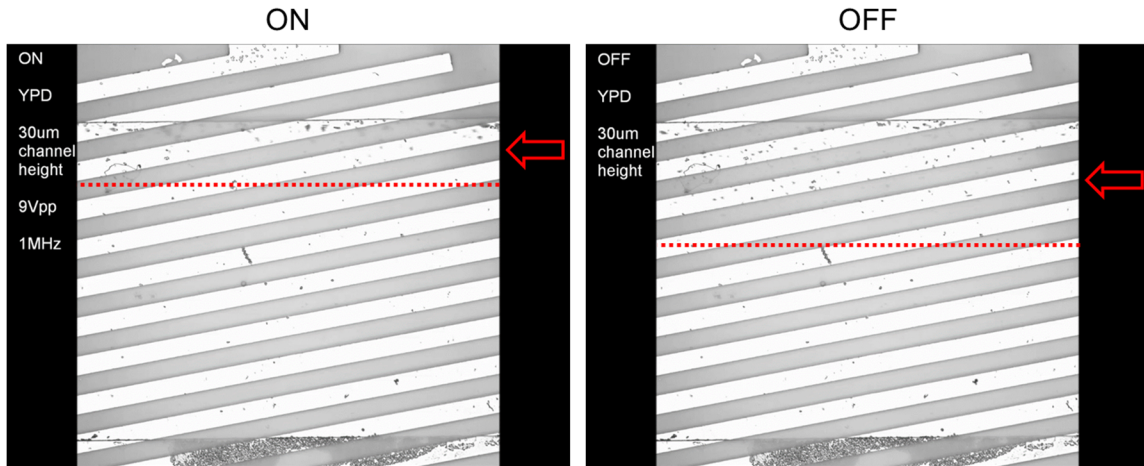
Figure 33. Yeast flowing over the interdigitated electrode (IDE) array of the dielectrophoresis (DEP) device in YPD medium (~5 mS/cm) were expected to deflect perpendicular to the flow direction toward the opposite channel wall. Left image shows the case when DEP was ON and the right when DEP was OFF. Yeast entered the image fields-of-view from the right (red arrows) and flowed into the main microchannel from the right side (top of image). Experimental conditions are shown in the black pane at left of each image. Cells were expected to deflect toward the opposite channel wall (toward bottom of image); however, upon DEP application, the cells deflected toward the right channel wall (top of image) even though the reduced channel height restrained them closer to the electrodes so that the DEP force would be greater than in Figs. 31 and 32. All yeast were confined between the red-dotted lines and the channel wall (horizontal black line).

2.1.18. Explanations for why nDEP results were not consistent with expectations

To explain this unexpected behavior in which yeast were deflected away from the channel center regardless of entering the separation region from the left or right, consider Fig. 34 which shows stationary yeast in YPD being manipulated by nDEP to align with the electrode centers. The left image of the figure shows the dispersed yeast positions before DEP is turned ON, and the right image was taken ~12 s after applying 20 V_{pp} at 10 kHz. Because of the medium conductivity and applied frequency, cells theoretically should experience nDEP that forces them to regions of lowest electric-field magnitude. For the IDE array, the electric-field minima occur at the centers of the electrodes (maxima occur at the electrode edges, see Fig. 22), and the right image of Fig. 34 shows yeast aligning with the electrode centers. Not shown in the figure but observed in

testing, after aligning with the electrode centers, the cells were slowly moved by DEP forces along the electrodes toward the outlet (toward the left in the image). Negative DEP thus forced cells to the electrode centers and then toward the outlet by constraining cells to track the electrode centers.
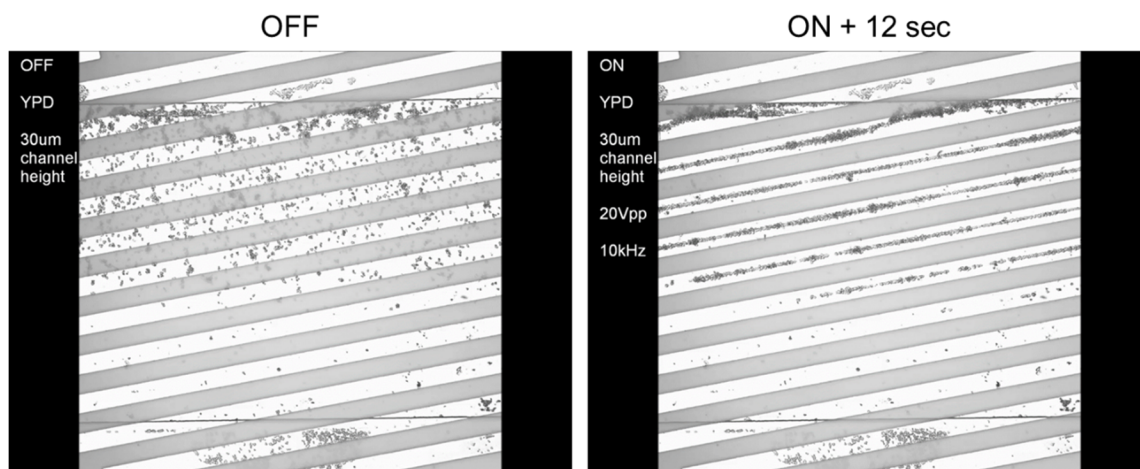
Figure 34. Stationary yeast suspended over the interdigitated electrode (IDE) array of the dielectrophoresis (DEP) device in YPD medium (~5 mS/cm) were repelled to the channel top in the regions above the electrode centers where electric-field magnitude was lower. Left image shows the case when DEP was OFF and the right ~12 s after DEP was applied at 20 V_{pp} and 10 kHz. Regardless of the cell locations within the microchannel, DEP forced them to the nearest electrode center. After aligning with the electrode centers, the yeast were slowly pushed along the electrode center toward the device outlet (toward right of image).

To explain the unexpected deflection behavior, consider that once DEP was turned ON, yeast were immediately attracted to the nearest electrode center regardless of their positions in the microchannel. This initial movement of yeast to the nearest electrode center may have caused the unexpected behavior in which yeast were deflected toward the initial channel wall (right of left) regardless of which side of the channel the cells were on when they entered the IDE array. For example, when yeast entered the separation region from the right side of the channel, they may have been flowing fast enough that they moved through the electric-field peak near the first

electrode they crossed of the IDE array. After moving through this peak, the yeast may have experienced forces toward the right side of the channel where the nearest electric-field minimum was located, in the direction opposite to what we expected in order to achieve size-based separation. Using lower flow rates may possibly produce the desired behavior in which cells deflect toward the opposite channel wall; however, we could not reduce the flow rates much more than what were used in the experiments because the yeast started randomly sticking to the channel walls. That is, the excessively low flow rates contributed to cells and cell clumps becoming caught on the channel walls rather than constantly flowing toward the outlet.

In addition to the initial attraction of cells to the nearest electric-field minima leading to the unexpected deflection behavior, the inlet and outlet designs may have contributed to the non-ideal results. The inlet in our design does not have buffer channels on both sides of the cell inlet like the design used in Han *et al.*[65] Our device flow focused cells completely against the channel wall, whereas the device in Han *et al.* focused cells between two buffer inlets such that the cells were not directly against the channel wall. This difference in inlet designs could have led to yeast being deflected away from the channel center regardless from which side of the channel the cells started. Additionally, the outlets of our device are positioned after the end of the IDE array such that no electrodes are located in the outlet channels. When the IDE array ends, the electric-field magnitude quickly goes to zero (see Fig. 22) in a spatial pattern parallel to the last electrode length. Because nDEP forces yeast to regions of lowest electric-field, the electric-field pattern at the end of the IDE array may have manipulated cells in such a way to produce the unexpected deflection behavior that we observed. A potential improvement on the design is to adjust the positions of outlets to overlap the IDE array so that the PDMS outlet walls prevent cells from following the electric-field drop-off at the end of the IDE array.

Our final explanation for why yeast were deflected toward the channel walls from which they started is that fluidic leaks through the channel sides helped produce the unexpected results. In our experiments, we observed that with DEP ON the yeast seemed to flow more quickly toward the device outlet, i.e., DEP appeared to increase the flow rate. Additionally, we observed many cells escape through the main channel sides and become trapped between the PDMS and Au electrode. These cells can be seen outside of the channel boundaries in Figs. 33 and 34. The increase in flow rate and evidence of cells flowing through the channel sides support the hypothesis that fluid medium was pulled outside of the channel between the PDMS and electrodes (which are not irreversibly bonded together) even when the flow rates were not excessively high. In other words, we believe that DEP might have pulled cells and medium out through the right and left channel walls, and this outflow through the channel walls could have led to the unexpected deflection direction that we observed in our testing.

We had hypothesized that we could separate yeast by size in much the same way that nDEP separated blood cells by size[65]; however, blood cells and yeast have somewhat different CM factors across moderate to high frequencies, and differences in CM factor create dissimilar DEP forces. Sano *et al*. plotted the CM factor for red blood cells suspended in relatively low conductivity medium (0.01 S/m).[84,85] Compared to yeast in low conductivity medium (0.001 S/m) which have $f_{CM}>0$ across all frequencies, blood cells have $f_{CM}<0$ for frequencies up to ~15 kHz and $f_{CM}>0$ when frequency is >15 kHz. Yeast must be suspended in high conductivity medium (~0.1 S/m) to have $f_{CM}<0$ for frequencies up to ~1 MHz. Thus because the CM factor of yeast differs from that of blood cells, we should not have expected similar size-based separation in our experiments.

2.1.19. DEP showed poor separation of yeast by size and potential for harmful heat generation

In summary, the DEP device we designed and tested did not separate yeast by size as expected. DEP heat generation, the production of nDEP versus pDEP, and size-based separation resolution are largely determined by fluid medium conductivity and electric-field frequency. Using low conductivity medium ($\sigma \sim 0.05$ mS/cm) in DEP devices is recommended to reduce Joule heating that can harm biological cells; however, for best size-based separation resolution of yeast traveling over an IDE array, higher conductivity medium ($\sigma \sim 5$ mS/cm) should be used along with low to moderate frequencies. High conductivity medium results in large Joule heating and thus requires adding electrode passivation to limit heat generation. Passivation, though, can reduce electric-field magnitude such that the DEP force is less noticeable. In our experiments, even when using high conductivity medium that likely allowed excess heat, we did not observe promising size-based separation of yeast. Future designs of the yeast DEP device could (i) include an extra buffer inlet (see § 2.1.18) to focus cells further from channel wall, (ii) let the outlet channel walls overlap the IDE array, and (iii) reduce the electrode widths to limit fluid leaks. These changes might improve separating yeast; however, because high conductivity medium, which is needed to produce nDEP, can generate biologically-unsafe Joule heating, we concluded DEP was not the best option for the size-based separation subsystem of our aged yeast generator.

2.1.20. Theory for size-based acoustic separation

After selecting DEP and acoustic techniques as candidates for our aged yeast generator, we began investigating both in parallel for this application. With DEP ruled out as a candidate, we now discuss the background of acoustophoresis and our experimental progress in applying it to yeast aging.

Particles flowing through a microchannel in which standing acoustic waves have been formed experience an acoustic force given by[86]

$$F_a = -\left(\frac{\pi p^2 V_c \beta_m}{2\lambda}\right)\Phi(\beta,\rho)\sin(2kx)$$

$$\Phi(\beta, \rho) = \frac{5\rho_c - 2\rho_m}{2\rho_c + \rho_m} - \frac{\beta_c}{\beta_m}$$

where p is the pressure amplitude of the standing waves, V_c is the cell volume, ρ_c (β_c) and ρ_m (β_m) are the densities (compressibilities) of the cell and medium, respectively, k is wave number, and λ is wavelength. As the equation above shows, $F_a \propto V_c$, so larger cells experience larger acoustic forces compared to smaller cells. In Fig. 35, as cells enter a microchannel at approximately the same location, acoustic forces deflect cells toward the center of the microchannel where an acoustic node has been formed. Acoustic nodes are regions of high acoustic pressure, while antinodes are regions of low pressure. The locations and number of nodes/antinodes are determined by the acoustic frequency relative to the channel width. For a single node to form at the channel center and antinodes at the channel walls as shown in Fig. 35, the acoustic wavelength must be 2x the channel width. Such standing waves are referred to as first-order harmonics. Knowing the speed of sound in a given medium thus allows us to calculate the required acoustic frequency to create standing waves in a channel with known width. Also, for a channel of known width, higher-order harmonics with more nodes and anti-nodes than what are shown in Fig. 35 can be generated by increasing the frequency by multiples of half the wavelength.

$$F_a = -\left(\frac{\pi p^2 V_c \beta_m}{2\lambda}\right)\Phi(\beta,\rho)\sin(2kx) \qquad \Phi(\beta,\rho) = \frac{5\rho_c - 2\rho_m}{2\rho_c + \rho_m} - \frac{\beta_c}{\beta_m}$$

⇐ Acoustophoresis ⇒
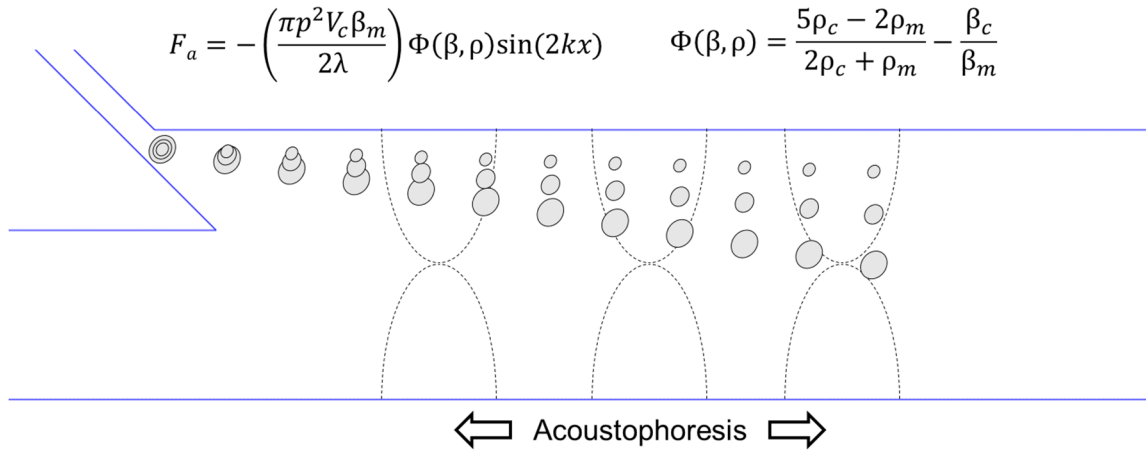
Figure 35. Particles flowing through a microchannel experience acoustic forces that deflect them toward the channel center where an acoustic node from standing waves has formed. Particles with larger volume experience larger acoustic forces and thus deflect more than smaller cells.

Acoustophoresis has been well-developed in the literature.[27,62,63,86-97] For instance, Yang and Soh developed a high-throughput system to separate live mammalian cells from a mixture also containing apoptotic cells.[27] Live mammalian cells have larger volume but similar density and compressibility compared to dead cells, so the acoustic forces are stronger on live cells. We aim to exploit this same size-dependence to separate larger mother yeast from smaller daughters. As discussed in § 2.1.7, acoustic separation is gentle, efficient, and label-free, which make acoustophoresis a promising approach for this application.

2.1.21. Design and operational parameters for acoustic deflection device

To investigate the size-based separation resolution of acoustic forces, we fabricated and tested the microfluidic device in Fig. 36. Using this device in experiments, we found promising separation of yeast by size (discussed below), after which we aimed to optimize the acoustic power and outlet y-position cut-off at the device outlet (bottom Fig. 36).
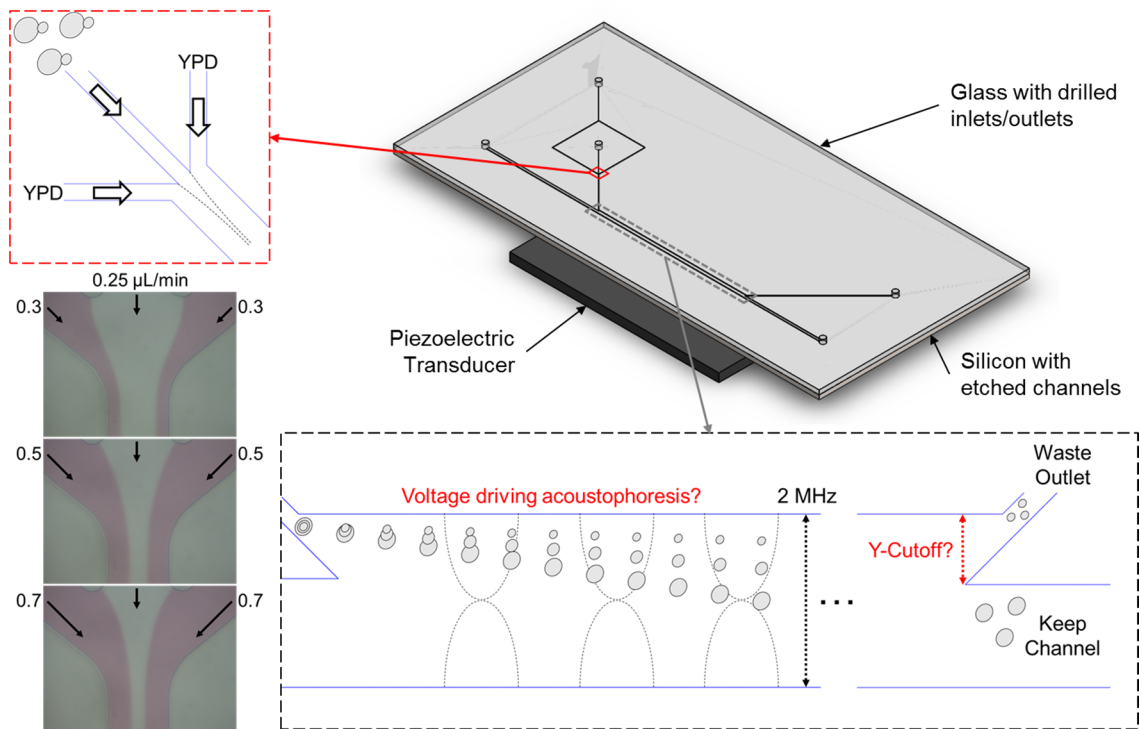
Figure 36. Microfluidic acoustic deflection device for testing the size-based separation of yeast. Device is illustrated at top right and consists of a transducer, silicon with etched microfluidic channels, and glass with inlets/outlets. Yeast enter the device through the center inlet and are flow focused by size channels carrying yeast extract peptone dextrose (YPD) in inset at top left. Flow focusing is achieved because laminar flow dominates at the microscale. At bottom left, laminar flow between red dye and water allows the fluids to flow side by side without mixing. Yeast are flow focused into the separation region (bottom of figure) where acoustic forces separate the yeast by size. The separation is finalized when smaller cells flow into a waste outlet and larger cells into a keep channel. Important operational and design parameters that must be defined are the voltage applied to produce the acoustic waves and the y-cutoff separating cells that are discarded from those that are kept.

The device consisted of a glass layer with drilled inlets/outlets, a silicon layer with etched microfluidic channels, and a piezoelectric transducer (PZT) to generate the acoustic standing waves. Cells and culture media enter the device as shown in the red inset at top left. Mother and daughter yeast are flow focused by streams of culture medium (YPD) on both sides of the cell inlet. Flow focusing is possible because of the dominance of laminar flow at the microscale that allows liquids to flow side by side in a microchannel and mix only by diffusions.

Examples of laminar flow are shown at bottom left of the figure. In these examples, water flowed through the center channel of all three images at a flow rate of 0.25 µL/min, and red dye entered the junction at three different flow rates (0.3, 0.5, 0.7 µL/min). As the red dye flow rate increased, the center channel narrowed because laminar flow between the water and red dye prevented convective mixing of the fluids. In the acoustic device, the yeast are flow focused by programming the side inlet buffers appropriately. Flow focusing improves size-based separation resolution because cells enter the separation region at approximately the same location and thus deflect toward the channel center starting at the same initial y-position (defined perpendicular to the channel wall). Because of flow focusing, the trajectories as cells flow through the acoustic radiation would depend only on size and would not vary by start position. After yeast are flow focused, they enter the main channel. As cells flow from left to right through the main channel with acoustic radiation OFF, laminar flow keeps them at approximately the same y-position through the entire channel length; diffusion is the only mechanism deflecting them toward the channel center (downward in the diagram). If acoustic radiation is applied, cells experience a force deflecting them to the channel center where an acoustic node is formed from standing waves generated by the PZT. In this scenario, the frequency is chosen to create a single node at the channel center.

Referring to the lower diagram in Fig. 36, we now consider the design and operational parameters that must be defined. First, the acoustic frequency is determined by the channel width. For channel width of 375 µm (see Fig. 37 for device dimensions), the acoustic frequency is ~2 MHz if the fluid in the microchannel is water. Second, the PZT is driven by an amplified function generator, so in addition to defining the excitation frequency, the voltage applied to the PZT must also be selected. As shown in the equation for acoustic force F_a, the acoustic pressure amplitude p directly determines F_a, and p depends on the voltage driving the piezoelectric

transducer. Thus the applied voltage largely impacts the distances that cells are deflected in the acoustic region. Third, an ideal y-cutoff must be chosen for the distance between the channel wall and intersection of the outlet channels. As shown at bottom in Fig. 36, after separating by size, larger yeast flow into the outlet labeled "Keep Channel" while the smaller cells flow to the "Waste Outlet." The y-cutoff must be optimized for separating the yeast. If we set the main channel length at ~17 mm (Fig. 37) and the width at 375 μm, we should select the y-cutoff somewhere between (i) the y-position at the intersection of the inlet and main channels and (ii) the middle of the channel where acoustic nodes are formed. With the main channel length/width and y-cutoff defined, all important device dimensions are set. The only remaining operational parameters are the inlet flow rates, which were defined during testing as described in § 2.1.22.
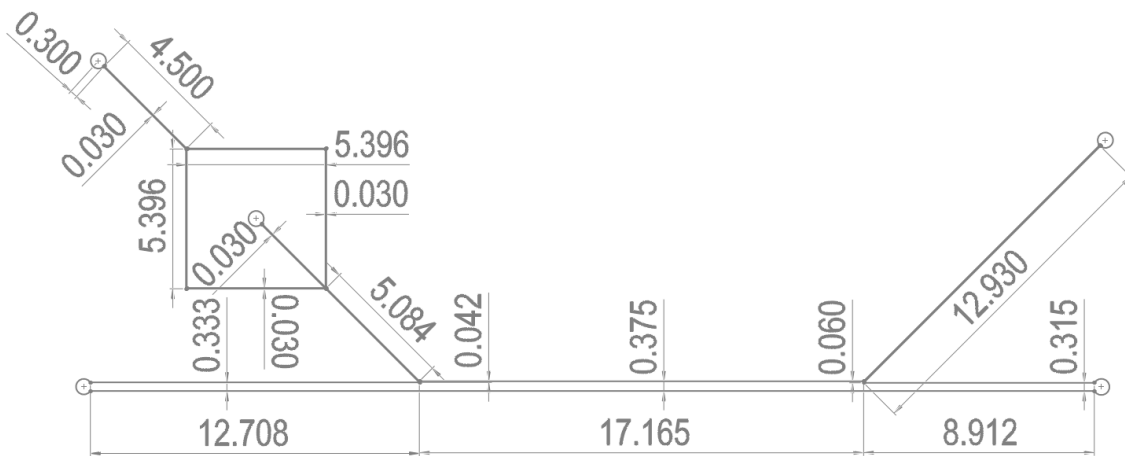
Figure 37. Dimensions of the microfluidic channels of the acoustic deflection device in Fig. 36. All units are mm.

2.1.22. Acoustic device fabrication and experimental procedure

The acoustic device dimensions are provided in Fig. 37. We thank Dr. Sungman Kim and Dr. Han Wang for providing these initial designs and fabricating test devices. The microfluidic channel was etched in silicon using standard processing. First, aluminum was sputtered onto

Piranha-cleaned silicon wafers using a Lesker PVD 75 Metal Sputter to achieve a thickness of ~500 nm. Shipley S1818 (Micro-Chem) was spin-coated onto the aluminum at 4000 rpm for 30 s to obtain a ~1.5 µm layer of photoresist. The wafers were soft-baked at 110°C for 5 min. An MA6 mask aligner with film masks from CAD Art Services exposed the photoresist with UV light at 168 mW/cm^2. After developing with MF-319 for ~1 min and post-baking at 120°C for 10 min, the aluminum was etched using aluminum etchant for ~30 min. Resist was removed by rinsing in acetone. After patterning the aluminum, the wafers were loaded into Oxford PlasmaLab 100 ICP machine, and microfluidic channels were etched into Si using reactive-ion etching (RIE) at -100°C, APC 10 mTorr, SF$_6$ at 70 sccm, O$_2$ at 4 sccm, FP (DC) 12W, ICP 900W, at a rate of ~3 µm/min to achieve a final depth of ~50 µm. The aluminum etch mask was removed using aluminum etchant. Next, inlets/outlets were drilled into a glass slide using a drill press, and the microfluidic channels in the silicon were sealed by anodically bonding the glass by applying 700 V for 40 min at 400°C. A dicing saw was used to separate the individual devices of a wafer. Plastic luer fittings were glued to the inlets/outlets using Quik-Set Epoxy (Loctite), and 0.01-in inner-diameter plastic tubing was subsequently epoxied into the plastic luer fittings. A PZT transducer square (PZ26 transducer) was attached to the backside of the silicon layer using wax (Crystalbond). Electrical wires were soldered onto both sides of the PZT.

After fabricating the acoustic device, it was sterilized by flowing ethanol, PBS, and YPD through the device. Yeast were prepared and loaded into syringes as described in § 2.1.2. YPD was also loaded into several syringes to be used as buffers. The syringes were attached to the plastic tubing of the device, which was placed on the stage of an upright microscope (Nikon Eclipse LV100) with camera (Hamamatsu ORCA-Flash4.0 V2 C11440-22CU) and supporting software (NIS-Elements Br Microscope Imaging Software). After attaching all syringes to syringe pumps (Chemyx Fusion 400 Touch Syringe Pump), yeast flowed into the device through

the inlets at rates between 5 µL/hr and 20 µL/hr. The flow rates for side focusing channels were

set between 10 µL/hr and 40 µL/hr, and those for main channel between 50 µL/hr and 150 µL/hr.

Acoustic radiation was produced by programming a 1.73 MHz sinusoidal wave at voltages

between 20 mV and 80 mV on a function generator (Tektronix AFG 3021B Single Channel

Arbitrary/Function Generator). The signal from the function generator was passed through a

50dB RF Power Amplifier (E&I). Alligator connectors from the amplifier were attached to the

electrical wiring that was previously soldered to the PZT. While observing yeast under the

microscope at different locations along the channel length, voltage was increased until cells just

started deflecting toward the channel center. Voltage was increased until most cells were

deflected to the channel center. For several voltages between the lowest value that just deflected

cells and the highest that deflected most cells, videos were captured at the middle of the channel

length and at the outlet. Videos were not recorded until >30 s after the voltage was changed.

After the experiments, videos were processed in MATLAB (MathWorks) to determine

the relations between cell size and y-position (how much the cell had deflected toward the

channel center) for several applied voltages.

2.1.23. Promising size-based separation of yeast using acoustic deflection device

As mentioned above, our initial testing of the acoustic deflection device showed promising

separation of yeast by size. Figure 38 shows images of the device outlet. Each image

corresponds to a different applied voltage from 0 V (OFF) or 25 mV to 70 mV in 5 mV

increments. With the exception of the top left color image, all black/white images are the sum of

several frames of videos that have been black/white thresholded so that more yeast could be

viewed simultaneously than what can be observed in a single video frame. The dark black ovals

in the channel consistent in all images are debris and fabrication scars, while the yeast are the

gray objects. Yeast enter the image field-of-view from the left indicated by the red arrow which is aligned approximately to the average y-position of all visible yeast. As the voltage driving the PZT was increased from OFF to 70 mV, the yeast were deflected more toward the channel center. With the acoustic OFF, most yeast were near the channel wall at the top of the "OFF" image. At >60 mV, most yeast have been deflected to the center of the channel where the acoustic node has been formed. This behavior agrees very well with expectations. In addition to cells being forced more to the channel center as acoustic amplitude increased, we observed larger cells and cell clumps (groups of 2+ attached yeast) deflected more than smaller cells. Although this size-based separation is promising, it foreshadows a problem we address in § 2.3: because cell clumps are deflected approximately proportionate to combined cell volume, smaller cells that should be removed from the device through the waste outlet may flow into the keep channel because they are attached to other cells. Thus cell clumps may worsen size-based separation resolution and motivate the need for adding an agitation mechanism to the system to promote separation of cell clumps (see § 2.3).
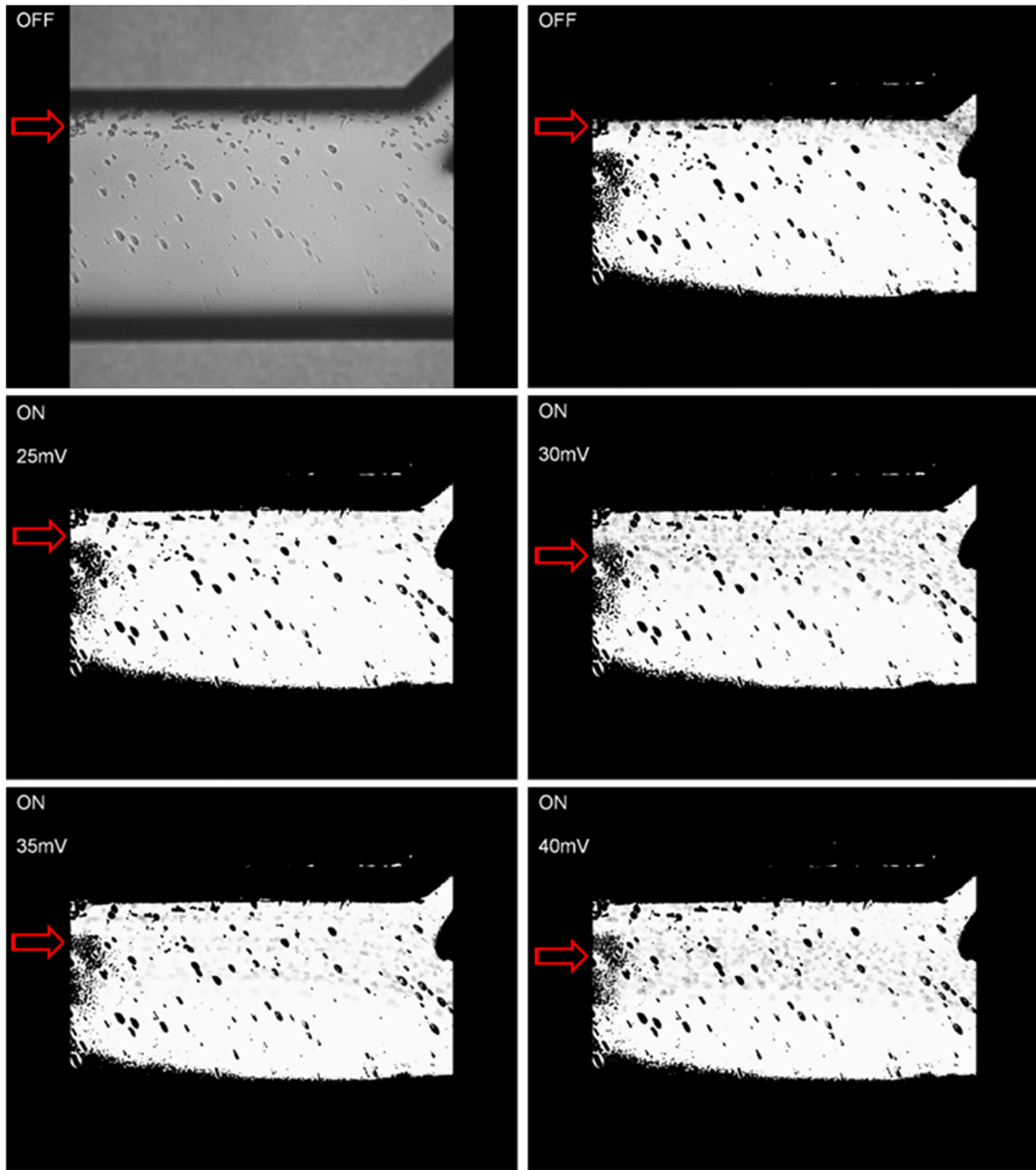
Figure 38. Experimental results of the acoustic deflection device show promising size-based separation of yeast. Each image corresponds to a different applied voltage. Except for the top left image, all black/white images are stacked, thresholded frames from videos captured under the experimental conditions indicated in the black panes at left of images. The yeast are the gray objects in the microchannels and flowed from left to right in the experiment. The red arrows approximate the average y-position of all yeast in the field-of-view. Consistent with expectations, as acoustic power was increased, more cells were deflected toward the channel center where standing waves formed an acoustic node.
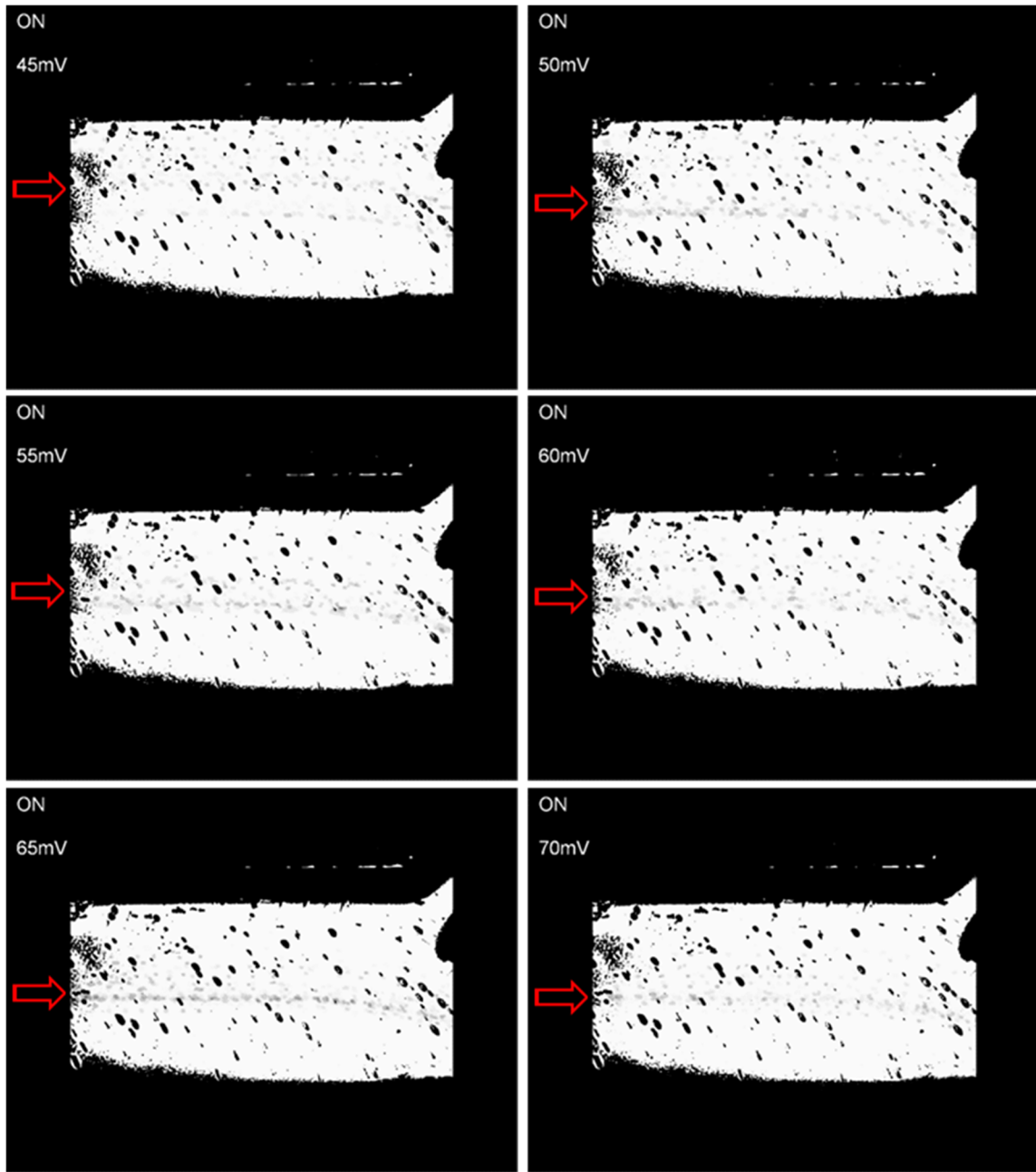
Figure 38. (continued)

2.1.24. Yeast size analysis at acoustic device outlet using circle-fit algorithm

Our goal with this test deflection device was to determine the optimal applied voltage and y-cutoff (see Fig. 36) for yeast separation; therefore, we processed the videos for each acoustic

power in MATLAB to evaluate how final y-position for each cell varied with cell size. More specifically, we cropped each frame of a video to isolate a single region-of-interest (ROI) indicated by the red-dotted rectangle over the outlet image at bottom in Fig. 39.
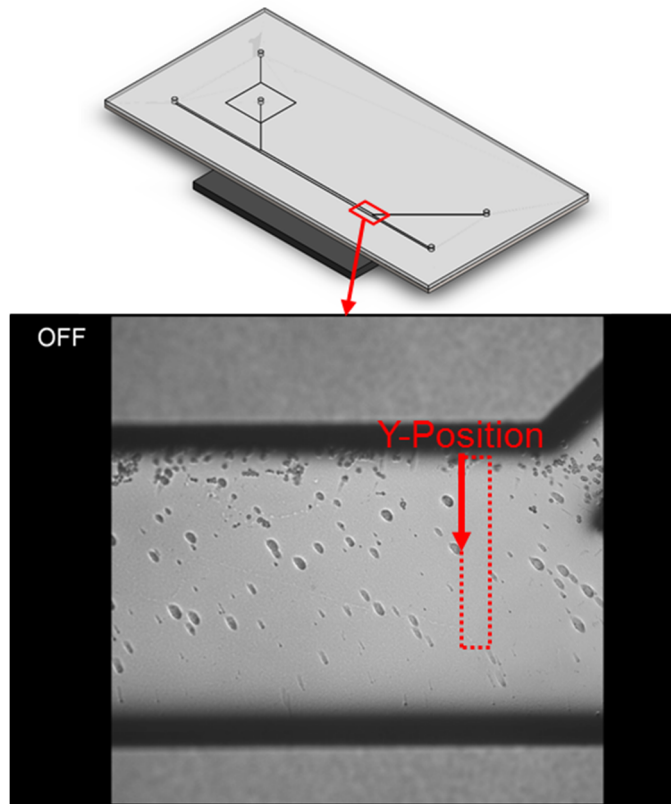
Figure 39. In order to analyze the relation between cell size and y-position as acoustic power varied, videos were captured at the device outlet (top of diagram) and a region-of-interest was identified (bottom). The region-of-interest was processed in MATLAB as shown in Fig. 40. The y-position in the analyses was defined as shown at bottom.

For each cropped ROI, we applied a built-in MATLAB function that fits objects in the image to circles based on several user-defined parameters (see § 2.1.3 for more detail). We used the function to calculate cell diameter and x/y-coordinates of its center, after which we plotted the cell y-position versus cell size. Example images illustrating this process are shown in Fig. 40.
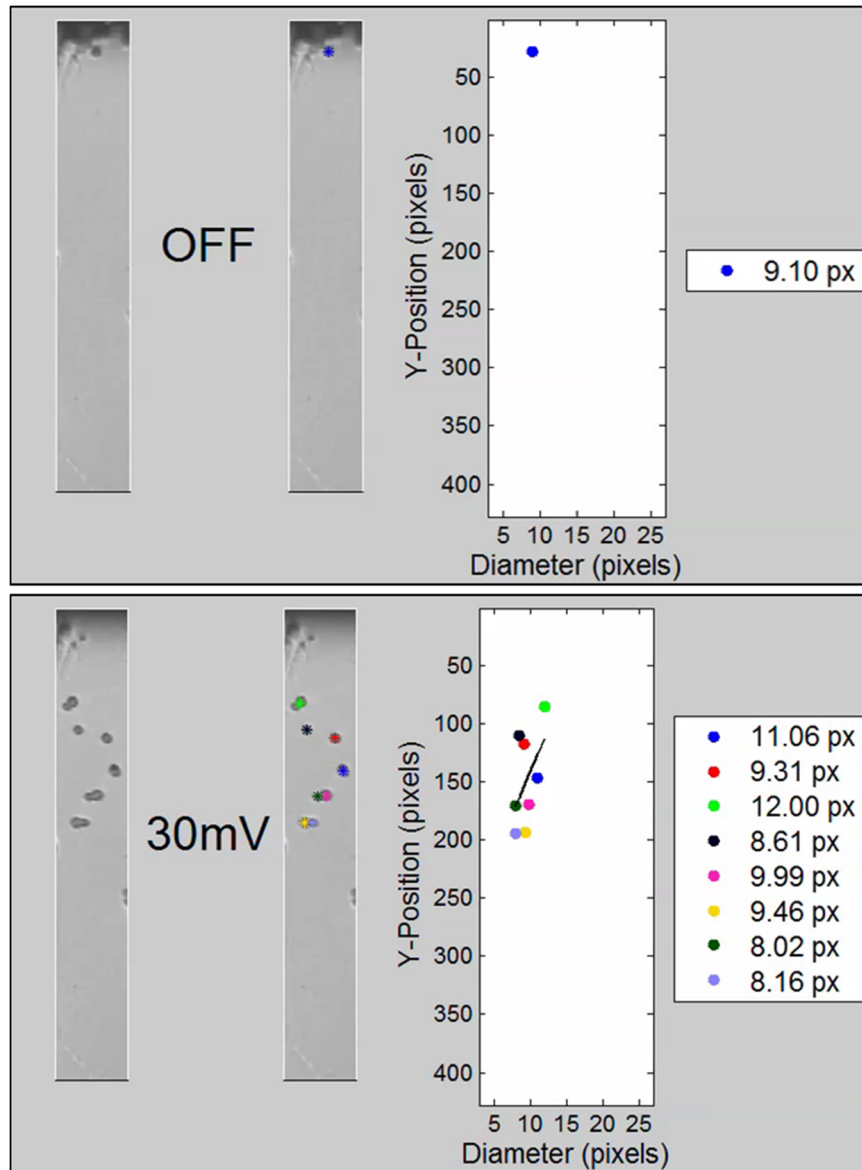
Figure 40. Example images from the procedure to analyze the relation between cell size and y-position as acoustic power varied. The regions-of-interest (ROIs) identified at the acoustic deflection device outlet (Fig. 39) are shown at far left of each image. The voltage driving the acoustophoresis is displayed next to the original ROI. Next in each image is the ROI with colored asterisks plotted over the yeast in the images that have been fit to circles using a function from the MATLAB Image Processing Toolbox. The yeast y-positions relative to the image coordinates are plotted against the cell diameter at right of each image. A legend displays the precise cell size. If >1 yeast was identified in the ROI, a linear regression relating y-position and diameter was also plotted.
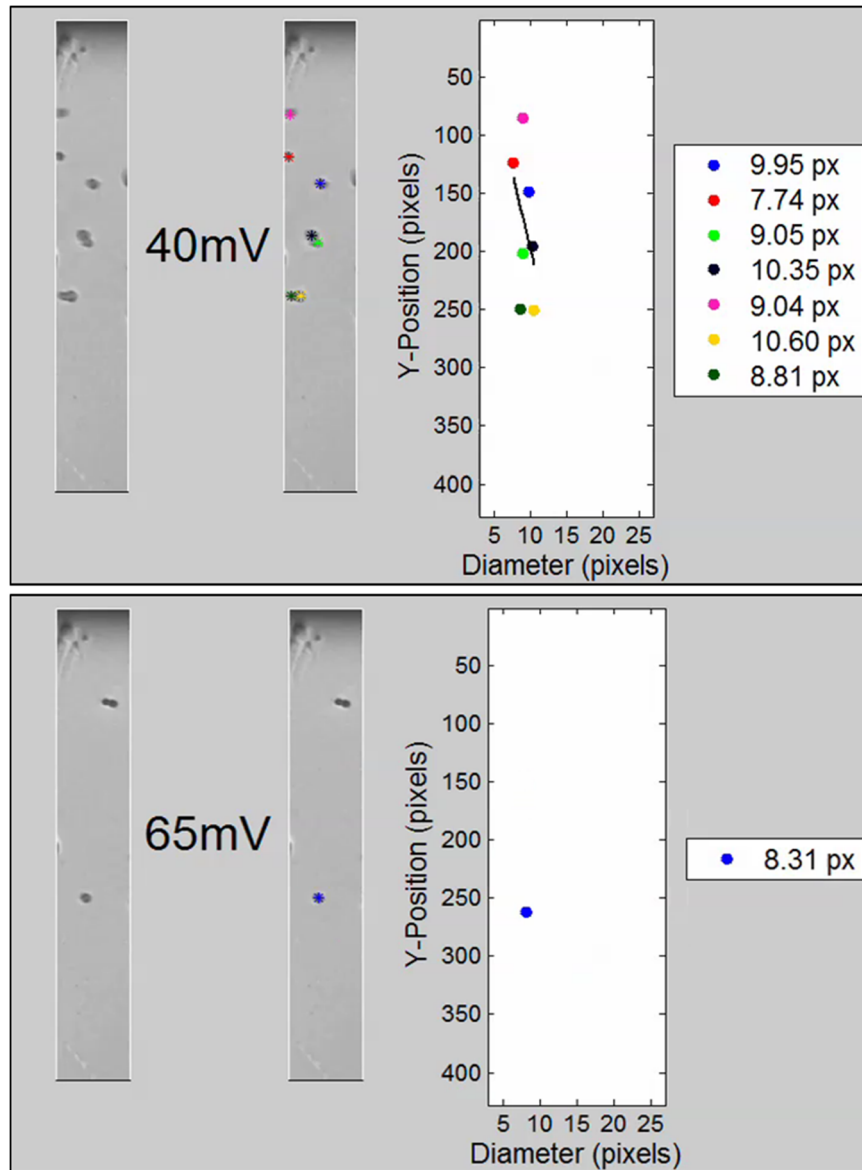
Figure 40. (continued)

In each of these examples, the original ROI is plotted at left, the applied voltage is indicated to the right of the original ROI, and then the original ROI is shown along with the circle centers plotted on top with asterisks of varying colors. The far right plot of each image shows y-position against diameter, and the legend indicates the circle size. If 2 or more circles were identified in the image, a linear regression describing y-position vs cell size was plotted.

The y-axis of this plot is reversed to correspond with the pixel at which the circle is located in the actual image (pixel at row 1, column 1 is at top left in the image). After processing all videos for the different applied voltages, we produced a single plot of yeast size vs y-position for all data points. Figure 39 bottom indicates how y-position is defined relative to the ROI at the device outlet, and Fig. 41 shows the results; therefore, according to this convention, yeast experiencing more deflection toward the channel center have larger y-positions. Figure 41 top shows data points for all applied voltages. Along with the individual data points which are color-coded for a particular voltage, a linear regression is also plotted in the graph to discern how yeast diameter varies with y-position for that voltage. The linear fit lines are also plotted in their own plot without any data points (bottom Fig. 41).

The trend of yeast diameter versus y-position in these plots agrees with expectations. With no acoustic radiation, yeast diameter is not correlated with a particular y-position as indicated by the vertical line in the plot for the case when acoustic was OFF. As applied voltage increased, the slopes of the linear regression lines decrease (relative to the way in which the axes are defined) and approach 45° relative to the axes. As voltage was increased further, more and more cells were deflected to the channel center and so the slopes of the linear regressions for these higher voltages become more vertical, indicating less size-based differentiation by y-position. Ideally, we would choose the voltage whose linear fit is close to 45° relative to the plots because this behavior reflects the best size-based separation.
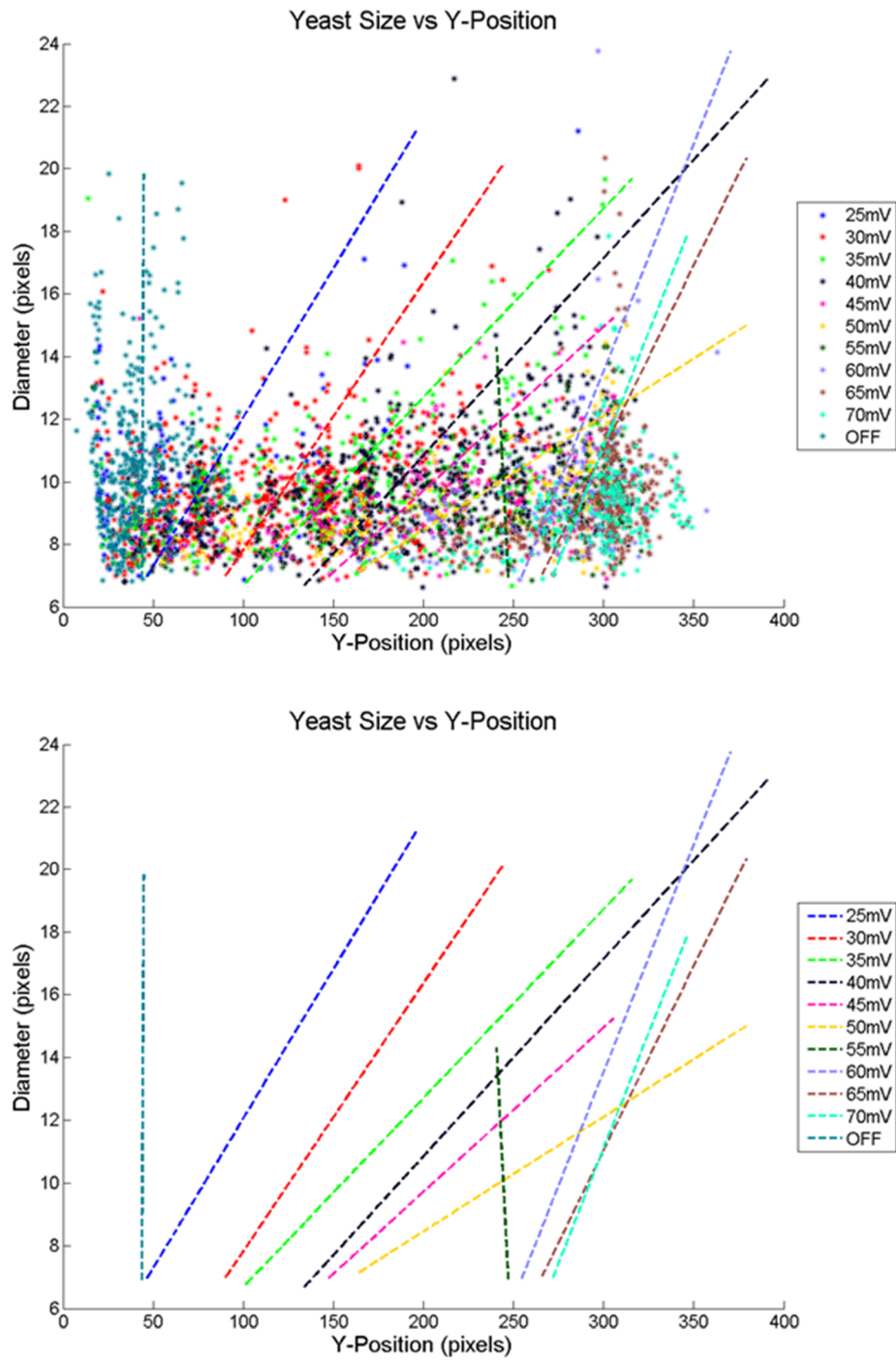
Figure 41. Results of the procedure described in Figs. 39 and 40 to determine the relation between yeast positions at the acoustic deflection device outlet and yeast size as acoustic power varied. Top plot shows data points for all applied voltages along with linear regressions for each voltage. Bottom plot shows only the linear regressions. The trend in size vs y-position as acoustic power increased is consistent with expectations (see § 2.1.26).

2.1.25. Fitting yeast to circles skews the analysis of size vs y-position

Although the plots of yeast diameter versus y-position in Fig. 41 show the expected trends, the results are skewed because fitting individual cells to circles did not correctly find the size and y-position for cell clumps. Consider the series of images in Fig. 42. Part A shows the original ROI, and B displays the original ROI with circles fit to the cells. In B, we see that fitting circles to the cells is useful when we want to identify cells that may be attached to each other as seen with the lowest pair of cells in the images. Fitting cells to circles also improves calculating the true cell size for the case when cells are at the edges of the field-of-view. Finally, using the circle-fit procedure also allows us to find circles that are in the shadow at the top of the image. If we black/white threshold the image as in C, we would not be able to find this cell in the shadow. Also notice how fitting circles to cells in thresholded images can produce false cells as seen in D.
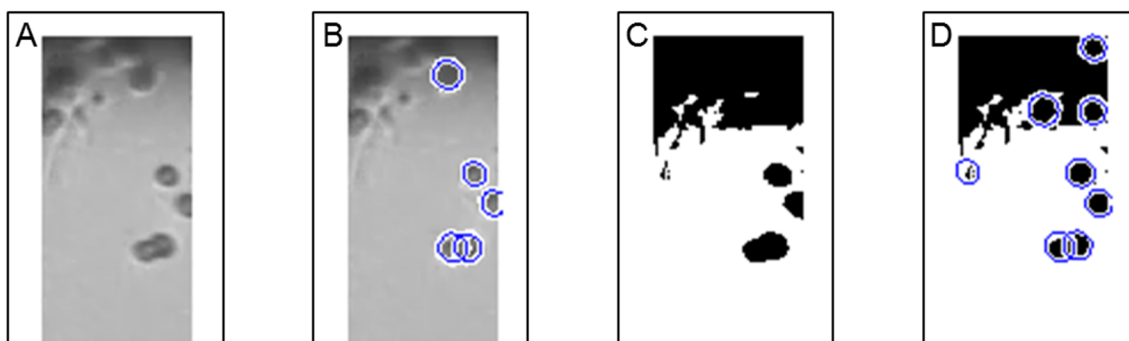
Figure 42. Illustration of the error that occurred when yeast were fit to circles during the investigation of y-position vs yeast size. A) Original image of region-of-interest (ROI). B) Circles plotted over the yeast in the original ROI. The cells closest to the bottom of the image were identified as 2 separate cells rather than a single object that had deflected toward the channel center because of the acoustic forces. C) Black/white thresholded image of the ROI. D) Using the circle-fit procedure on the thresholded image did not correctly identify the yeast in the image.

Fitting cells to circles skews the results because cell clumps, consisting of various-sized cells, were often deflected toward the channel center more than single cells. The circle-fit

algorithm identifies the individual cells comprising the clump, and thus some cells especially the smaller ones were calculated to have larger y-positions (measured from the top of the image) than what they would have if they were not attached to other cells.

2.1.26. Yeast size analysis repeated using region-find procedure

A more accurate correlation between cell size and y-position can be determined if we compute the total two-dimensional area of cells and cell clumps after black/white thresholding the images like in Fig. 42C. We therefore repeated the acoustic outlet analysis by thresholding the ROI in each video frame, finding the centroid and total area for relevant black objects in the thresholded images, and reproducing the size versus y-position plots. Figure 43 shows examples of this procedure laid out similar to the images representing the circle-fit analysis in Fig. 40. The size and y-position data for all cells and cell clumps at all acoustic voltages is displayed at top in Fig. 44. The plots also include linear regressions for each applied voltage. Figure 44 bottom shows only these linear regressions, and their trend as voltage increased is consistent with expectations. For acoustic radiation OFF, the slope of the line is nearly vertical indicating no relation between cell area and y-position. As voltage increased up to ~45 mV, the slopes of the linear-fit lines decrease and approach a 45° angle relative to the plot axes. For voltages >45 mV, the slopes become steeper because cells and cell clumps of all sizes are deflected more to the channel center and the correlation between cell size and y-position diminishes.
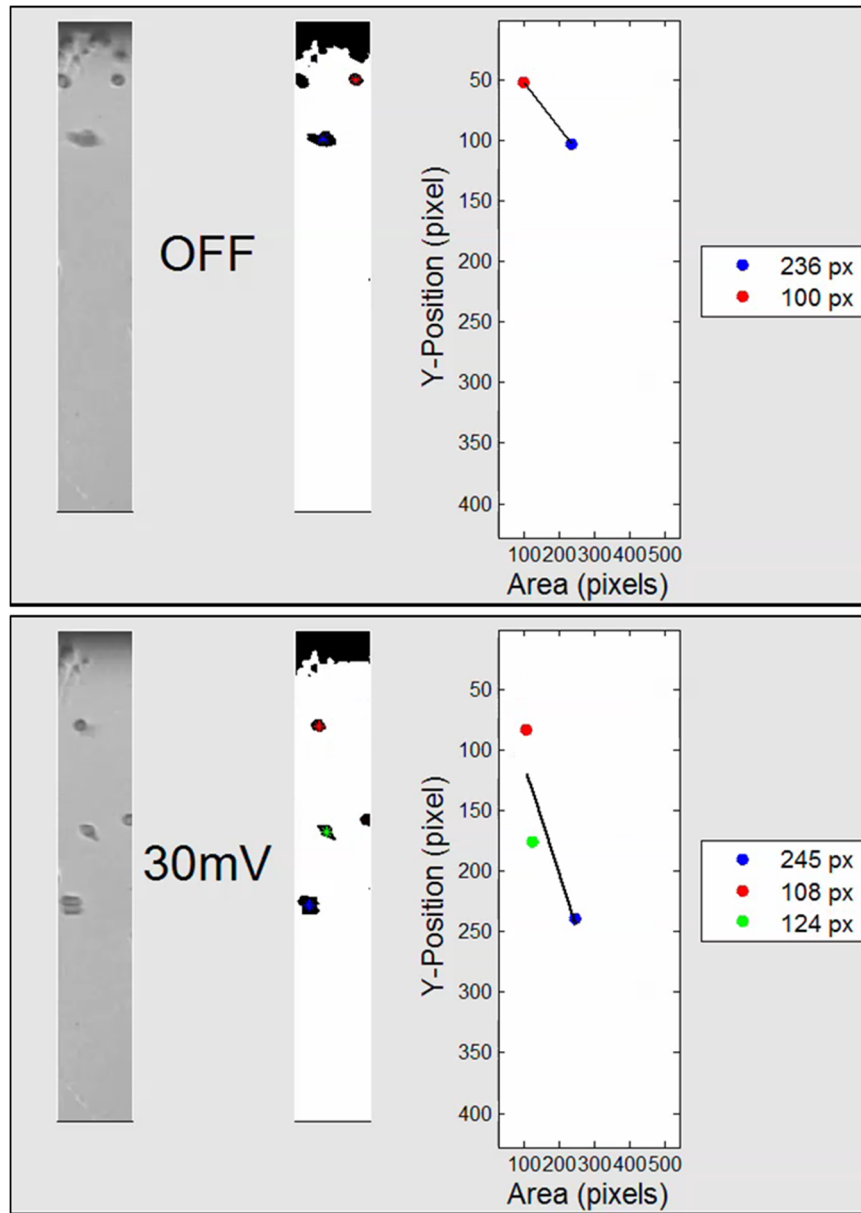
Figure 43. Example images from a new procedure to analyze the relation between cell size and y-position as acoustic power varied. The regions-of-interest (ROIs) identified at the acoustic deflection device outlet (Fig. 39) are shown at far left of each image. The voltage driving the acoustophoresis is displayed next to the original ROI. Next in each image is the black/white thresholded ROI with colored asterisks plotted over the objects that have been identified using an image processing function in MATLAB. The yeast y-positions relative to the image coordinates are plotted against the black region area at right of each image. A legend displays the precise area. If >1 area was identified in the ROI, a linear regression relating y-position and area was also plotted.
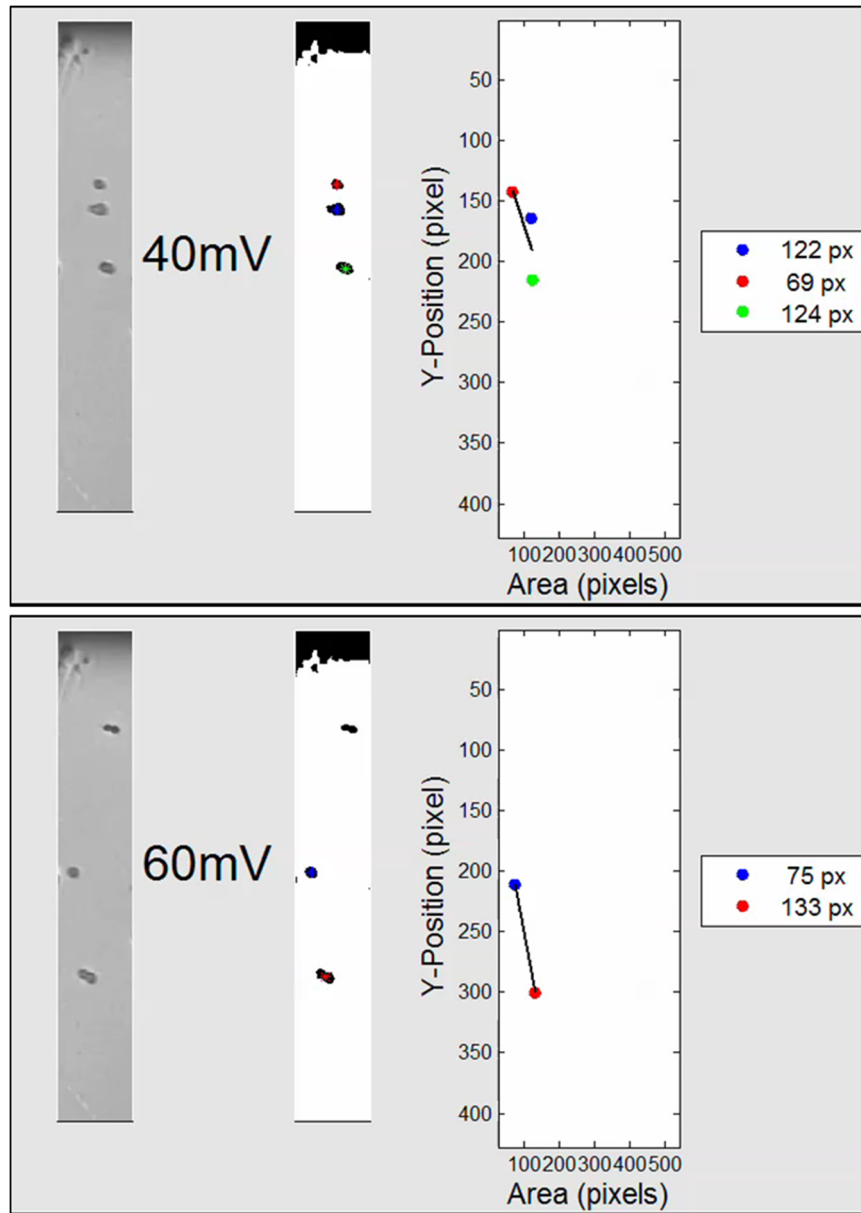
Figure 43. (continued)
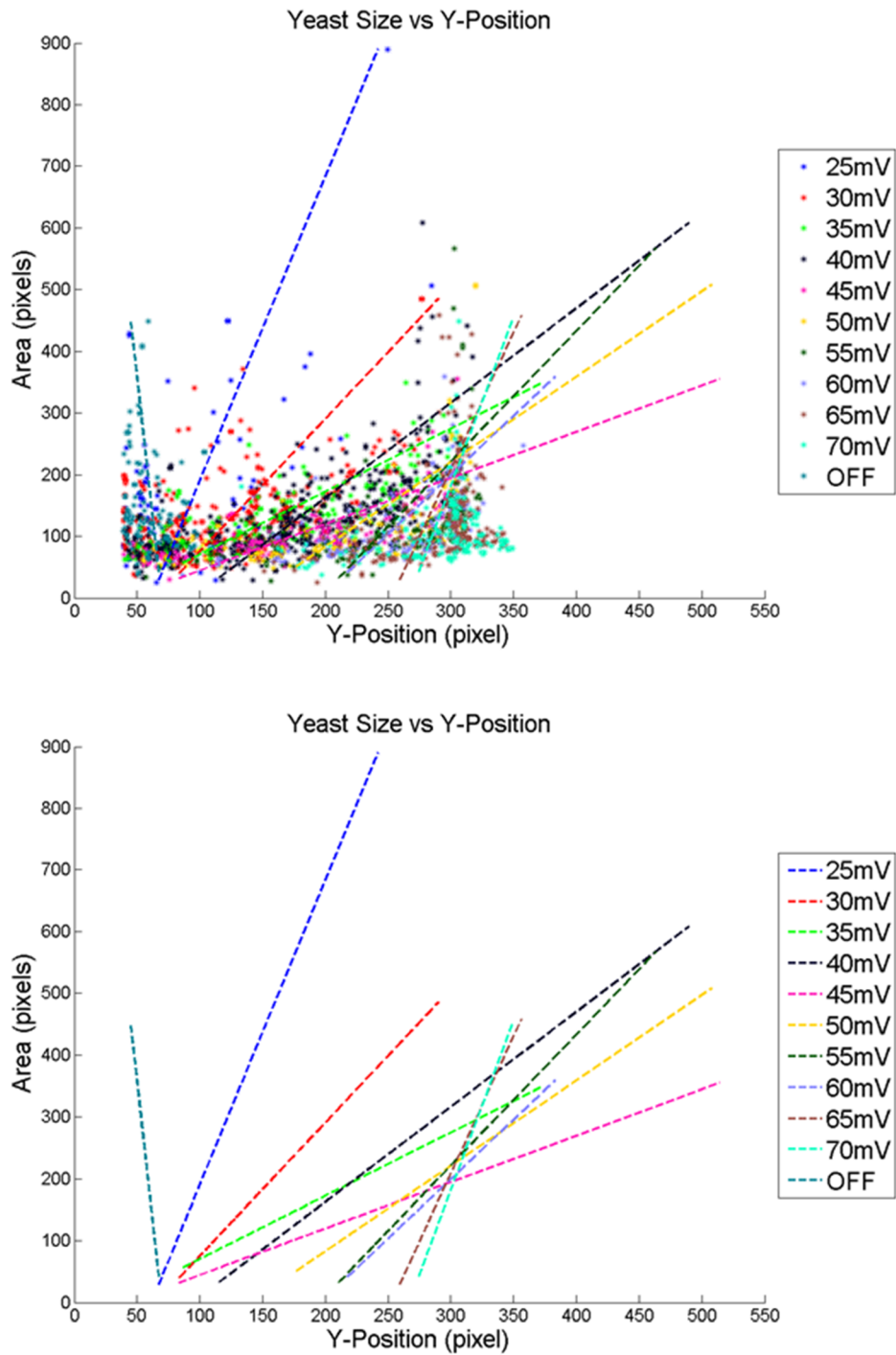
Figure 44. Results of the procedure described in Fig. 43 to determine the relation between yeast positions at the acoustic deflection device outlet and yeast size as acoustic power varied. Top plot shows data points for all applied voltages along with linear regressions for each voltage. Bottom plot shows only the linear regressions. The trend in size vs y-position as acoustic power increased is consistent with expectations (see § 2.1.26).

To improve visibility of the data points for a particular applied voltage in the plot with all data, we show in Fig. 45 all data points plotted in gray except for one voltage for the cases of OFF and 30 mV to 70 mV in 10 mV increments. Because the data for each voltage does not closely follow the linear regression, we did not attempt to use the lines for determining optimal applied voltage. The linear regressions are provided in the images only to help visualize the y-position versus size trends.

We repeated this analysis for videos captured at the middle of the channel length for applied voltages from 20 mV to 60 mV. The top of Fig. 46 shows the area versus y-position for all objects identified as relevant regions in the region-find algorithm described above. The trend of the linear regression lines for the applied voltages is similar to what we observed at the outlet, and thus the trend is repeatable. The linear regression slopes of the voltages at the midway point of the device are not directly comparable to the corresponding voltages at the outlet of the device because cells have experienced acoustic radiation for less time when they are at the channel length center compared to at the outlet. Thus cells will not have deflected as much midway through the device as they will have at the device outlet.
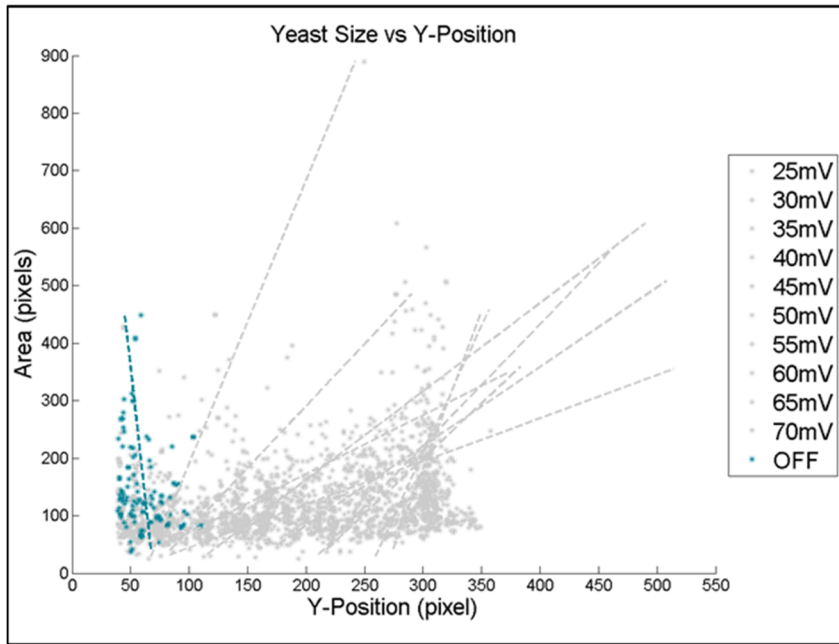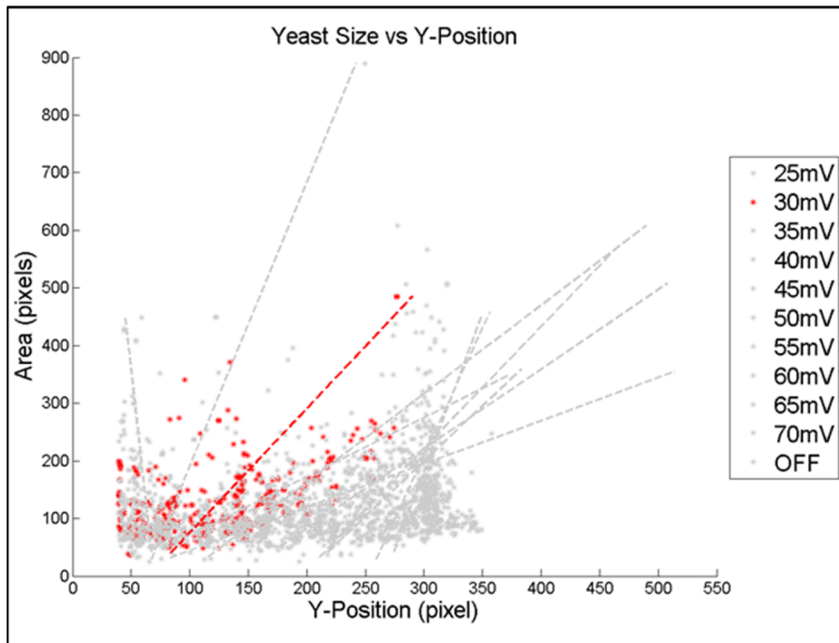
Figure 45. Selected images from the results in Fig. 44 to investigate how yeast size and y-position varied with changes in acoustic power. In each image, all but one of the data sets is plotted in gray. The data points do not closely follow the linear regressions, thus we did not heavily rely on the linear regressions for drawing conclusions but used them for better visualization of how yeast area trended with y-position.

40mV
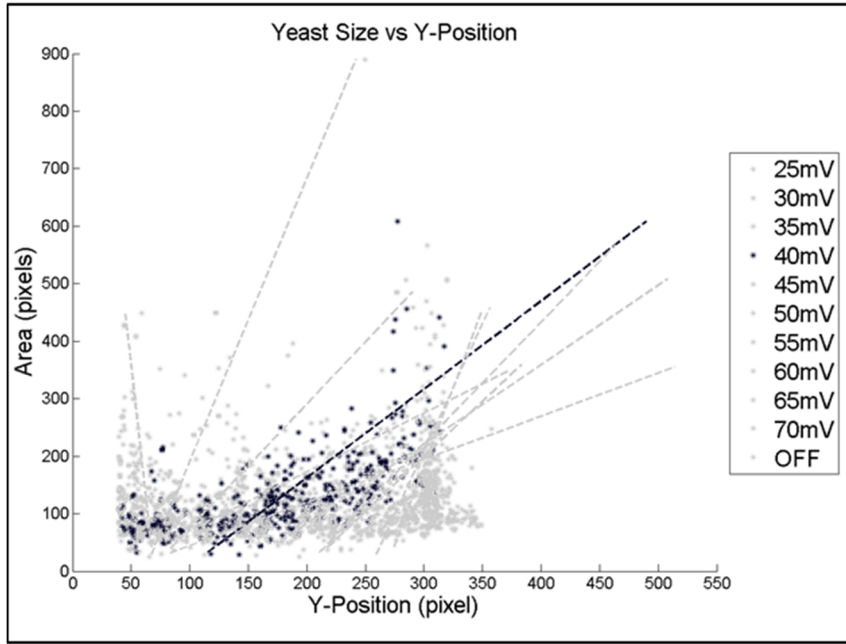
50mV
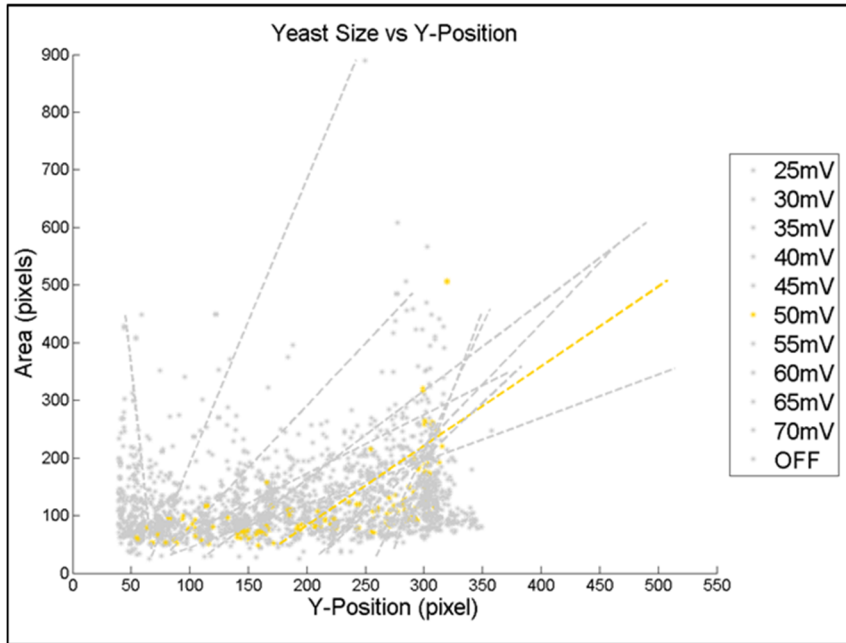
Figure 45. (continued)

60mV
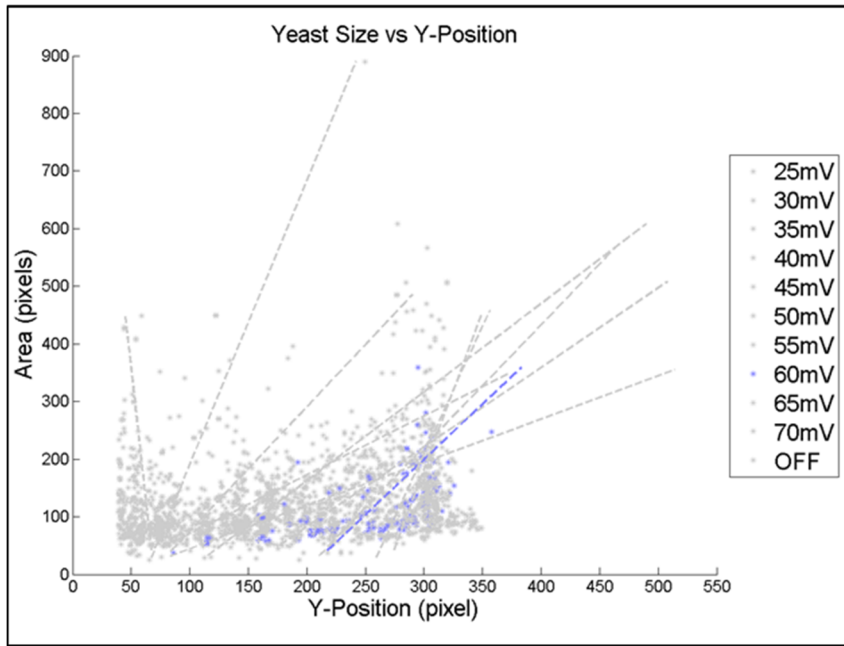
70mV
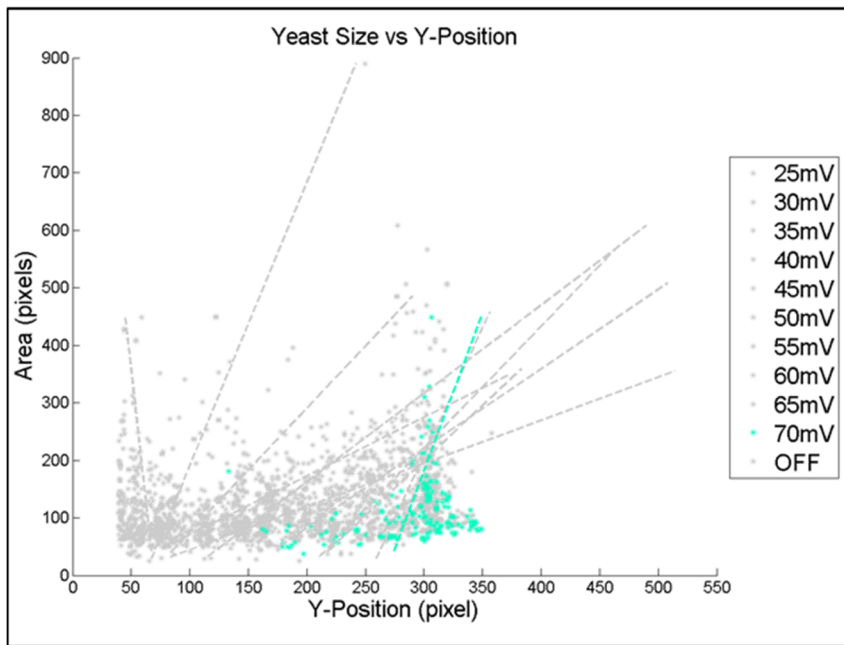
Figure 45. (continued)
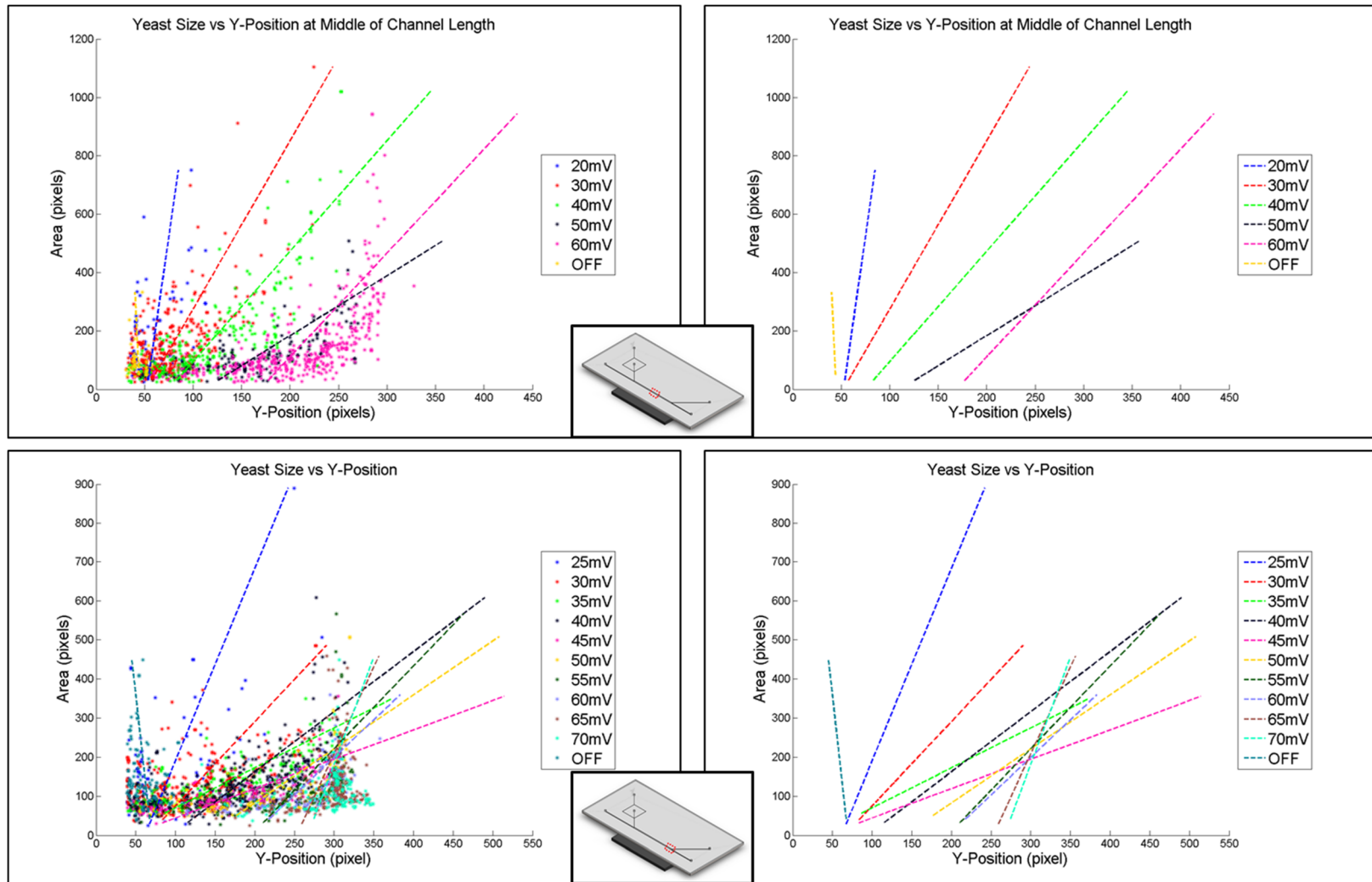
Figure 46. After repeating the procedure described in Fig. 43 on experimental videos of yeast flowing midway down the fluidic channel length of the acoustic deflection device (top half), the results showed similar trends as what we found in videos of yeast at the device outlet (bottom half, repeated from Fig. 44).

2.1.27. Ideal applied voltage and outlet y-cutoff for acoustic deflection device

Because the slopes of the linear regressions are vertical in Figs. 44 and 46 at low applied voltages, approach a 45° angle relative to the plot axes as voltage increased, and return to vertical at high applied voltages, an optimal applied voltage must exist somewhere between the minimum and maximum values. Additionally, an ideal y-cutoff can be chosen for dividing the separated cells and cell clumps into those that are kept and those that are discarded (see Fig. 36). To determine the optimal combination of voltage and y-cutoff, we first defined several size-thresholds and y-cutoffs for each applied voltage. For example, Fig. 47 shows a 240 pixel size-threshold and 150 pixel y-cutoff for the 40 mV data.

These size and y-position cutoffs divide the data points into 4 regions: (i) y > y-cutoff & area > threshold, (ii) y > y-cutoff & area < threshold, (iii) y < y-cutoff & area > threshold, and (iv) y < y-cutoff & area < threshold. With the data divided into quadrants, we calculated how "pure" the separation was for all combinations of 2 adjacent regions. For instance, to calculate the purity for area > threshold, we took the total number of data points with area > threshold and y > y-cutoff divided by the total number of data points with area > threshold. In Fig 47, these purities are displayed at the top of the plots along with how they were calculated according to the colors of data points displayed in the plots. For instance, y > y-cutoff purity was calculated as (# black points) / (# black points + # green points). For each voltage {0 mV, 20 mV to 70 mV in 5 mV increments}, we calculated these 4 purities for several y-cutoffs {120 pixels to 300 pixels in increments of 15 pixels} and size-thresholds {125 pixels to 300 pixels in increments of 25 pixels}. We defined the size-thresholds in pixels because the 2D regions may not correlate well with actual cell sizes due to poor image quality and other reasons (see § 2.1.4).

116
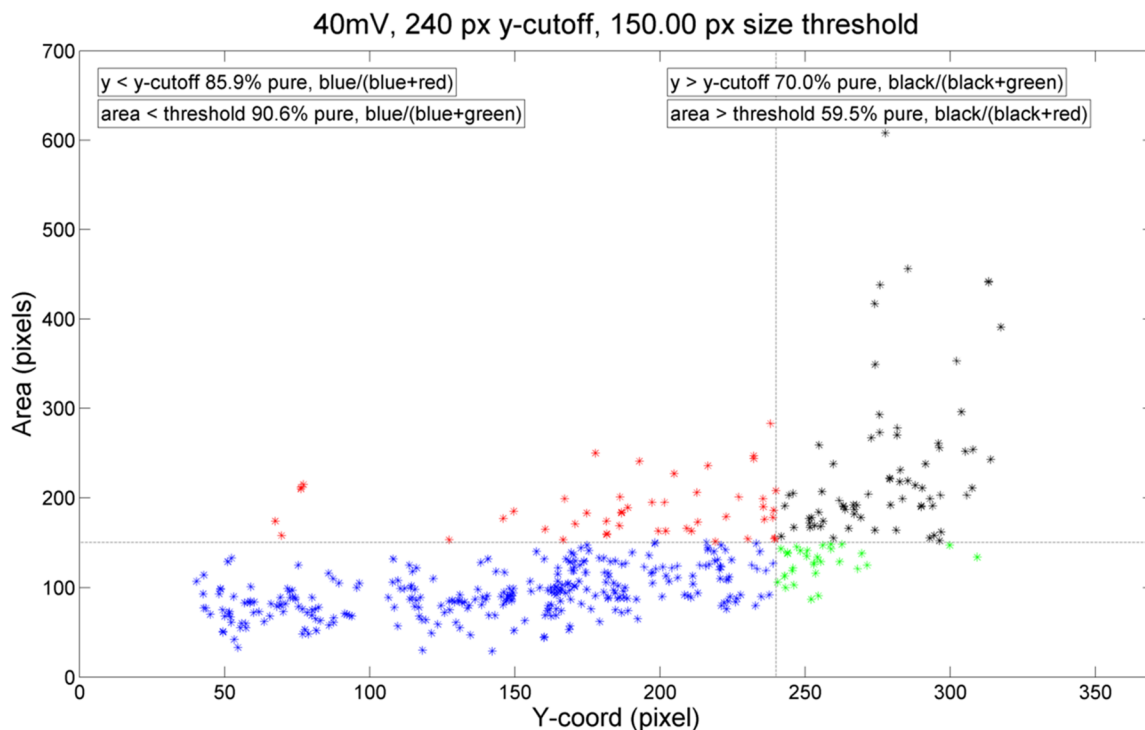
Figure 47. To optimize the acoustic power and y-cutoff (see Fig. 36), all of the experimental data from the acoustic deflection device was analyzed using four figures-of-merit for each data set. An example plot is shown here, with the figures-of-merit listed near the top of the plot. The data for each voltage was divided into quadrants by defining several y-cutoffs {120-300 pixels in increments of 15 pixels} and size-thresholds {125-300 pixels in increments of 25 pixels}. The figures-of-merit were calculated for all combinations of two adjacent quadrants in the plots (see § 2.1.27). In this way, we could identify the ideal applied voltage and y-cutoff for the acoustic deflection device.

With all these combinations of voltages, y-cutoffs, and size-thresholds, we sorted the results by size-threshold (in descending order) and then by each calculated purity (in descending order) starting with y > y-cutoff, then area > threshold, area < threshold, and y < y-cutoff. The resulting list of all parameters provided us with an optimal choice of y-cutoff and applied voltage. Some of the list entries, especially those with 25 mV, were artificially high on the list because the purities for 25 mV were close to the ideal value of 100% due to very few data points. After ignoring these entries, we observed a pattern for the optimal applied voltage and y-cutoff for all size-thresholds. Table 8 shows the best options for the size-cutoffs. As shown in the table,

the optimal acoustic power is 35-40 mV and the ideal y-cutoff is 270-300 pixels relative to the ROI that was cropped out of the original videos of the acoustic device outlet. The cell area versus y-position plots for these optimal combinations are shown in Fig. 48. Figure 49 shows the calculated optimal y-cutoff plotted on top of the original device outlet.

Table 8. Figures-of-merit for the ideal combinations of applied voltage and y-cutoff

Design & Operation			Purities			
Size Cutoff (pixels)	Applied Voltage (mV)	Y-Cutoff (pixel)	y < y-cutoff (%)	y > y-cutoff (%)	area < threshold (%)	area > threshold (%)
300	40	300	98.8	36.8	98.4	43.8
300	25	120	92.4	31.7	72.3	68.4
275	40	300	97.9	47.4	98.6	37.5
275	30	270	99.1	40.0	99.5	25.0
250	40	300	96.7	63.2	99.0	33.3
250	30	270	96.8	60.0	99.7	12.5
225	40	300	94.8	73.7	99.3	26.9
225	35	270	97.9	66.7	97.9	66.7
200	40	300	90.6	89.5	99.7	20.0
200	30	225	94.5	88.9	99.5	40.7
175	40	300	83.1	89.5	99.7	12.1
175	30	240	88.2	87.5	99.5	21.9
150	35	240	85.4	93.8	98.7	54.1
150	40	270	81.1	93.7	99.1	37.0
125	35	255	65.2	100.0	100.0	24.6
125	25	150	40.4	100.0	100.0	20.5

35mV, 255 px y-cutoff, 150.00 px size threshold

y < y-cutoff 81.1% pure, blue/(blue+red)
area < threshold 99.7% pure, blue/(blue+green)
y > y-cutoff 97.6% pure, black/(black+green)
area > threshold 36.9% pure, black/(black+red)

40mV, 285 px y-cutoff, 125.00 px size threshold

y < y-cutoff 64.9% pure, blue/(blue+red)
area < threshold 100.0% pure, blue/(blue+green)
y > y-cutoff 100.0% pure, black/(black+green)
area > threshold 16.1% pure, black/(black+red)

Figure 48. Experimental data plotted and scored against the figures-of-merit (see § 2.1.27) that helped determine the optimal applied voltage and outlet y-cutoff for separating yeast by size using acoustic deflection. The ideal acoustic power is 35-40 mV and the ideal y-cutoff is 270-300 pixels (see Fig. 36).
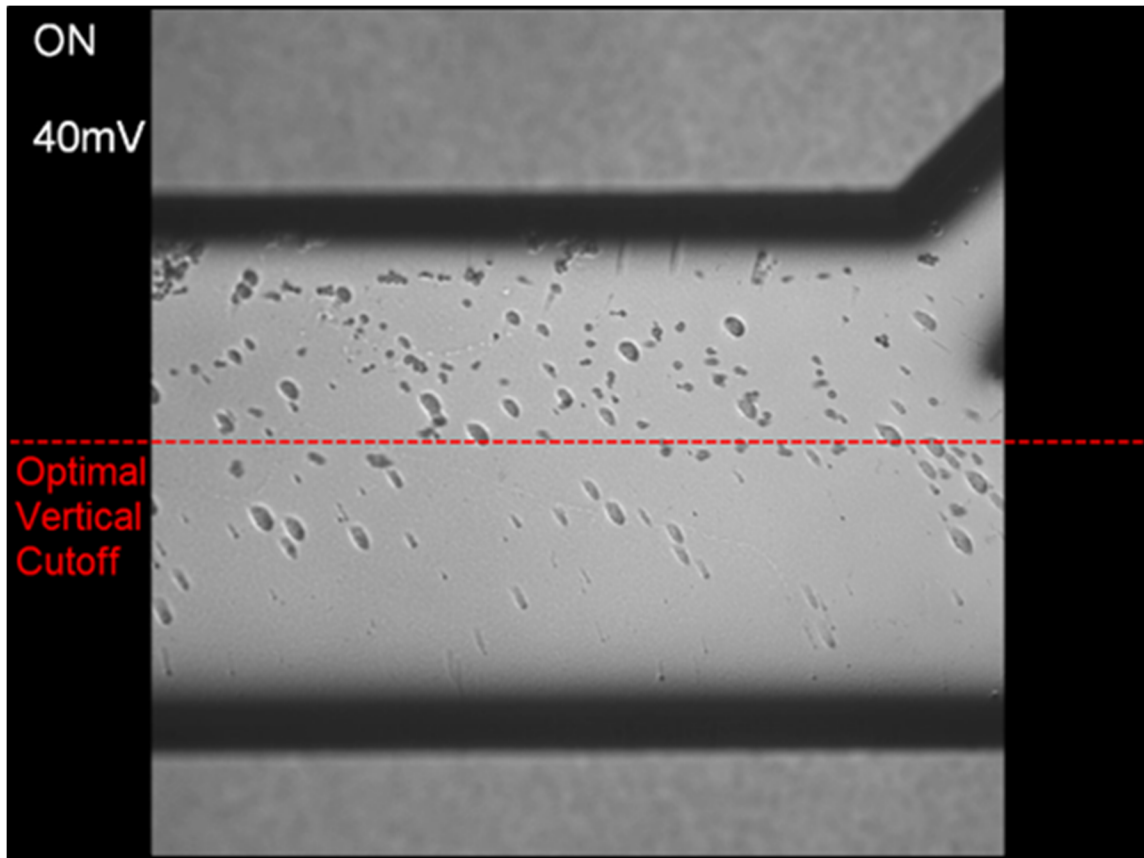
Figure 49. Optimal applied voltage and outlet y-cutoff for using the acoustic deflection device to separate yeast by size. Values were determined using the procedure described in § 2.2.27.

2.1.28. Optimal acoustic device design for separating yeast by size

After calculating the ideal y-cutoff based on analysis of cell size versus y-position, we designed

the size-based separation subsystem of the aged yeast generator as shown in Fig. 50.
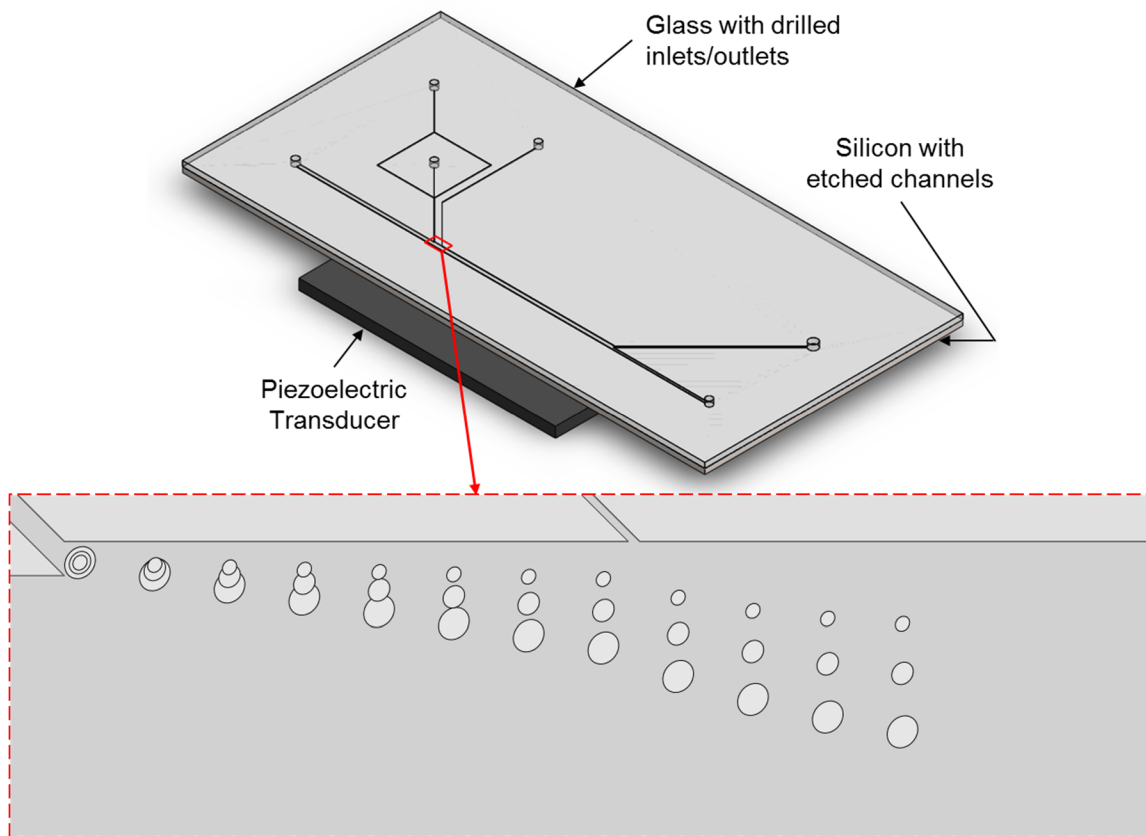
Figure 50. Acoustic deflection device design with the optimal y-cutoff and an additional inlet channel to enhance flexibility. The design is very similar to the acoustic test device (Figs. 36 and 37). The outlet was redesigned to implement the ideal y-cutoff from Fig. 49. An extra inlet channel was added near the cell inlet to the main channel in order to create an adjustable y-cutoff. Fluid entering the main channel through this extra inlet deflects all cells downward by the same amount (bottom of figure). This adjustment effectively changes the y-cutoff at the device outlet to allow for more flexibility.

Most of the device dimensions (Fig. 51) are similar to those of the test device so that the performance we observed in testing will be similar to behavior of this new device. Two significant differences are (i) the optimal y-cutoff is implemented at the main channel outlets and (ii) an extra inlet channel is connected to the main channel near where cells enter the acoustic separation region. This additional inlet allows us to adjust the y-cutoff at the outlet that determines cells we keep and those we discard (see Fig. 36); thus the device has an adjustable outlet that enhances flexibility. Instead of needing to re-design and fabricate a completely new

121

device whenever the y-cutoff needs to be changed (e.g. if separating cells other than yeast), we can simply increase the flow from this extra inlet. The inlet should not change the separation behavior whenever it is not in use. Alternative methods to adjust the y-cutoff are to change the flow rates and/or the acoustic power (by adjusting voltage applied to the PZT); however, these options are not as straightforward as the extra inlet channel. Adjusting all flow rates significantly affects the separation behavior because cells spend less or more time in the separation region, and fine-tuning several flow rates can be challenging to produce a desired change in y-cutoff at the device outlet. Changing the acoustic power is simpler for adjusting the y-cutoff compared to changing flow rates; however, increasing acoustic power obviously costs more energy, and adjusting power can decrease the maximum separation between the largest and smallest cells. In Fig. 44 we observed that for very low and very high acoustic powers, yeast were at similar y-positions at the device outlet (and the linear regressions for cell size versus y-position were nearly vertical). To maintain the greatest degree of separation between small and large cells, we desired to keep applied voltage in the 35-40 mV range. To adjust the y-cutoff while keeping this maximum separation we added the extra inlet that linearly adjusts the y-positions of all cells. Note that the y-cutoff can only be decreased with the extra inlet because all cells are deflected downward; therefore, we designed the y-cutoff very close to the center of the channel where the acoustic node is formed so that the y-cutoff of the device with no flow from the extra inlet would be a sort of maximum.
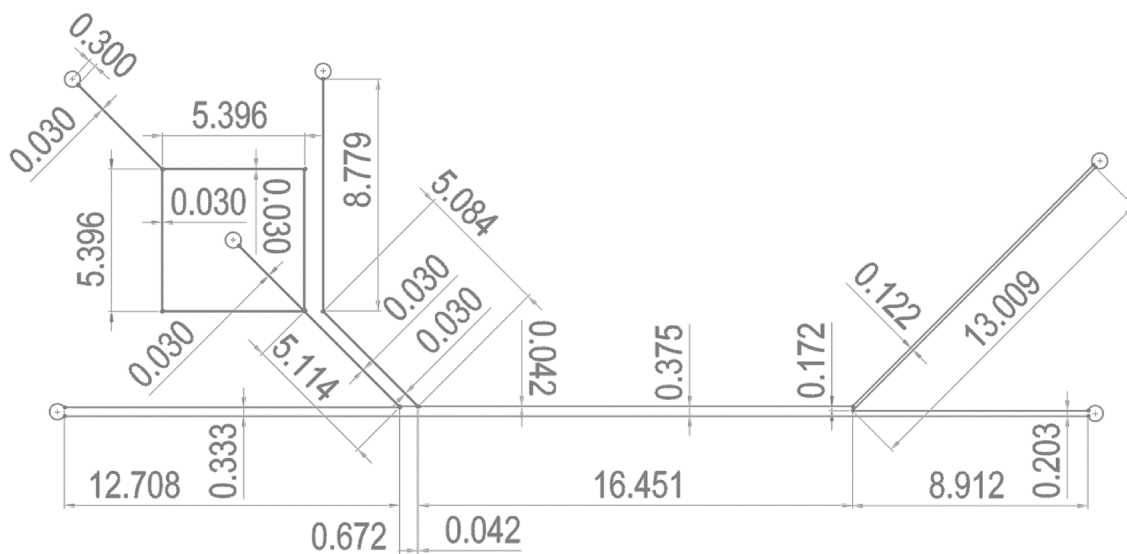
Figure 51. Dimensions of the microfluidic channels of the optimized acoustic deflection device in Fig. 50. All units are mm.

2.1.29. Future testing of acoustic deflection device with optimized design

At the time of this writing, the new acoustic separation device had not been fabricated and tested. After fabricating the device using the process described in § 2.1.22, testing will proceed as follows. All cell preparation steps will be the same as those in § 2.1.2 except the syringe containing cells will have plain YPD withdrawn into it both before and after the cells are loaded. In other words, ~100 µL of YPD will be withdrawn into the syringe, ~100 µL of cells+YPD will be withdrawn, and finally ~50 µL of YPD will be loaded. This procedure creates a cell "plug" surrounded by YPD on both sides so that when the syringe contents flow into the device, the cells will follow and be followed by buffer. The purpose of introducing buffer both before and after cells enter the device is to repeat the separation several times after reversing the flow in between each separation. We discuss the reasoning and procedure in more detail in § 2.2. After repeating the acoustic separation several times, the yeast populations flowing through the waste outlet and keep channel will be processed using a Beckman Coulter Z2 Particle Count and Size

Analyzer with Z2 AccuComp Software to determine yeast sizes of the keep channel and of the waste channel and verify that the size-based separation is effective.

2.2. Continuous/repeated separation to age the yeast

2.2.1. Old yeast are very rare in a cell population

In this section we discuss the second subsystem of the aged yeast generator that recirculates the yeast remaining in the device after size-based separation. The kept cells are the larger mothers that are manipulated by this subsystem so that they periodically pass through the separation subsystem. Repeated separation is required because very old yeast (>15 generations) are extremely rare in a given population. Consider Fig. 52A which shows ~1,500 yeast in the four fields-of-view.

Because yeast grow exponentially in number, ~50% of these 1,500 cells are virgin daughters that have not yet budded any offspring. In Fig. 52B, ~50% of the cells are highlighted with blue circles. Similarly, of the 1,500 yeast, ~25% are first generation mothers (yeast that have completed exactly 1 division) represented in Fig. 52B and highlighted in green circles. Note that the highlighted cells in Fig. 52B and C are not all virgin daughters or first generation mothers; we created these figures to illustrate that old cells are very rare because yeast population grows exponentially. Figure 52D shows that only 1 cell of the 1,500 is 10-11 generations old (has produced 9-10 daughters), which is still relatively young considering yeast continue budding until they divide 20-30 times. Additionally, Vanoni *et al.* found that the proportion of virgin daughters in a population is closer to 80%, 12% are first generation mothers, 6% have budded twice, 3% have budded three times, etc.,[98] so the percentage of very old cells may be even smaller than what was considered in Fig. 52.
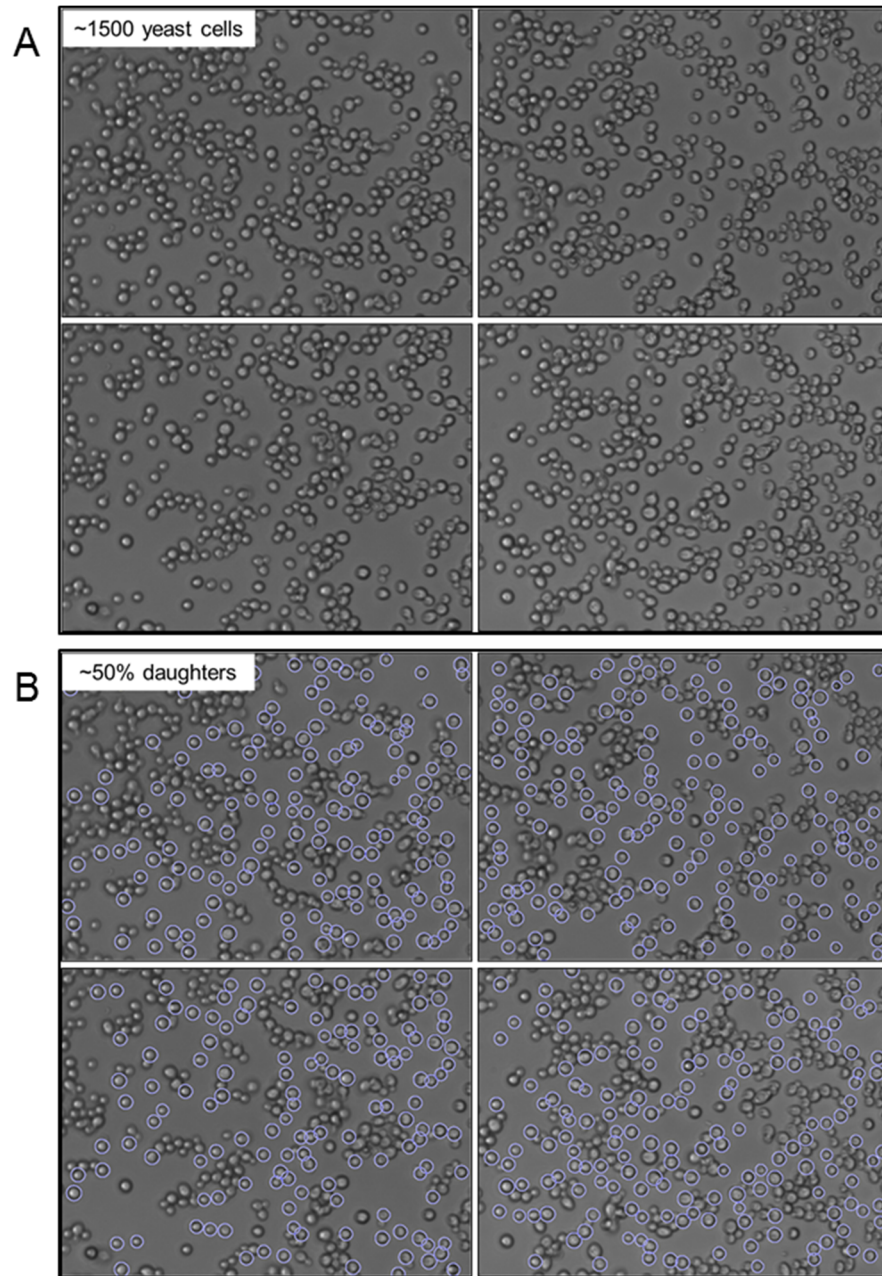
Figure 52. Approximately 1,500 yeast are captured in each set of four images. Of the ~1,500 cells (A), 50% are virgin daughters (B), 25% have divided once (C), and only one cells is >10 generations old (D). Because of the very small number of very old yeast in a given population, performing size-based separation once is not likely to have a very high yield of aged yeast.
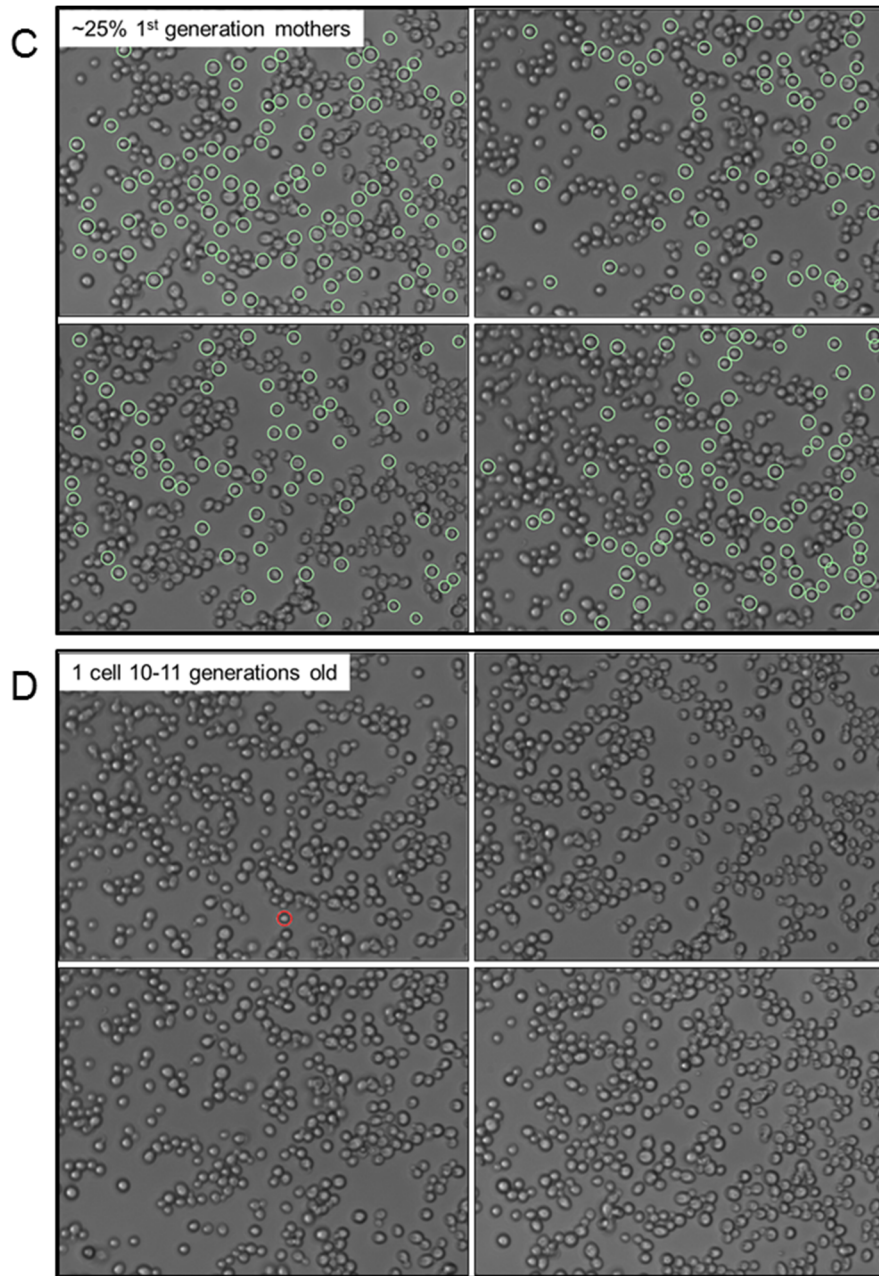
Figure 52. (continued)

2.2.2. A single separation run is not likely to yield a large number of aged yeast

This number exercise motivates the need for a subsystem that continuously or repeatedly cycles

yeast through the separation region. Because of the very low percentage of old yeast in a given

population, if we process several millions of yeast through the size-based separation region one time and keep only the largest cells, we are not likely to obtain a large quantity of aged yeast. Rather than starting with a large number of yeast and separating once to keep the largest cells, we are better off still starting with a large number of yeast, potentially reducing the size-threshold separating the yeast that are kept and discarded, and continuously perform the size-based separation over several hours. Ideally, the same yeast are kept after each separation and only the daughters are removed. The size separation threshold could be increased gradually as the yeast that are kept grow in size and age. After several hours of repeated separation, the yeast that have been kept are aged (>15 generations), and we have achieved a higher yield of aged cells than what is possible with a single separation run.

2.2.3. Straightforward approach to recirculate the yeast

The promise of larger numbers of aged yeast using repeated separation motivated us to develop a method of recirculating yeast through the separation subsystem. The simplest approach for repeating the separation is to add an on-chip recirculation channel to the acoustic device design. Figure 53 shows the recirculation channel. As mother and daughter yeast enter the device at top left and are focused by side buffer channels into the separation region, they are separated such that smaller daughters exit the device through the upper outlet and larger mothers enter the recirculation channel through the lower outlet. As the mothers flow through the recirculation channel, they grow, bud daughters, and age. After this aging, the yeast from the original population along with new daughters flow through the inlet channels where they are again focused to undergo repeated size-based separation. After several hours of this periodic separation, the final yeast population ideally consists of a high yield of yeast which belonged to the original population that entered the device but are now aged.
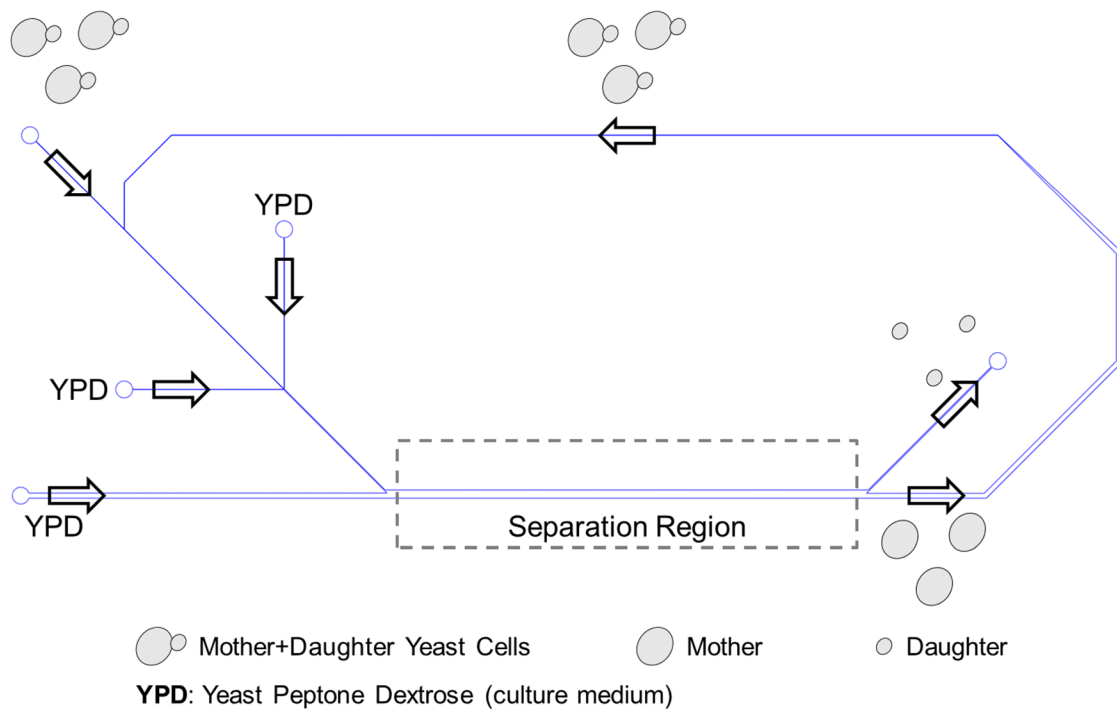
Figure 53. Recirculation channel added to the original acoustic deflection device. Mother and daughter yeast enter the device at top left as before and are separated by size in the separation region. The smaller yeast are discarded while the larger enter a recirculation channel. In the recirculation channel, the yeast grow, bud, and age. The recirculation channel delivers the kept yeast to the original inlet where they repeat separation. By allowing yeast to complete several cycles through the device, a higher yield of aged cells can be obtained.

2.2.4. Simulations show on-chip recirculation cannot be designed

Although adding the on-chip recirculation channel to the acoustic device is the simplest method for repeating the size-based separation, COMSOL simulations show that fluid prefers flowing through the outlet instead of the recirculation channel. Figure 54 shows a single-phase flow simulation for the simplest recirculation channel design.
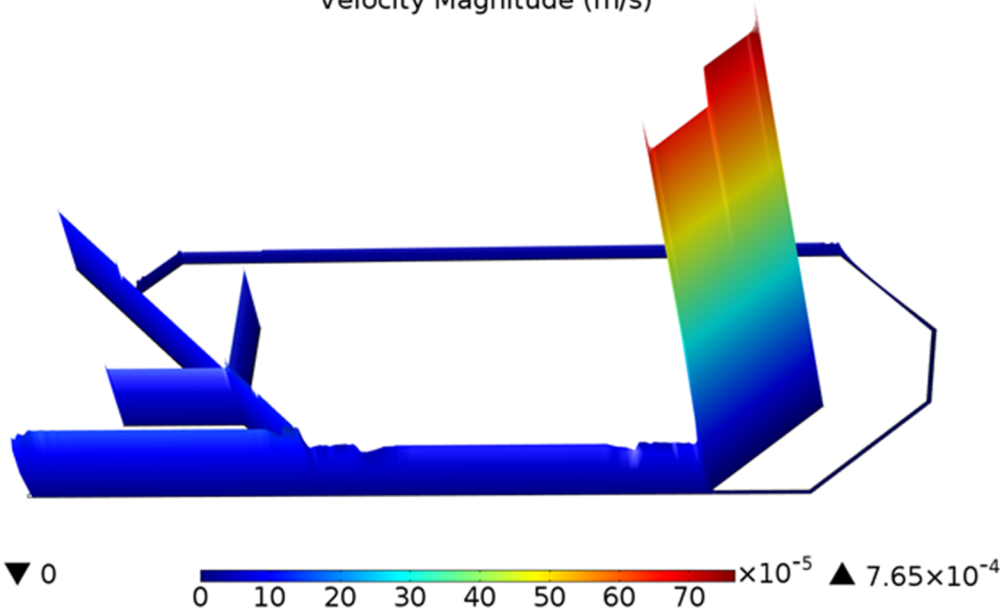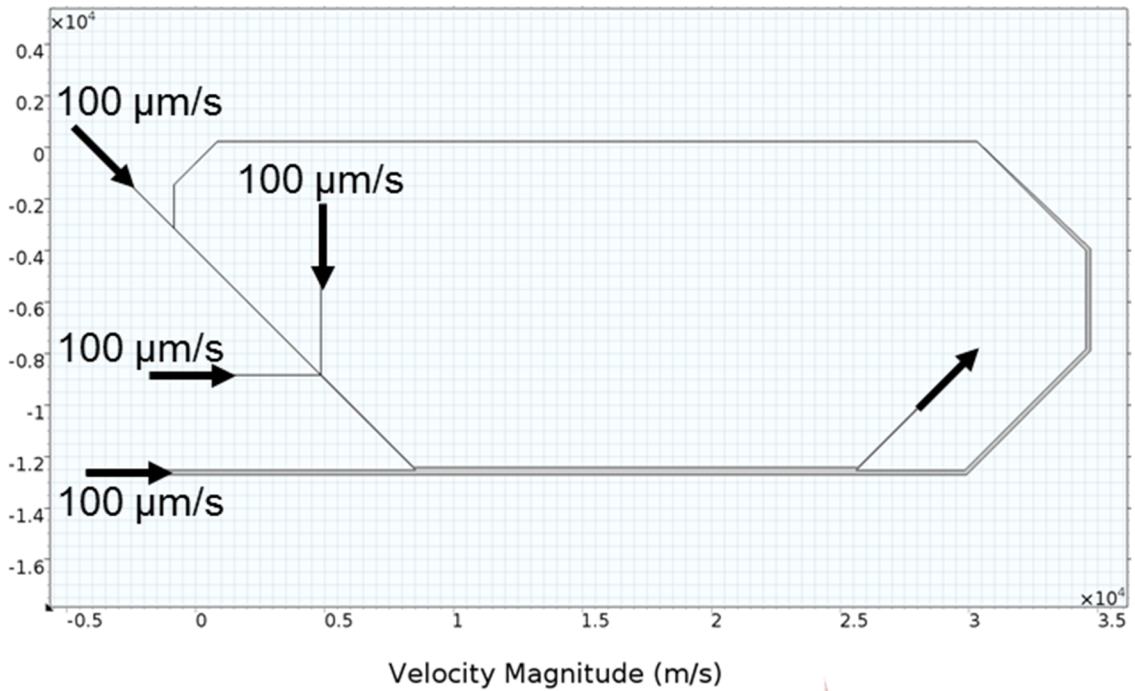
Figure 54. COMSOL single-phase flow simulations showing that fluid does not readily flow into the recirculation channel but instead exits through the outlet. The microfluidic channel geometries and inlet flow rates are displayed in the top half of the figure. The bottom half plots the velocity magnitude over the channel geometry. The color scale and the relative heights of the channels portray the velocity magnitude, e.g., tall and red-colored channels correspond to large velocity magnitudes.
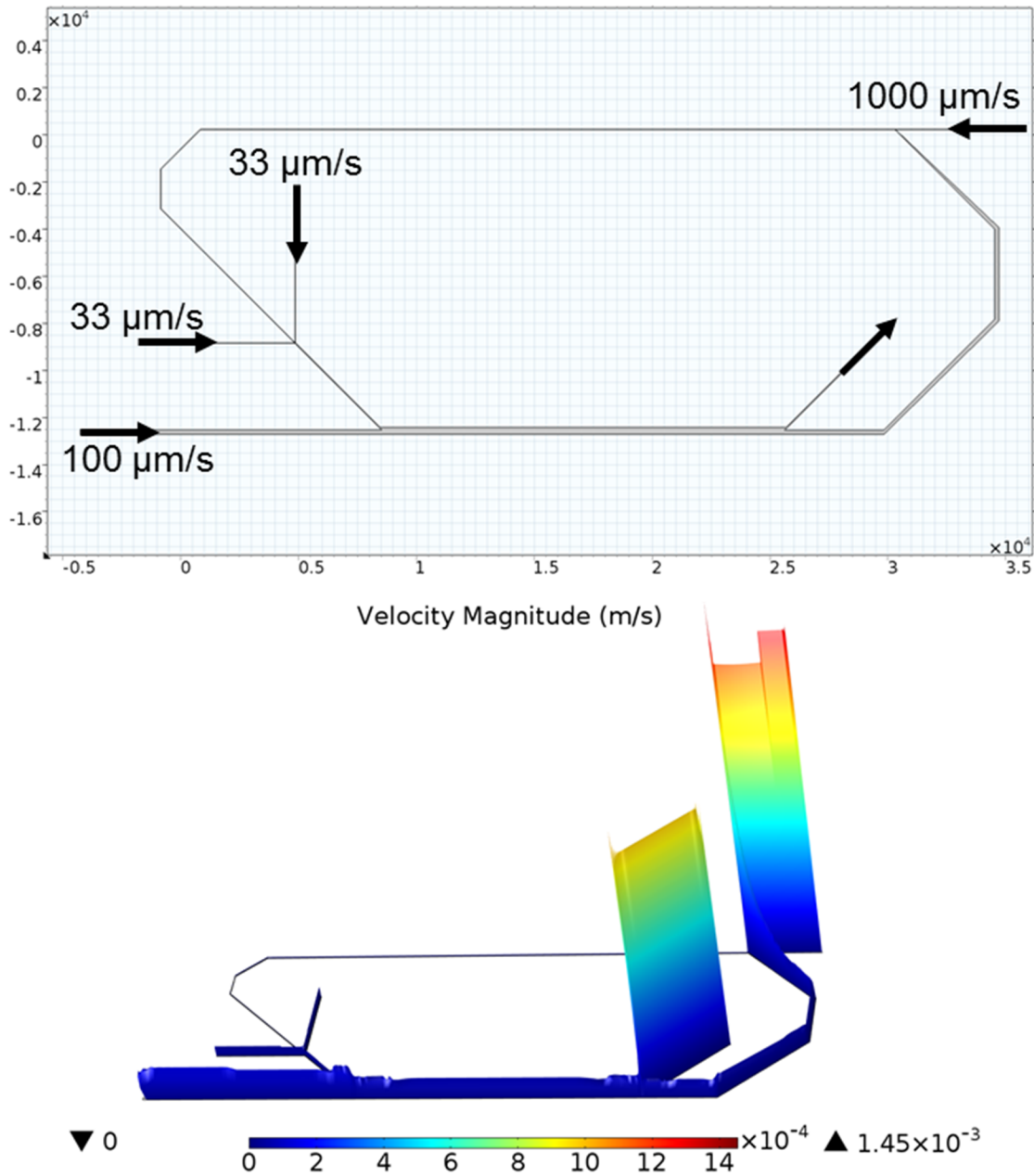
Figure 55. COMSOL single-phase flow simulations showing that fluid does not readily flow into the recirculation channel but instead exits through the outlet. Compared to the simulation in Fig. 54, even when an inlet is added to the recirculation channel (top right of geometry), the fluid still does not readily flow through the recirculation channel.

The top half of the figure displays the geometry along with flow rates of the inlets.

Although all flow rates were equal in this simulation, increasing or decreasing them did not

significantly alter the simulation results. In particular, no combination of flow rates changed the behavior in which all flow traveled into the outlet as shown in the Velocity Magnitude plot at figure bottom. This surface-height plot correlates high velocities in the microchannels with red colors and low velocities with blue colors. The heights of the channels are also proportional to the velocity magnitudes: channels with higher velocities have larger (and red-color) heights. The bottom half of Fig. 54 shows most of the flow traveling through the outlet as opposed to the recirculation channel. We simulated several variations of this geometry, and all results supported that on-chip recirculation cannot be designed. One variation is shown in Fig. 55, in which an inlet is added at the top right of the geometry to increase flow through the recirculation channel. Even with the high flow rate of this new inlet, fluid does not flow through the recirculation channel but prefers to travel through the original outlet; the fluid entering the device from this inlet prefers changing direction by ~135° to exit through the outlet rather than flow straight into the recirculation channel. We did not simulate many variations in which additional outlets were added anywhere along the recirculation channel because any fluid entering the recirculation channel and containing yeast should be kept and not discarded through an outlet.

Fluid preferred to flow through the outlet instead of the recirculation channel in Figs. 54 and 55 because of the high fluidic resistance of the recirculation channel. We therefore simulated similar 2D recirculation designs that better equalize the fluidic resistance between the outlet and recirculation channel. Figure 56A displays the Velocity Magnitude plot for one such design. The units of the x-/y-axes are microns, and colors close to blue on the color scale correspond to low velocities while colors close to red correspond to high velocities. In Fig. 56A with the inlet flow rates as indicated in the plot, a majority of the fluid travels through the recirculation channel that is not yet connected to the inlet. As expected, some of the flow also travels through the outlet at top right, but a majority travels through the loop as indicated by the high velocities through this

channel. As soon as the looped channel is connected to the inlet at top left (Fig. 56B), so that it becomes a true recirculation channel, all of the inlet flow immediately exits the geometry through the outlet at top right. Little to no fluid travels through the recirculation channel because of the higher fluidic resistance compared to the outlet. To increase the outlet resistance so that fluid will travel through the recirculation channel, we decreased the outlet width to 1 µm. Figure 56C shows all fluid traveling through this extraordinarily small outlet rather than through the recirculation channel. With the outlet width still very small, we disconnected the recirculation channel very close to the inlet (Fig. 56D), and all flow travels through this new outlet as opposed to the one with very small width. All other variations of this geometry that we simulated produced the same results; thus we concluded that a 2D on-chip recirculation channel fundamentally cannot be designed to achieve our goal of repeatedly cycling yeast through the separation region.
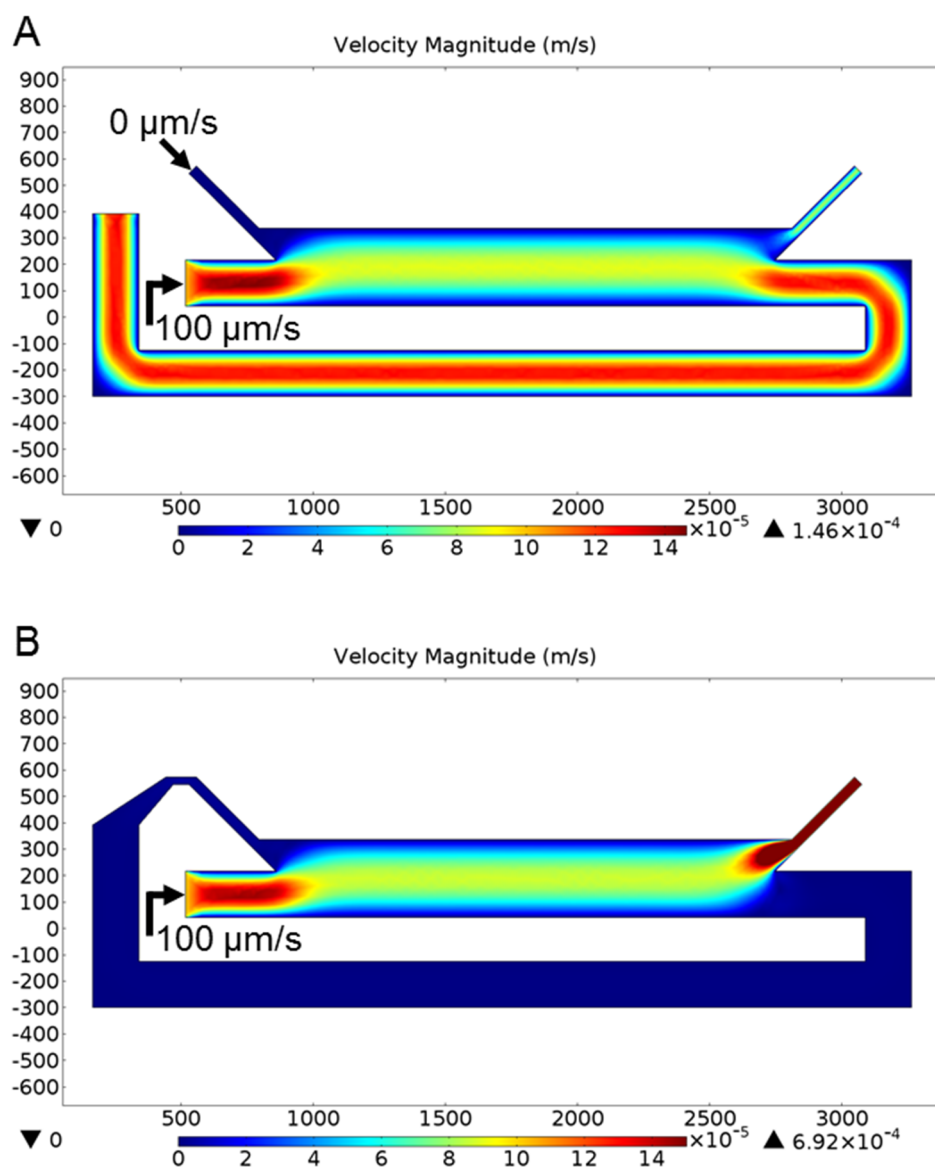
Figure 56. COMSOL single-phase flow simulations showing that fluid does not readily flow into the recirculation channel but instead exits through the outlet. The microfluidic channel geometries, inlet flow rates, and velocity magnitudes are displayed in each simulation result. A) Consistent with expectations, fluid flows through the beginning of the recirculation channel as well as through the outlet. B) As soon as the recirculation channel connects to the inlet, all fluid flows through the outlet while none goes into the recirculation channel. C) Even after decreasing the outlet width to 1 µm and thus significantly increasing the fluidic resistance, fluid still does not flow through the recirculation channel. D) By disconnecting the recirculation channel so that it becomes another outlet while maintaining the very small width at the outlet at top right, the fluid no longer flows through the small outlet. From these simulations, we concluded two-dimensional on-chip recirculation cannot be designed.
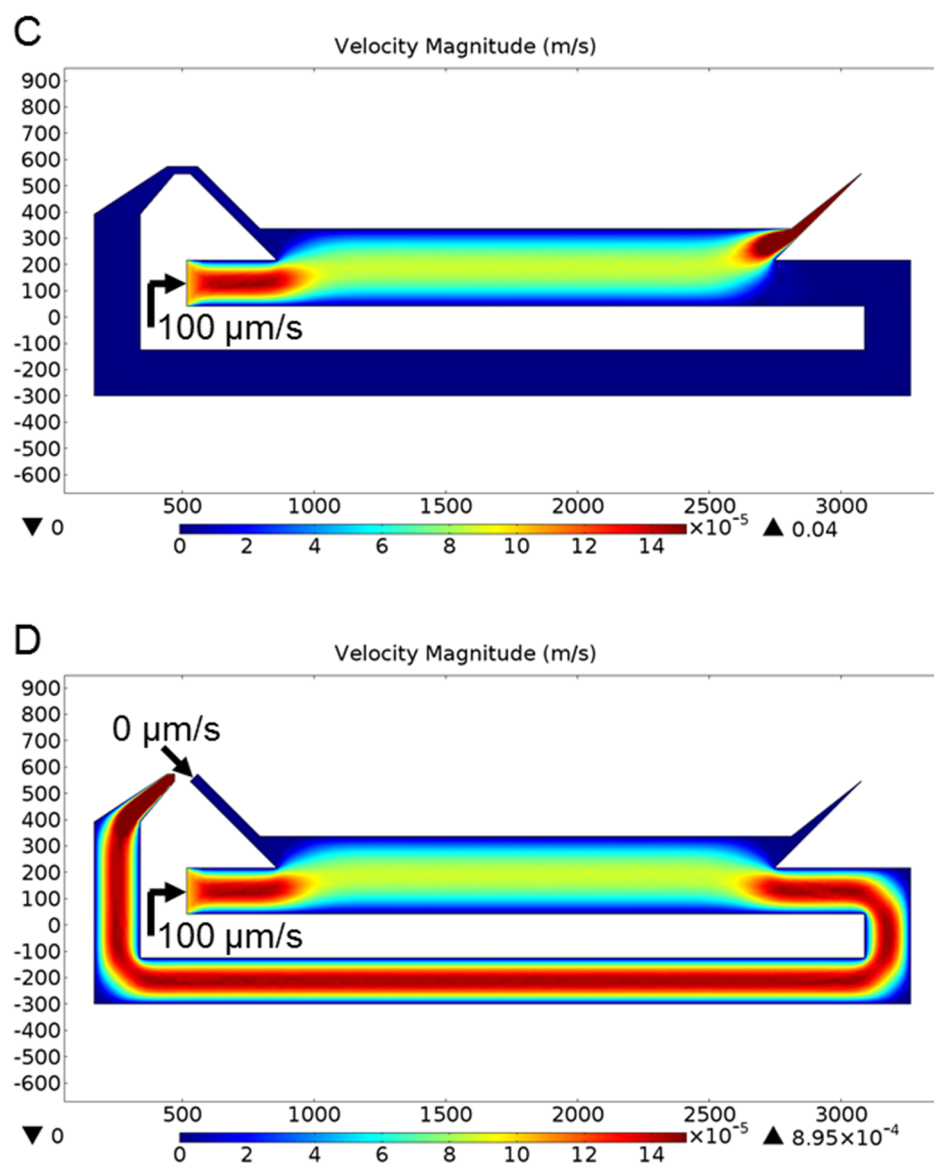
Figure 56. (continued)

2.2.5. Periodic forward/reverse flow as alternative strategy to repeat separation

Because 2D on-chip recirculation cannot be designed, we propose an alternative procedure that periodically passes yeast through the separation region. Figure 57 describes the steps for periodic forward/reverse flow.
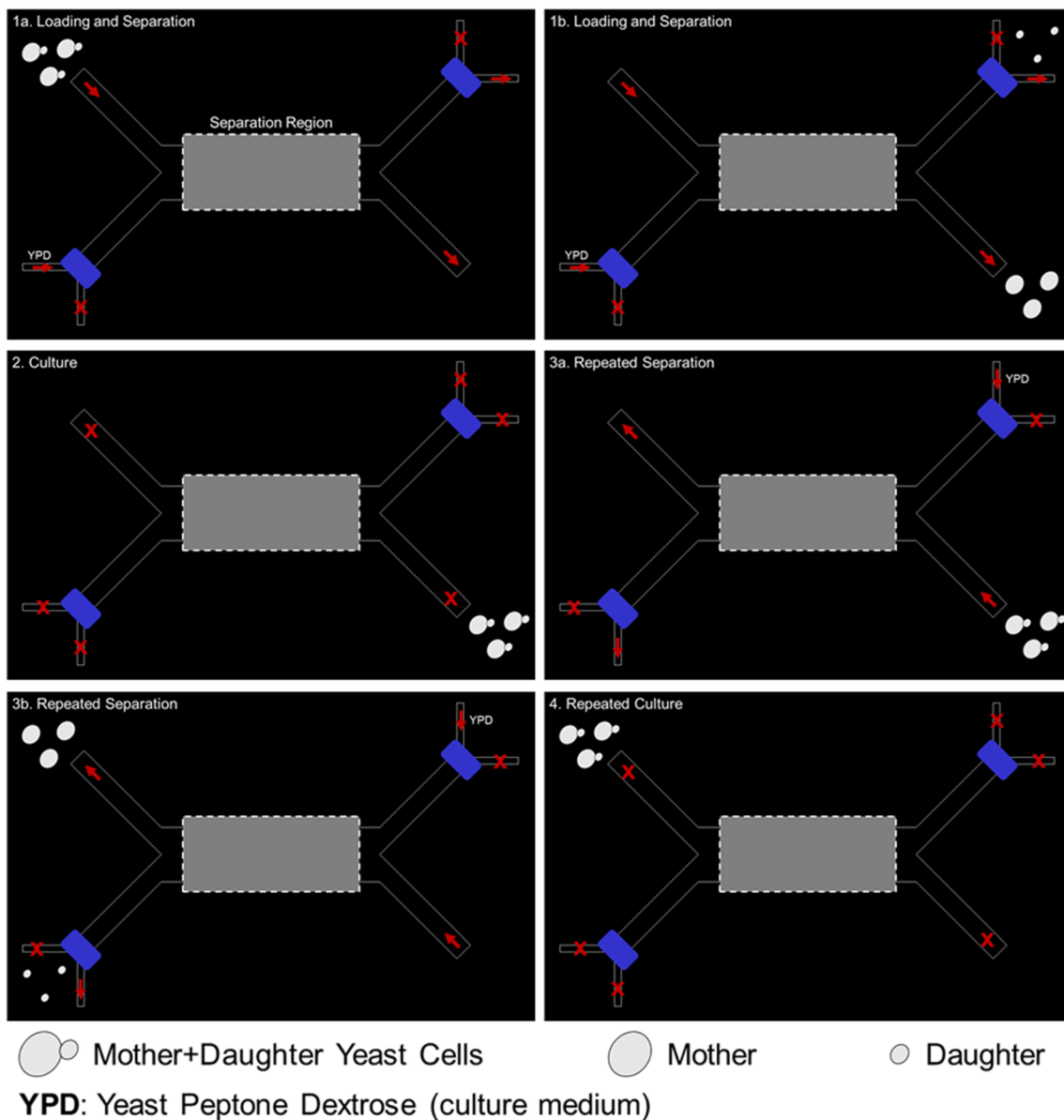
Figure 57. Alternative recirculation strategy to repeat the size-based separation because on-chip recirculation cannot be designed (see Figs. 54-56). Directions of flow are indicated by red arrows, and blocked flows have red x's. Mother and daughter yeast enter the device at top left (step 1a), are separated by size, and flow through different outlets (step 1b). Smaller yeast exit the device. All flows stop, and the kept yeast are cultured so they can grow, bud, and age (step 2). The flows are reversed, and the culturing yeast flow through the separation region where they are again separated by size (step 3). The unwanted yeast exit the device while the larger yeast are cultured again once the flows are blocked (step 4). After culturing, the flows return to their original directions to repeat the separation (step 5). After several repeated separations and times for culturing the cells, the final yeast population should consist of a large number of aged yeast.

In step 1a, mothers and daughters are loaded into the device through the inlet at top left. Red arrows denote directions of fluid flow, and red x's signify blocked channels (no flow). The channels are simplified for convenience (e.g. the inlet does not have flow focusing for the yeast before they enter the separation region). Cells flow through the inlet at top left and enter the separation region where they are separated by size such that daughters are discarded through the top right outlet while mothers flow to the bottom right (step 1b) where they are kept in the device. In step 2, all channels are blocked and the mothers are allowed to grow, bud, and age. In step 3a, the appropriate channels are flowed so that the culturing yeast once again travel through the separation region after which daughters exit the device at bottom left and mothers return to the original inlet (step 3b). The fluidic channel in the figure was designed to have rotational symmetry for all inlets and outlets so that separation can be performed as cells travel in both directions through the separation region. Additionally, to separate cells as they travel in both directions through the separation region, the separation mechanism must deflect larger cells toward the opposite channel wall more than smaller cells. Both DEP and acoustic separation accomplish this size-based differential deflection. The bottom right and top left channels are designed to split into smaller channels because fluid must flow either into or out of the device depending on the operation step. The blue rectangles at these inlets/outlets denote that more complicated flow controls (e.g. microvalves) can potentially be implemented instead of simple channel junctions. In step 4, the channels are blocked, again allowing the kept mothers to bud and age. After a designated culture time, the flows can resume as shown in step 5 to separate cells again by size. This process repeats for as long as needed so that yeast from the original population that entered the device are aged.

The microchannel design in Fig. 57 to implement this periodic forward/reverse flow is rotationally symmetric so that cells can be separated by size each time they flow through the

separation region. For the case that the separation cannot be performed in both directions or the device is not designed symmetrically—as with the acoustic separation device in Fig. 50— repeated separation can still be accomplished by (i) blocking and reversing the flows of appropriate channels after cells have undergone separation, (ii) deactivating the separation as cells flow through the separation region in the opposite direction to the original inlet, and (iii) resuming the flow rates and directions and activating the separation after cells have returned to the original inlet. This periodic forward/reverse flow must be programmed with a certain frequency, which we found is determined by the cell division patterns of the yeast. As yeast divide, they spend a certain amount of time budding before exiting mitosis and releasing the buds. We predicted that this attachment of mothers and daughters could worsen the performance of the aged yeast generator.

2.2.6. Budding daughters still attached to mothers are incorrectly kept after separation

Although the periodic forward/reverse flow can be implemented with the acoustic separation device, a major concern with smaller daughters being kept in the device must be addressed. In Fig. 58 we show an acoustic separation experiment observed near the middle of the device channel length. The two images present conditions with acoustic OFF (at left) and ON with 40 mV applied (at right). As expected, applying acoustic radiation deflected yeast toward the channel center; however, most of the cells in the image do not exist alone, that is, they were currently budding a daughter and were attached to this smaller cell. Examples of attached cells are highlighted with the red arrows. Notice how the cells that deflected the most in the acoustic device were the larger cells and the larger cell clumps.
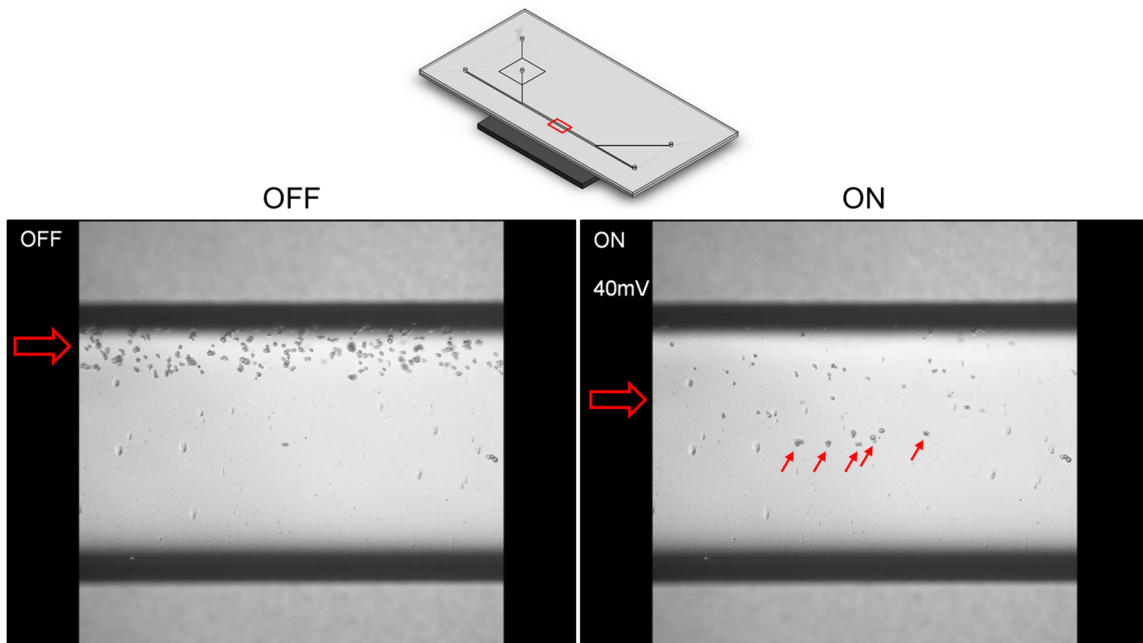
Figure 58. Acoustic deflection of yeast flowing mid-way along the channel length (bottom of figure). Acoustic forces were OFF at left and ON (40 mV applied) at right. Red arrows show the flow directions and the approximate average y-position of the yeast in the field-of-view. With acoustic OFF, yeast are relatively close to the left channel wall (top of image). With acoustic ON, yeast are deflected toward the channel center. Many of the yeast closest to the channel center, i.e., those yeast experiencing the greatest acoustic forces, consist of cell clumps. These cell clumps can worsen separation resolution because smaller cells in the clumps may not be removed from the device as desired.

Ideally, all daughters would be removed after yeast travel through the separation region once; however, yeast spend a certain amount of time budding a daughter before that bud is released. Thus sometimes a mother will not exist as a single cell but will be attached to its daughter, which is problematic when cells are traveling through the separation region because the daughter will be kept with the mother. After some time, however, the mother will finish budding and release this daughter that will start to grow and bud itself. To ensure that this daughter does not remain with the kept cells after it is released, we must perform the separation again before the daughter is allowed enough time to grow such that it is larger than the separation size-threshold. In other words, the separation must be repeated at a high enough

138

frequency so that daughters incorrectly kept in the device because they were attached to mothers cannot grow above the size-threshold. Because of the heterogeneity in division time among yeast in a given population, the cell cycles are far from synchronized, and so any number of yeast may exist as a single cell, be attached to a very small bud, be close to releasing a new daughter, etc.

2.2.7. Simulation model to determine separation frequency and predict aged yeast purity

To determine the optimal frequency for how often the size-based separation should be performed, we developed a model in MATLAB that simulates the aged yeast generator. The software (i) accepts several inputs including separation purity and frequency, (ii) simulates an experiment as if the aged yeast generator were actually being used to produce a large quantity of aged yeast, and (iii) outputs the purity of the resulting aged yeast population, among other results. Figure 59 schematically depicts the model. Nine inputs are accepted into the model, and the output of the model is the aged yeast purity.
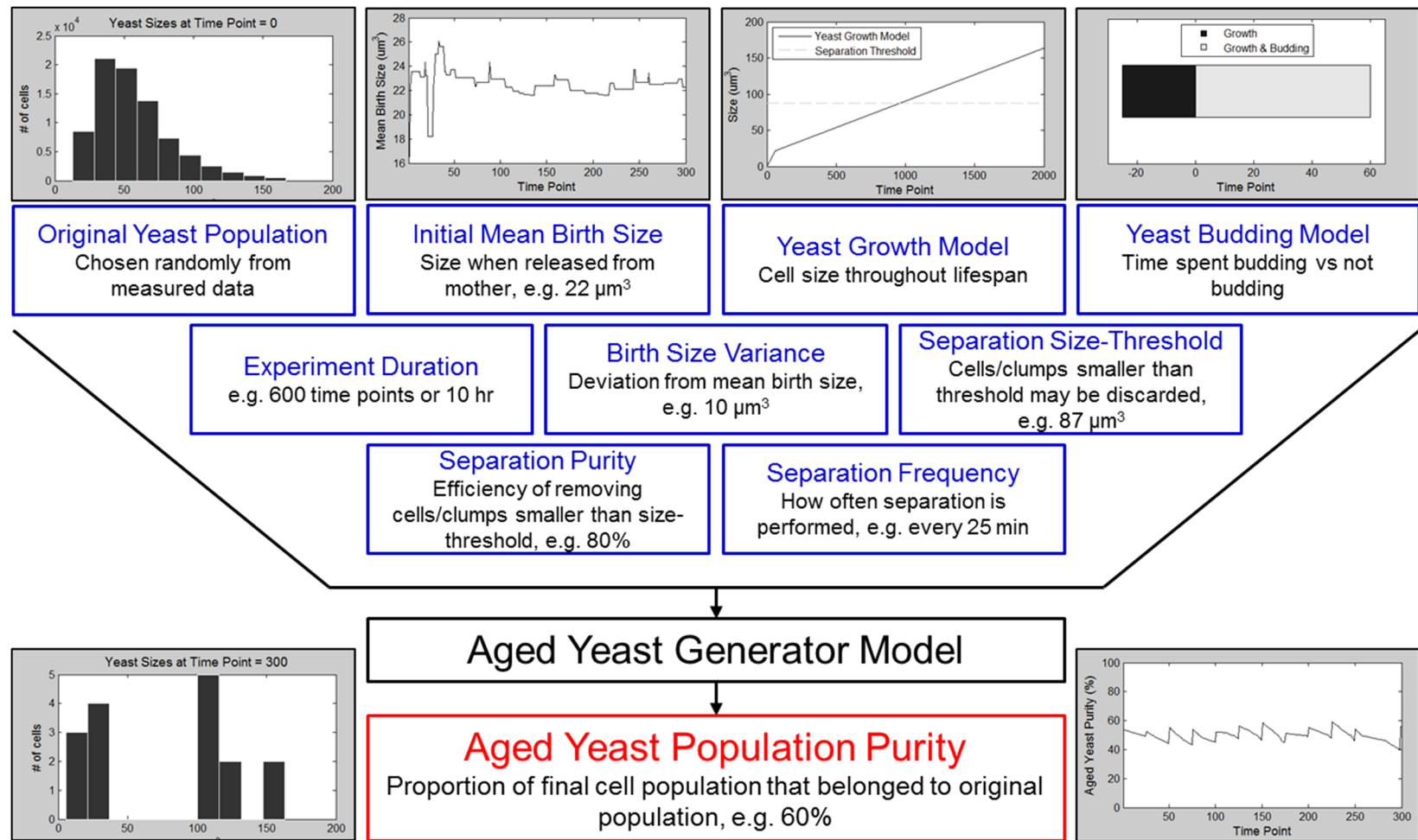
Figure 59. Diagram of the MATLAB simulation model of the aged yeast generator. Nine input parameters determine the output of aged yeast population purity. Plots at top of figure display examples of the parameters in the boxes immediately below them. The lower plots demonstrate the size distribution (lower left) and purity (lower right) of the final yeast population after a simulation with the model.

2.2.8. Input parameters of the aged yeast generator model

The first input is the original yeast population consisting of a user-defined number of yeast (e.g. 100 or 1000 cells) with sizes selected randomly from an actual Coulter Cell-Size Counter measurement of ~340,000 cells (see Fig. 8). The plot above this input in Fig. 59 shows the size distribution of 80,000 randomly selected yeast that enter the model.

The experiment duration, as well as several other inputs, is defined in terms of *time points* which are units that simply must be consistent in the model. For convenience, take 1 time point to equal 1 min. The experiment duration, for example, can thus equal 600 time points or 10 hr.

A yeast growth model is the next input to the simulation, and it contains a typical yeast growth curve from minimum size up to maximum size across the entire yeast lifespan. In the case of the example yeast growth model plotted in the schematic, the yeast size starts at 0 μm^3 at time 0, increases linearly to the birth size at 60 min, and increases linearly to the max yeast size (equal to the max size of the actual data) over ~2,000 time points or 33 hr. Explanation for choosing the particular values defining the models is provided in § 2.2.11. The sizes of all yeast in the simulation follow this growth curve throughout an experiment.

The yeast budding model is then defined in the simulation, which describes the amount of time a mother yeast spends budding a daughter relative to the amount of time the yeast is without a bud in a single cell cycle. More specifically, the budding model quantifies the amount of time a yeast spends in G1 phase without a bud versus the amount of time the mother spends budding in the remaining stages of a cell cycle. The plot in the schematic above the yeast budding model input displays (i) a black segment of 25 time points (or min) representing how much time mother yeast in the simulation spend without a bud and (ii) a gray segment of 60 time points quantifying how long the mother spends budding before the daughter is released. This

time can also be observed in the yeast growth model in which the yeast start at size 0 at time 0 and increase to the mean birth size (~ 21 μm^3 in the plot) over 60 time points. In both segments of the yeast budding model the mother yeast will grow (all cells grow at all time points). Mothers continuously circulate through the budding model, i.e., once a cell reaches the end of the second segment (time point 60), it will immediately start over at the beginning of the first segment (time point -25). When a mother reaches time point 0 or the beginning of the "Growth & Budding" segment, it will start budding a new daughter from size 0. This new daughter is released from the mother after it grows from time point 0 to time point 60. Once the daughter is released, it becomes a mother and enters the budding model at the beginning of the "Growth" segment (time point -25).

The initial mean birth size is equal to the mean birth size of the actual yeast measurement in Fig. 8. This value was 21.44 μm^3. The mean birth size of yeast in the experiment (i.e. the size at which yeast daughters are released from mothers) varies randomly in a Gaussian distribution around the initial mean birth size. The variance is a user-entered percentage of the range from minimum birth size (smallest cell size) to maximum birth size (mode of the size distribution of the experimental data, defined as in ref. 52). The variance value is used in a built-in MATLAB function that generates a random number from a Gaussian distribution centered on the initial mean birth size and having standard deviation equal to the square root of the user-defined variance. The plot above the initial mean birth size variable of the schematic shows how birth size can vary throughout an experiment. The mean size appears more erratic at the beginning of the plot and becomes less variable as time progresses because the mean birth size as plotted is a running average. The exact variance does not change throughout an experiment.

The separation size-threshold determines the yeast that are kept in the experiment and those that are discarded. Single yeast and cell clumps (consisting of mothers and their still-

attached daughters) with volumes below the size-threshold may be removed. An example size-threshold is plotted horizontally on the yeast growth model. The separation purity describes the efficiency of the separation or how well the separation can remove cells and cell clumps below the size-threshold. Out of the total number of cells that should be removed because their volumes are below the size-threshold, a certain percentage remain in the experiment based on the separation purity. For example, if separation purity is 90%, 10% of the cells that should be removed will stay in the experiment. The particular cells that should be removed but stay, if any, are selected randomly.

Finally, the separation frequency quantifies how often the separation is performed. For instance, the user can define that the separation be performed every 5 time points or every 60 time points. How the separation frequency relates to the different segments of the yeast budding model is especially important because this relation can influence the resulting aged yeast population purity, which is the percentage of the final cell population at the end of the experiment that belonged to the original population. After yeast grow, bud, and undergo separation several times throughout an experiment, the resulting yeast size distribution might look like the example plot at the left of the aged yeast purity box at bottom of Fig. 59. In this plot, the cell sizes are either close to the maximum size or close to the minimum size; no cells have intermediate sizes. An example aged yeast purity plot over an experiment is displayed at bottom right of Fig. 59.

2.2.9. Aged yeast generator model simulates yeast separation, growth, and budding

All of these inputs influence how the original yeast population of an experiment is transformed into the final population with a certain figure-of-merit given by the aged yeast purity. Figure 60 portrays the steps completed at each time point of a simulation. The original population, which is

143

loaded into the "device" in step 1, is constructed by first randomly selecting a user-defined number of cells from experimental measurements of yeast sizes (see Fig. 8). The selected yeast are then randomly assigned a particular time location in the budding model that determines whether the cell is currently budding and how close it is to releasing the bud. Some yeast are not attached to buds (if assigned to the "Growth" segment of the model), some are budding ("Growth & Budding" segment), some are about to release the bud (end of "Growth & Budding" segment), etc. The budding yeast mothers are assigned daughter buds with size proportional to the mothers' time locations in the budding model. Mothers at the beginning of the "Growth & Budding" segment will have smaller buds than cells near the end of this segment. As soon as a mother reaches the end of the "Growth & Budding" segment, it releases its bud and immediately returns to the beginning of the "Growth" segment.

After all the initial yeast have been assigned time locations on the bud model and daughter buds as necessary, the resulting population—called the original population—enters the aged yeast generator experiment (step 1 in Fig. 60). An experiment consists of several steps performed periodically. In step 2, some yeast may be removed from the experiment depending on the size-threshold and separation purity parameters. Yeast and yeast clumps having volume below the size-threshold may potentially be removed depending on the separation purity, which determines the percentage of cells below the size-threshold that remain in the experiment. These cells that should be removed but remain in the experiment, if any, are selected randomly. Once a cell is removed from the population of interest, its bud time and size are no longer increased, i.e., cells removed from the experiment no longer bud or grow.
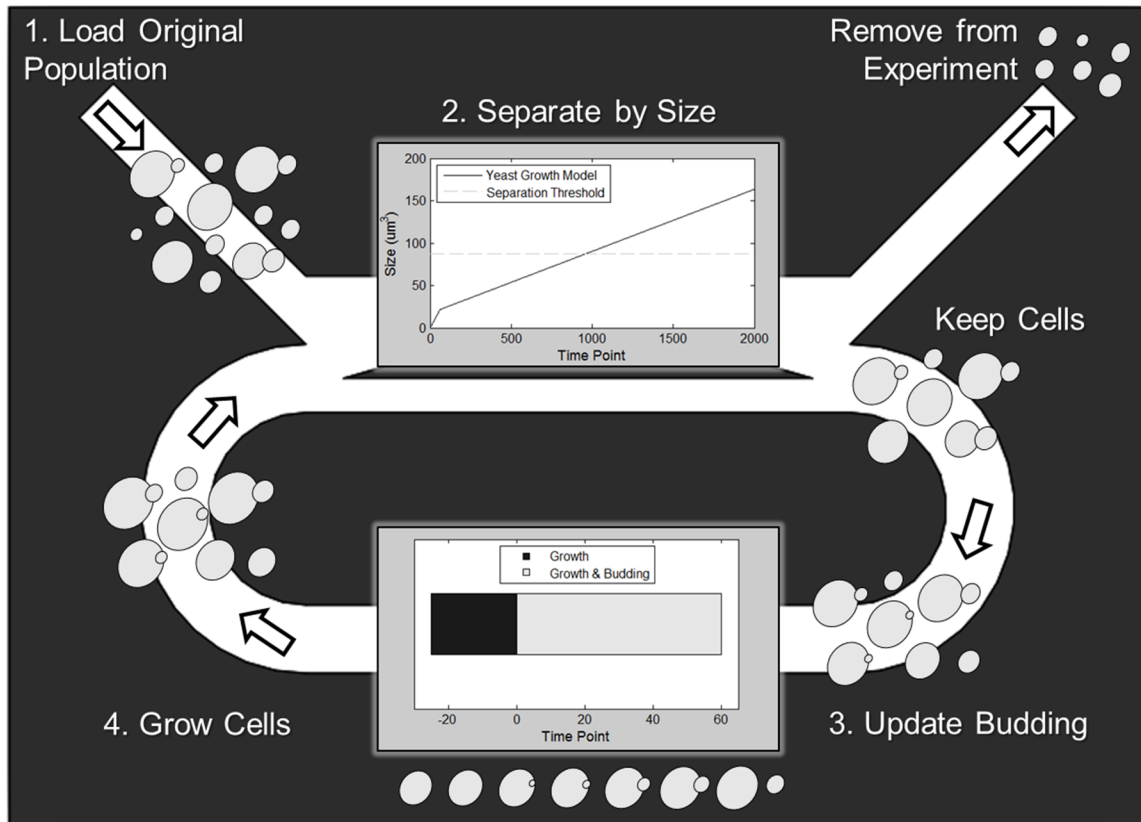
Figure 60. The aged yeast generator model depicted in Fig. 59 follows these steps throughout a simulation (see text). An original population of yeast enter at top left (step 1) and are separated by size (step 2). Smaller cells are removed from the experiment. Larger yeast that remain in the experiment divide/bud (step 3) and grow (step 4) before they either re-enter the separation module or bypass separation and continue to bud and grow. At each time point of a simulation, steps 3 and 4 occur. The user-input of separation frequency defined at the beginning of the simulation determines how often separation occurs (e.g. every 25 time points).

The cells that remain in the experiment proceed to step 3 during which the bud times of all mothers are increased by 1 time point. In other words, all yeast that are not buds advance forward 1 time point in the budding model (displayed mid-bottom of Fig. 60). Mothers that enter the final time point of the budding model (time point 60 at far right of the "Growth & Budding" segment) release their daughters and start over at the far left of the "Growth" segment. Mothers that enter the first time point of the "Growth & Budding" segment are given a new bud of size close to 0. All mothers continuously repeat this budding cycle throughout the experiment, so

cells undergo approximately equivalent cell cycle times throughout their lifespans. Random variation in the cell cycle times produces daughters that are born/released with varying sizes. Variation in yeast birth size and division time is observed in real experiments with yeast. Specifically, for actual yeast, cell cycle time is slow at the beginning of the lifespan during the first 3 generations, rapid during the middle generations (~75 min per division), and very slow during the last few divisions before cell death (often lasting several hours). In the model, however, the variation in division time and birth size has no dependency on the age of a cell. The model could be improved relatively easily to account for this dependence of division time on cell age.

After updating mothers' bud time locations in the budding model, all yeast are grown 1 time point according to the growth model (shown at mid-top of Fig. 60, step 2), i.e., the yeast sizes advance 1 time point on the curve so that the cells grow. Yeast at the end of the growth model (at the largest possible size) do not grow any larger and stay this maximum size for the remainder of the experiment.

After updating bud times and growing the yeast, the population of interest follows one of two paths depending on the separation frequency. At every time point of an experiment, the yeast complete steps 3 and 4 in Fig. 60: their bud times and sizes are updated. The yeast will not, however, undergo size-based separation at every time step. Separation occurs only when the current time point is a certain number of time points advanced from the previous separation's time point. For example, if separation frequency is every 30 time points, the yeast population will skip the separation path of the model 29 times in between every separation. This periodic separation is illustrated in Fig. 60 with the branched channels where one path undergoes separation while the other bypasses it.

2.2.10. Simulation results are displayed throughout an experiment

After each time point of an experiment, the current state of the aged yeast generator model is displayed along with the results of all past time points. In this way, the final display shows the progression of important model outputs including mean birth size and aged yeast population purity. One such experiment is displayed in Fig. 61. Part A plots the yeast growth model and the separation size-threshold. Parts B and C show the cells that have been removed from and kept in the experiment, respectively. The cell sizes in these plots correspond to the cell volumes. The blue cells belonged to the original population that entered the experiment, and red cells are the progeny of the original cells. Part D shows the budding model. Parts E and F plot the size distributions of the original population and the final population, respectively. The mean birth size (a running average throughout the experiment) is plotted in part G. The model input parameters are displayed in part H. Finally, part I shows the purity of the yeast population of interest at each time point. The purity is the percentage of yeast from the original population that are kept in the model (not removed).
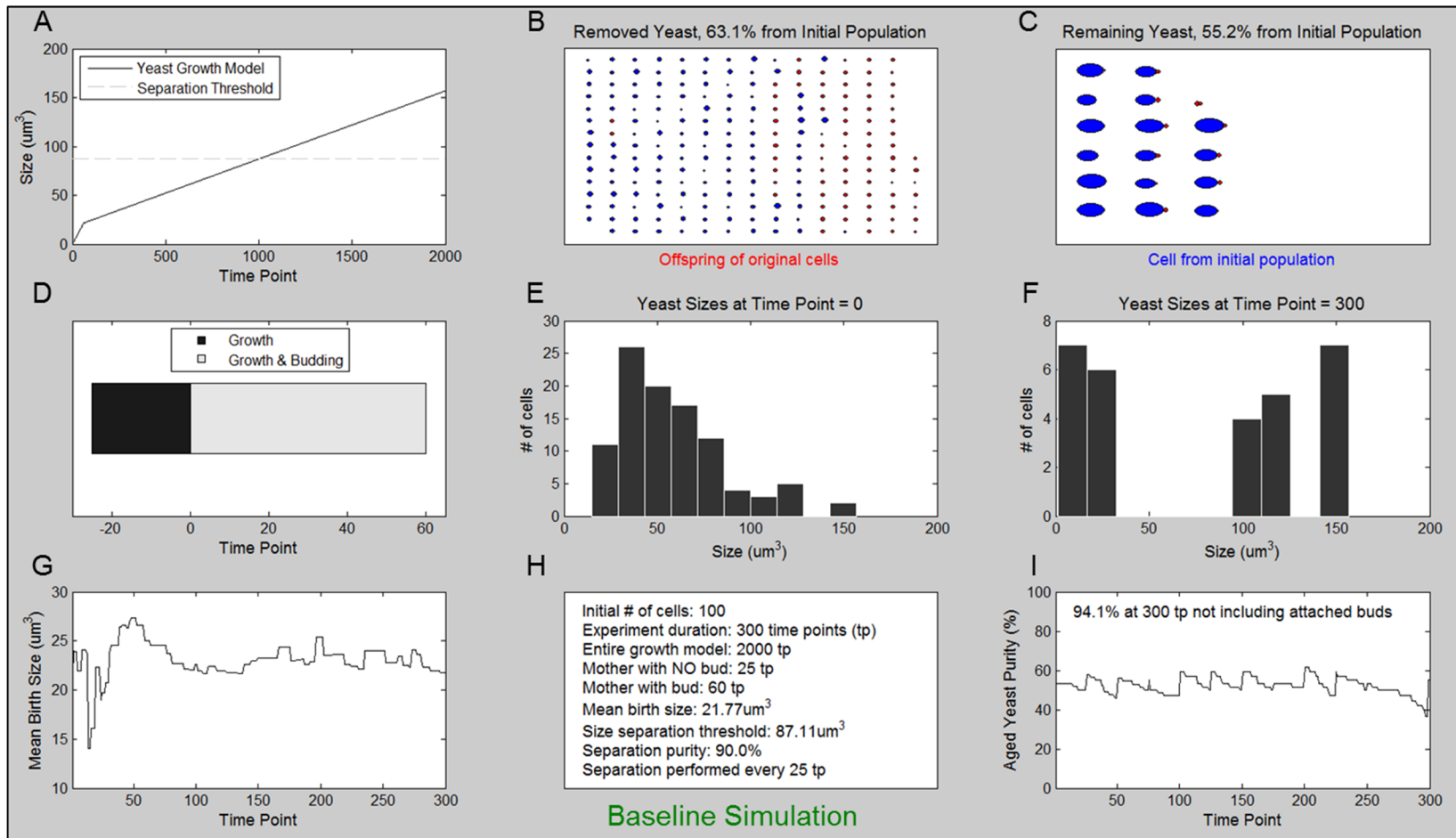
Figure 61. Simulation results of the aged yeast generator model showing a baseline simulation. A) Yeast growth model and size-separation threshold. B) Yeast that are removed from an experiment. C) Yeast that are kept in an experiment after separation. D) Yeast budding model. E) Size distribution of the original yeast population at the beginning of the simulation. F) Size distribution of the final yeast population. G) Mean birth size throughout the simulation. H) Simulation parameters. I) Final aged yeast population purity throughout the simulation. With these inputs parameters, the final aged yeast purity was 55%.

2.2.11. Scientific reasoning for selection of simulation model parameters

Before showing the results of several aged yeast generator simulations with various input parameters, we describe in this section the evidence supporting our choice of model parameters including the yeast size and budding models. First, the cell cycle time was set to ~85 min which was observed in our own experiments and very commonly in the literature. Crane *et al.* discovered that the first 3 cell cycle times for wild-type yeast in 2% glucose in XY media ranged from 60 min to 410 min with a majority of yeast dividing in ~80 min.[9] Yeast from the GFP library grown in YPD from Rowat *et al.* divided every ~100 min.[48] Lee *et al.* observed cell cycle time to last 65-80 min for wild-type yeast grown in YPD.[18]

With the cell cycle time defined at ~85 min, the following data analyses and journal papers informed our decision to program the yeast budding model such that a cell spends ~25 time points (or min) in G1 phase growing without a bud and ~60 time points in the remaining cell cycle stages. Charvin *et al.* published a video in which mother yeast are stained with a yeast bud marker (CDC10-YFP) in order to monitor the particular gene associated with anaphase and the mitotic exit.[15] Analysis of this video using MATLAB (Fig. 62) showed that a particular mother yeast spent ~45% of the time not budding and existing as a single cell in G1 phase. At left in Fig. 62, a red-dotted box identifies the yeast of interest. The plot at right calculates the number of image pixels that are yellow indicating the presence of a bud. Whenever the red-dotted box in the video did not have any yellow pixels, the yeast was not budding. Figure 63 shows the number of yellow pixels for all frames of the video. The data points in red denote that no yellow was detected in the region-of-interest, and the red data points are ~45% of the total video duration, indicating that the cell spent ~45% of the time not budding, which corresponds to ~30-40 min of the cell cycle. The yeast strain used by Charvin *et al.* was a variant of the W303 background, and the cells were grown in SD medium with the appropriate Met dosage. In other

149

experiments, Charvin *et al.* observed wild-type yeast to spend 20-25 min in G1 phase not attached to a bud.
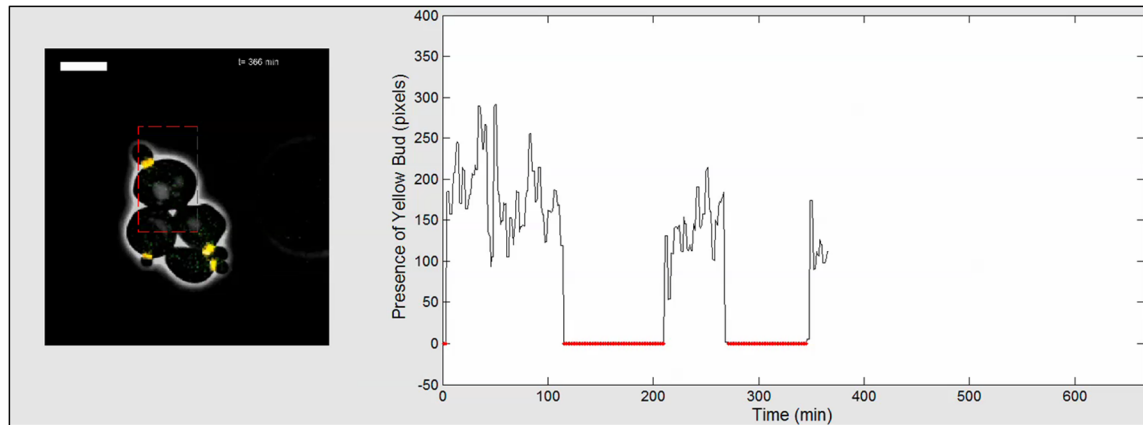
Figure 62. Analysis of an experimental video published by ref. 15 to determine a yeast budding model for the aged yeast generator simulation. A region-of-interest (red-dotted box at left of figure) was identified in each frame of a yeast culture time-lapse in which mothers were stained with a yeast bud marker (CDC10-YFP) such that yellow fluorescence was emitted whenever the mother was budding. The plot at right displays the number of yellow pixels measured in the region-of-interest at left.
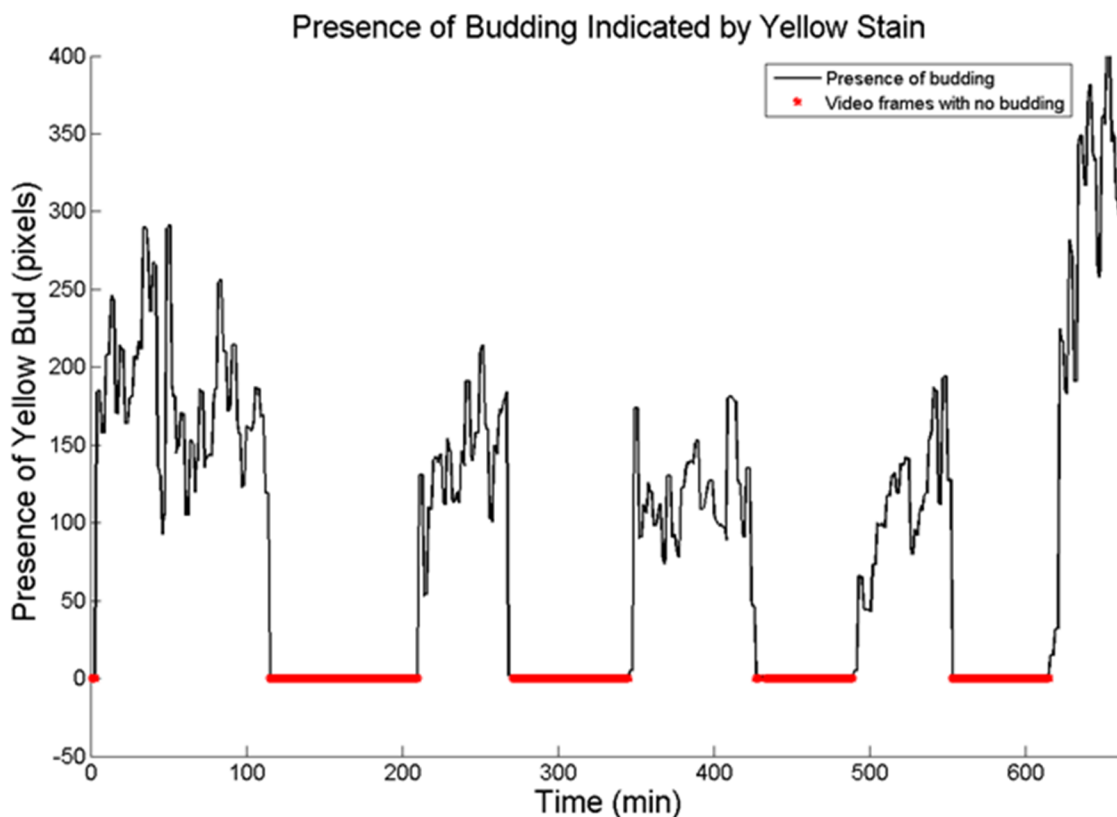
Figure 63. Results of analyzing the yeast culture time-lapse with a yellow fluorescent bud marker from ref. 15 (see Fig. 62) showed that the mother yeast of interest spent ~45% (~30-40 min) of the cell cycle not budding.

Analysis of a yeast lifespan time-lapse from Lee *et al.* showed that a mother yeast spent ~25% of its lifespan not budding.[18] The original video shows a trapped mother yeast as fluid flow selectively removed its daughters from the field-of-view (top left of Fig. 64). We determined the approximate time the yeast is not budding by black/white thresholding each frame of the video (top right of Fig. 64) and using MATLAB to calculate the sizes of cells in the field-of-view. We plot the combined cell size in image pixels for each frame of the video at bottom of Fig. 64. In a stand-alone plot of the combined cell size for each frame (Fig. 65), the video frames in which we identified only 1 cell in the field of view have red data points indicating the combined cell size was that of a single cell. The total number of video frames in

151

which the mother cell was alone and not budding was ~25% of the yeast lifespan. This proportion translates to the yeast existing alone without a bud for ~20 min of the cell cycle. The yeast used by Lee *et al.* was wild-type and cultured in YPD.
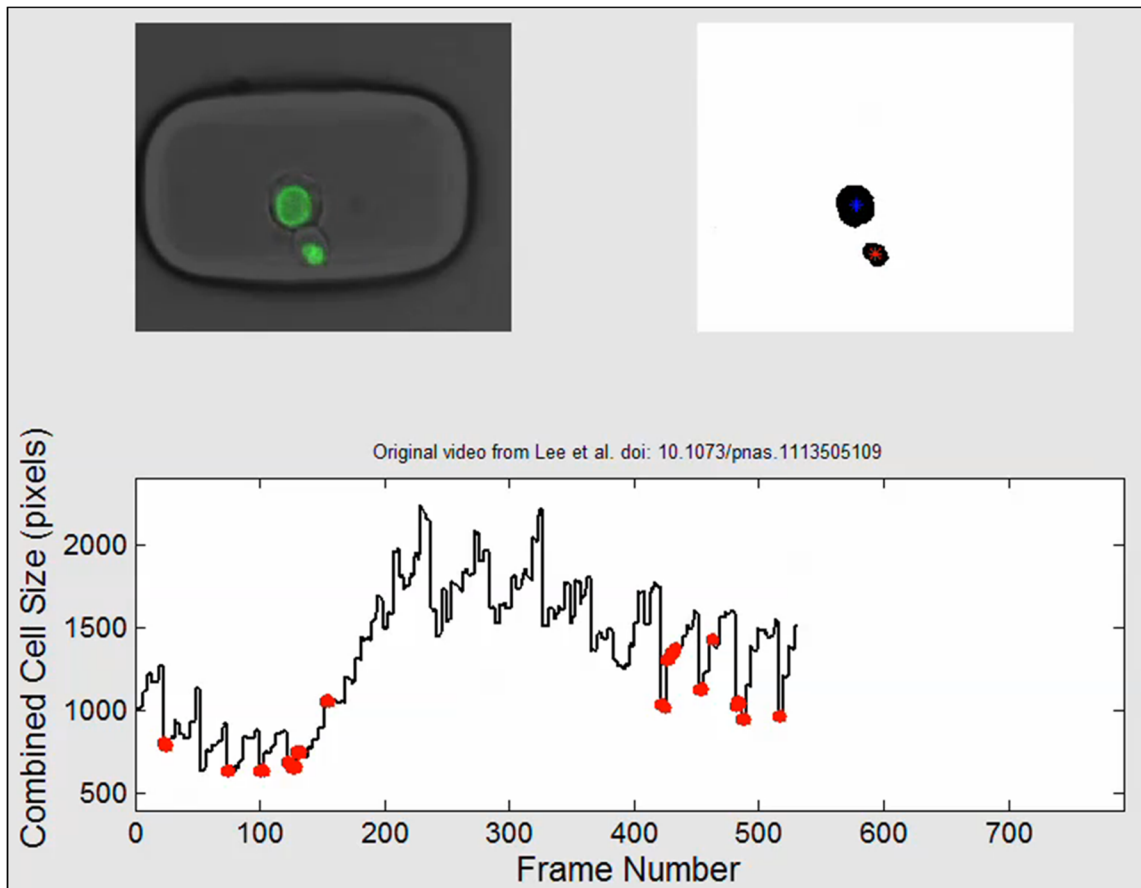
Figure 64. Analysis of an experimental video published by ref. 18 to determine a yeast budding model for the aged yeast generator simulation. At top left, the original video frame is displayed, while the black/white thresholded image is plotted at top right. A function from the MATLAB Image Processing Toolbox is used to identify the centroids and areas of all black objects in the thresholded image. The combined cell size in each video frame is plotted at bottom.
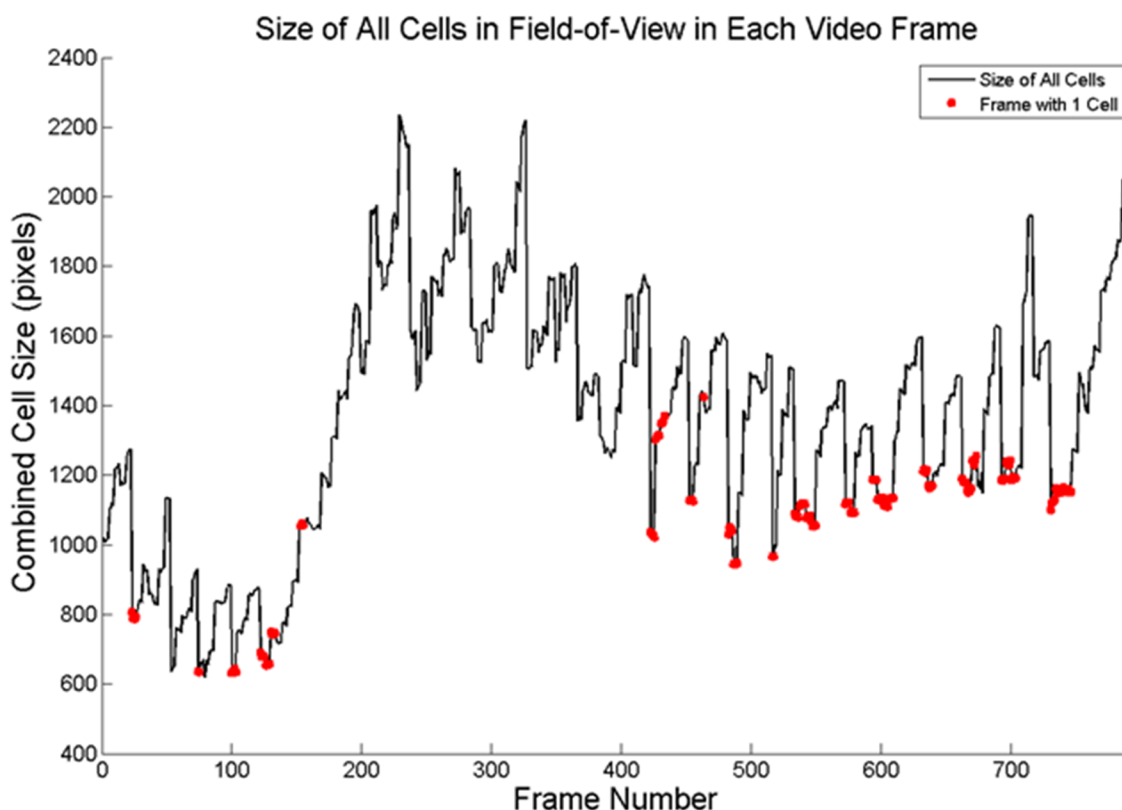
Figure 65. Results of analyzing the yeast culture time-lapse from ref. 18 (see Fig. 64) showed that the mother yeast of interest spent ~25% (~20 min) of the cell cycle not budding.

After analyzing the experimental results from Charvin *et al.* and Lee *et al.* to find that mother yeast spend ~20-25 min not budding, we reviewed a very recent publication by Liu *et al.* who found that modified wild-type CLN3 yeast grown in synthetic dextrose with 2% glucose spend 10-25 min of the cell cycle without a bud.[99] From these analyses and helpful discussion with Dr. Michael Polymenis (Texas A&M University), we decided to define in our model that mother yeast spend ~25 min of an ~85 min cell cycle in G1 phase not attached to a bud.

When researching how to define the yeast growth model over the entire yeast lifespan, we found very little analysis in the literature and could not obtain enough experimental data to conclude with high confidence. Investigating how yeast size trends over time throughout its

entire lifespan was not possible until microfluidics were applied to yeast aging in 2005. Of the two dozen publications we have reviewed (see § 1.9), the research that was closest to solving this problem of cell size over lifespan was discussed in Lee *et al.*[18] In experiments with wild-type yeast, Lee *et al.* observed yeast size to trend approximately linearly after birth in terms of number of buds before death (see Figs. 2C and 3E of Lee *et al.*). Yeast size versus generation is linear up until the last few divisions before cell death. Because cell cycle time is relatively constant throughout the middle of a yeast lifespan (~75-85 min), we can assume the yeast size trends nearly linearly with time. Although the yeast size exhibited increased growth rate during the last few divisions before death, this increase is offset by an increase in the cell cycle time during these least few divisions (~225 min).

2.2.12. Inaccuracies of the aged yeast generator simulation model

From analysis in Lee *et al.*,[18] we concluded that yeast size is linear across the entire yeast lifespan. Even if a linear model is incorrect, this error should not greatly skew the results of a simulation with our aged yeast generator model. The growth trend—whether linear, exponential, piecewise, etc.—once the yeast is larger than the size-threshold is not relevant to the simulation results. Also, the exact shape of the curve is not as important as (i) the yeast birth size and (ii) the elapsed time between when a cell is born and when that cell exceeds the size-threshold.

Other potentially more concerning inaccuracies of the model are not accounting for (i) age-associated changes in the yeast cell cycle time and (ii) the dependence of a daughter's division time and size on the age of its mother. For the first concern, Fehrmann *et al.* showed that the yeast cell cycle time changes from ~75 min at the beginning and middle of the yeast lifespan to ~225 min near the lifespan end.[3] Variance in cell cycle time among yeast in the experiment also increased as the yeast aged. Fehrmann *et al.* experimented with wild-type yeast

154

grown in SD medium. Zhang *et al.* also observed an increase from ~85 min to ~220 min and more heterogeneity in cell cycle time as wild-type yeast in YPD aged and approached death.[23] Xie *et al.* observed similar differences in cell cycle time as yeast aged.[19] An increase in cell cycle time as yeast age, however, does not worsen the aged yeast population purity in our simulation; in fact, it may improve the purity. The separation frequency must simply be high enough to remove the offspring of yeast that have the shortest division times. Such a frequency would also eliminate the offspring of yeast with much longer division times.

The dependence of a daughter's cell cycle time and birth size on the age of its mother is not programmed into our aged yeast generator model. Cookson *et al.* found that cell cycle time is influenced by whether a daughter is born from an old or a young mother and whether the mother has entered senescence.[16] The yeast used by Cookson *et al.* were a variant of K699 grown in synthetic drop-out medium supplemented with amino acids and 2% glucose. We discussed in § 1.6 how mother yeast are larger than their daughters except at the beginning and end of the mothers' lifespans.[22] Although the birth size variance input to the model improves the model realism in this aspect, it does not fully characterize these mother-daughter size similarities which can worsen the aged yeast population purity (see next section).

2.2.13. Aged yeast generator simulation results for varying input parameters

After building and verifying our aged yeast generator model, we simulated several test cases with varying inputs to determine which parameters have greater influence on the purity of the final aged yeast population. The results of a sort of baseline simulation are displayed in Fig. 61. The experiment's input parameters are shown in part H of the figure. In particular, the original population consisted of 100 yeast with size distribution shown in E. With a size-threshold of 87.11 μm^3, 90% separation purity, and separation performed every 25 time points, the final aged

yeast population purity was 55% after 300 time points or 5 hr. We first increased the sample size from 100 yeast in the baseline simulation to 80,000 yeast in the simulation shown in Fig. 66. This significant increase in sample size did not worsen the final aged yeast purity, which was ~56%. We can therefore assume our results with a moderate number of yeast in the simulations will be preserved if we process billions of cells in an actual aged yeast generator experiment. For the following analyses, we simulated the model with 100 initial cells.

After the simulation with large initial cell number, we then modestly increased the birth variance and observed little change in the resulting aged yeast purity. In Fig. 67, the mean birth size ranged between 18 μm^3 and 50 μm^3 (compared to between 14 μm^3 and 27 μm^3 in the baseline simulation of Fig. 61), and the aged yeast purity was 56%. A further increase in the variance such that birth size ranged between 15 μm^3 and 110 μm^3 (Fig. 68) significantly reduced the final aged yeast purity. Several simulations repeated with these input parameters produced similar results. These simulations show that if daughters are born close or greater in size than the separation size-threshold, they will contaminate the final yeast population; therefore, the size-threshold should be selected greater than the largest birth size. Such a choice could exclude more of the aged mothers and is not possible for the case when daughters are born similar in size to their mothers.
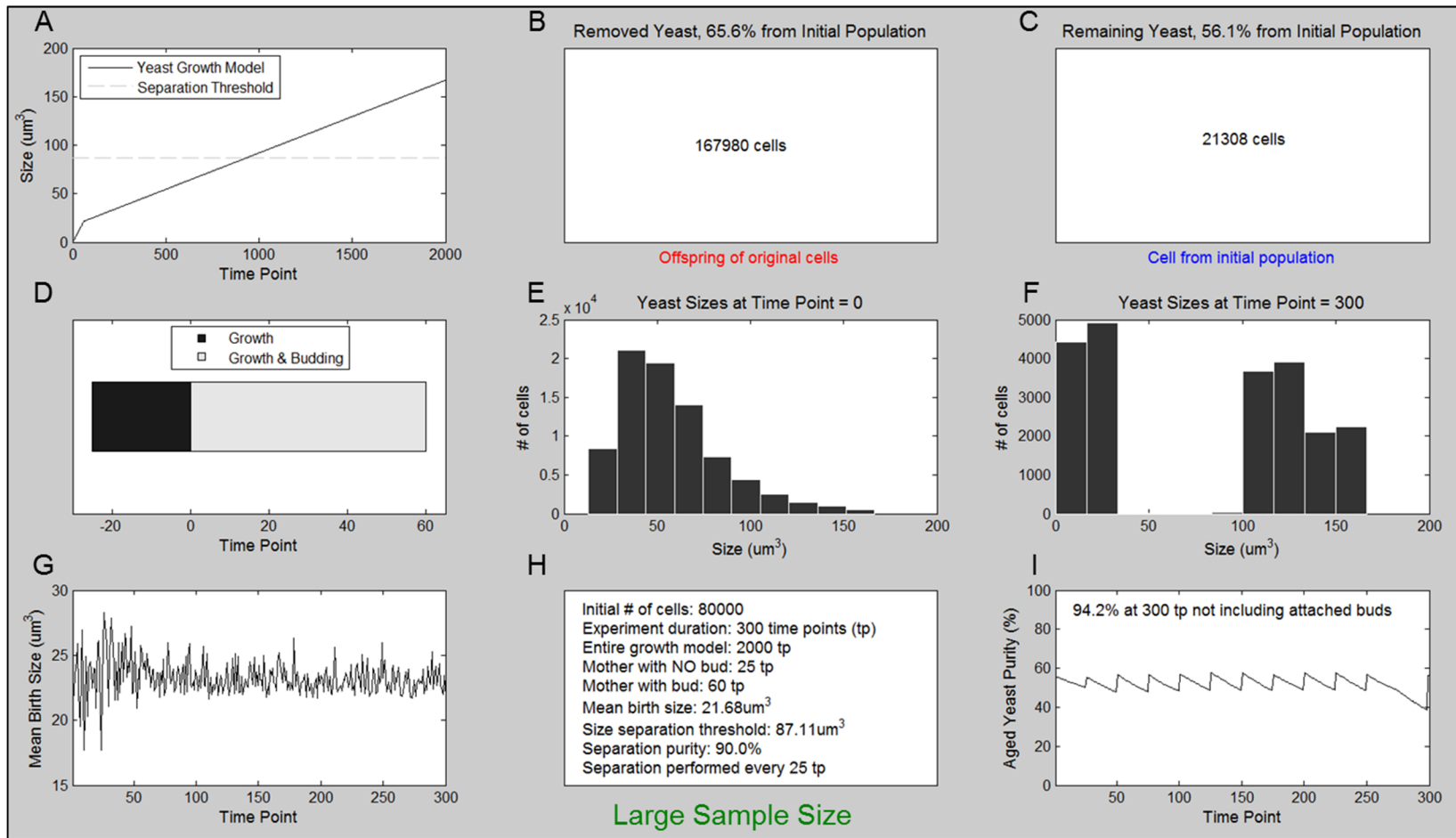
Figure 66. Simulation results of the aged yeast generator model with large sample size. Increasing the sample size from 100 cells (Fig. 61) to 80,000 cells did not change the resulting final aged yeast population purity (~55% in both cases), indicating that the simulation results with relatively low cell number (Figs. 61, 67-75) should be preserved when a much larger number of yeast is processed in the aged yeast generator.

157
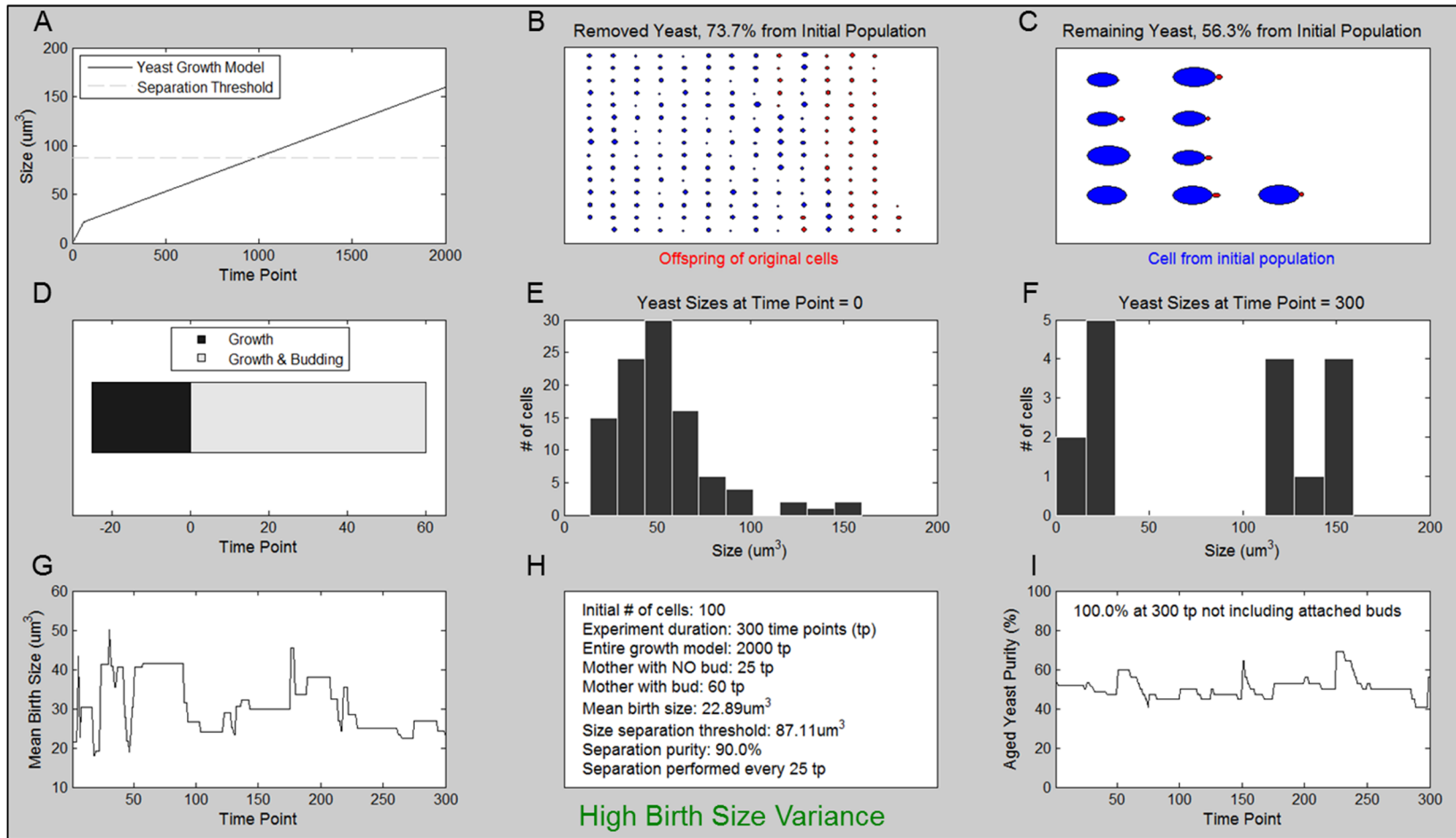
Figure 67. Simulation results of the aged yeast generator model after increasing the birth size variance compared to the results in Fig. 61. After an increase in birth size variance so that the birth size ranged between 18 μm³ and 50 μm³ (rather than between 14 μm³ and 27 μm³, Fig. 61), the final aged yeast purity of 56% was not significantly different compared to the purity of 55% in the baseline simulation.
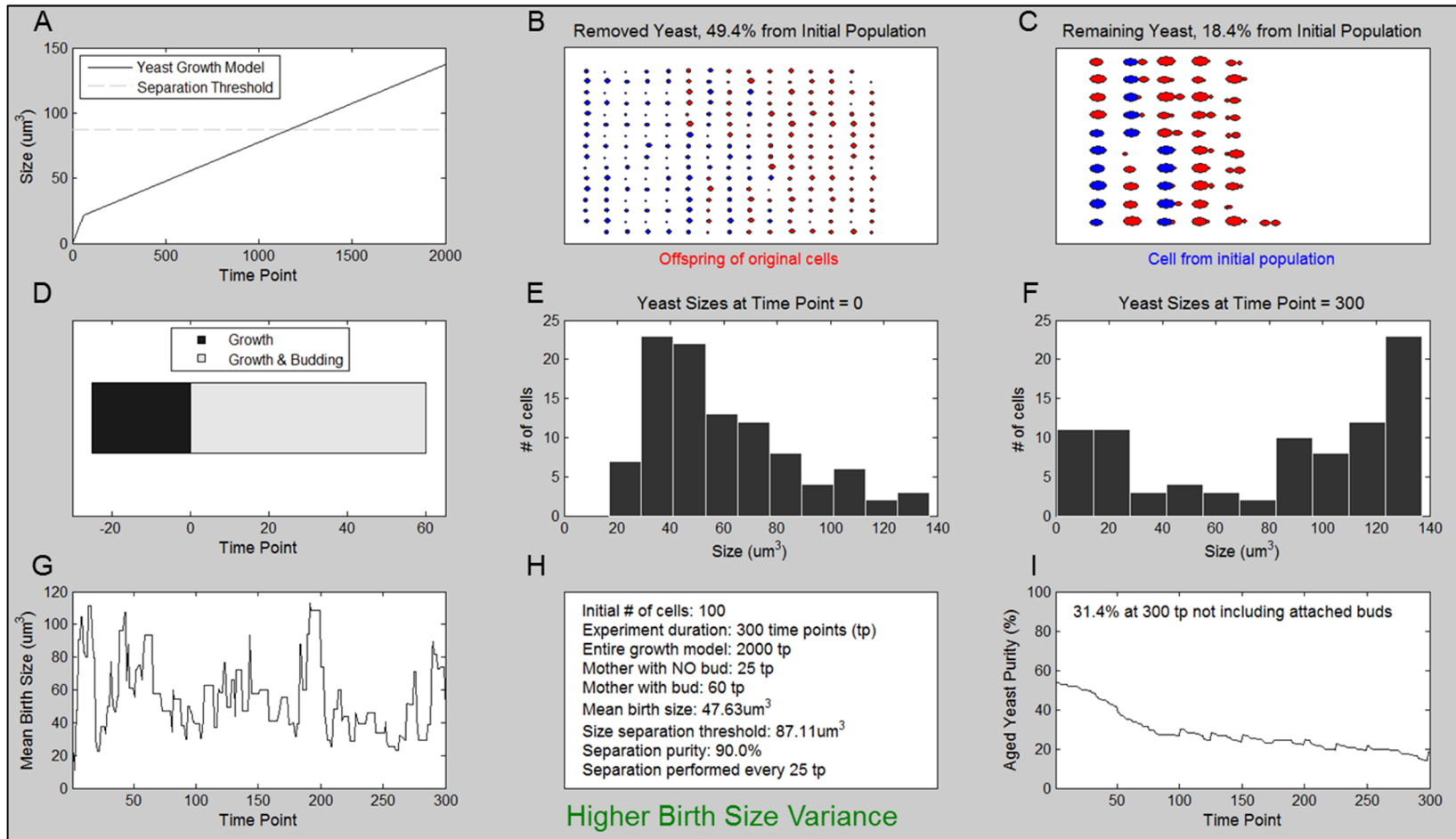
Figure 68. Simulation results of the aged yeast generator model after further increasing the birth size variance compared to the results in Fig. 61. With a birth size varying between 15 μm³ and 110 μm³ (rather than between 14 μm³ and 27 μm³, Fig. 61), the final aged yeast purity of 18% dropped significantly compared to that of the baseline simulation (55%).

After finding that birth size variance can significantly worsen the aged yeast purity, we experimented with a low separation size-threshold. Figure 69 verifies expectations that lower threshold (33.51 μm^3 instead of 87.11 μm^3) produced low aged yeast purity (40% instead of 55%). These results further support the need for relatively high size-separation threshold.

For the simulation results shown in Fig. 70, we decreased the separation purity to 40%, which meant that 60% of the yeast that should have been removed from the experiment (because their sizes were below the size-threshold during a particular separation event) incorrectly remained in the experiment. By the end of the experiment (300 time points), the aged yeast purity dropped to 35%. The minimum separation purity that did not significantly reduce the aged yeast purity was ~60%. Even this low of a separation purity produced an aged yeast purity of 47% (Fig. 71). These results imply that the size-separation subsystem of the aged yeast generator should efficiently remove smaller yeast with >60% purity.
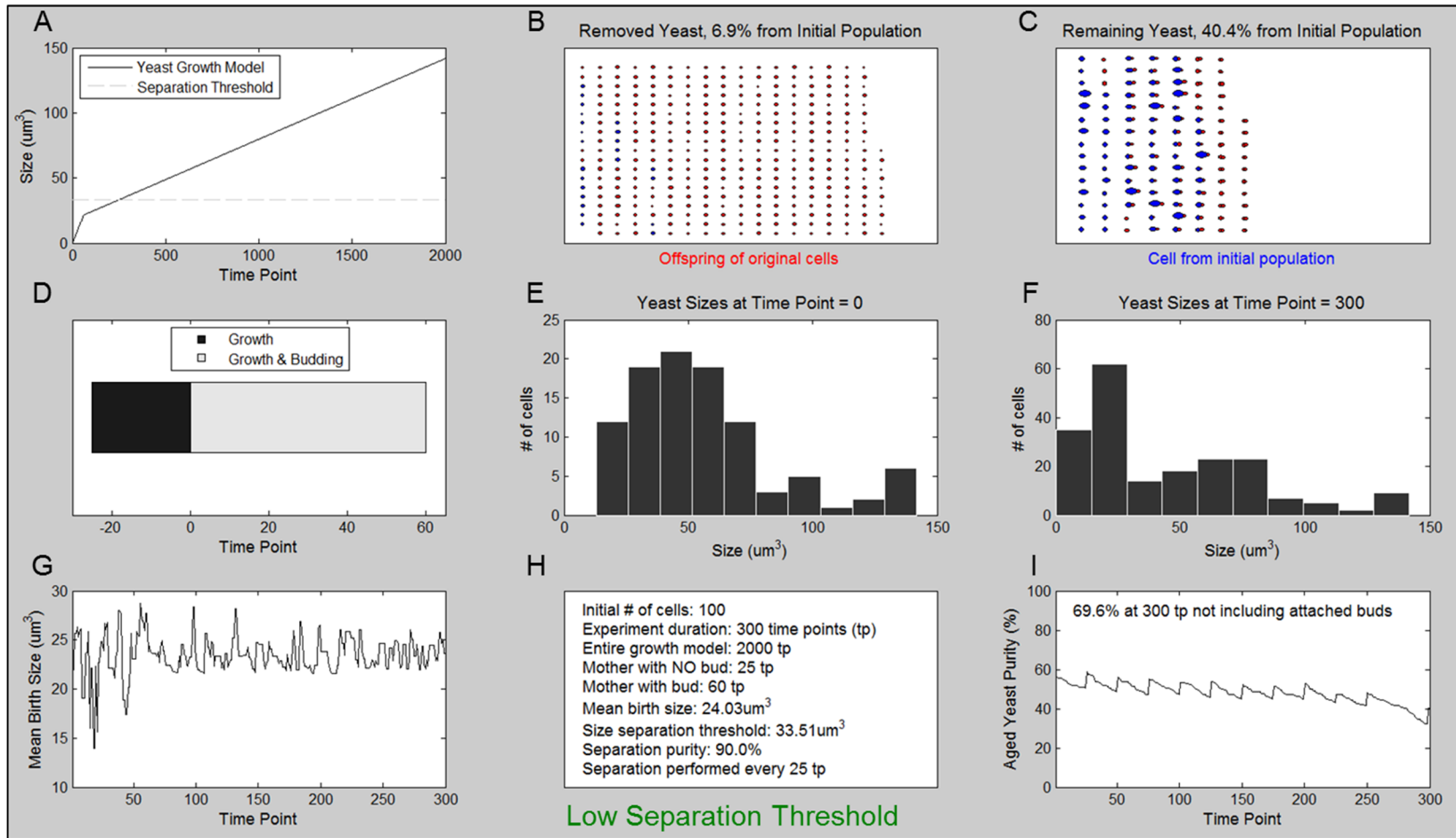
Figure 69. Simulation results of the aged yeast generator model with lower separation threshold compared to the results in Fig. 61. Decreasing the separation threshold from 87 μm³ to 33.5 μm³ reduced the final aged yeast population purity from 55% to 40%. These results motivate the need for programming the actual aged yeast generator to have a relatively high separation threshold compared to the yeast birth size.

161
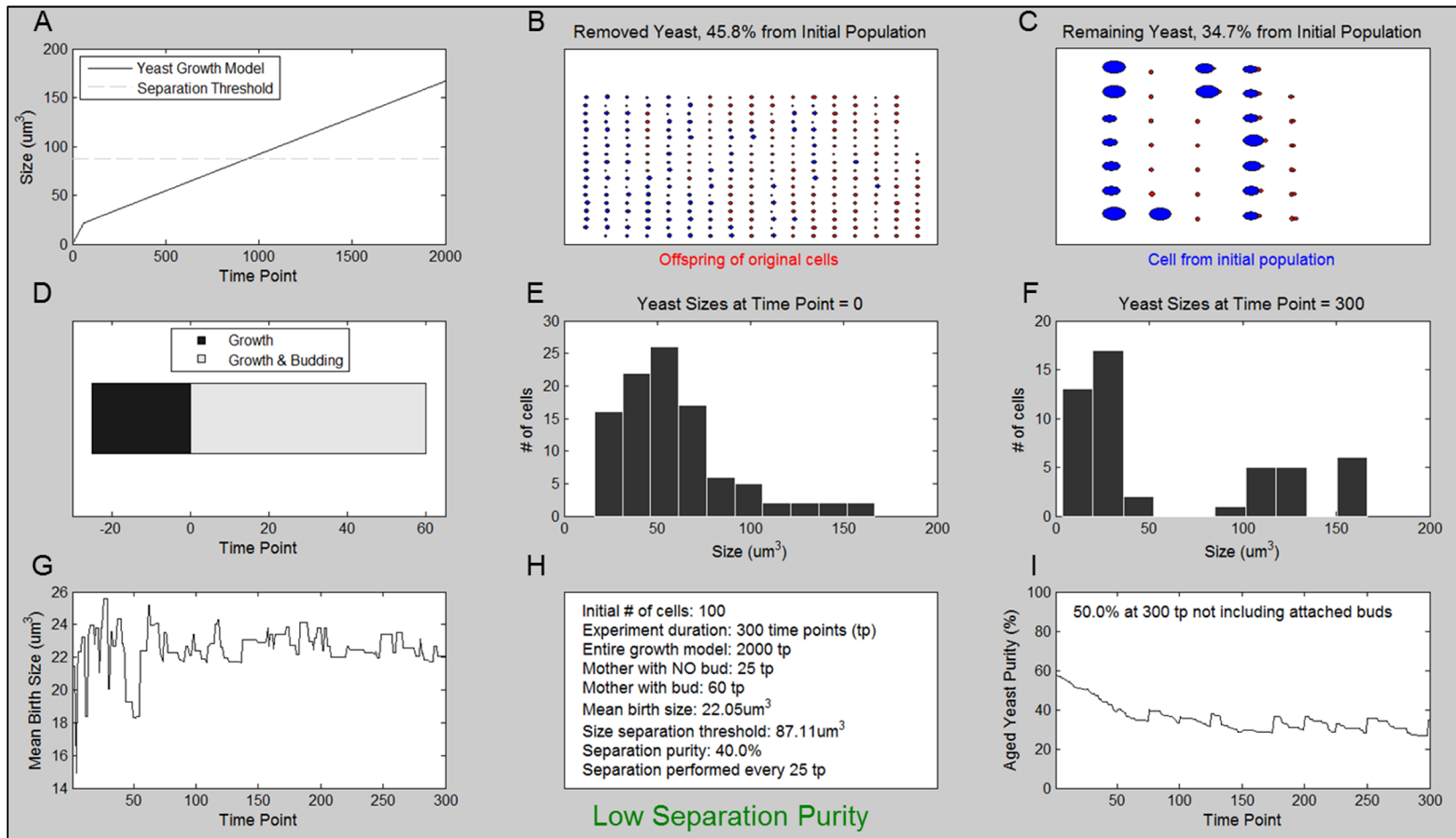
Figure 70. Simulation results of the aged yeast generator model with lower separation purity compared to the results in Fig. 61. Decreasing the separation purity from 0.9 to 0.4 reduced the final aged yeast population purity from 55% to 35%.
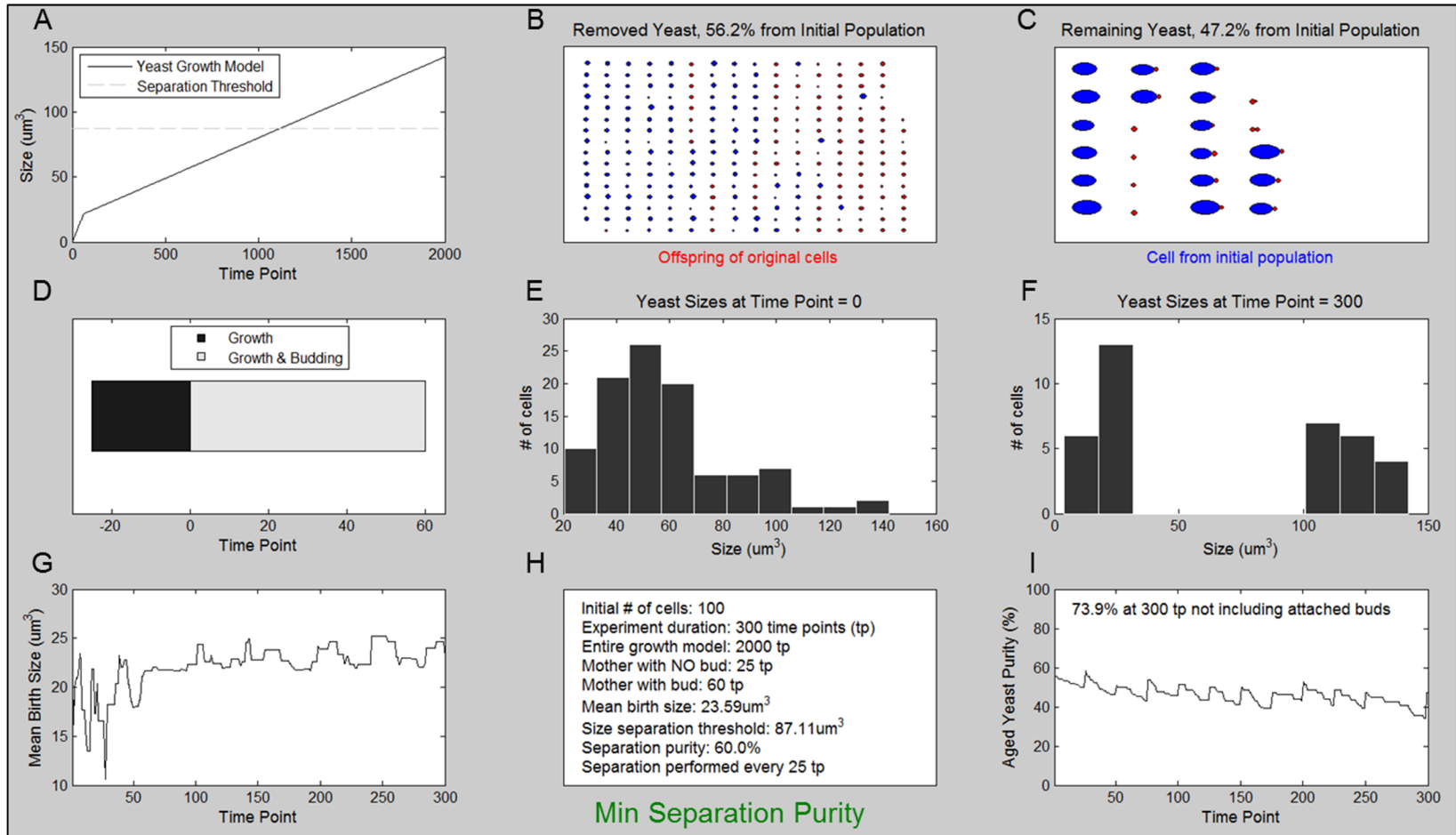
Figure 71. Simulation results of the aged yeast generator model with an estimated minimum separation purity. As long as the size-based separation subsystem of the aged yeast generator removes smaller yeast with >60% purity, the final aged yeast population purity will not be reduced.

163

Low separation frequency also worsens the aged yeast population purity. Figure 72 shows the simulation results with separation performed every 150 time points over a total experiment duration of 3000 time points. The aged yeast purity oscillated between 15% and 45% as the separation was performed at this relatively low rate. After simulating the model with several separation frequencies, we found that the minimum separation frequency that does not significantly worsen the aged yeast purity is ~90 time points (Fig. 73). The periodic forward/reverse flow in the aged yeast generator thus should operate more often than every ~90 min. Even a very high separation frequency of every 5 time points produced aged yeast purity of ~60% (Fig. 74). The inability of the aged yeast generator to create a very high purity of aged yeast results from mothers spending a majority (~70%) of the cell cycle budding. Therefore, a mother spends more time attached to its bud than existing as a single cell, and the bud will stay in the experiment because the combined size of the mother and bud is greater than the size-threshold. The resulting aged yeast purity thus can never exceed ~70% when the budding model is defined as shown in the simulations.

We observed that performing an experiment for an extraordinarily long amount of time (30,000 time points or 500 hr, Fig. 75) did not improve or worsen the final aged yeast purity relative to the baseline value (50-60% aged yeast purity for experiments lasting 300 or 30,000 time points). This simulation verifies that the experiment should last only long enough to age the yeast of interest as desired, and increasing the experiment length does not accrue additional benefits. To produce yeast that are >15 generations old, the maximum experiment duration should be ~20 hr.

164
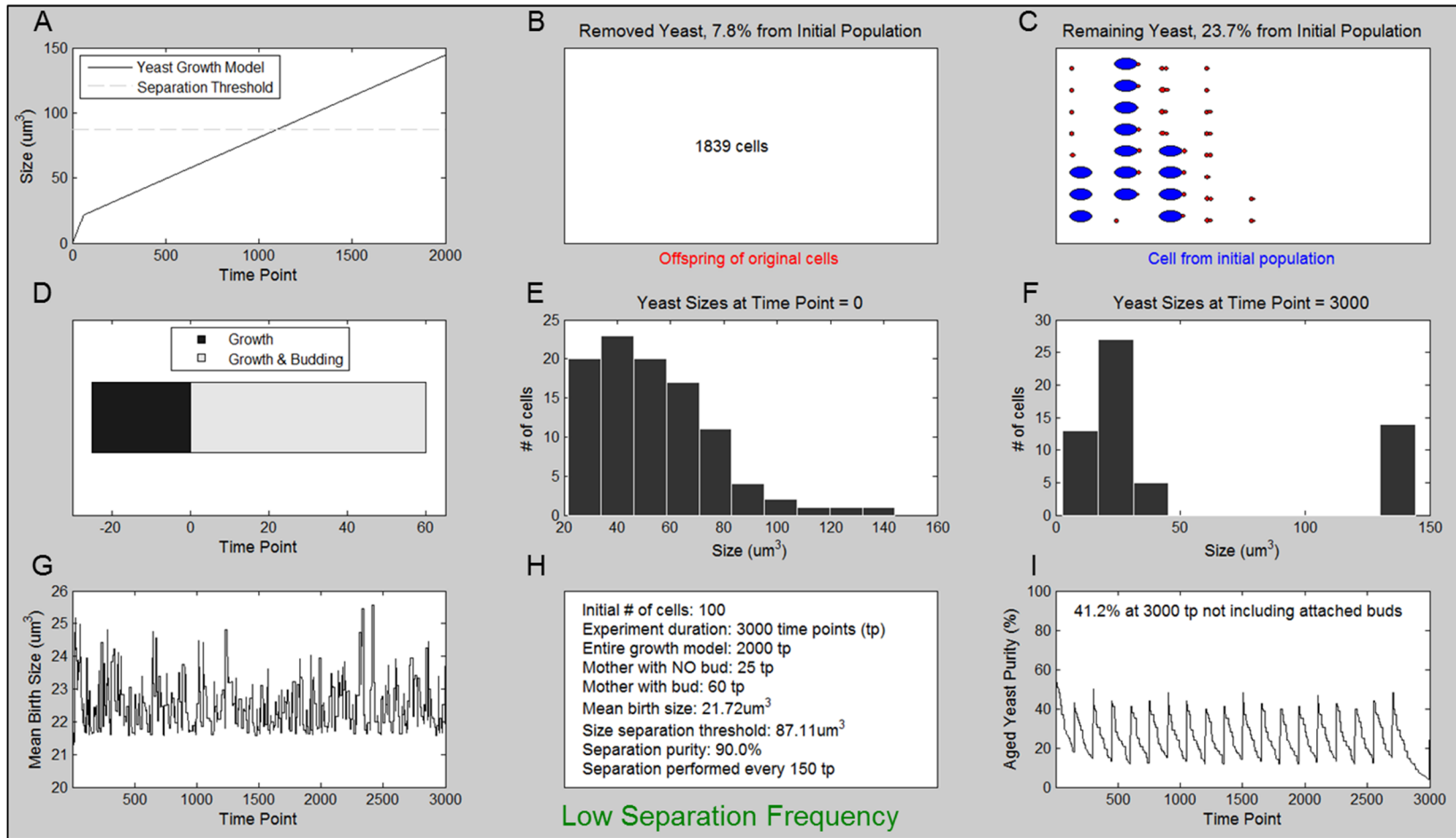
Figure 72. Simulation results of the aged yeast generator model with lower separation frequency compared to the results in Fig. 61. Changing the separation frequency from every 25 time points to every 150 time points reduced the final aged yeast population purity from 55% to 24%.
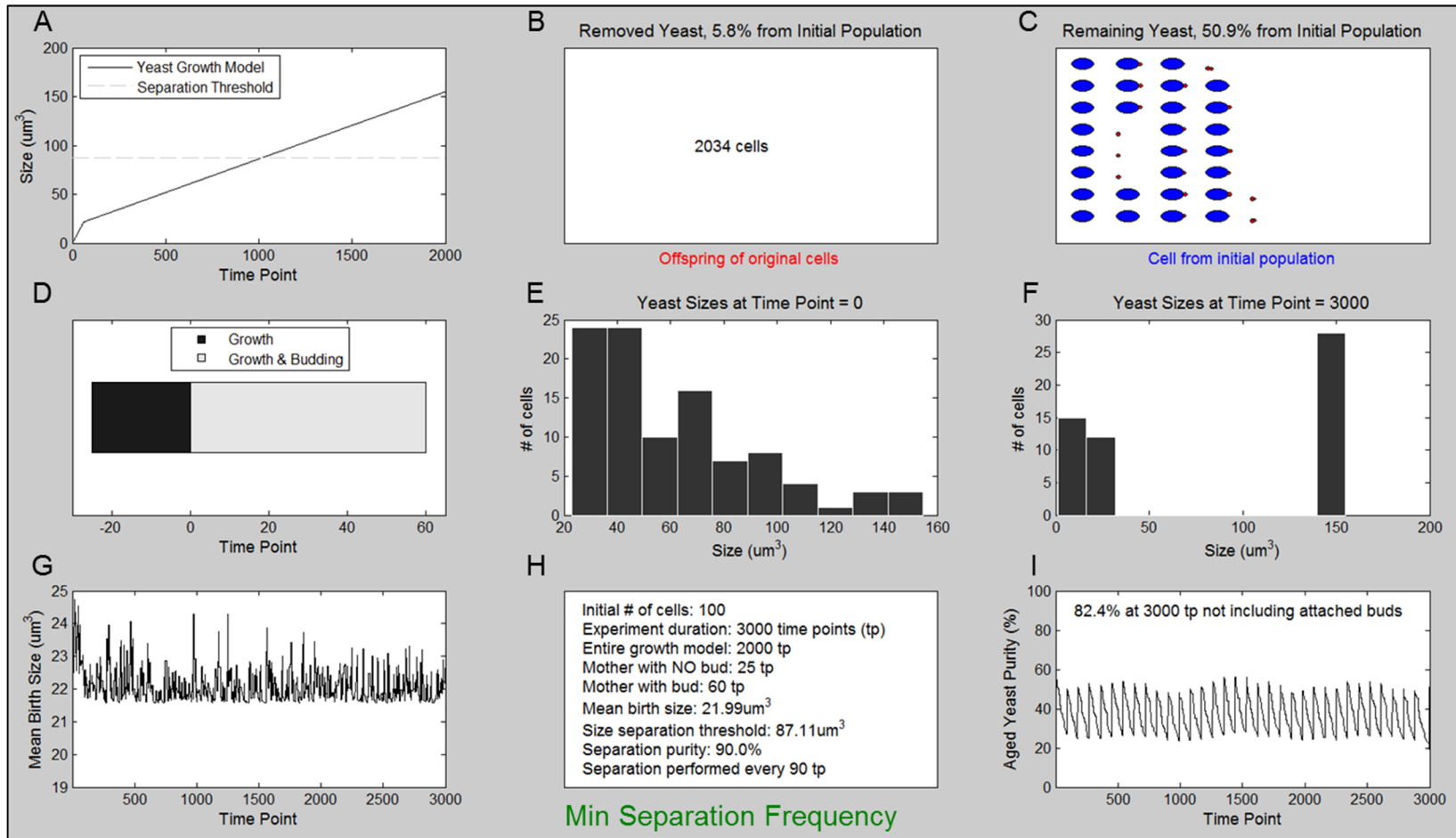
Figure 73. Simulation results of the aged yeast generator model with an estimated minimum separation frequency. As long as the size-based separation of the aged yeast generator is repeated more often than every 90 time points, the final aged yeast population purity will not be reduced.

166
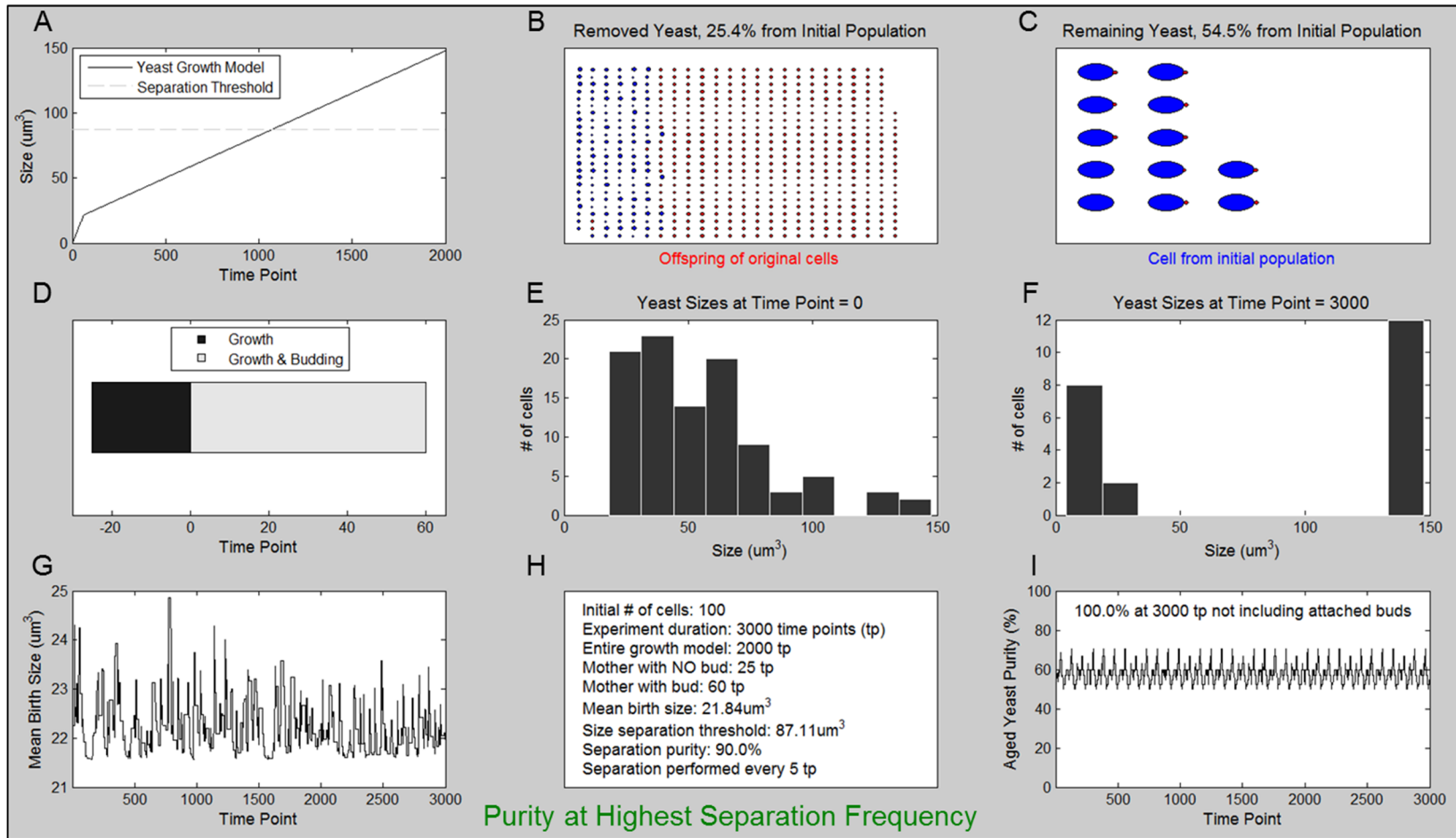
Figure 74. Simulation results of the aged yeast generator model with high separation frequency. Even when the size-based separation was performed every 5 time points, the final aged yeast population purity was never >70%. This upper limit on the final purity results from mother yeast spending ~70% of the cell cycle attached to a daughter bud so that the bud is not removed by the size-based separation.
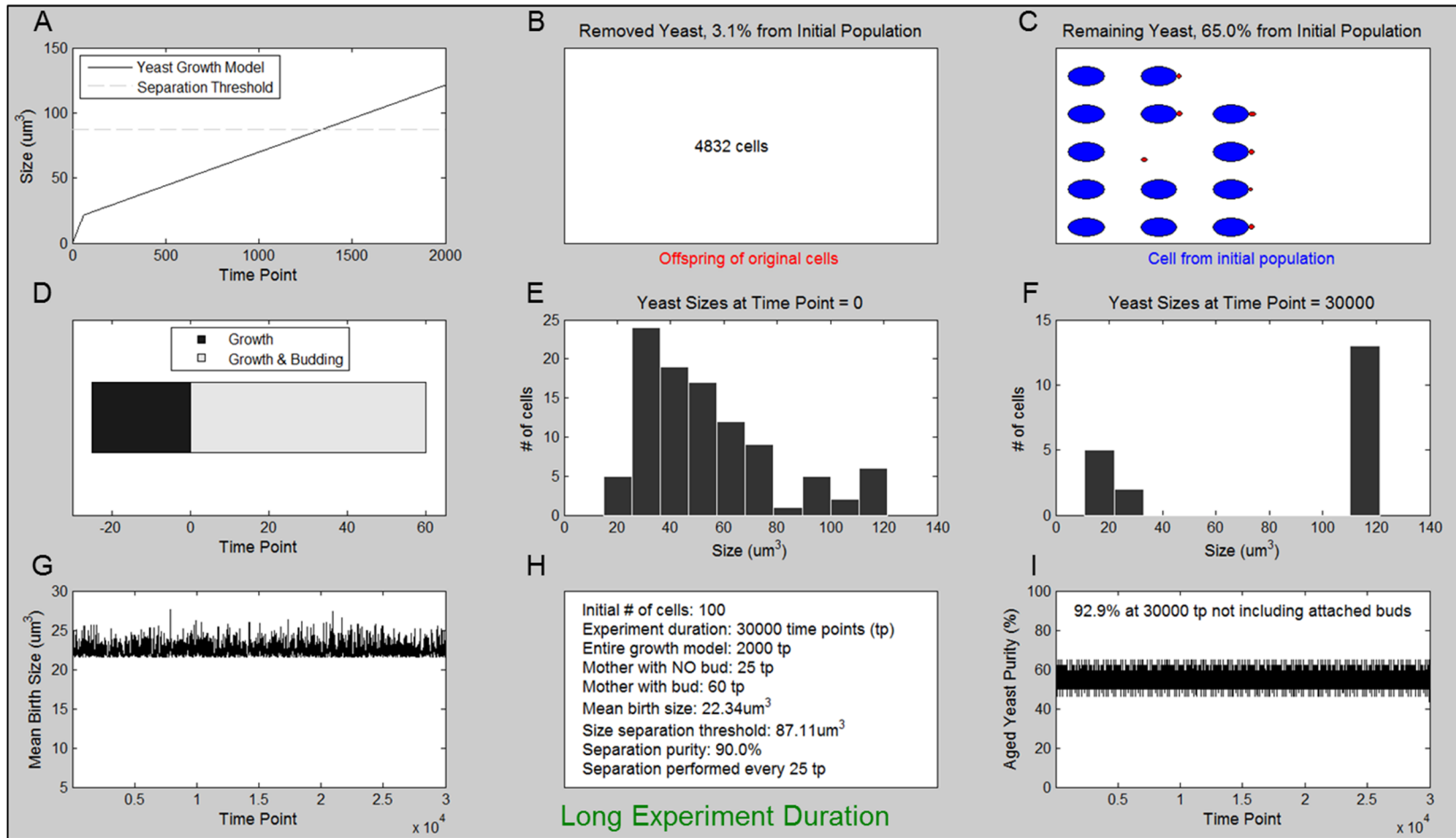
Figure 75. Simulation results of the aged yeast generator model with long experiment duration. Increasing the experiment duration does not accrue additional benefits; therefore, an actual experiment with the aged yeast generator needs to last just long enough to produce aged yeast (<25 hr).

168

After finding that the final aged yeast population purity may have some sort of an upper bound (see Fig. 74), we simulated several cases in which the purity was also calculated by considering only the mothers; we did not include the attached daughter buds when calculating how pure the final aged yeast population is. By calculating the aged yeast purity in this way, we observed that it was no longer bounded at ~70%. Figure 76 shows the simulations results with 1000 initial cells, 100% separation purity, and separation performed every 25 time points. Although the aged yeast purity was 62% when daughter buds were included in the calculation, the aged yeast purity was 100% when considering only the mothers in the calculation. These results agree well with expectations: the final population consists of only aged mothers from the initial cell population when the separation efficiency is 100%, i.e. when 100% of cells below the size-threshold are removed from the experiment during each separation run. As we decreased the separation purity, the aged yeast purity decreased similarly. Figures 77, 78, 79, 80, and 81 show the results when separation purity was 90%, 70%, 50%, 30%, and 10%, respectively. For these separation purities, the aged yeast purities were 94%, 83%, 65%, 35%, and 12%, respectively. In summary, when aged yeast purity was calculated such that still-attached daughter buds were excluded, the final aged yeast population purity was close to or higher than the separation purity.
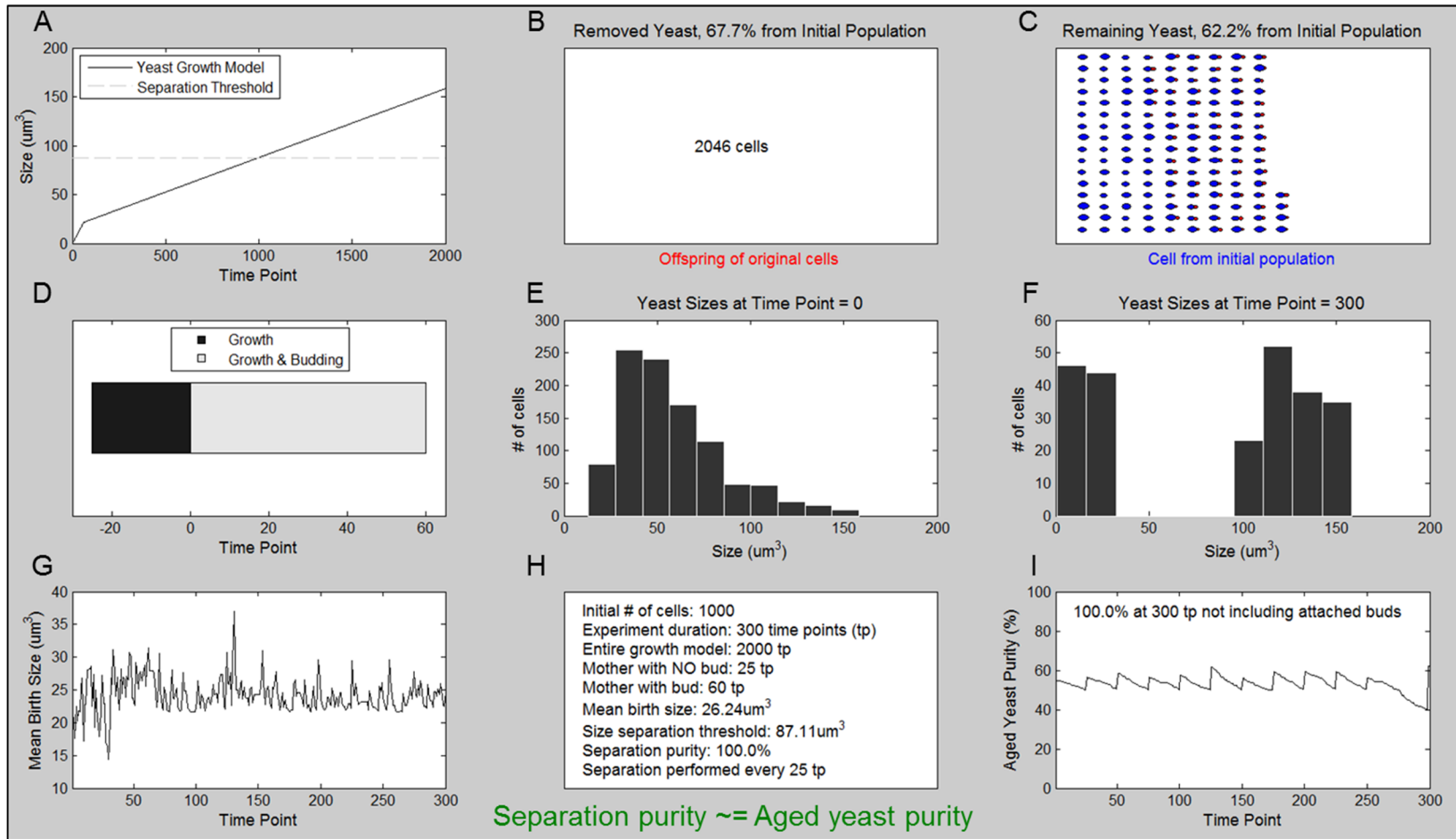
Figure 76. Simulation results of the aged yeast generator model for which the final aged yeast population purity was calculated by excluding still-attached daughters. For 100% separation purity, aged yeast purity was 100% (62% when including still-attached buds).
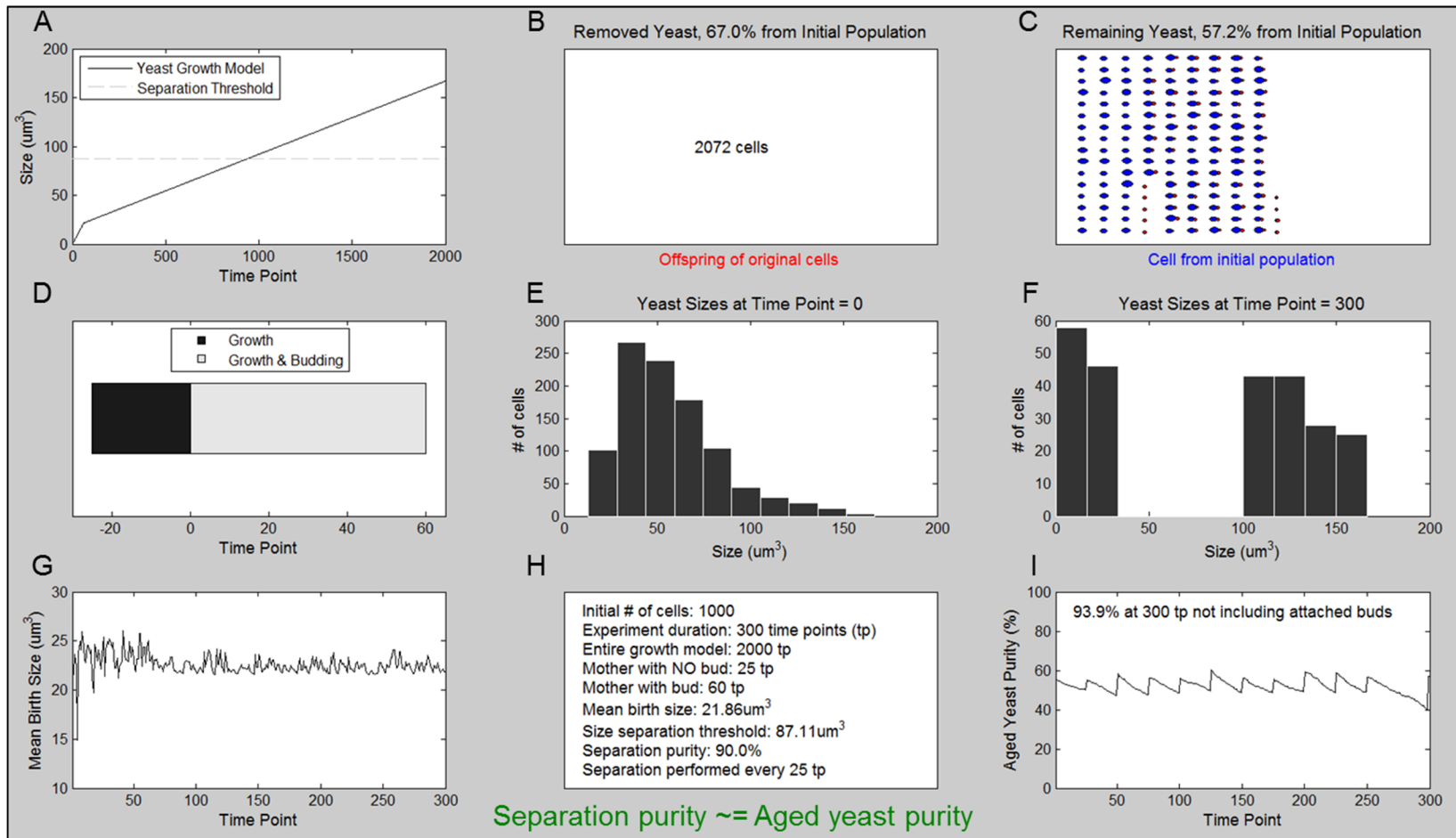
Figure 77. Simulation results of the aged yeast generator model for which the final aged yeast population purity was calculated by excluding still-attached daughters. For 90% separation purity, aged yeast purity was 94% (57% when including still-attached buds).

171
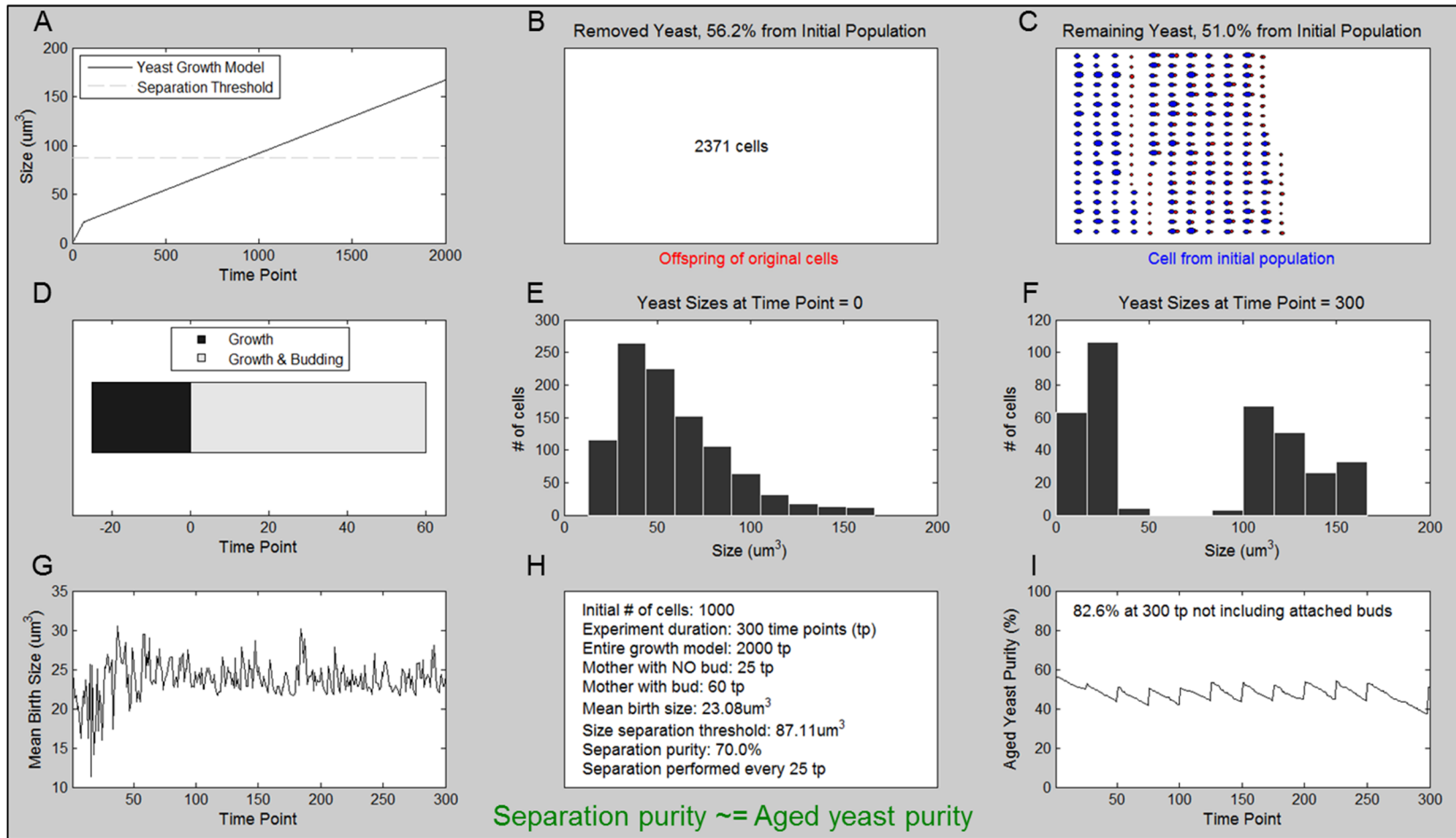
Figure 78. Simulation results of the aged yeast generator model for which the final aged yeast population purity was calculated by excluding still-attached daughters. For 70% separation purity, aged yeast purity was 83% (51% when including still-attached buds).
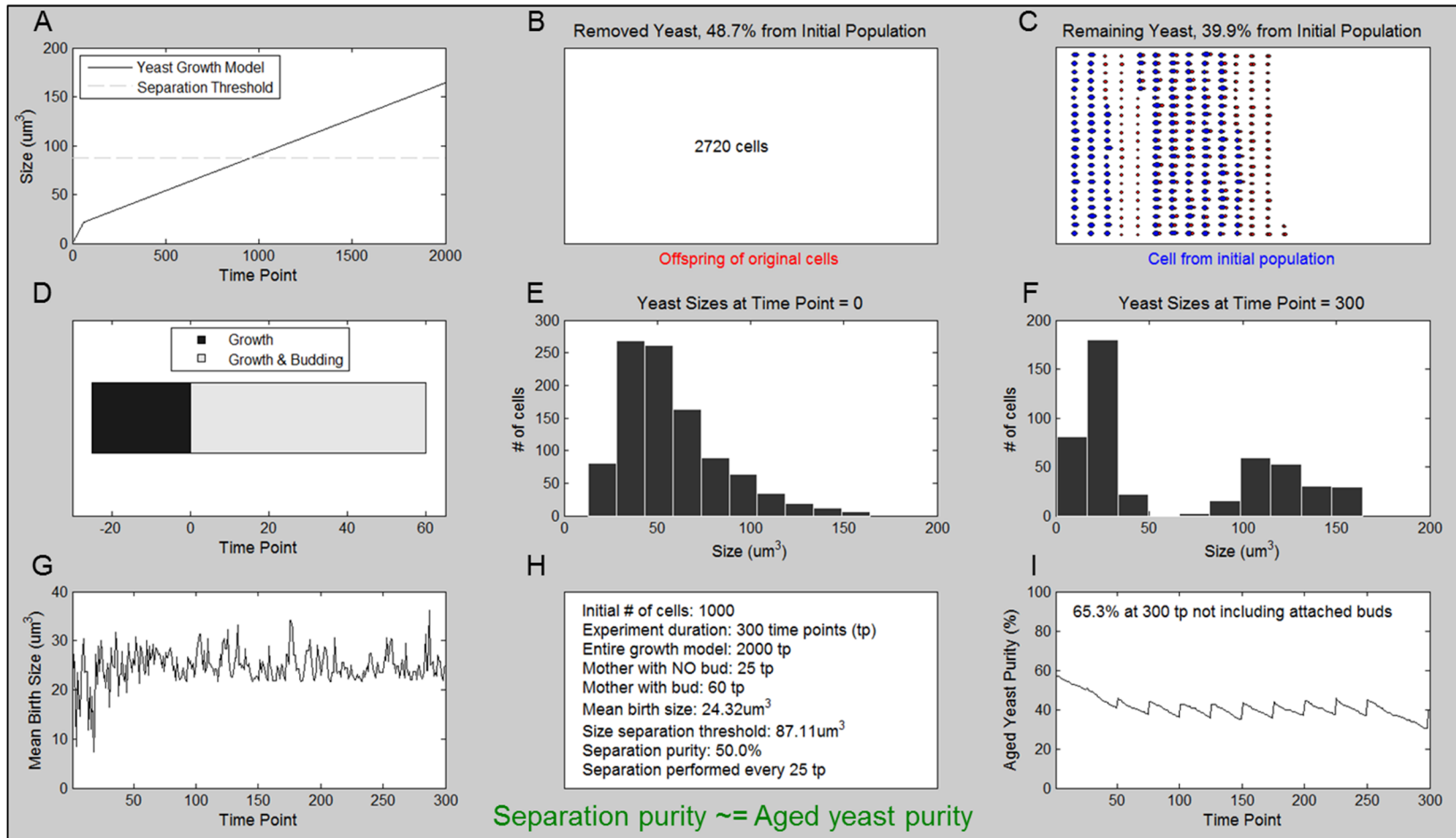
Figure 79. Simulation results of the aged yeast generator model for which the final aged yeast population purity was calculated by excluding still-attached daughters. For 50% separation purity, aged yeast purity was 65% (40% when including still-attached buds).
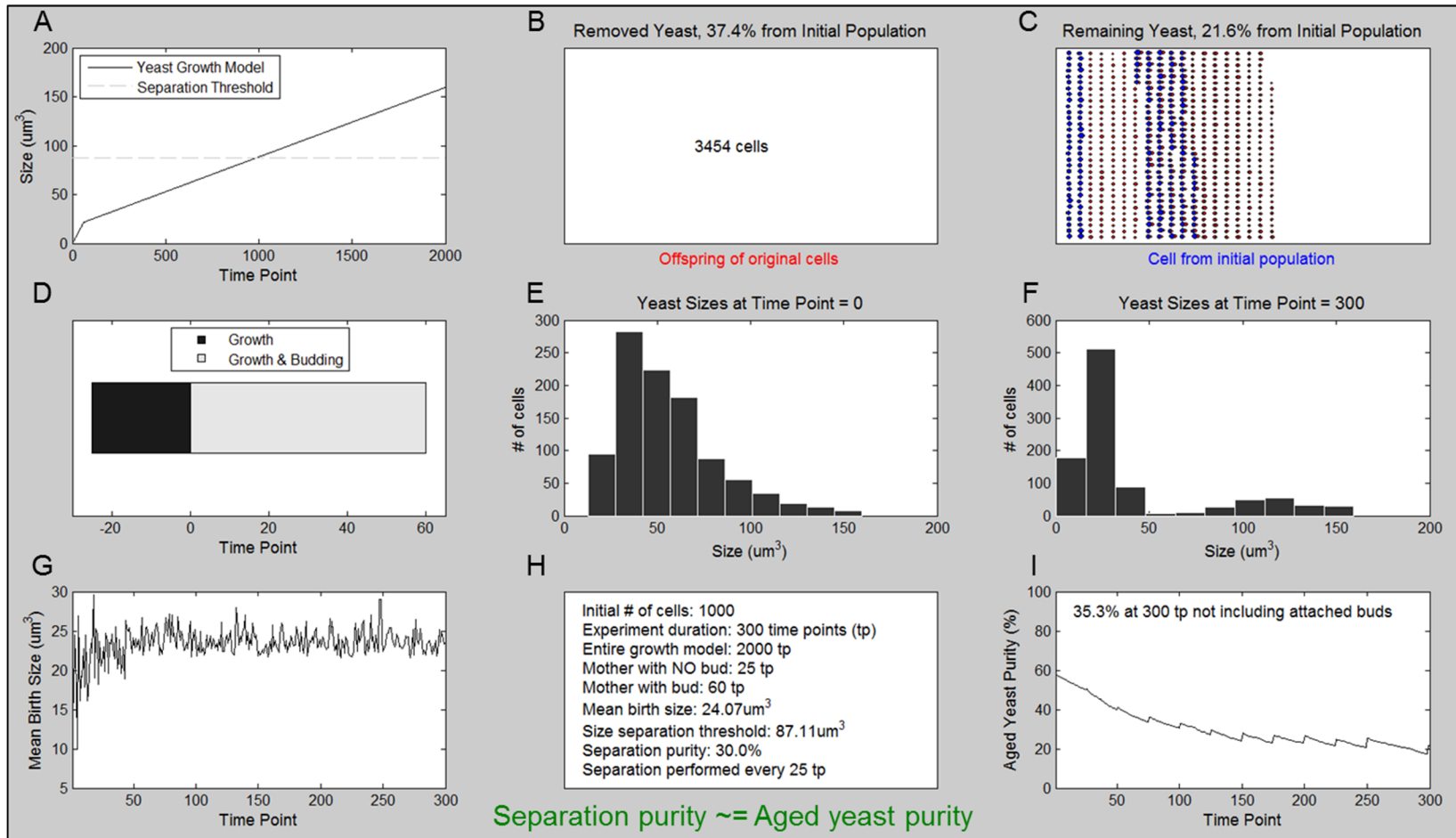
Figure 80. Simulation results of the aged yeast generator model for which the final aged yeast population purity was calculated by excluding still-attached daughters. For 30% separation purity, aged yeast purity was 35% (22% when including still-attached buds).
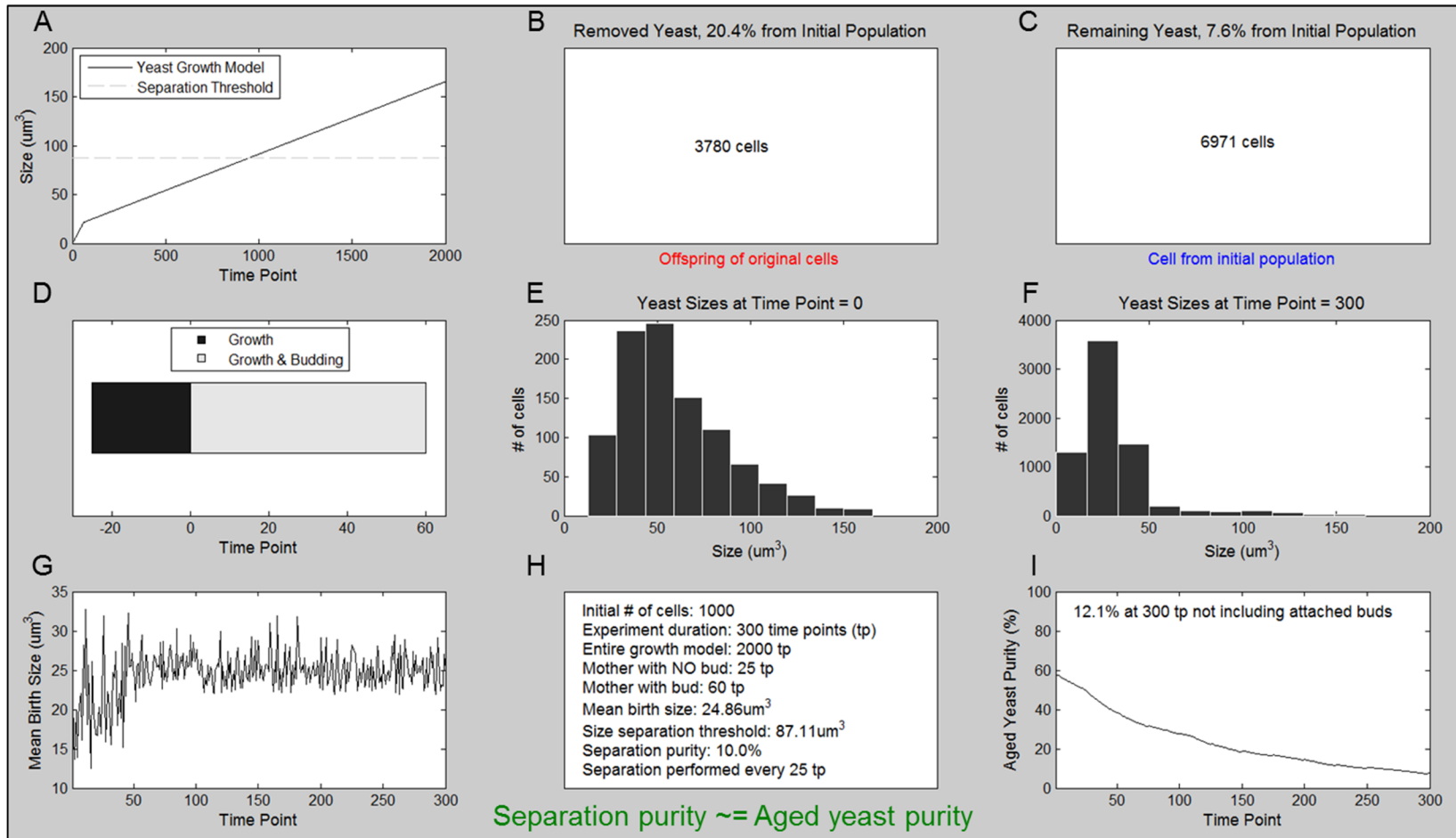
Figure 81. Simulation results of the aged yeast generator model for which the final aged yeast population purity was calculated by excluding still-attached daughters. For 10% separation purity, aged yeast purity was 12% (8% when including still-attached buds).

2.2.14. Simulation model helped determine experimental parameters for aged yeast generator

In summary, our aged yeast generator model helped us determine which experimental parameters can worsen the purity of our final yeast population and provided helpful guidelines for defining some of these variables. For actual experiments with the aged yeast generator, we should program the system to have relatively high separation threshold so that only the largest yeast are kept in the device. A combination of relatively low size-threshold and high separation frequency, for example, is not advantageous to produce high aged yeast purity. The size-based separation subsystem of the aged yeast generator should remove smaller cells from the device with >60% purity. The system's separation frequency, i.e., the frequency of periodic forward/reverse flow of the repeated separation subsystem, should be more often than every 90 min assuming yeast follow the budding model defined in the simulations. Because a mother yeast spends a majority of the cell cycle budding a daughter, many daughters will stay in the aged yeast generator instead of being removed. These daughters contaminate the final aged yeast population so that it can never exceed ~70%. An experiment with the aged yeast generator does not need to last >20 hr because no additional benefits are gained by increasing the experiment duration. Finally, the simulation results above should be preserved if we are processing billions of cells in the aged yeast generator.

2.2.15. Prediction of low purity for final aged yeast population is not alarming

The aged yeast generator model showed that the final population (i) may not be very pure (may consist of up to ~45% daughters) and (ii) may be relatively small in number. The second point results from the rarity of very large yeast—which we assumed to be the older mothers—in a given population. The first point predicting that the final population may be relatively impure and contaminated by daughters is not as problematic as it may seem. Buds still attached to their

mothers are the primary source of impurities. These daughters are smaller than their mothers (at least before the mother enters the final 1-3 divisions before death) and thus are easily identifiable as impurities. In subsequent biochemical analyses of aged yeast and these contaminants, the researcher can simply ignore the experimental data from impurities. For example, if fluorescent intensity of a biomarker is being measured in an image of yeast, the fluorescence of cells below a certain size-threshold can be filtered out of the measurements.

The aged yeast generator simulation developed here is currently simple in that it applies a single growth model and a single budding model to all cells with minor, adjustable variation. Improving the model to be more realistic, however, would not be difficult. For example, a relatively straightforward addition would be considering the yeast age when determining the cell cycle time and daughter birth size.

2.3. Agitation to improve separation resolution

2.3.1. Cell clumps can introduce impurities into the aged yeast population

In addition to repeated separation, an agitation mechanism should be included in the aged yeast generator to break up cell clumps that would worsen separation resolution. This cell clumping is likely the result of interactions between cell wall glycoproteins and/or sugar residues on the surfaces of yeast.[100] We saw in Fig. 58 how acoustic deflection forces larger cells and cell clumps toward the fluidic channel center. Deflection of cell clumps is problematic because the clumps consist partially of smaller yeast that we want to remove from the aged yeast generator.

In our continuous-flow microfluidic experiments, we often observed cell clumps consisting of >2 yeast. Figure 82 shows images from experiments of an acoustic microfluidic device employed to trap yeast in a circular channel.
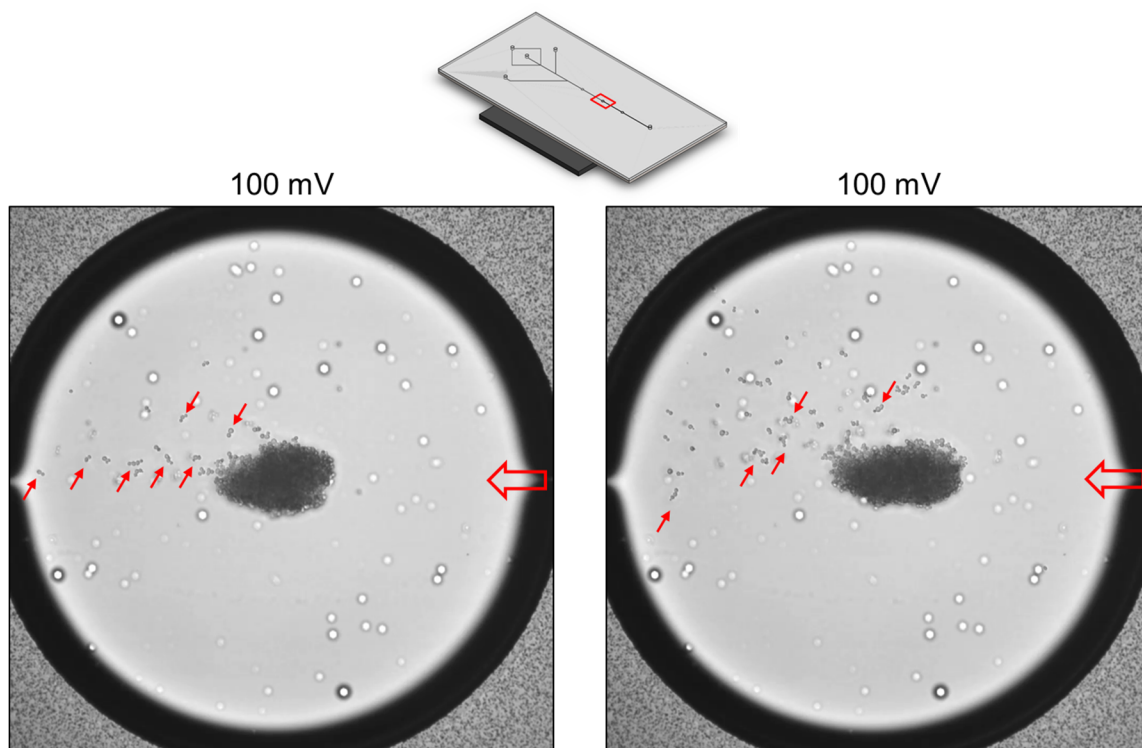
Figure 82. Yeast in a circular acoustic trap often exist in clumps of two or more cells. The images were from experiments with an acoustic trap device (at top). Flow was from right to left in the images (indicated by large red arrows). A standing acoustic wave in the circular region trapped yeast from flowing toward the outlet. Flow removed some yeast from the large cell cloud at the center of the trap, and most of these yeast are in clumps of two or more cells (small red arrows). The acoustic radiation was driven by a 100 mV sinusoidal wave.

The diagram at top of the figure depicts the acoustic trap device which was designed and fabricated similar to the device in Han *et al*.[101] The experimental protocol for testing the acoustic trap with yeast was similar to what was used for the acoustic deflection device in § 2.1.22. A syringe filled with yeast and YPD was connected to the inlet of the acoustic trap device. Only one of the inlets was used because the others were not needed in this particular experiment. Buffer flows containing pure YPD were not needed either. The syringe with yeast was attached to a syringe pump (Chemyx Fusion 400 Touch Syringe Pump) that flowed yeast into the device and through the circular trap at a rate between 10 µL/hr and 50 µL/hr. A 100 mV sinusoidal wave from a function generator (Tektronix AFG 3021B Single Channel Arbitrary/Function

Generator) was passed through a 50 dB amplifier (E&I) and applied to the piezoelectric transducer glued to the bottom of the acoustic device. The microscope was aligned to one of the circular traps and videos were captured of the yeast becoming trapped in the circular region as they were forced to the circle center where the node of a standing acoustic wave was formed. In the images of Fig. 82, flow was from right to left through the circular acoustic trap. A large cell cloud was formed in the center of both images while flow gradually pulled cells and cell clumps out of the cloud and toward the outlet at the left of the circular region. Red arrows identify cell clumps in which 2 or more cells were attached as they flowed toward the outlet. Most of the cells outside of the cell cloud—even those not highlighted by red arrows—were attached to other cells. Some of the clumps contain >2 cells, indicating that cells of these clumps were attached to each other not simply because a mother was dividing to produce a daughter.

To prevent contamination in the final aged yeast population by daughters that are budding from their mothers, we developed the simulation in § 2.2.7 to determine an optimal separation frequency. Our goal was to perform the size-based separation often enough to remove these attached buds after they are released but before they grow too large. On the other hand, by adding some agitation mechanism to the aged yeast generator, we aim to address the problem of >2 cells attached as they flow through fluidic channels, although the agitation would also promote separation of mothers and daughters after the daughters have completed budding. In the case of >2 cells clumped together, not all of the cells can be daughter buds still attached to their mothers. These cell clumps should be broken up before performing size-based separation because some cells that are smaller than the size-threshold may be wrongly kept in the device and thereby contaminate the final aged yeast population. If these clumps are not broken up, laminar flow would keep the cells together. Without turbulence or deliberate agitation, the cell clumps would likely never break apart. With this agitation subsystem we are not aiming to break

179

up mother-daughter pairs prematurely before budding is completed. In other words, the agitation must be gentle enough that mother-daughter pairs are not broken up before the daughter is fully developed or before the required events that produce healthy mothers and daughters are completed.[102] In summary, the frequent occurrence of cell clumps that we observed in flow-through tests with yeast motivated the need for adding agitation to the aged yeast generator to promote breaking up of cell clumps that would worsen the aged yeast population purity.

2.3.2. Acoustic excitation is not sufficient for breaking up cell clumps

Because our size-based separation subsystem employs an acoustic device, we naturally considered using acoustic agitation to break up cell clumps. Figure 83 shows images from the same acoustic trap used in Fig. 82. The applied voltage was increased to 300 mV to produce greater acoustic forces on yeast in the acoustic trap. We reduced the number of yeast within the field of view in the images of Fig. 83 so that we could more easily observe how the acoustic radiation affected cell clumps. The red arrows in the images highlight cell clumps that were not broken up by the large acoustic forces. Many of the clumps in the images consist of >2 cells, indicating that not all of the cells in these clumps can be buds still attached to mothers. The high acoustic forces in the traps were insufficient for separating the clumps composed of >2 yeast.
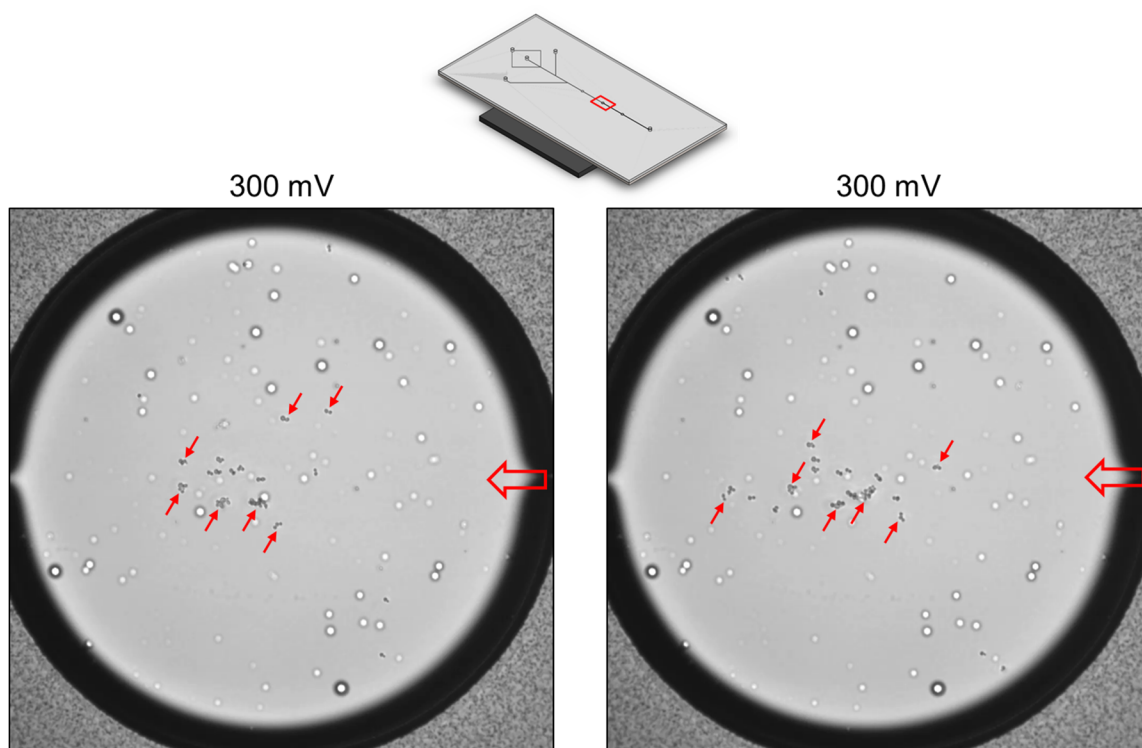
Figure 83. Large acoustic radiation is insufficient for breaking up cell clumps that can worsen size-based separation resolution in the aged yeast generator. The images at bottom were from experiments with an acoustic trap device (top). Flow was from right to left in the images (indicated by large red arrows). A standing acoustic wave in the circular region trapped yeast from flowing toward the outlet. Even with relatively large acoustic forces on the yeast, cell clumps consisting of >2 cells were not broken up. The acoustic radiation was driven by a 300 mV sinusoidal wave.

2.3.3. Proposed agitation subsystem consists of periodic constriction channels

Because large acoustic forces could not break up cell clumps of 2+ yeast that can worsen

separation resolution, we propose using a microfluidic device with periodic constriction regions

that break up clumps. Figure 84 shows a simplified diagram of the device which consists of

PDMS with channels and inlets/outlets bonded to a glass substrate. A cross-section through the

center of the fluidic channel length is shown at bottom in Fig. 84. Constriction channels 50 µm

long and 4 µm tall are separated by 100 µm long channels having 30 µm heights. As yeast flow

from left to right through the constriction channels, the cell clumps simply cannot pass altogether

through the narrow regions; they must break up in order to pass. The minimum channel height

was chosen so that mothers still attached to buds can pass without prematurely separating the

bud. This design is relatively simple, and additional features like serpentine channels or lateral

channel constrictions to increase turbulence could be added.

Other researchers have successfully dissociated cell aggregates using mechanical

features in microfluidic devices. Often the features increase fluidic turbulence to break up the

cell clumps[103,104] or may physically cleave cell aggregates.[105] Dissociation efficiency and cell

viability were relatively high for these reported examples. However, because the cells were

much larger in size compared to yeast, we can only speculate on the efficiency of our proposed

agitation mechanism to break up yeast clumps. Future testing will investigate the performance of

our proposed device.
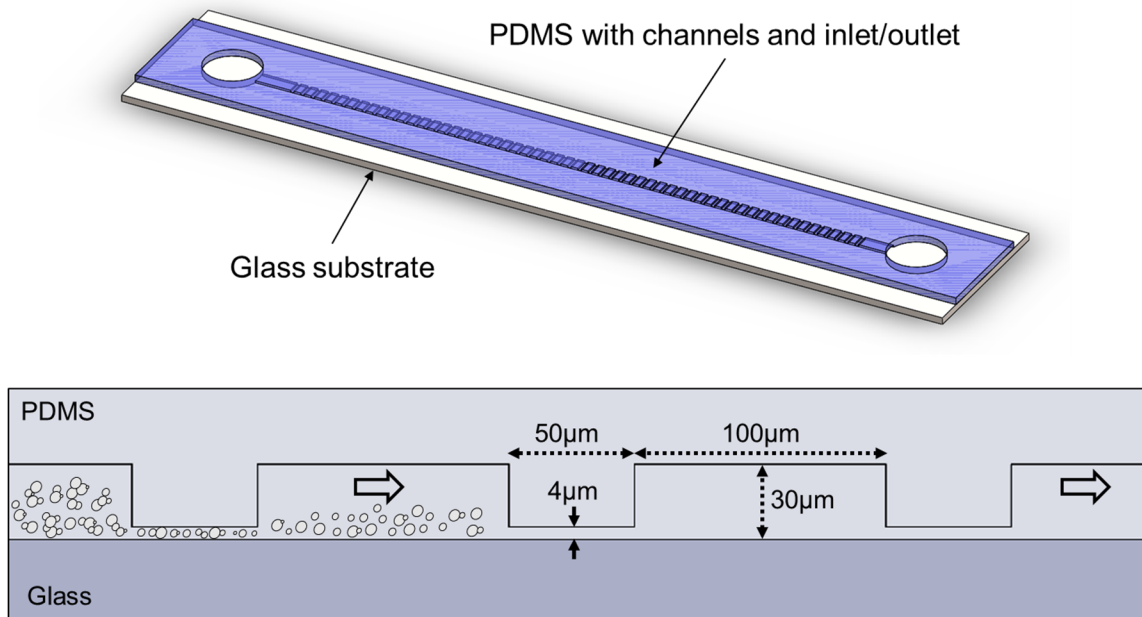
Figure 84. Proposed agitation mechanism to break up cell clumps that can worsen separation resolution in the aged yeast generator. At top, the agitation is accomplished with a PDMS and glass microfluidic device. The PDMS has periodic constriction channels (bottom) that force cell clumps to break up in order for the cells to pass.

3. CONCLUSIONS

In this work, we aimed to develop a high-throughput microfluidic system that generates a large number ($>10^5$) of aged yeast (>15 generations) because current technologies are not able to do so without relying on genetic modification or complex and costly purification steps. Such a system can aid biomedical researchers in creating (i) a more holistic understanding of aging and (ii) improved treatments for age-related diseases including neurodegeneration and cancer.

We quantified the size differences of mother and daughter yeast and concluded that the mothers can be separated successfully from the daughters if the separation technique has sub-500 nm separation resolution. We investigated multiple size-based separation strategies, demonstrated acoustic deflection can separate yeast by size, and optimized the design and operational parameters for the acoustic deflection device. We proposed a method of periodically repeating the separation to age the yeast and produce a higher yield of aged cells. We developed a simulation model of the aged yeast generator that helped determine important experimental parameters including separation frequency and efficiency. Finally, we recommended an agitation mechanism that breaks up cell clumps to improve separation purity.

3.1. Subsystem integration of the aged yeast generator

After developing the three subsystems, the finalized aged yeast generator that combines the subsystems is shown in Fig. 85. The original population of mother and daughter yeast enter the PDMS device with periodic constriction channels that break up cell clumps. The cells flow into an inlet of the acoustic separation device and are flow-focused by side buffer channels so that all yeast enter the separation region at approximately the same location. The yeast are acoustically separated by size. Daughters flow into the waste outlet where they are removed from the device.

183

Mothers enter the keep channel where they are not discarded. Once all cells flow through the separation region once, the acoustic radiation is deactivated, and all flows are blocked except those of the yeast inlet and the keep channel. The flows are reversed so that the yeast pass through the agitation subsystem again. After the kept yeast return to the original inlet, the flows are programmed to flow forward as before, and the acoustic separation is activated. The separation is repeated, and this cycle continues for several hours until the yeast are aged as desired.
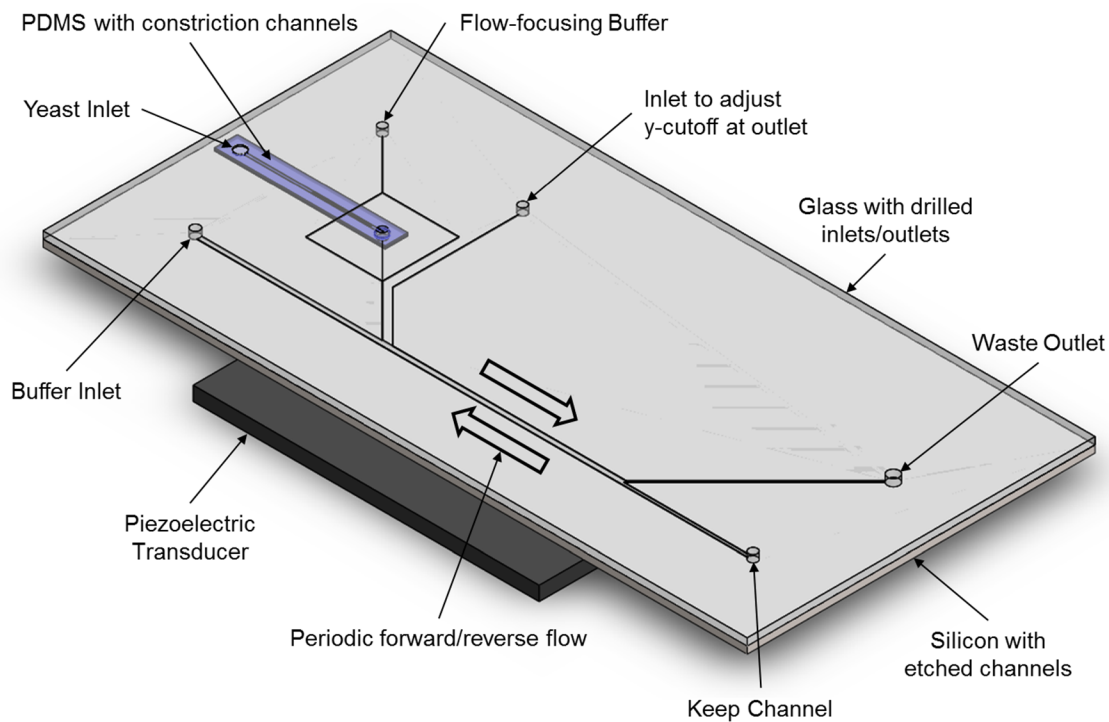
Figure 85. Finalized aged yeast generator that combines the three subsystems: size-based separation of mother and daughter yeast, periodic forward/reverse flow to repeat the separation, and agitation to improve separation efficiency.

Future testing of the finalized aged yeast generator will involve performing a long-term experiment to age the largest yeast in the original cell population. After each size-based

separation of the yeast, we will capture microscopic images of the cells at both outlets (waste outlet and keep channel). These images will be processed to calculate yeast size over time or separation run. The aged yeast generator is successful if we observe an overall increase in size of the yeast in the keep channel as separation number increases. In other words, an upward trend in size of the kept yeast over time indicates that the aged yeast generator indeed ages mothers while removing daughters.

3.2. Anticipated concerns for the aged yeast generator

The two most significant potential problems of the aged yeast generator are (i) the possibility that the final aged yeast population will not be very pure as predicted by the simulation model (see § 2.2.13) and (ii) impurities due to daughters being born similar in size as their mothers at the beginning and end of the mother lifespan. For the first concern of low purity in the final yeast population, we discussed in § 2.2.15 how the data from the impurities can be disregarded in subsequent analyses of the cells. The main source of these impurities are small daughter buds that are attached to their mothers during the size-based separation and are thus not removed from the experiment like they would if they completed budding. Even at relatively high separation frequency, we predicted that these impurities will still contaminate the final aged yeast population. Fortunately, because of their small size, they can be ignored in biochemical analyses.

For the second potential problem, we are not concerned by daughters that are born similar in size to their mothers at the beginning of the mother lifespan. The mother is still relatively small at that time and will be removed along with its daughter assuming the separation size-threshold is programmed large enough, which will certainly be the case in the aged yeast generator. Daughters born similar in size to their mothers at the end of the mother lifespan, however, presents perhaps the greatest obstacle for the aged yeast generator. The mother-

daughter size similarities occur during the last few cell divisions before the mother dies, i.e., during the 25-30 cell divisions. The number of yeast at this end point in their lifespans will be incredibly small due to the exponential growth in cell number. We aim to produce yeast that are >15 generations old, which is several generations before cell death and before the mother-daughter size difference is not observed. This particular problem affects all yeast aging systems that rely on size-based separation of mothers and daughters, and to overcome it researchers have had to rely on using labels to tag mothers or genetic modification, both of which have their own disadvantages (see § 1.8).

Finally, the aged yeast generator benefits biomedical researchers simply because it can purify and age the larger cells within a mixed population. Cell size is correlated with several aspects of cellular physiology and is thus a very important characteristic to study.[106] For example, cell size may determine when a mother enter certain stages of the cell cycle. Because cell size significantly influences cell function, creating a tool that ages the largest cells in a population has merit in its own way.

REFERENCES

1   Phipps, S. M. O., Berletch, J. B., Andrews, L. G. & Tollefsbol, T. O. Aging cell culture: methods and observations. *Methods in Molecular Biology* **371**, 9-19 (2007).

2   Longo, V. D., Shadel, G. S., Kaeberlein, M. & Kennedy, B. Replicative and chronological aging in Saccharomyces cerevisiae. *Cell Metabolism* **16**, 18-31, doi:10.1016/j.cmet.2012.06.002 (2012).

3   Fehrmann, S. *et al.* Aging yeast cells undergo a sharp entry into senescence unrelated to the loss of mitochondrial membrane potential. *Cell Reports* **5**, 1589-1599, doi:10.1016/j.celrep.2013.11.013 (2013).

4   Kaeberlein, M., Burtner, C. R. & Kennedy, B. Recent developments in yeast aging. *PLoS Genetics* **3**, 0655-0660, doi:10.1371/journal.pgen.0030084.g001 (2007).

5   Polymenis, M. & Kennedy, B. K. High-tech yeast ageing. *Nature* **486**, 37-38, doi:10.1111/ (2012).

6   Campisi, J. Aging, cellular senescence, and cancer. *Annual Review of Physiology* **75**, 685-705, doi:10.1146/annurev-physiol-030212-183653 (2013).

7   Price, A. K. & Culbertson, C. T. Chemical analysis of single mammalian cells with microfluidics. *Analytical Chemistry*, 2614-2621 (2007).

8   Avesar, J., Ben Arye, T. & Levenberg, S. Frontier microfluidic techniques for short and long-term single cell analysis. *Lab on a Chip* **14**, 2161-2167, doi:10.1039/c4lc00013g (2014).

9   Crane, M. M., Clark, I. B. N., Bakker, E., Smith, S. & Swain, P. S. A microfluidic system for studying ageing and dynamic single-cell responses in budding yeast. *PLoS One* **9**, doi:10.1371/journal.pone.0100042 (2014).

10   Lippuner, A. D., Julou, T. & Barral, Y. Budding yeast as a model organism to study the effects of age. *Fems Microbiology Reviews* **38**, 300-325, doi:10.1111/1574-6976.12060 (2014).

11   Mirisola, M. G., Braun, R. J. & Petranovic, D. Approaches to study yeast cell aging and death. *FEMS Yeast Research*, doi:10.1111/1567-1364.12112 (2013).

12   Sinclair, D. A. Studying the replicative life span of yeast cells. *Methods in Molecular Biology* **1048**, 49-63, doi:10.1007/978-1-62703-556-9_5 (2013).

13   Banaeiyan, A. A., Ahmadpour, D., Adiels, C. B. & Goksor, M. Design and fabrication of high-throughput application-specific microfluidic devices for studying single-cell responses to extracellular perturbations. *Bio-Mems and Medical Microdevices* **8765**, doi:10.1117/12.2017301 (2013).

14   Bennett, M. R. *et al.* Metabolic gene regulation in a dynamically changing environment. *Nature* **454**, 1119-1122, doi:10.1038/nature07211 (2008).

15   Charvin, G., Cross, F. R. & Siggia, E. D. A microfluidic device for temporally controlled gene expression and long-term fluorescent imaging in unperturbed dividing yeast cells. *PLoS One*, doi:10.1371/journal.pone.0001468.g001 (2008).

16   Cookson, S., Ostroff, N., Pang, W. L., Volfson, D. & Hasty, J. Monitoring dynamics of single-cell gene expression over multiple cell cycles. *Molecular Systems Biology* **1**, 2005 0024, doi:10.1038/msb4100032 (2005).

17   Denervaud, N. *et al.* A chemostat array enables the spatio-temporal analysis of the yeast proteome. *PNAS* **110**, 15842-15847, doi:10.1073/pnas.1308265110 (2013).

18   Lee, S. S., Vizcarraa, I. A., Hubertsc, D. H. E. W., Lee, L. P. & Heinemanna, M. Whole lifespan microscopic observation of budding yeast aging through a microfluidic dissection platform. *PNAS* **109**, 4916-4920 (2012).

19   Xie, Z. *et al.* Molecular phenotyping of aging in single yeast cells using a novel microfluidic device. *Aging Cell* **11**, 599-606 (2012).

20   Lindstrom, D. L. & Gottschling, D. E. The mother enrichment program: a genetic system for facile replicative life span analysis in Saccharomyces cerevisiae. *Genetics* **183**, 413-422, 411SI-413SI, doi:10.1534/genetics.109.106229 (2009).

21   Mortimer, R. K. & Johnston, J. R. Life span of individual yeast cells. *Nature* **183**, 1751-1752 (1959).

22   Park, P. U., McVey, M. & Guarente, L. Separation of mother and daughter cells. *Methods in Enzymology* **351**, 468-477 (2002).

23   Zhang, Y. *et al.* Single cell analysis of yeast replicative aging using a new generation of microfluidic device. *PLoS One* **7**, doi:10.1371/journal.pone.0048275.g001 (2012).

24   Woldringh, C. L., Fluiter, K. & Huls, P. G. Production of senescent cells of saccharomyces cerevisiae by centrifugal elutriation. *Yeast* **11**, 361-369 (1995).

25   Marbouty, M., Ermont, C., Dujon, B., Richard, G. F. & Koszul, R. Purification of G1 daughter cells from different Saccharomycetes species through an optimized centrifugal elutriation procedure. *Yeast* **31**, 159-166, doi:10.1002/yea.3005 (2014).

26   Kim, S. M. & Huberman, J. A. Regulation of replication timing in fission yeast. *Embo Journal* **20**, 6115-6126, doi:10.1093/emboj/20.21.6115 (2001).

27   Yang, A. H. & Soh, H. T. Acoustophoretic sorting of viable mammalian cells in a microfluidic device. *Analytical Chemistry* **84**, 10756-10762, doi:10.1021/ac3026674 (2012).

28   Smeal, T., Claus, J., Kennedy, B., Cole, F. & Guarente, L. Loss of transcriptional silencing causes sterility in old mother cells of S. cerevisiae. *Cell* **84**, 633-642 (1996).

29   Jarolim, S. *et al.* A novel assay for replicative lifespan in Saccharomyces cerevisiae. *FEMS Yeast Research* **5**, 169-177, doi:10.1016/j.femsyr.2004.06.015 (2004).

30   Whitesides, G. M. The origins and the future of microfluidics. *Nature* **442**, 368-373, doi:10.1038/nature05058 (2006).

31   Barbulovic-Nad, I., Au, S. H. & Wheeler, A. R. A microfluidic platform for complete mammalian cell culture. *Lab on a Chip* **10**, 1536-1542, doi:10.1039/c002147d (2010).

32   Chen, Q. *et al.* Microfluidic isolation of highly pure embryonic stem cells using feeder-separated co-culture system. *Scientific Reports* **3**, 2433, doi:10.1038/srep02433 (2013).

33   Di Carlo, D., Wu, L. Y. & Lee, L. P. Dynamic single cell culture array. *Lab on a Chip* **6**, 1445-1449, doi:10.1039/b605937f (2006).

34   Gomez-Sjoberg, R., Leyrat, A. A., Pirone, D. M., Chen, C. S. & Quake, S. R. Versatile, fully automated, microfluidic cell culture system. *Analytical Chemistry* **79**, 8557-8563 (2007).

35   Hong, S., Pan, Q. & Lee, L. P. Single-cell level co-culture platform for intercellular communication. *Integrative Biology: Quantitative Biosciences from Nano to Macro* **4**, 374-380, doi:10.1039/c2ib00166g (2012).

36   Rhee, S. W. *et al.* Patterned cell culture inside microfluidic devices. *Lab on a Chip* **5**, 102-107, doi:10.1039/b403091e (2005).

37   Toh, Y. C. *et al.* A novel 3D mammalian cell perfusion-culture system in microfluidic channels. *Lab on a Chip* **7**, 302-309, doi:10.1039/b614872g (2007).

38   Zhang, B., Kim, M. C., Thorsen, T. & Wang, Z. A self-contained microfluidic cell culture system. *Biomedical Microdevices* **11**, 1233-1237, doi:10.1007/s10544-009-9342-4 (2009).

39   Denoth-Lippuner, A., Krzyzanowski, M. K., Stober, C. & Barral, Y. Role of SAGA in the asymmetric segregation of DNA circles during yeast ageing. *Elife* **3**, doi:10.7554/eLife.03790.001 (2014).

40   Eriksson, E. *et al.* A microfluidic system in combination with optical tweezers for analyzing rapid and reversible cytological alterations in single cells upon environmental changes. *Lab on a Chip* **7**, 71-76, doi:10.1039/b613650b (2007).

41   Falconnet, D. *et al.* High-throughput tracking of single yeast cells in a microfluidic imaging matrix. *Lab on a Chip* **11**, 466-473, doi:10.1039/c0lc00228c (2011).

42   Fernandes, J. T. S. *et al.* Modulation of alpha-synuclein toxicity in yeast using a novel microfluidic-based gradient generator. *Lab on a Chip* **14**, 3949-3957, doi:10.1039/c4lc00756e (2014).

43   Hersen, P., McClean, M. N., Mahadevan, L. & Ramanathan, S. Signal processing by the HOG MAP kinase pathway. *PNAS* **105**, 7165-7170, doi:10.1073/pnas.0710770105 (2008).

44   Huberts, D. *et al.* Construction and use of a microfluidic dissection platform for long-term imaging of cellular processes in budding yeast. *Nature Protocols* **8**, 1019-1027, doi:10.1038/nprot.2013.060 (2013).

45   Koschwanez, J. *et al. Automated Lifetime Analysis of a Single Yeast Cell.* (2005).

46   Lee, P., Helman, N., Lim, W. & Hung, P. A microfluidic system for dynamic yeast cell imaging. *BioTechniques* **44**, 91-95, doi:10.2144/000112673 (2008).

47   Mirzaei, M. *et al.* Microfluidic perfusion system for culturing and imaging yeast cell microarrays and rapidly exchanging media. *Lab on a Chip* **10**, 2449-2457, doi:10.1039/c004857g (2010).

48   Rowat, A. C., Bird, J. C., Agresti, J. J., Rando, O. J. & Weitz, D. A. Tracking lineages of single cells in lines using a microfluidic device. *PNAS* **106**, 18149-18154, doi:10.1073/pnas.0903163106 (2009).

49   Ryley, J. & Pereira-Smith, O. M. Microfluidics device for single cell gene expression analysis in Saccharomyces cerevisiae. *Yeast* **23**, 1065-1073, doi:10.1002/yea.1412 (2006).

50   Spivey, E. C., Xhemalce, B., Shear, J. B. & Finkelstein, I. J. 3D-printed microfluidic microdissector for high-throughput studies of cellular aging. *Analytical Chemistry* **86**, 7406-7412, doi:10.1021/ac500893a (2014).

51   Tian, Y., Luo, C. X. & Ouyang, Q. A microfluidic synchronizer for fission yeast cells. *Lab on a Chip* **13**, 4071-4077, doi:10.1039/c3lc50639h (2013).

52   Truong, S. K., McCormick, R. F. & Polymenis, M. Genetic determinants of cell size at birth and their impact on cell cycle progression in Saccharomyces cerevisiae. *G3-Genes Genomes Genetics* **3**, 1525-1530, doi:10.1534/g3.113.007062 (2013).

53   Lee, S. S., Avalos Vizcarra, I., Huberts, D., Lee, L. P. & Heinemann, M. Whole lifespan microscopic observation of budding yeast aging through a microfluidic dissection platform. *PNAS* **109**, 4916-4920, doi:10.1073/pnas.1113505109 (2012).

54   Sajeesh, P. & Sen, A. K. Particle separation and sorting in microfluidic devices: a review. *Microfluidics and Nanofluidics* **17**, 1-52, doi:10.1007/s10404-013-1291-9 (2014).

55   Gossett, D. R. *et al.* Label-free cell separation and sorting in microfluidic systems. *Analytical and Bioanalytical Chemistry* **397**, 3249-3267, doi:10.1007/s00216-010-3721-9 (2010).

56   Tsutsui, H. & Ho, C. M. Cell separation by non-inertial force fields in microfluidic systems. *Mechanics Research Communications* **36**, 92-103, doi:10.1016/j.mechrescom.2008.08.006 (2009).

57   Lenshof, A. & Laurell, T. Continuous separation of cells and particles in microfluidic systems. *Chemical Society Reviews* **39**, 1203-1217, doi:10.1039/b915999c (2010).

58   VanDelinder, V. & Groisman, A. Perfusion in microfluidic cross-flow: separation of white blood cells from whole blood and exchange of medium in a continuous flow. *Analytical Chemistry* **79**, 2023-2030, doi:10.1021/ac061659b (2007).

59   Yamada, M., Nakashima, M. & Seki, M. Pinched flow fractionation: continuous size separation of particles utilizing a laminar flow profile in a pinched microchannel. *Analytical Chemistry* **76**, 5465-5471, doi:10.1021/ac049863r (2004).

60   Bhagat, A. A. S., Hou, H. W., Li, L. D., Lim, C. T. & Han, J. Y. Pinched flow coupled shear-modulated inertial microfluidics for high-throughput rare blood cell separation. *Lab on a Chip* **11**, 1870-1878, doi:10.1039/c0lc00633e (2011).

61   Jain, A. & Posner, J. D. Particle dispersion and separation resolution of pinched flow fractionation. *Analytical Chemistry* **80**, 1641-1648, doi:10.1021/ac0713813 (2008).

62   Petersson, F., Aberg, L., Sward-Nilsson, A.-M. & Laurell, T. Free Flow Acoustophoresis: microfluidic-based mode of particle and cell separation. *Analytical Chemistry* **79**, 5117-5123 (2007).

63   Destgeer, G., Ha, B. H., Jung, J. H. & Sung, H. J. Submicron separation of microspheres via travelling surface acoustic waves. *Lab on a Chip* **14**, 4665-4672, doi:10.1039/c4lc00868e (2014).

64   Jung, B., Fisher, K., Ness, K. D., Rose, K. A. & Mariella, R. P. Acoustic particle filter with adjustable effective pore size for automated sample preparation. *Analytical Chemistry* **80**, 8447-8452, doi:10.1021/ac8011768 (2008).

65   Han, S. I., Lee, S. M., Joo, Y. D. & Han, K. H. Lateral dielectrophoretic microseparators to measure the size distribution of blood cells. *Lab on a Chip* **11**, 3864-3872, doi:10.1039/c1lc20413k (2011).

66   Zhu, J. J. *et al.* Continuous-flow particle and cell separations in a serpentine microchannel via curvature-induced dielectrophoresis. *Microfluidics and Nanofluidics* **11**, 743-752, doi:10.1007/s10404-011-0839-9 (2011).

67   Yunus, N. A. M. & Green, N. G. Continuous separation of submicron particles using angled electrodes. *Electrostatics 2007* **142**, doi:10.1088/1742-6596/142/1/012068 (2009).

68   Huang, L. R., Cox, E. C., Austin, R. H. & Sturm, J. C. Continuous particle separation through deterministic lateral displacement. *Science* **304**, 987-990, doi:10.1126/science.1094567 (2004).

69   Morijiri, T., Yamada, M., Hikida, T. & Seki, M. Microfluidic counterflow centrifugal elutriation system for sedimentation-based cell separation. *Microfluidics and Nanofluidics* **14**, 1049-1057, doi:10.1007/s10404-012-1113-5 (2013).

70   Huh, D. *et al.* Gravity-driven microfluidic particle sorting device with hydrodynamic separation amplification. *Analytical Chemistry* **79**, 1369-1376, doi:10.1021/ac061542n (2007).

71   Johnston, I. D. *et al.* Dean flow focusing and separation of small microspheres within a narrow size range. *Microfluidics and Nanofluidics* **17**, 509-518, doi:10.1007/s10404-013-1322-6 (2014).

72   Nam, J., Lim, H., Kim, D., Jung, H. & Shin, S. Continuous separation of microparticles in a microfluidic channel via the elasto-inertial effect of non-Newtonian fluid. *Lab on a Chip* **12**, 1347-1354, doi:10.1039/c2lc21304d (2012).

73   Sai, Y., Yamada, M., Yasuda, M. & Seki, M. Continuous separation of particles using a microfluidic device equipped with flow rate control valves. *Journal of Chromatography A* **1127**, 214-220, doi:10.1016/j.chroma.2006.05.020 (2006).

74   Xia, N. *et al.* Combined microfluidic-micromagnetic separation of living cells in continuous flow. *Biomedical Microdevices* **8**, 299-308, doi:10.1007/s10544-006-0033-0 (2006).

75   Zheng, S. *et al.* Membrane microfilter device for selective capture, electrolysis and genomic analysis of human circulating tumor cells. *Journal of Chromatography A* **1162**, 154-161, doi:10.1016/j.chroma.2007.05.064 (2007).

76   Milne, G., Rhodes, D., MacDonald, M. & Dholakia, K. Fractionation of polydisperse colloid with acousto-optically generated potential energy landscapes. *Optics Letters* **32**, 1144-1146, doi:10.1364/ol.32.001144 (2007).

77   Khoshmanesh, K. *et al.* Dielectrophoretic-activated cell sorter based on curved microelectrodes. *Microfluidics and Nanofluidics* **9**, 411-426, doi:10.1007/s10404-009-0558-7 (2010).

78   Li, S. B. *et al.* High-throughput particle manipulation by hydrodynamic, electrokinetic, and dielectrophoretic effects in an integrated microfluidic chip. *Biomicrofluidics* **7**, doi:10.1063/1.4795856 (2013).

79   Doh, I. & Cho, Y. H. A continuous cell separation chip using hydrodynamic dielectrophoresis (DEP) process. *Sensors and Actuators A-Physical* **121**, 59-65, doi:10.1016/j.sna.2005.01.030 (2005).

80   Patel, S. *et al.* Microfluidic separation of live and dead yeast cells using reservoir-based dielectrophoresis. *Biomicrofluidics* **6**, doi:10.1063/1.4732800 (2012).

81   Lewpiriyawong, N., Kandaswamy, K., Yang, C., Ivanov, V. & Stocker, R. Microfluidic characterization and continuous separation of cells and particles using conducting poly(dimethyl siloxane) electrode induced alternating current-dielectrophoresis. *Analytical Chemistry* **83**, 9579-9585, doi:10.1021/ac202137y (2011).

82   Han, K. H., Han, S. I. & Frazier, A. B. Lateral displacement as a function of particle size using a piecewise curved planar interdigitated electrode array. *Lab on a Chip* **9**, 2958-2964, doi:10.1039/b909753h (2009).

83   Steenbakkers, P. G. A., Hubers, H. & Rijnders, A. W. M. Efficient generation of monoclonal-antibodies from preselected antigen-specific B-cells - efficient immortalization of preselected B-cells. *Molecular Biology Reports* **19**, 125-134, doi:10.1007/bf00997158 (1994).

84   Sano, M. B., Henslee, E. A., Schmelz, E. M. & Davalos, R. V. Contactless dielectrophoretic spectroscopy: examination of the dielectric properties of cells found in blood. *Electrophoresis* **32**, 3164-3171, doi:10.1002/elps.201100351 (2011).

85   Sano, M. B., Caldwell, J. L. & Davalos, R. V. Modeling and development of a low frequency contactless dielectrophoresis (cDEP) platform to sort cancer cells from dilute whole blood samples. *Biosensors & Bioelectronics* **30**, 13-20, doi:10.1016/j.bios.2011.07.048 (2011).

86   Nilsson, A., Petersson, F., Jonsson, H. & Laurell, T. Acoustic control of suspended particles in micro fluidic chips. *Lab on a Chip* **4**, 131-135, doi:10.1039/b313493h (2004).

87   Gao, L., *et al.* Two-dimensional spatial manipulation of microparticles in continuous flows in acoustofluidic systems. *Biomicrofluidics* **9** 014105, doi:10.1063/1.4905875 (2015).

88   Kapishnikov, S., Kantsler, V. & Steinberg, V. Continuous particle size separation and size sorting using ultrasound in a microchannel. *Journal of Statistical Mechanics: Theory and Experiment*, doi:10.1088/1742-5468/2006/01/p01012 (2006).

89   Franke, T., Wixforth, A. & Weitz, D. A. Cell and droplet sorting with surface acoustic waves in microfluidics. *Biophysics* **98**, 193A-194A (2010).

90   Franke, T., Braunmuller, S., Schmid, L., Wixforth, A. & Weitz, D. A. Surface acoustic wave actuated cell sorting (SAWACS). *Lab on a Chip* **10**, 789-794, doi:10.1039/b915522h (2010).

91   Nam, J., Lim, H. & Shin, S. Manipulation of microparticles using surface acoustic wave in microfluidic systems: a brief review. *Korea-Australia Rheology Journal* **23**, 255-267, doi:10.1007/s13367-011-0031-5 (2011).

92   Jeong, J. S. *et al.* Particle manipulation in a microfluidic channel using acoustic trap. *Biomedical microdevices* **13**, 779-788, doi:10.1007/s10544-011-9548-0 (2011).

93   Jo, M. C. & Guldiken, R. in *Smart Biomedical and Physiological Sensor Technology Viii* Vol. 8025 *Proceedings of SPIE* (eds B. M. Cullum & E. S. McLamore) (Spie-Int Soc Optical Engineering, 2011).

94   Lenshof, A., Magnusson, C. & Laurell, T. Acoustofluidics 8: applications of acoustophoresis in continuous flow microsystems. *Lab on a Chip* **12**, 1210-1223, doi:10.1039/c2lc21256k (2012).

95   Ding, X. Y. *et al.* Standing surface acoustic wave (SSAW) based multichannel cell sorting. *Lab on a Chip* **12**, 4228-4231, doi:10.1039/c2lc40751e (2012).

96   Guldiken, R., Jo, M. C., Gallant, N. D., Demirci, U. & Zhe, J. Sheathless size-based acoustic particle separation. *Sensors* **12**, 905-922, doi:10.3390/s120100905 (2012).

97   Ding, X. Y. *et al.* Surface acoustic wave microfluidics. *Lab on a Chip* **13**, 3626-3649, doi:10.1039/c3lc50361e (2013).

98   Vanoni, M., Vai, M., Popolo, L. & Alberghina, L. Structural heterogeneity in populations of the budding yeast Saccharomyces-cerevisiae. *Journal of Bacteriology* **156**, 1282-1291 (1983).

99   Liu, X. L. *et al.* Reliable cell cycle commitment in budding yeast is ensured by signal integration. *Elife* **4** (2015).

100   Li, J. R. *et al.* Polygenic molecular architecture underlying non-sexual cell aggregation in budding yeast. *DNA Research* **20**, 55-66, doi:10.1093/dnares/dss033 (2013).

101   Wang, H. *et al.* Microfluidic acoustophoretic force based low-concentration oil separation and detection from the environment. *Lab on a Chip* **14**, 947-956, doi:10.1039/c3lc51032h (2014).

102   Yeong, F. M. Severing all ties between mother and daughter: cell separation in budding yeast. *Molecular Microbiology* **55**, 1325-1331, doi:10.1111/j.1365-2958.2005.04507.x (2005).

103   Lin, C. H., Lee, D. C., Chang, H. C., Chiu, I. M. & Hsu, C. H. Single-cell enzyme-free dissociation of neurospheres using a microfluidic chip. *Analytical Chemistry* **85**, 11920-11928, doi:10.1021/ac402724b (2013).

104   Qiu, X. L., De Jesus, J., Pennell, M., Troiani, M. & Haun, J. B. Microfluidic device for mechanical dissociation of cancer cell aggregates into single cells. *Lab on a Chip* **15**, 339-350, doi:10.1039/c4lc01126k (2015).

105   Wallman, L. *et al.* Biogrid-a microfluidic device for large-scale enzyme-free dissociation of stem cell aggregates. *Lab on a Chip* **11**, 3241-3248, doi:10.1039/c1lc20316a (2011).

106   Turner, J. J., Ewald, J. C. & Skotheim, J. M. Cell size control in yeast. *Current Biology* **22**, R350-R359, doi:10.1016/j.cub.2012.02.041 (2012).

APPENDIX

MATLAB script for aged yeast generator simulation

```matlab
clc; clear all; close all;
datestr(now)

% Randomly generated yeast size data
% numYeast = 1e1;
% momIDs = 1:numYeast;
% yeast = struct(...
%     'sizeInd',num2cell(ceil(numel(allSizes).*rand(1,numYeast))),... %
index, allSizes(sizeInd) tells the yeast size
%
'budTimeInd',num2cell(ceil(numel(budTimes).*rand(1,numYeast))),... %
index, not necessarily an exact time, if NaN then currently attached to
another cell
%     'momID',num2cell(momIDs));

% Experimental yeast size data
load('...\YeastSizeData.mat');

% Save final results of simulation to an image
fileName = 'AgedYeastGenerator.png';

% Pre-processing of yeast size data
numYeast = sum(hits);
yeastSizes = ones(1,numYeast);
yeastSizes(1:hits(1)) = volumeBins(1)*ones(1,hits(1));
ind = hits(1);
for j = 2:numel(hits)
    yeastSizes(ind+1:ind+hits(j)) = volumeBins(j)*ones(1,hits(j));
    ind = ind+hits(j);
end

% Down sample for faster processing
numYeast = 1000;
indices = randperm(numel(yeastSizes));
yeastSizes = yeastSizes(indices(1:numYeast));

% Or up sample
% multiplyBy = 2;
% for j = 1:multiplyBy
%     yeastSizes = [yeastSizes yeastSizes];
% end
% numYeast = numel(yeastSizes);

maxYeastPlot = 1500; % max # of cells to plot (to waste time plotting
in graph)
```

```matlab
skipWasteCalcs = 0; % logical value determining whether we calculate
purity of removed yeast

% Define parameters that influence experimental outcome
maxExperimentTime = round(300); % time points
timePoints = 1:maxExperimentTime; % does not need to be a real unit of
time, can be an index, for convenience assume 1 time point = 1 min
numSizesGrowthModel = 2000; %floor(0.5*maxExperimentTime);

% Ratio of budTimes < budTimeStartInd (given by timeGrowthNoBud) and
budTimes > budTimeStartInd (given by timeGrowthYesBud) will determine
outcome of experiment
timeGrowthNoBud = 25; % time points
timeGrowthYesBud = 60; % time points
budTimes = -timeGrowthNoBud:timeGrowthYesBud; % time points, budTimes <
budTimeStartInd means cell is NOT budding, budTimes > budTimeStartInd
means cell is attached to daughter, new bud is released at
max(budTimes)
budTimeStartInd = floor(find(budTimes==0)); % index, new bud starts
growing at budTimeStartInd

avgBirthSize = 21.44; % um^3, special definition
http://www.ncbi.nlm.nih.gov/pmc/articles/PMC3755912/pdf/1525.pdf, this
value is from Coulter Counter
minBirthSize = min(yeastSizes);
maxBirthSize = mode(yeastSizes);
allSizes1 = linspace(0,avgBirthSize,timeGrowthYesBud);
if numSizesGrowthModel < numel(budTimes)
    disp('Increased numSizesGrowthModel to match numel(budTimes)')
    numSizesGrowthModel = numel(budTimes);
end
allSizes2 = linspace(avgBirthSize,max(yeastSizes),numSizesGrowthModel-
timeGrowthYesBud+1); % volume um^3, only needed for computing size-
based separation
% Construct yeast growth model (how cells grow in size throughout
experiment)
allSizes = [allSizes1 allSizes2(2:end)];
avgBirthSizeInd = max(1,find(allSizes>=avgBirthSize,1,'first')-1); %
index
minBirthSizeInd = max(1,find(allSizes>=minBirthSize,1,'first')-1);
maxBirthSizeInd = max(1,find(allSizes>=maxBirthSize,1,'first')-1);
sigmaInd = 0.5*mean([(maxBirthSizeInd-avgBirthSizeInd)
(avgBirthSizeInd-minBirthSizeInd)]); % need sigma for a function later
on, determines how much avg birth size varies

% Size threshold and separation efficiency parameters
sizeThreshVal = 4/3*pi*2.75^3; %0.5*max(allSizes); % an actual value
sizeThreshInd = find(allSizes<sizeThreshVal,1,'last'); % index, a
percentage (defined by separationPurity) of yeast (or mother+daughter)
with size < sizeThreshInd are removed
separationPurity = 0.9; % relative to the ideal case where 100% of
smaller cells go into the smaller size-bin. Of the smaller cells that
```

```matlab
should be removed, (1-separationPurity)% are kept in the larger size-
bin

% How often separation is performed (relative to total timePoints for
yeast cell cycle) is important parameter
removeEveryNth = 25; %round(0.1*range(timePoints)); % time points
removeThisTime = floor(1:removeEveryNth:numel(timePoints));
removeThisTime(end) = numel(timePoints);

% For sizeInd field of the yeast (see struct definition below), find
each experimental measurement's closest equivalent value in allSizes
sizeInd = zeros(1,numel(yeastSizes));
for j = 1 : numel(yeastSizes)
    sizeInd(j) = max(1,find(allSizes>=yeastSizes(j),1,'first')-1);
end
momIDs = 1:numYeast;
yeast = struct(...
    'sizeInd',num2cell(sizeInd),... % index, allSizes(sizeInd) tells
the yeast size
    'budTimeInd',num2cell(ceil(numel(budTimes).*rand(1,numYeast))),...
% index, not necessarily an exact time, if NaN then currently attached
to another cell
    'momID',num2cell(momIDs));

initialMomIDs = [yeast.momID];
initialSizes = allSizes([yeast.sizeInd]);
wasteYeast = yeast(1); % collect all removed yeast here for plotting
wasteYeast(1).sizeInd = []; wasteYeast(1).budTimeInd = [];
wasteYeast(1).momID = [];

% Add buds to the initial yeast population
indStartBud = find([yeast.budTimeInd] >= budTimeStartInd);
indOffset = numel(yeast);
yeast(end+1:end+numel(indStartBud)) = struct(...
    'sizeInd',[],...
    'budTimeInd',[],...
    'momID',[]);
if indStartBud
    for j = 1:numel(indStartBud)
        tempYeast = yeast(indStartBud(j));
%         tempYeast.sizeInd = max([1
(floor(normrnd(avgBirthSizeInd,sigmaInd)) + (numel(budTimes)-
tempYeast.budTimeInd))]); % index
        tempYeast.sizeInd = max([1
(floor(normrnd(avgBirthSizeInd,sigmaInd))-
timeGrowthYesBud+tempYeast.budTimeInd)]); % index
        tempYeast.budTimeInd = NaN;
        % tempYeast is the new daughter bud having the same momID as
its mother cell (important when identifying later)
        yeast(indOffset+j) = tempYeast;
    end
end
```

```matlab
colors = [0 0 1; 1 0 0]; % blue and red
fontSizeTitle = 12;
fontSizeAxis = 11;
fontSizeLegend = 10;
fontSizeText = 11;

% Define variables to calculate stats throughout the simulation
avgBirthSizes = avgBirthSize;
purities = [];


for timeInd = 1:numel(timePoints)
    % Update budTime for all yeast having a budTimeInd (all yeast not
attached to a mother)
    indMom = find(~isnan([yeast.budTimeInd]));
    for m = 1:numel(indMom) % not able to assign all elements of struct
in a single command, thus must loop
        yeast(indMom(m)).budTimeInd = yeast(indMom(m)).budTimeInd + 1;
% index
    end
    anyTooHigh = find([yeast(indMom).budTimeInd] > numel(budTimes));
    % Account for case that yeast reaches end of budTimes and must
release its daughter
    if anyTooHigh
        % Release all buds from their mothers if mothers' budTimeInds
exceed the max budTime
        tempAvgBirth = [];
        for k = 1:numel(anyTooHigh)
            releaseID =
find([yeast(anyTooHigh(k)).momID]==[yeast.momID] &
isnan([yeast.budTimeInd]));
            yeast(releaseID).budTimeInd = 1;
            yeast(releaseID).momID = max([[yeast.momID]
initialMomIDs])+1; % should be unique
            avgBirthSize = mean([avgBirthSize
allSizes(yeast(releaseID).sizeInd)]);
            tempAvgBirth = nanmean([tempAvgBirth avgBirthSize]);
            yeast(anyTooHigh(k)).budTimeInd = 1;
        end
        avgBirthSizes(end+1) = tempAvgBirth;
    else
        avgBirthSizes(end+1) = avgBirthSizes(end);
    end

    % See if we need to add new buds (if a yeast starts
budTimeStartInd)
    indStartBud = find([yeast.budTimeInd] == budTimeStartInd);
    indOffset = numel(yeast);
    yeast(end+1:end+numel(indStartBud)) = struct(...
        'sizeInd',[],...
        'budTimeInd',[],...
        'momID',[]);
    if indStartBud
        for j = 1:numel(indStartBud)
```

```matlab
            tempYeast = yeast(indStartBud(j));
            tempYeast.sizeInd = max([1
(floor(normrnd(avgBirthSizeInd,sigmaInd))-timeGrowthYesBud)]); % index
            tempYeast.budTimeInd = NaN;
            % tempYeast is the new daughter bud having the same momID
as its mother cell (important when identifying later)
            yeast(indOffset+j) = tempYeast;
        end
    end

    % Grow all yeast by updating sizeInd, which cannot exceed
numel(allSizes)
    for m = 1:numel(yeast)
        yeast(m).sizeInd = min([(yeast(m).sizeInd+1) numel(allSizes)]);
% index
    end

    % Remove yeast below a certain size threshold
    if any(removeThisTime==timeInd)
        % First remove yeast not currently attached to a daughter
(those that are not currently budding, budTimeInd is below
budTimeStartInd)
        indNotAttach = find([yeast.budTimeInd] < budTimeStartInd);
        indRemove = find([yeast.budTimeInd] < budTimeStartInd &
allSizes([yeast.sizeInd]) < allSizes(sizeThreshInd));
        if indNotAttach
%            indRemove = allSizes([yeast.sizeInd]) <
allSizes(sizeThreshInd);
%            indRemove = indRemove & [yeast.budTimeInd] <
budTimeStartInd;
            % Of the smaller cells that should be removed, (1-
separationPurity)% are kept in the larger size-bin
            numElements = round((1-separationPurity)*numel(indRemove));
            indices = randperm(numel(indRemove));
            indKeep = indices(1:numElements);
            indRemove(indKeep) = [];
            wasteYeast(end+1:end+numel(indRemove)) = yeast(indRemove);
            yeast(indRemove) = [];
        end
        % Now remove mom+daughter sizes that do not exceed size
threshold
        indAttachedMom = find([yeast.budTimeInd] >= budTimeStartInd);
        if indAttachedMom
            indRemove = [];
            for m = 1:numel(indAttachedMom)
                indAttachedDaughter =
find([yeast(indAttachedMom(m)).momID]==[yeast.momID] &
isnan([yeast.budTimeInd]));
                sizeIndMom = yeast(indAttachedMom(m)).sizeInd; % needed
to calculate combined size of mother+daughter
                sizeIndDaughter = yeast(indAttachedDaughter).sizeInd;
                combinedSize = allSizes(sizeIndMom) +
allSizes(sizeIndDaughter);
```

```matlab
                if combinedSize < allSizes(sizeThreshInd)
                    indRemove(end+1) = indAttachedMom(m);
                    indRemove(end+1) = indAttachedDaughter;
                end
            end
            % Of the smaller volumes that should be removed, (1-
separationPurity) are kept in the larger size-bin
            % Tricky here because mother index is immediately followed
by daughter index in indRemove, and if we want to keep a mother (or
daughter), we must also keep the daughter (or mother)
            numElements = round((1-
separationPurity)*(numel(indRemove)/2));
            indices = randperm(numel(indRemove)/2);
            indKeep = 2*indices(1:numElements);
            indKeep = [indKeep indKeep-1];
            indRemove(indKeep) = [];
            wasteYeast(end+1:end+numel(yeast(indRemove))) =
yeast(indRemove);
            yeast(indRemove) = [];
        end
    end

    % Handle yeast moms not currently attached to daughters
    indAloneMoms = find([yeast.budTimeInd] < budTimeStartInd);
    numOriginal = 0;
    for k = 1:numel(indAloneMoms)
        if any(initialMomIDs == yeast(indAloneMoms(k)).momID)
            numOriginal = numOriginal + 1;
        end
    end
    % Handle yeast moms still attached to daughters
    indAttachedMom = find([yeast.budTimeInd] >= budTimeStartInd);
    if indAttachedMom
        for m = 1:numel(indAttachedMom)
            if any(initialMomIDs == yeast(indAttachedMom(m)).momID)
                numOriginal = numOriginal + 1;
            end
        end
    end
    percentOriginal = 100*numOriginal/numel(yeast);
    purities(end+1) = percentOriginal;

end

% Plot the results
figHand = figure('Position',[1 1 1920 994]); hold on

% Plot growth/size model
subplot(3,3,1), hold on
plot(1:numSizesGrowthModel,allSizes,'k');
plot([1 numSizesGrowthModel],[allSizes(sizeThreshInd)
allSizes(sizeThreshInd)],'--','Color',[0.8 0.8 0.8]);
```

```matlab
legend({'Yeast Growth Model','Separation
Threshold'},'Location','NorthWest','FontName','Arial','FontSize',fontSi
zeLegend);
xlabel('Time Point','FontName','Arial','FontSize',fontSizeAxis);
ylabel('Size (um^3)','FontName','Arial','FontSize',fontSizeAxis);
box on

% Plot budding model
subplot(3,3,4), hold on
yLevel = 1; % arbitray
rectHeight = 1; % arbitrary
rect1 = [budTimes(1) yLevel (budTimes(budTimeStartInd)-budTimes(1))
rectHeight];
%       rect2 = [budTimes(budTimeStartInd) yLevel
(numel(budTimeStartInd)) rectHeight];
rect3 = [budTimes(budTimeStartInd) yLevel (budTimes(end)-
budTimes(budTimeStartInd)) rectHeight];
handr1 = rectangle('Position',rect1,'FaceColor',[0.1 0.1 0.1]);
p1=plot(nan,nan,'s','markeredgecolor',get(handr1,'edgecolor'),'markerfa
cecolor',get(handr1,'facecolor'));
%       handr2 = rectangle('Position',rect2,'FaceColor','g');
p2=plot(nan,nan,'s','markeredgecolor',get(handr2,'edgecolor'),'markerfa
cecolor',get(handr2,'facecolor'));
handr3 = rectangle('Position',rect3,'FaceColor',[0.9 0.9 0.9]);
p3=plot(nan,nan,'s','markeredgecolor',get(handr3,'edgecolor'),'markerfa
cecolor',get(handr3,'facecolor'));
legend([p1 p3],{'Growth';'Growth &
Budding'},'FontName','Arial','FontSize',fontSizeLegend,'Location','Nort
h');
xlabel('Time Point','FontName','Arial','FontSize',fontSizeAxis);
set(gca,'YTick',[]);
xOffset = 5; yLim = ylim; yDiff = 0.9*(yLim(2)-yLim(1));
axis([budTimes(1)-xOffset budTimes(end)+xOffset yLim(1)-yDiff
yLim(2)+yDiff])
box on

% Plot graph of initial cell sizes
subplot(3,3,5), hold on
hist(initialSizes);
handHist = findobj(gca,'Type','patch');
set(handHist,'FaceColor',[0.2 0.2 0.2],'EdgeColor','w');
title('Yeast Sizes at Time Point =
0','FontSize',fontSizeTitle,'FontName','Arial')
xlabel('Size (um^3)','FontName','Arial','FontSize',fontSizeAxis);
ylabel('# of cells','FontName','Arial','FontSize',fontSizeAxis);
box on

% Plot graph of cell sizes at currrent time point
subplot(3,3,6), hold on
hist(allSizes([yeast.sizeInd]));
handHist = findobj(gca,'Type','patch');
set(handHist,'FaceColor',[0.2 0.2 0.2],'EdgeColor','w');
```

```matlab
title(sprintf('Yeast Sizes at Time Point =
%0.0d',timePoints(timeInd)),'FontSize',fontSizeTitle,'FontName','Arial'
)
xlabel('Size (um^3)','FontName','Arial','FontSize',fontSizeAxis);
ylabel('# of cells','FontName','Arial','FontSize',fontSizeAxis);
box on

% Plot cells that have been removed by creating unique x,y coords for
each yeast
subplot(3,3,2), hold on
if skipWasteCalcs
    xLim = xlim; yLim = ylim;
    text('String',{sprintf('%0.0d cells',numel(wasteYeast)-1)},...
        'Position',[0.35*(xLim(2)-xLim(1)) yLim(2)/2],...
        'HorizontalAlignment','left',...
        'FontSize',fontSizeText,...
        'FontName','Arial',...
        'BackgroundColor',[1 1 1],...
        'Color',[0 0 0]);
    numOriginal = NaN;
elseif numel(wasteYeast) < maxYeastPlot
    squareDim = ceil(sqrt(numel(wasteYeast)));
    [squareGridX, squareGridY] = meshgrid(1:squareDim,1:squareDim);
    squareGridX = squareGridX*2*max(allSizes); squareGridY =
squareGridY*2*max(allSizes);
    numOriginal = 0;
    for k = 2:numel(wasteYeast) % first waste yeast is an empty struct
        if any(initialMomIDs == wasteYeast(k).momID)
            circleColor = colors(1,:);
            numOriginal = numOriginal + 1;
        else
            circleColor = colors(2,:);
        end
        sideLength = allSizes(wasteYeast(k).sizeInd);
        rectangle('Position',[squareGridX(k) squareGridY(k) sideLength
sideLength],...
            'Curvature',[1 1],...
            'FaceColor',circleColor);
    end
else
    numOriginal = 0;
    for k = 2:numel(wasteYeast) % first waste yeast is an empty struct
        if any(initialMomIDs == wasteYeast(k).momID)
            numOriginal = numOriginal + 1;
        end
    end
    xLim = xlim; yLim = ylim;
    text('String',{sprintf('%0.0d cells',numel(wasteYeast)-1)},...
        'Position',[0.35*(xLim(2)-xLim(1)) yLim(2)/2],...
        'HorizontalAlignment','left',...
        'FontSize',fontSizeText,...
        'FontName','Arial',...
        'BackgroundColor',[1 1 1],...
```

```matlab
        'Color',[0 0 0]);
end
percentOriginal = 100*numOriginal/numel(wasteYeast);
titleStr = sprintf('Removed Yeast, %0.1f%% from Initial
Population',percentOriginal);
title(titleStr,'FontSize',fontSizeTitle,'FontName','Arial')
set(gca,'XTick',[],'YTick',[]);
xlabel('Offspring of original
cells','FontName','Arial','FontSize',fontSizeAxis,'Color',[1 0 0])
box on

% Plot the results by creating unique x,y coords for each mother yeast
subplot(3,3,3), hold on
if numel(yeast) < maxYeastPlot
    squareDim = ceil(sqrt(numel(yeast)));
    [squareGridX, squareGridY] = meshgrid(1:squareDim,1:squareDim);
    squareGridX = squareGridX*2*max(allSizes); squareGridY =
squareGridY*2*max(allSizes);
    % Plot yeast moms not currently attached to daughters
    indAloneMoms = find([yeast.budTimeInd] < budTimeStartInd);
    numOriginal = 0;
    for k = 1:numel(indAloneMoms)
        if any(initialMomIDs == yeast(indAloneMoms(k)).momID)
            circleColor = colors(1,:);
            numOriginal = numOriginal + 1;
        else
            circleColor = colors(2,:);
        end
        sideLength = allSizes(yeast(indAloneMoms(k)).sizeInd);
        rectangle('Position',[squareGridX(k) squareGridY(k) sideLength
sideLength],...
            'Curvature',[1 1],...
            'FaceColor',circleColor);
    end
    % Plot yeast moms still attached to daughters
    indAttachedMom = find([yeast.budTimeInd] >= budTimeStartInd);
    if indAttachedMom
        for m = 1:numel(indAttachedMom)
            indAttachedDaughter =
find([yeast(indAttachedMom(m)).momID]==[yeast.momID] &
isnan([yeast.budTimeInd]));
            sizeIndMom = yeast(indAttachedMom(m)).sizeInd; % needed to
calculate combined size of mother+daughter
            sizeIndDaughter = yeast(indAttachedDaughter).sizeInd;
            combinedSize = allSizes(sizeIndMom) +
allSizes(sizeIndDaughter);
            if any(initialMomIDs == yeast(indAttachedMom(m)).momID)
                circleColor = colors(1,:);
                numOriginal = numOriginal + 1;
            else
                circleColor = colors(2,:);
            end
            sizeMom = allSizes(sizeIndMom);
```

```matlab
            sizeDaughter = allSizes(sizeIndDaughter);
            indOffset = max([k 0]);
            rectangle('Position',[squareGridX(indOffset+m)
squareGridY(indOffset+m) sizeMom sizeMom],...
                'Curvature',[1 1],...
                'FaceColor',circleColor);
            rectangle('Position',[squareGridX(indOffset+m)+sizeMom
squareGridY(indOffset+m)+0.5*sizeMom-0.5*sizeDaughter sizeDaughter
sizeDaughter],...
                'Curvature',[1 1],...
                'FaceColor',colors(2,:));
        end
    end
else
    squareDim = ceil(sqrt(numel(yeast)));
    [squareGridX, squareGridY] = meshgrid(1:squareDim,1:squareDim);
    squareGridX = squareGridX*2*max(allSizes); squareGridY =
squareGridY*2*max(allSizes);
    % Handle yeast moms not currently attached to daughters
    indAloneMoms = find([yeast.budTimeInd] < budTimeStartInd);
    numOriginal = 0;
    for k = 1:numel(indAloneMoms)
        if any(initialMomIDs == yeast(indAloneMoms(k)).momID)
            numOriginal = numOriginal + 1;
        end
    end
    % Handle yeast moms still attached to daughters
    indAttachedMom = find([yeast.budTimeInd] >= budTimeStartInd);
    if indAttachedMom
        for m = 1:numel(indAttachedMom)
            if any(initialMomIDs == yeast(indAttachedMom(m)).momID)
                numOriginal = numOriginal + 1;
            end
        end
    end
    xLim = xlim; yLim = ylim;
    text('String',{sprintf('%0.0d cells',numel(yeast))},...
        'Position',[0.35*(xLim(2)-xLim(1)) yLim(2)/2],...
        'HorizontalAlignment','left',...
        'FontSize',fontSizeText,...
        'FontName','Arial',...
        'BackgroundColor',[1 1 1],...
        'Color',[0 0 0]);
end
percentOriginal = 100*numOriginal/numel(yeast);
purities(end+1) = percentOriginal;
titleStr = sprintf('Remaining Yeast, %0.1f%% from Initial
Population',percentOriginal);
title(titleStr,'FontSize',fontSizeTitle,'FontName','Arial')
set(gca,'XTick',[],'YTick',[]);
xlabel('Cell from initial
population','FontName','Arial','FontSize',fontSizeAxis,'Color',[0 0 1])
xLim = xlim; yLim = ylim;
```

```matlab
axis([xLim(1) max(max(squareGridX))+2*max(allSizes) yLim(1)
max(max(squareGridY))+2*max(allSizes)])
box on

% Show input parameters and simulation stats
subplot(3,3,8), hold on
set(gca,'XTick',[],'YTick',[]), box on
textStr = sprintf(['Initial # of cells: %0.0d\nExperiment duration:
%0.0d time points (tp)\n'...
    'Entire growth model: %0.0d tp\nMother with NO bud: %0.0d
tp\nMother with bud: %0.0d tp\n'...
    'Mean birth size: %0.2fum^3\nSize separation threshold:
%0.2fum^3\nSeparation purity: %0.1f%%\n'...
    'Separation performed every %0.0d
tp'],numYeast,maxExperimentTime,...

numel(allSizes),timeGrowthNoBud,timeGrowthYesBud,avgBirthSize,sizeThres
hVal,100*separationPurity,min(removeEveryNth,inf));
xLim = xlim; yLim = ylim;
text('String',{textStr},...
    'Position',[0.05*(xLim(2)-xLim(1)) yLim(2)/2],...
    'HorizontalAlignment','left',...
    'FontSize',fontSizeText,...
    'FontName','Arial',...
    'BackgroundColor',[1 1 1],...
    'Color',[0 0 0]);

% Plot average birthsize vs time
subplot(3,3,7), hold on
timeArray =
linspace(timePoints(1),timePoints(timeInd),numel(avgBirthSizes));
plot(timeArray,avgBirthSizes,'k')
xlabel('Time Point','FontName','Arial','FontSize',fontSizeAxis);
ylabel('Mean Birth Size
(um^3)','FontName','Arial','FontSize',fontSizeAxis);
yLim = ylim;
axis([timePoints(1) timePoints(end) yLim(1) yLim(2)])
box on

% Plot average purity vs time
subplot(3,3,9), hold on
timeArray =
linspace(timePoints(1),timePoints(timeInd),numel(purities));
plot(timeArray,purities,'k')
xlabel('Time Point','FontName','Arial','FontSize',fontSizeAxis);
ylabel('Aged Yeast Purity
(%)','FontName','Arial','FontSize',fontSizeAxis);
axis([timePoints(1) timePoints(end) 0 100])
box on

% Different way of calculating purity (without including daughters
currently attached to mothers)
indMoms = ~isnan([yeast.budTimeInd]);
```

```matlab
percentOriginal = 100*numOriginal/sum(indMoms);
textStr = sprintf('%0.1f%% at %0.0d tp not including attached
buds',percentOriginal,timePoints(end));
xLim = xlim; yLim = ylim;
text('String',{textStr},...
    'Position',[0.05*(xLim(2)-xLim(1)) 0.9*yLim(2)],...
    'HorizontalAlignment','left',...
    'FontSize',fontSizeText,...
    'FontName','Arial',...
    'BackgroundColor',[1 1 1],...
    'Color',[0 0 0]);

frame = getframe(figHand);
imwrite(frame.cdata,fileName);

datestr(now)
```

Yeast size data used in aged yeast generator simulation model

Table 9. Data from Coulter Counter measurement of yeast sizes

Volume Bins (µm)	Diameter Bins (µm)	Radius Bins (µm)	Hits
13.18	2.930706	1.465353	673
13.84	2.978831	1.489415	606
14.49	3.024753	1.512377	623
15.15	3.069997	1.534999	673
15.81	3.113946	1.556973	606
16.47	3.156688	1.578344	623
17.13	3.198303	1.599151	539
17.79	3.238862	1.619431	791
18.44	3.277838	1.638919	825
19.11	3.317065	1.658533	1077
19.77	3.354821	1.67741	892
20.43	3.391745	1.695873	1279
21.09	3.427883	1.713941	1431
21.74	3.462743	1.731372	1818
22.41	3.497957	1.748978	1986
23.07	3.531964	1.765982	2138
23.72	3.564829	1.782414	2189
24.39	3.598082	1.799041	2710
25.04	3.629765	1.814883	2593
25.69	3.660905	1.830453	2744
26.35	3.691991	1.845996	2879
27.02	3.723022	1.861511	3855

Table 9. (continued)

Volume Bins (µm)	Diameter Bins (µm)	Radius Bins (µm)	Hits
27.68	3.753092	1.876546	3333
28.32	3.781797	1.890898	4242
29	3.811827	1.905913	3720
29.65	3.840096	1.920048	4394
30.3	3.867954	1.933977	4781
30.96	3.895837	1.947918	4411
31.64	3.924153	1.962077	4394
32.29	3.950843	1.975422	4495
32.94	3.977178	1.988589	3990
33.61	4.003962	2.001981	4916
34.27	4.030001	2.015001	4478
34.94	4.056095	2.028047	5303
35.59	4.081093	2.040546	4377
36.25	4.106166	2.053083	4158
36.91	4.130936	2.065468	5151
37.56	4.155044	2.077522	4226
38.21	4.178876	2.089438	4663
38.88	4.20316	2.10158	4798
39.55	4.227166	2.113583	4444
40.19	4.249845	2.124923	4848
40.85	4.272983	2.136491	4461
41.51	4.295872	2.147936	4478
42.18	4.318862	2.159431	4461
42.83	4.340934	2.170467	4933
43.49	4.363118	2.181559	4141
44.15	4.385078	2.192539	4949
44.82	4.407149	2.203575	4596
45.46	4.428027	2.214014	4327
46.14	4.449996	2.224998	4697
46.8	4.471114	2.235557	4074
47.46	4.492034	2.246017	4646
48.1	4.512136	2.256068	4646
48.77	4.532989	2.266495	4141
49.42	4.553039	2.27652	4529
50.07	4.572914	2.286457	4175
50.73	4.592919	2.296459	4933
51.4	4.61305	2.306525	3502
52.07	4.633007	2.316504	4293

Table 9. (continued)

Volume Bins (µm)	Diameter Bins (µm)	Radius Bins (µm)	Hits
52.71	4.651912	2.325956	3468
53.36	4.670956	2.335478	4343
54.05	4.691003	2.345501	3468
54.71	4.710019	2.35501	4209
55.34	4.728029	2.364015	3939
56.01	4.747034	2.373517	4478
56.68	4.765887	2.382943	3215
57.33	4.784036	2.392018	3889
57.98	4.802048	2.401024	3502
58.63	4.819927	2.409963	3805
59.29	4.837945	2.418973	3215
59.96	4.856101	2.42805	3619
60.63	4.874121	2.437061	3384
61.3	4.892009	2.446005	3872
61.94	4.908975	2.454488	2828
62.59	4.926087	2.463044	3535
63.28	4.944123	2.472062	3384
63.93	4.960994	2.480497	3316
64.59	4.978008	2.489004	3165
65.25	4.994906	2.497453	3114
65.88	5.01093	2.505465	2761
66.56	5.028111	2.514056	3148
67.23	5.044926	2.522463	2963
67.87	5.060884	2.530442	2424
68.52	5.076989	2.538495	2879
69.21	5.093974	2.546987	2643
69.87	5.110115	2.555058	2609
70.52	5.125913	2.562956	2155
71.19	5.142095	2.571048	2576
71.81	5.15698	2.57849	2508
72.48	5.172969	2.586484	2239
73.16	5.189096	2.594548	2273
73.79	5.203948	2.601974	2071
74.47	5.219885	2.609942	1885
75.12	5.235028	2.617514	2138
75.77	5.250084	2.625042	1919
76.46	5.265972	2.632986	1784
77.12	5.281081	2.64054	2020
77.78	5.296103	2.648052	1633

Table 9. (continued)

Volume Bins (µm)	Diameter Bins (µm)	Radius Bins (µm)	Hits
78.44	5.311041	2.655521	1650
79.06	5.324997	2.662499	2104
79.73	5.339997	2.669999	1633
80.4	5.354914	2.677457	1751
81.04	5.369085	2.684542	1784
81.72	5.38406	2.69203	1650
82.36	5.398079	2.69904	1549
83.04	5.412895	2.706447	1768
83.69	5.426981	2.713491	1549
84.34	5.440995	2.720497	1027
84.99	5.454937	2.727468	1566
85.65	5.469021	2.73451	1296
86.31	5.483033	2.741516	1380
86.97	5.496973	2.748487	1162
87.64	5.511053	2.755526	1279
88.31	5.525061	2.762531	1128
88.98	5.538999	2.769499	1330
89.61	5.55204	2.77602	1061
90.29	5.566049	2.783024	1162
90.92	5.578965	2.789482	1229
91.61	5.593042	2.796521	1414
92.25	5.606036	2.803018	1195
92.89	5.618971	2.809485	1077
93.59	5.63305	2.816525	976
94.24	5.646061	2.82303	976
94.89	5.659012	2.829506	909
95.54	5.671904	2.835952	892
96.2	5.684935	2.842467	741
96.86	5.697906	2.848953	774
97.53	5.711014	2.855507	976
98.2	5.724061	2.862031	1027
98.87	5.73705	2.868525	943
99.49	5.749017	2.874509	657
100.2	5.76266	2.88133	1145
100.8	5.77414	2.88707	1111
101.5	5.787475	2.893738	825
102.2	5.800749	2.900375	623
102.8	5.812079	2.906039	690
103.4	5.823364	2.911682	859

Table 9. (continued)

Volume Bins (µm)	Diameter Bins (µm)	Radius Bins (µm)	Hits
104.1	5.836476	2.918238	774
104.8	5.849529	2.924764	690
105.4	5.860671	2.930335	640
106.1	5.873617	2.936808	859
106.8	5.886505	2.943253	741
107.4	5.897508	2.948754	690
108.1	5.910293	2.955147	657
108.7	5.921208	2.960604	606
109.4	5.933891	2.966946	572
110.1	5.94652	2.97326	488
110.7	5.957303	2.978651	404
111.4	5.969833	2.984917	707
112	5.980532	2.990266	522
112.7	5.992965	2.996483	875
113.3	6.003582	3.001791	269
114	6.01592	3.00796	370
114.6	6.026456	3.013228	471
115.3	6.038701	3.019351	438
116	6.050897	3.025449	370
116.6	6.061312	3.030656	370
117.3	6.073417	3.036709	488
118	6.085475	3.042737	505
118.6	6.095772	3.047886	354
119.3	6.107741	3.05387	404
119.9	6.117963	3.058982	286
120.6	6.129846	3.064923	505
121.3	6.141683	3.070841	421
121.9	6.151793	3.075896	505
122.6	6.163546	3.081773	370
123.2	6.173584	3.086792	438
123.9	6.185254	3.092627	253
124.5	6.195223	3.097611	337
125.2	6.206812	3.103406	438
125.9	6.218358	3.109179	505
126.5	6.22822	3.11411	253
127.2	6.239687	3.119844	219
127.8	6.249483	3.124741	303
128.5	6.260872	3.130436	387
129.2	6.27222	3.13611	286

Table 9. (continued)

Volume Bins (µm)	Diameter Bins (µm)	Radius Bins (µm)	Hits
129.8	6.281915	3.140957	404
130.5	6.293187	3.146593	219
131.1	6.302817	3.151408	168
131.8	6.314015	3.157007	370
132.4	6.323582	3.161791	337
133.1	6.334706	3.167353	185
133.7	6.344211	3.172105	286
134.4	6.355263	3.177632	370
135.1	6.366278	3.183139	202
135.7	6.375688	3.187844	269
136.4	6.386632	3.193316	320
137.1	6.397539	3.19877	202
137.7	6.406858	3.203429	269
138.4	6.417696	3.208848	101
139.1	6.428498	3.214249	269
139.7	6.437728	3.218864	236
140.4	6.448462	3.224231	253
141	6.457635	3.228818	168
141.7	6.468304	3.234152	219
142.3	6.477421	3.23871	135
143	6.488024	3.244012	337
143.7	6.498594	3.249297	185
144.3	6.507626	3.253813	135
145	6.518132	3.259066	202
145.7	6.528604	3.264302	286
146.3	6.537553	3.268777	101
146.9	6.546478	3.273239	135
147.6	6.55686	3.27843	135
148.3	6.567209	3.283605	152
148.9	6.576054	3.288027	135
149.6	6.586343	3.293171	168
150.3	6.5966	3.2983	118
150.9	6.605366	3.302683	118
151.6	6.615564	3.307782	152
152.2	6.62428	3.31214	135
152.9	6.63442	3.31721	269
153.6	6.644529	3.322264	152
154.2	6.653169	3.326585	118
154.9	6.663222	3.331611	101

Table 9. (continued)

Volume Bins (µm)	Diameter Bins (µm)	Radius Bins (µm)	Hits
155.5	6.671814	3.335907	84
156.1	6.680384	3.340192	152
156.8	6.690355	3.345177	152
157.5	6.700296	3.350148	101
158.2	6.710208	3.355104	185
158.8	6.71868	3.35934	67
159.5	6.728538	3.364269	185
160.1	6.736964	3.368482	67
160.8	6.746768	3.373384	67
161.5	6.756544	3.378272	51
162.1	6.764901	3.382451	67
162.8	6.774625	3.387312	118
163.4	6.782937	3.391469	84
164.1	6.79261	3.396305	67
164.7	6.800878	3.400439	84
165.4	6.810499	3.40525	67
166.1	6.820094	3.410047	84
166.8	6.829661	3.41483	67